Liver Segmentation and its Application to Hepatic Interventions

Andrea Schenk

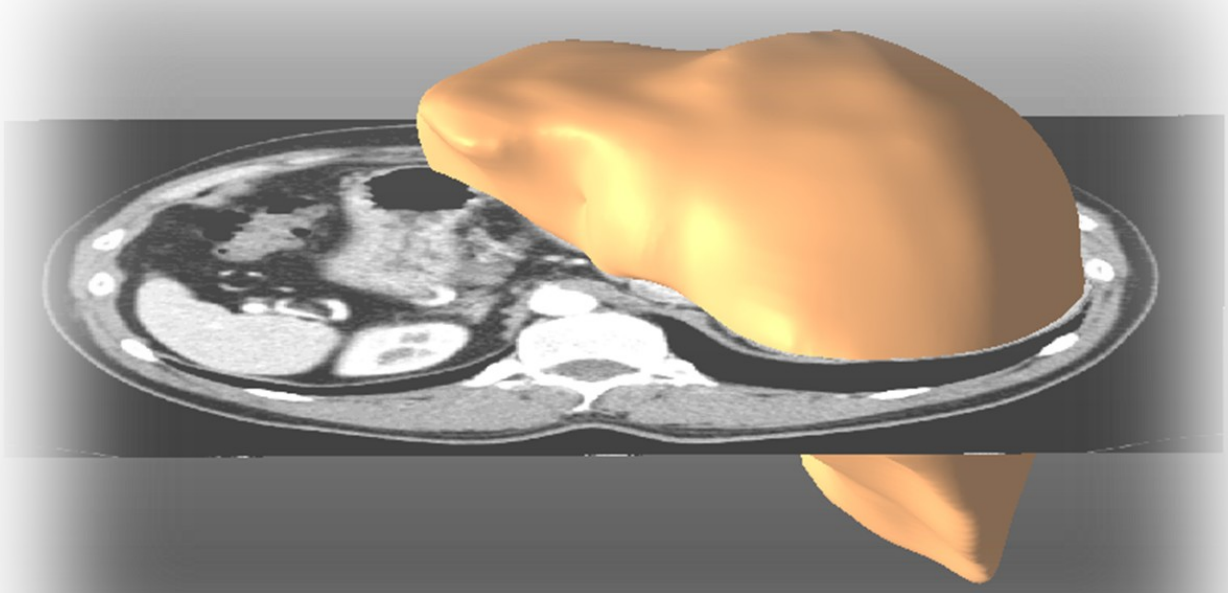

Fraunhofer MEVIS
2012

Datum des Promotionskolloquiums: 24. September 2012

Gutachter: Prof. Dr. rer. nat. Heinz-Otto Peitgen,
Universität Bremen

Prof. Dr.-Ing. Bernhard Preim,
Otto-von-Guericke-Universität Magdeburg

Liver Segmentation and its Application to Hepatic Interventions

von Dipl.-Math. Andrea Schenk

Dissertation

zur Erlangung des akademischen Grades
eines Doktors der Ingenieurwissenschaften
- Dr.-Ing. -

Vorgelegt im Fachbereich 3 (Mathematik und Informatik)
der Universität Bremen

Juli 2012

© 2012 Andrea Schenk. All rights reserved

This work was conducted at
Fraunhofer MEVIS - Institute for Medical Image Computing

Andrea Schenk
Fraunhofer MEVIS
Universitätsallee 29, 28357 Bremen, Germany
Email: andrea.schenk@mevis.fraunhofer.de

Content

1 Introduction

"The King of Babylon stood at the parting of the ways, at the head of the two ways, to use divination; he made arrows bright, he consulted with images, he looked in the liver."
The Bible, Ezekiel 21:21

1.1 Why Hepatic Surgery needs Liver Segmentation

A surgeon typically resects a liver for two reasons: to remove a malignant or benign lesion or to split the organ for living donor liver transplantation (LDLT). In both cases, hepatic tissue will be removed, and liver volume and the related liver function will be temporarily decreased. For the safety and survival of the patient, a certain amount of liver tissue should remain. This 'certain amount' of required remnant liver volume leads to the issue of how this amount can be computed and how the organ size of an individual human is determined.

In general, the volume of a healthy liver correlates to the individually required organ function. When a liver grows during childhood and adolescence, it adapts to the needs and increases in size. Later, when an adult gains or loses weight, the organ will also change to match the new metabolic demand. How can the individual liver volume be computed?

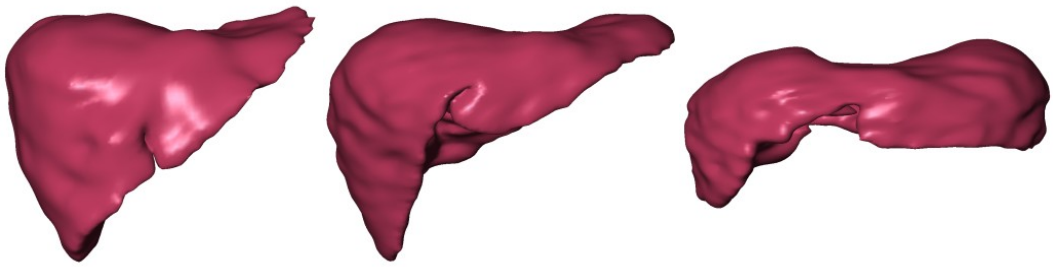

Figure 1: Variability of liver shapes: A typical Caucasian liver show a large right lobe (left), while Asian organs often extend to the left body side (right), although variations are common (middle).

As reported in early studies, the total liver volume is closely related to a person's weight and accounts for about 2.0%-2.7% of body weight [Henderson et al., 1981, Heymsfield et al., 1979]. Several published formulas estimate the total liver volume from the weight, body surface area (BSA, for details see [Bois and Bois, 1989, Mosteller, 1987]), or a combination of body weight and age [Chan et al., 2011, Poovathumkadavil et al., 2010, Yuan et al., 2008]. A comprehensive list of formulas can be found in [Fu-Gui et al., 2009] and [Pomposelli et al., 2012]. The basis for the computations were liver volumes from autopsies [DeLand and North, 1968, Heinemann et al., 1999, Yoshizumi et al., 2003] or volumes of liver masks extracted from computed tomography (CT) data [Pomposelli et al., 2012, Urata

et al., 1995, Vauthey et al., 2002]. In most studies, the results are derived from and limited to an ethnic group, e.g., Asian or Caucasians, but also to subgroups, e.g., Japanese, Chinese, or Arab adults [Poovathumkadavil et al., 2010, Urata et al., 1995, Yoshizumi et al., 2008]. Figure 1 illustrates the variability in liver shape. Organ volume formulas are typically used to estimate the demand for a transplant recipient whose existing liver volume cannot be used as a reference, due to oncologic, cirrhotic, or other diseases that have significantly changed the original organ size and weight.

Recently, some authors have even published formulas for parts of the organ, such as the right liver lobe, derived from body weight [Chan et al., 2011, Harada et al., 2004, Salvalaggio et al., 2005], but considering the wide interindividual variation of these other formulas, the purpose and usability of these computations remain doubtful. Although formulas for the total liver volume might be helpful for a very rough estimation of the functional demand for a recipient, the computation of remnant liver after extended surgery needs to be more precise.

A patient's liver volume can be computed from radiological images. For this purpose, the liver boundary contours have to be determined for all images slices of the abdominal data. Different approaches have been developed, ranging from manual drawing to fully automatic algorithms. An overview of liver segmentation methods is given in Section 2.1.

For hepatic surgery, the volume of the remnant organ after resection is important for patient safety. Unfortunately, the minimal required remnant volume is not only a fixed percentage of the full volume, but also strongly depends on the condition of the liver parenchyma. For patients with otherwise healthy livers, a functional volume of 25% of the original liver volume is sufficient for survival [Breitenstein et al., 2009, Chen et al., 2003, Lo et al., 1999]. Due to the high regenerative power of the liver, the organ grows within a couple of months until the liver volume is similar to pre-surgery levels. For diseased livers, e.g., cirrhotic or steatotic organs or organs that have undergone chemotherapy, the required remnant volume increases to 30% - 90%, depending on the stage of the disease and the remaining hepatic function. Unfortunately, the exact minimum volume necessary for organ and patient survival is difficult to predict in these cases [Breitenstein et al., 2009].

Furthermore, not only a pre-existing hepatic disease but also the resection itself can cause a functional problem. Resecting the liver with its complex vessel structure can truncate supplying or draining veins and liver arteries (cf. Figure 2). As a consequence of reduced or interrupted blood flow, the dependent local liver regions can exhibit liver dysfunction that can extend to a complete necrosis in the worst cases. To analyze the risks and plan the surgical interventions, this functionally limited tissue has to be considered and the predicted functional remnant liver volume adjusted. For tumor resections, the risk analysis is computed for the re-

maining liver, whereas in living donor liver transplantations, it has to be evaluated for both the remnant liver of the donor and the graft given to the recipient.

In conclusion, the remaining liver volume may be one of the most critical factors for a surgical intervention, depending on the liver condition and extent of the resection. Therefore, the computation of total liver volume as well as prediction of remnant liver volume is important for surgical planning. The segmentation of the liver in radiological data, i.e., the separation of the organ tissue from all other surrounding structures in the images, typically represents the first step in computer-assisted liver surgery planning.

Liver segmentation is not only the prerequisite for planning hepatic surgery but also for several other medical applications, including local tumor ablations by radiofrequency or laser energy, tumor load computation for radiation therapy, and therapy monitoring during chemotherapy. The applications have varying demands for accuracy, and the clinical routine often limits the available interaction time. Therefore, dedicated techniques or individual parameterizations for liver segmentation methods are needed.

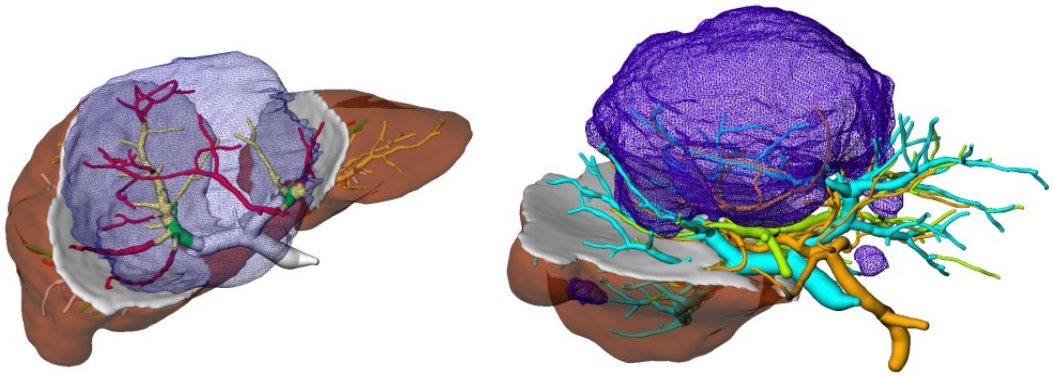

Figure 2: Example of a complex tumor resection case. Left: Color-coded vessel surfaces show the minimal distance of subbranches to the tumor (tumor in blue; vessels red: 5mm, yellow 10mm, green 15mm distance). Brown: remnant liver after central resection. Right: Plan of an extended left liver resection for the same case with the risk of insufficient remaining liver volume (brown). The visualization shows tumors, the remnant liver, and the triad of portal vein (cyan), hepatic artery (orange), and bile ducts (green).

1.2 Objectives of the Thesis

This work is dedicated to the topic of liver segmentation and its applications to liver surgery. The development and evaluation of a clinically applicable segmentation algorithm and its integration into a software assistant that can be used by medical experts represents one major focus of the thesis. The second objective addresses the remaining liver volume after hepatic resections at the example of adult living donor liver transplantation (ALDLT). The anatomical volume can be computed from the liver segmentation mask and the virtual resection line quite easily, but may not represent the remaining liver function. The hepatic tissue can be impaired by a disease or outflow obstruction induced by the transection of hepatic vein branches. The relevance of this outflow obstruction to liver function and regeneration and the mechanisms of reperfusion were investigated in this thesis. Human and animal studies were performed and evaluated in cooperation with clinical partners. New algorithms and software applications were developed to support the research in this field.

The following issues have been addressed by this work in different ways:

- What methods are appropriate to achieve highly accurate liver segmentation?
- How can the interaction effort for liver segmentation be reduced and corrected in an intuitive way?
- How much time is invested by users for segmentation and correction and what are the differences between intial and corrected liver segmentation?
- Which steps are included in a comprehensive software assistant for liver surgery planning and how can this workflow be realized?
- How could 3D planning data be used in laparoscopic liver surgery?
- Can the vascular cooling effect in radiofrequency ablation be estimated by numerical models?
- How can the risk of a resection be quantified and can this measure be used to provide immediate feedback during resection planning?
- To which extend does the transection of middle hepatic vein branches influence global and local liver regeneration?
- When do collaterals develop between truncated vein branches and neighbored hepatic veins?
- How do outflow obstructions change perfusion and how do collaterals between the outflow obstructed and normal zones develop?
- Can MRI serve as a sole imaging modality for liver surgery planning?

1.3 Outline of the Thesis

Chapter 1 introduces the relation between the technical issue of liver segmentation and hepatic interventions. The ojectives of the thesis are described followed by an overview of the thesis structure.

Chapter 2 presents an in-depth review of liver segmentation methods and their application to different types of radiological data (Section 2.1). The review also highlights the problems and gaps which further support the objectives and purpose of this work. The background of liver anatomy and the different types of hepatic interventions are presented in Section 2.2. It is complemented by an overview of computer-assistance for hepatic applications and the methods and tools developed at MeVis, other research institutions, and commercial companies.

Chapter 3 presents the achievements of this thesis. Section 3.1 summarizes the methodical developments for the liver segmentation approach developed in the years 1999 and 2000 based on live wire, shape-based interpolation and correction algorithms. The basic concept is described and several improvements are presented. This section concludes with an evaluation of the approach on first clinical data sets and more than 2000 CT data sets.
Section 3.2 presents the first comprehensive software assistant for liver surgery and the first integration of planning information into liver laparoscopy. The numerical modeling of radiofrequency ablation and the evaluation of lesions is introduced, followed by an overview of recent software developments for liver surgery.
Section 3.3 provides the application of liver segmentation and computer-assisted planning to the field of ALDLT. Decision algorithms, anatomical observations, and derived concepts developed on basis of the 3D evaluations are presented. Studies in humans and animals and new software for the evaluation of outflow obstruction and local regeneration are provided, including the investigation of collateral formation in animals. The section concludes with the first approach in computer-assisted surgical planning based on MRI data, a comparison of results from CT and MRI data in live liver donors, and perspectives on MRI-based intervention planning.

Chapter 4 provides a summary of the thesis and recommendations for future research.

Chapter 5, 6, and 7 include the publications of this thesis. Chapter 5 is related to the developments and evaluation of the liver segmentation approach based on live wire and interpolation (Section 3.1), Chapter 6 includes the papers presented in Section 3.2, and Chapter 7 provides publications about ALDLT in the areas of risk analysis, liver regeneration, and planning on MRI data, related to Section 3.3.

2 Preliminary and Related Work

Time is a great teacher, but unfortunately it kills all its pupils.
Hector Berlioz

2.1 Liver Segmentation

Many methods for liver segmentation have been published, and we will introduce different approaches in the following sections. In most cases, the segmentation algorithms are applied to contrast-enhanced CT data. Few approaches have been developed for the image analysis of livers in MRI data. Independent of the image modality used, manifold error sources and challenges for liver segmentation exist, because several other organs and structures with similar density or gray values are near the liver. For example, the heart and diaphragm are in direct contact with the liver, but the spleen and the pancreas also exhibit the same gray level in CT data as the liver. Furthermore, the liver shape varies greatly, and the organ tissue itself often appears inhomogenous in the images. This can be due to a liver disease such as cirrhosis (liver tissue scarring) or can be related to the imaging technique, e.g., inhomogeneities in MR images. Other factors hampering the value-based segmentation process include intrahepatic structures and pathologies with varying intensity values. Typical examples are contrast-enhanced vessels, hypointense and enlarged bile ducts, and in oncologic patients, malignant lesions with different appearances and locations. Challenges for liver segmentation are shown in Figure 3.

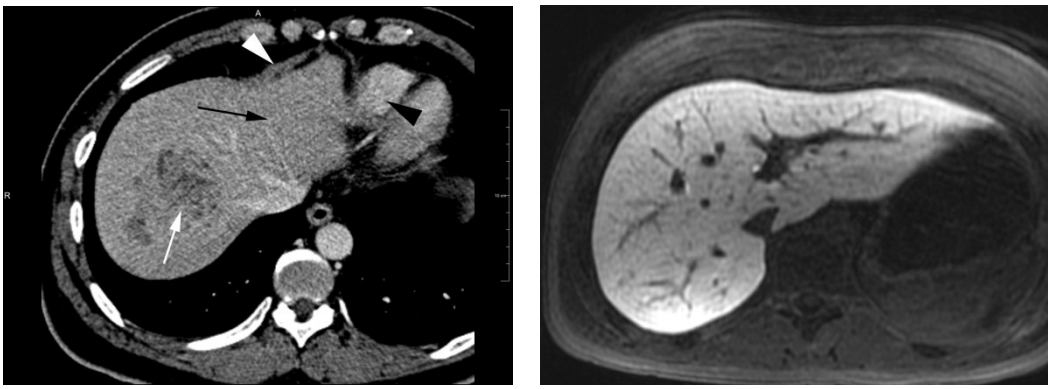

Figure 3: Challenges for liver segmentations methods. Left: CT image of the liver (black arrow), with tumor (white arrow), and neighboring structures: heart (black arrowhead) and diaphragm (white arrowhead); Right: MR image showing lower resolution and typical inhomogeneities that lead to varying gray values in the liver.

The gold standard of liver segmentation is a liver contour manually drawn by a radiological expert on the two-dimensional image slice. High quality is achieved at the expense of tedious work. Because time in clinical routine is limited, this elaborative work is only applied in selected cases or is reduced to a fast and rough approximation of the liver volume typically performed by drawing contours on

very thick or distant (10-20mm) image slices. To reduce the amount of manual drawing, computer-assisted methods for semi- and fully-automatic liver segmentation have been developed. A survey of different algorithms presented until 2006 can be found in the paper of Campadelli et al. [Campadelli et al., 2009].

2.1.1 Region-based Segmentation

Initial approaches for computer-assisted liver segmentation were based on gray-value analysis [Bae et al., 1993, Gao et al., 1996]. These algorithms use explicit thresholds or estimate the liver gray values by statistical analysis of manually segmented images or by histogram analysis. The determined upper and lower thresholds are used to generate a binary mask that is typically postprocessed by morphological operations to separate the organ from other structures. Several thresholding methods for the liver have been presented in recent years [Platero et al., 2008, Seo and Park, 2005, Soler et al., 2001].

To overcome the typical problem of over-segmentation with global thresholding, algorithms based on region-growing have been developed. Approaches for the liver are based either on the images of a single acquisition [Pohle and Toennies, 2001, Ruskó et al., 2007] or on multi-phase images that consider the changing gray values at different time points in the contrast-enhanced liver [Ruskó et al., 2009].

Other approaches try to estimate not only the gray levels but also other image features of the liver, neighbored organs, and the background from existing segmentations in CT images. The learning procedure is implemented with methods based on neural networks and subsequently applied to a new data set for automatic detection and labeling of the liver area [Koss et al., 1999, Lee et al., 2003]. The methods strongly depend on the training data sets and the given variability of organ anomalies and selected image features.

All region-based approaches applied for liver segmentation struggle to separate the organ from adjacent organs and to include intrahepatic structures as lesions or vessels appearing darker or brighter than the tissue. Furthermore, depending on the time after contrast application and the patient's cardiovascular state, the liver gray values of the parenchyma itself show a high variability. Texture features can vary between healthy and diseased livers in CT data, whereas in MR images, in-plane inhomogeneities and intensity variations over the 3D volume are common. In conclusion, liver segmentation cannot be solved alone by a simple global region-based approach and, these algorithms are therefore typically combined with other methods.

2.1.2 Contour-based Segmentation

Two basic approaches are used to determine the liver contours in radiological images: the user-steered interactive live wire algorithm and energy-minimizing contour algorithms as snakes and level sets.

In the live wire approach, invented in 1992, the image is described as an undirected, weighted graph where vertices of the graph represent image pixels while edges connect neighboring pixels [Mortensen et al., 1992, Udupa et al., 1992]. The weights are computed as costs for the connection from one pixel to its neighbor and are based on image features. After calculating the cost graph, the user starts to segment by setting a first seed point on the boundary and moving the pointer of the mouse or another input device along the outline of the liver. Optimal paths, minimizing the accumulated costs from the seed to the current mouse position, are computed using Dijkstra's algorithm [Dijkstra, 1959, West, 1996]. Computation and display of the resulting live wire boundary segment is achieved in real-time, even for larger images. The live wire path snaps to the boundary while the user moves the mouse over the image, and a new seed point has to be set before the path starts to deviate from the desired contour. New shortest paths are computed from the new seed point, and the procedure is repeated. A final closure leads to a controlled, piecewise optimal segmentation result. Modifications of the basic approach including quality studies have been published, proving the high accuracy, efficiency, and reproducibility of the algorithm [Barrett and Mortensen, 1996, Barrett and Mortensen, 1997, Falcao et al., 1998, Falcao et al., 1999]. Details of the implementation, improvements and extension to 3D segmentation and application to liver segmentation are given in Chapter 3.

The second group of contour-based approaches is based on energy minimization with different mathematical background: active contours [Caselles, 1997, Montagnat and HerveDelingette, 1997, Kass et al., 1988] and level sets [Malladi and Sethian, 1997, Osher and Sethian, 1988]. Acrive contours, also known as snakes or deformable models, were placed in the image (2D) or volume (3D) and deformed iteratively by minimizing an energy functional summarizing so-called internal and external forces. Typically, the internal energy defines the physical property of the desired boundary (e.g., smoothness and flexibility) and the external forces drive the contour towards image characteristics as high gradients. Snakes have been applied to the liver, for example, by Xu and Liu [Xu and Prince, 1997, Xu and Prince, 1998, Liu et al., 2005] and recently by Lee, Chi, and Lassen [Chi et al., 2007, Lassen, 2009, Lee et al., 2007].

With level sets, an implicitly defined contour or surface is propagated towards the object boundary. The corresponding level set of dimension n is typically defined as the zero crossing of a function of dimension $n+1$. The deformation of the level set is steered by a speed function that often includes constraints of a priori knowledge about image features or the shape of the structure to be segmented.

The challenge in using this algorithm lies in the definition of an appropriate speed function and its parameters. Level sets were first used for liver segmentation by Pan & Dawant [Pan and Dawant, 2001]. The high computational demand of this algorithm limited its application in early years, but the method is now widely used, both directly for liver segmentation but also often as a final optimization step in combined approaches [Hermoye et al., 2005, Lassen, 2009, Oliveira et al., 2011, Shimizu et al., 2005].

2.1.3 Model-Based Segmentation

Model-based segmentation requires a set of training data sets with existing object segmentations for creating the model. During this process, the different shapes, gray-value information at the object surface, or the probability of each voxel belonging to the object can be taken into account. As a typical prerequisite, a sufficient number of corresponding landmarks in the images or masks have to be defined to align all training data sets.

In case of shape models, the liver surfaces of the training data are typically aligned based on a set of landmarks defined by the user. Subsequently, a principal component analysis is applied to compute the main shape variations of the organ. During the segmentation step, the average liver model is placed inside the new data set interactively by the user or in an automated fashion, and the landmark positions were optimized within the main shape variation. Additionally, gray value profiles learned from the training data at the landmarks or at surface normals can be applied (appearance models). Shape and appearance models have been applied for liver segmentation by several authors [Lamecker et al., 2004, Liu and Udupa, 2009].

Another approach for model-based segmentation creates a probabilistic model or probabilistic atlas of training images and related segmentation labels. Based on a few landmarks (manually or automatically determined), the different data sets are registered into a standard space. The probabilistic atlas is then generated by spatially averaging the registered objects and computing the probability of each voxel belonging to a certain label (e.g., organ). In the segmentation step, the new image is matched to the atlas space by registering landmarks, and the intended segmentation mask is defined by thresholding the existing probabilities of the corresponding object label. Probabilistic atlases have been employed for liver segmentation by different authors [Lassen, 2009, Park, 2003, Shimizu et al., 2006, Zhou et al., 2006].

One challenge of model-based methods is the initial construction of the model, which requires a large number of correctly segmented training images to capture all possible shapes and the correct distribution of probabilities. Because the typical liver shape is highly variable, even fundamentally different for Asian and Caucasian livers, more than one model with a sufficient number and distribution of

training data had to be constructed. Even when the model includes the variability of healthy livers, it may fail with diseased organs, since anomalies and pathologies are not represented in the model. Nevertheless, a model-based segmentation technique can supervise other approaches in cases or liver regions where no boundary information can be derived from the images.

2.1.4 Combined Segmentation

Neighboring organs and structures inside the liver may pose problems for automatic methods focusing on gray values, whereas the wide variability of the liver form prevents the general success of model-based approaches. Therefore, the most promising and successful automatic liver segmentation methods are combinations of both segmentation paradigms.

In 2007, a liver segmentation competition was performed as part of the *3D Segmentation in the Clinic: A Grand Challenge* workshop in conjunction with MICCAI 2007. Several algorithms were presented and evaluated on ten clinical CT data sets by developers attending the workshop [Heimann et al., 2009, van Ginneken et al., 2007]. The segmentation approaches were also executed on another set of ten cases prior to the workshop, and submitted results were evaluated by the organizers and presented on the workshop. Further segmentation results of improved or new algorithms could be submitted later via internet for additional rating. The evaluation included a combination of different metrics and the results are available on the workshop's homepage [MICCAI, 2007].
From the ten automatic and six interactive methods at the workshop, interactive approaches achieved some of the best results [Beck and Aurich, 2007, Dawant et al., 2007, Lee et al., 2007], while the most successful automatic approach was based on combination of shape models and intensity-based algorithms [Kainmueller et al., 2007]. However, the ground truth segmentations in the workshop were defined such that they included the entire liver tissue and parts of external vessels, such as the vena cava, when they were surrounded by liver parenchyma. This definition is beneficial for model-based approaches but does not match the clinical requirements. In contrast, the goal of our work is to segment the liver tissue accurately while excluding larger vascular structures.

The combination of approaches presented above was the composition of different segmentation algorithms. A second combination approach is to segment the liver in combination with organs and other structures. The goal of this so-called multi-organ segmentation is to identify the liver tissue by excluding the belonging to surrounding objects. There are several approaches that typically use a number of basic segmentation methods to classify image voxels. Examples of this type of multi-organ algorithms were presented in [Shimizu et al., 2006, Shimizu et al., 2007, Soler et al., 2001]. Soler extracted skin, bones, lungs, kidneys, and spleen by combining thresholding, morphological operations, and distance maps. Shimizu used thresholding and a statistical atlas for initial individual organ segmenta-

tions, followed by the expectation maximization algorithm for separation of these, and a level set method to define the final liver contour.

2.1.5 Segmentation Errors and Correction Methods

When analyzing the results of liver segmentations, the issue of the acceptable error arises. In one of the first liver segmentation publications in 1996, more than 20% of the slices had to be corrected due to insufficient results [Gao et al., 1996]. In the continuously updated list of the MICCAI contest, the results of the three best automatic methods show mean volume overlap errors of the ten test data sets between 6.0%-8.5% [MICCAI, 2007]. In the live contest of the MICCAI, where the teams had to perform the segmentation of ten data sets in three hours, the results were less convincing. The best three automatic approaches showed volume overlap errors of 8.4%, 12.4%, and 14.6%, while the best interactive approaches gave better results with error rates of 7.1%, 7.1%, and 8.1 %. The standard deviation of the three best methods was 2.8%, 4.3%, and 4.7% for the automatic and 2.1%, 2.4%, and 2.7% for the interactive segmentations, the latter showing a better consistency related to the direct user control.

User interaction and user control of all results on a large number of image slices clearly require more time than an automatic approach. If errors have to be corrected thereafter, however, a correction tool has to be applied, requiring additional user effort and sometimes even more time than the interactive algorithm for full segmentation. An early overview of interactive segmentation approaches, a discussion of the basic strategies and their evaluation is given in [Olabarriaga and Smeulders, 2001].

Only a few groups worldwide have focused on dedicated correction methods for segmentation in medical data. In most cases, some kind of manual correction on 2D images is applied, e.g., cutting or adding parts of the segmentation mask by drawing an intersection line or curve at the boundary ([Gao et al., 1996] and Chapter 3.3). The same type of manual correction is applied in 3D, in most cases on the basis of deformable 3D meshes [Bornik et al., 2006, Kang et al., 2004, Schwarz et al., 2008, Silva et al., 2010]. A typical example of correcting the segmentation result is presented by Silva et al., who modify the mask by removing and adding voxels in 3D by a spherical brush with a user-defined radius [Silva et al., 2010]. However, 3D correction tools are not intuitive, and these surface-based correction methods can result in strange modifications, as shown in the same paper.

Few authors have presented papers for dedicated correction of a liver segmentation mask. A contour-based manual correction algorithm has been developed by Heckel based on user-defined correct boundary paths in one image slice, live-wire extrapolation on neighbored slices, and morphological postprocessing [Heckel et al., 2009]. However, in the area where automatic approaches often fail and cor-

rections are necessary, the boundary information is low and challenging for image- based approaches, especially when applied to low-contrast or noisy images.

In summary, even the best automatic methods from worldwide groups were not able to segment the liver with high quality. Consequently, such automatic tools require a correction step to achieve the correct liver shape. Correction takes time, especially when it has to be performed on all image slices. Therefore, directly using an interactive user-controlled approach from the first segmentation step is a consequent conclusion. It also reduces user frustration when automatic results differ significantly from the expectations and cannot be corrected easily.

2.2 Application to Liver Interventions

Formerly, when religion was strong and science weak, men mistook magic for medicine, now, when science is strong and religion weak, men mistake medicine for magic.
Thomas Szasz, The Second Sin, 1973

The result of a liver segmentation is technically, a binary mask identifying the organ voxels in the image data[1]. This sounds simple, but the application of this information is manifold. From the binary mask itself, the liver volume can be computed; a further subdivision of the mask allows estimating the remnant liver volume, the graft volume in transplantation, or segmental volumes. The image voxel of the radiological data inside the mask can be classified and used for further interpretation, e.g., to support diagnosis, identification of vessels and detection and volumetry of lesions. Finally, the transformation of the binary mask into a three-dimensional liver model extends the slice-based radiological view to surgical reality and allows for resection planning and risk analysis.

The anatomy of the liver is important for clinical applications. This encompasses the different vascular systems supplying and draining the organ, and in the case of cancer treatment, their relation to tumors. The first section summarizes the vascular anatomy as well as surgical subdivisions of the liver. Different liver interventions including living donor liver transplantation, resection of hepatic tumors, and tumor ablations will be discussed in the following sections. A final section about state-of-the-art computer-assistance for hepatic interventions concludes the chapter.

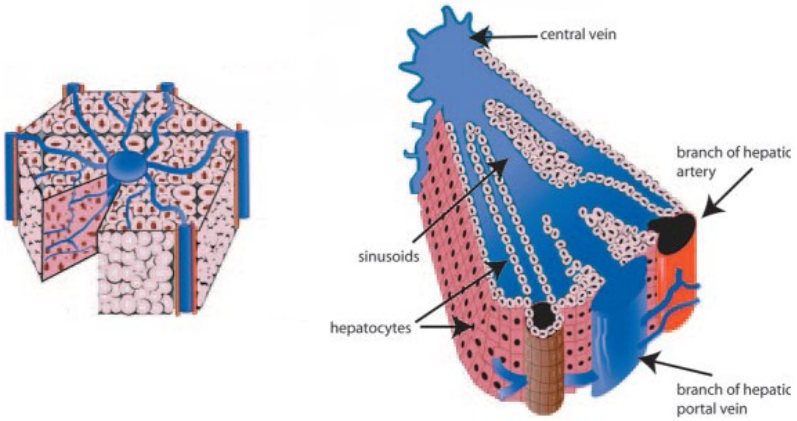

Figure 4: Anatomy of liver and vascular systems on microscopic scale, lobule (left) and portal triad (right). Portal vein (blue), bile ducts (brown), and hepatic arteries (red) run in parallel and build the portal triad. From the central veins the blood drains into the vena cava. Reprinted from [Aitsebaomo et al., 2008] with permission.

[1]For some approaches, the segmentation result may also be a mesh, a stack of contours, or another structure that can be converted into a binary mask.

2.2.1 Liver Anatomy and Anatomical Resections

The liver is located in the upper right quadrant of the abdominal cavity and is the largest gland in the body. The organ has a wide range of functions and consists of microscopic functional units called lobules (Figure 4). The classical anatomy divides the liver into the right and left liver lobe with the ligamentum falsiforme as surface landmark between the lobes. Functionally, the liver is divided according to the vascular supply and drainage into right and left hemiliver and further into segments or territories. These subdivisions build the basis for the anatomical resections introduced in the following section.

The Vascular Systems and the Liver Shape

The vascular anatomy of the liver is complex with four vascular systems supplying or draining the liver: hepatic veins (HV), portal vein (PV), hepatic arteries (HA), and bile ducts (BD) (Figure 11). The latter three vascular systems, the portal triad, run almost parallel on the microscopic level (Figure 4), but great inter-individual variability is present in the liver hilum, where these vessels enter into the organ [Imamura et al., 2000, Netter, 2006].

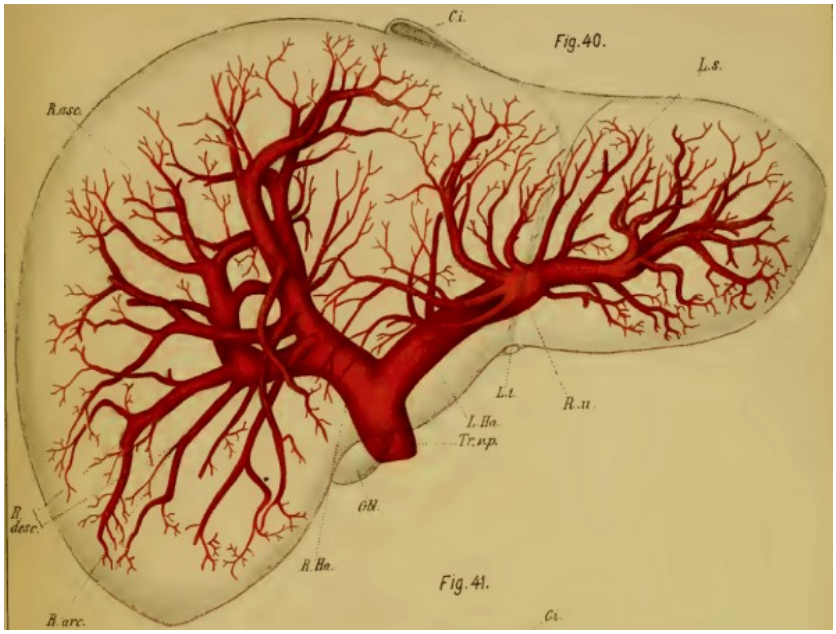

Figure 5: Historical illustration of the portal vein [Rex, 1888]. The portal vein trunc (Tr.v.p.) typically bifurcates into left and right portal vein branch, with a further division of the right branch into anterior and posterior branch (left part of the image). The left portal vein includes an umbilical part (the Recessus umbilicalis, R.u.) that was part of the prenatal umbilical vein. Other parts of the former umbilical vein build the ligamentum terres hepatis (L.t.), lying in a cleft of the liver surface that separates the left from the right liver lobe.

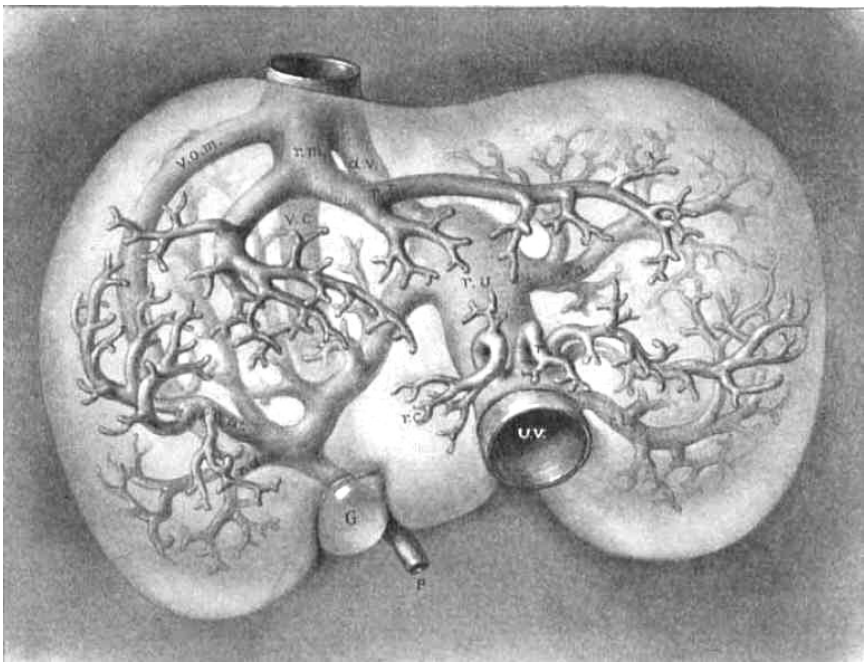

Figure 6: Drawing of the liver and vascular systems in an embryo [Mall, 1906]. The liver is supplied by the large umbilical vein (u.v., center) and by the portal vein (P). The umbilical vein is closed at the time of birth and a part of will remain as the umbilical part of the left portal vein (Recessus umbilicalis, r.u.).

The portal vein carries blood from the small intestine, stomach, and parts of the colon to the liver, accounting for about 70% of the overall blood flow to the organ. The remaining blood enters via the hepatic artery, supplying the liver with oxygen-rich blood. Blood from both vessel systems merges in the small sinusoids, the liver capillaries. From the sinusoids, the blood is recollected by small central veins, joining in the hepatic veins and draining finally into the inferior vena cava (Figure 4 and Figure 7).

During prenatal development of the organ, the blood reaches the liver through two major veins: the umbilical vein connected to the umbilical cord and the portal vein coming from the gastrointestinal tract and the spleen (Figure 6). The closure of the umbilical vein at time of birth causes a reverse flow in that vessel and subsequent remodeling of the portal vein system that also influences the liver shape. Parts of the umbilical vein build the ligamentum teres hepatis, a fibrous cord at the lower margin of the ligamentum falsiforme, which divides the liver into right and left lobe (Figure 5 and Figure 11).

The liver shows a high variability in both shape and size. Differences in the organ shape are common between ethnical groups, and the overall volume of the liver can change during live time. When a person grows or changes weight, the liver adapts to the required metabolic demand (cf. Section 1.1, Figure 1).

The Couinaud Scheme

It is difficult to mentally construct the internal 3D structure of the liver based on cross-sectional slices of radiological data, or to estimate which part of the four vessel systems would be damaged as a consequence of a surgical intervention. To enable surgeons to perform liver resections while respecting the vascular anatomy, a schematic 3D model of the liver is employed that was introduced by Couinaud in 1957, long before CT technology was developed [Couinaud, 1957]. At that time, preoperative evaluation of the individual vascular liver anatomy was not possible.

Couinaud subdivided the liver into eight functionally independent segments, each with its own vascular inflow, outflow and biliary drainage. The hepatic veins are located in the periphery of each segment (Figure 7). Related schemes were developed by Bismuth, Healey and Schroy, Hjortsjo, and others. An overview is given in [Fasel et al., 2010].

Dirrectly applying the widespread Couinaud scheme is questionable, because the liver segments do not correspond well to the individual territories (cf. Figure 8) and do not reflect common anatomical variants, such as trifurcations of the portal veins or inferior hepatic right veins draining directly into the inferior cava vein [Fasel et al., 1998]. In the following, we will use the term *segments* for the Couinaud-related liver regions and *territories* for the individual areas of portal venous supply computed from the patient's portal vein branches.

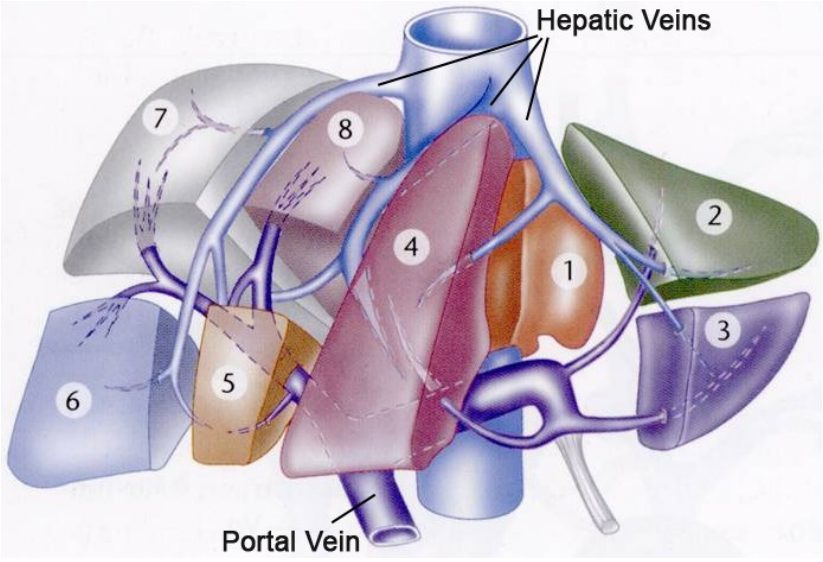

Figure 7: Couinaud Scheme: the liver is divided into eight segments determined according to the main branches of the portal vein and the hepatic veins. A liver segment is supposed to be defined by the supplied territory of a third-order branch of the portal vein with intermediate hepatic veins. The umbilical part of the portal vein is located between the left lateral segments 2 and 3 and the right liver lobe (segments 1,4-8). Reprint from [Castaing et al., 2006] with permission.

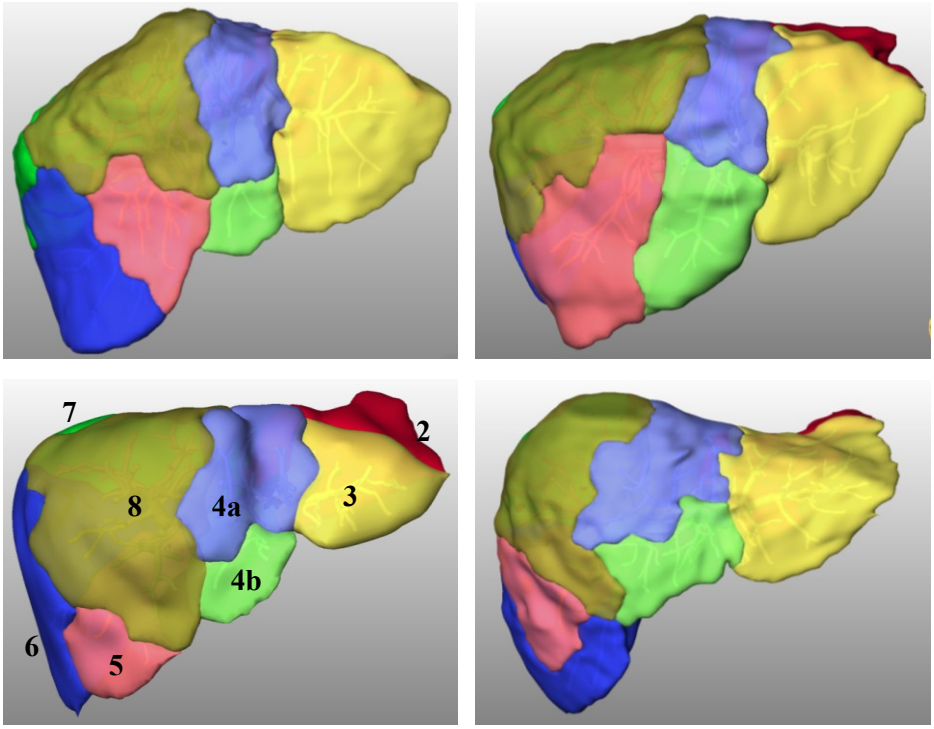

Figure 8: Variation in portal territories: Four different livers with the individual supplying areas of portal vein branches showing large deviations in shape and size. Corresponding portal vein territories are coded with identical colors: territory 2 (red), 3 (yellow), 4a (light blue), 4b (light green), 5 (light red), 6 (dark blue), 7 (green), 8 (dark yellow). Territory 1 is centrally located behind the other territories.

Anatomical Resections

Why is the knowledge of vascular anatomy and the individual liver territories so important for hepatic surgery? In 1954, John E. Healey summarized the previous unawareness of the vascular course with its consequences for liver resections to the point:

> '*Although radical operations upon the liver were performed as early as 1886, little advancement has been made in the surgical technic of such resections. This is due mainly to the fact that surgeons (and anatomists) have been total unaware of the intrahepatic course and distribution of the larger vascular and biliary channels and that, therefore, incisions through the hepatic parenchyma have been performed somewhat blindly. It is not surprising, therefore, that the present day mortality rate for partial hepatectomies is little changed from the mortality rate for similar procedures in 1897.*' [Healey, 1954].

The findings of Couinaud and the improvements in surgery by Healey and Hjortsjo heavily impacted surgical technique and surgery-related mortality and morbidity [Healey et al., 1953, Hjortsjo, 1951]. The mortality rate during or shortly after surgery, which reached 50% for right hemihepatectomies in the 1960s decreased significantly [Clavien and Breitenstein, 2010]. Nowadays, treatment-related mortality rates are below 1% in resections for primary liver tumors [Forner et al., 2012].

Standard resections now take into account Couinaud's liver subdivision and the related terminology of hepatic resections was defined by the International Hepatobiliary Pancreatic Association in 2000 [IHPBA, 2000]. This so-called *Brisbane 2000 Terminology* divides the organ following the prevailing anatomy of the portal vein and related Couinaud liver segments (see Figure 9). Nevertheless, these resections do not consider the patient's individual anatomy, which can only be determined by computer-assisted analysis.

2.2.2 Tumor Surgery

Malignant Liver Tumors

Liver tumors can be grouped into primary liver cancer, in which the disease begins in the cells of the liver, and secondary liver cancer or liver metastases which are malignant tumors that have spread to the liver from a primary cancer located somewhere else in the body. The distribution of primary and secondary liver tumors is different in Asian and Western countries. Metastases constitute the majority of malignant liver lesions in the West, whereas primary tumors are the most common liver cancer type in Asia. Hepatocellular cancer (HCC), the prevalent form of primary liver cancer, is the seventh most common form of cancer worldwide and the third most frequent cause of cancer-related death (about 500,000 people worldwide die each year from primary liver cancer). About 80% of HCCs originate from a chronic infection with hepatitis that may lead to cirrhosis and liver cancer. HCC is highly prevalent in Asia and southern Africa, but an increasing trend of the HCC incidence in Western countries has been observed in recent years [Salhab and Canelo, 2011]. With early diagnosis and modern therapies a 5-year survival rate above 50% can now be achieved [Forner et al., 2012].

The secondary malignant liver tumors are metastases of another cancer (like the colon, breast, or lung) that spread to the liver. From these, colorectal cancer is the third most common malignancy in the West and the second most common in Japan [Shimada et al., 2009]. The standard curative treatment is liver resection or local ablative therapies such as radio frequency or microwave ablation (see Section 2.2.4). The 5-year survival rate following liver resection ranges between 25% and 58% compared with 0% to 5% for patients who cannot or will not undergo surgery [Shimada et al., 2009].

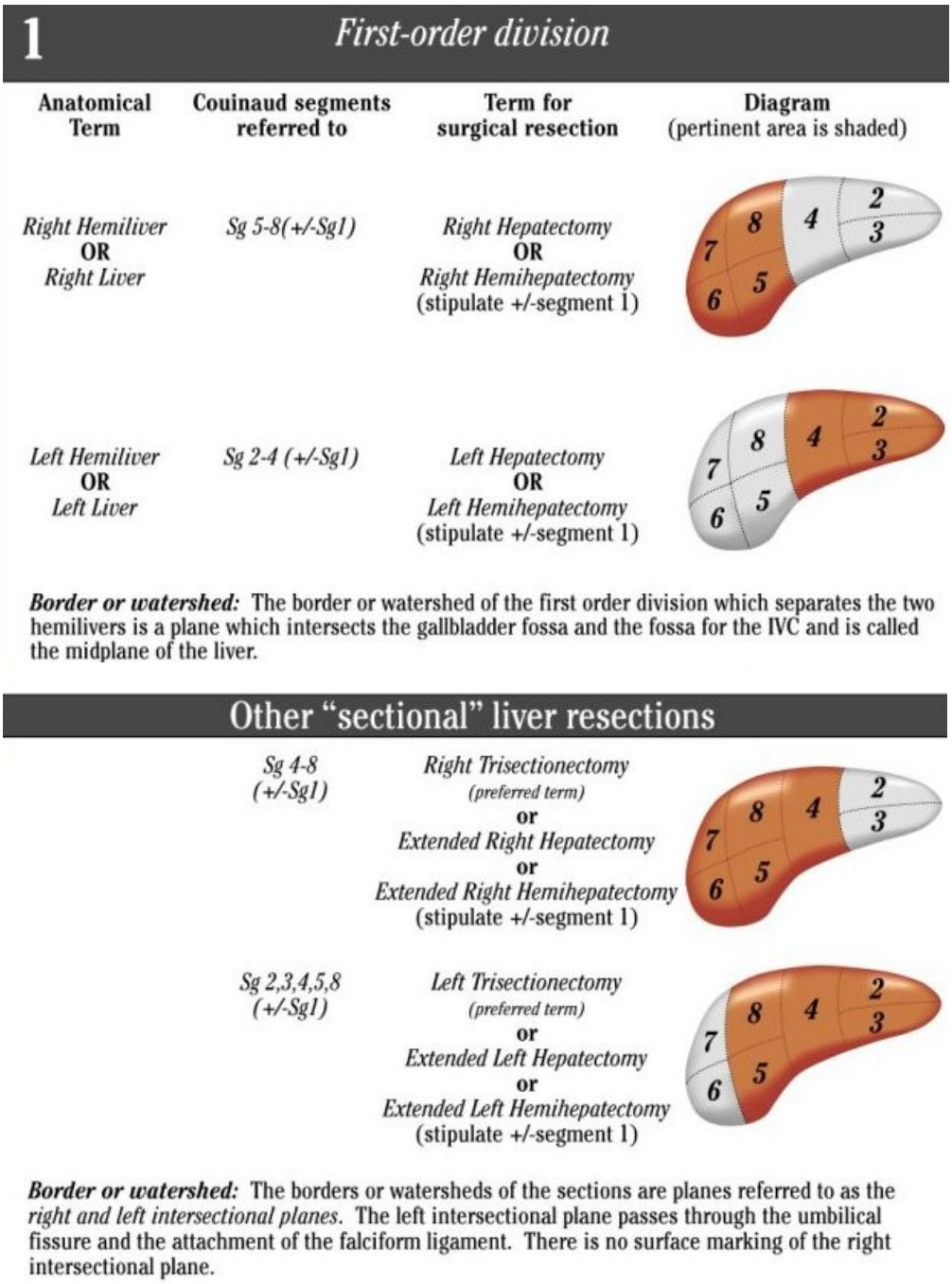

Figure 9: Examples of the Brisbane Terminology of Liver Resections for different orders of liver subdivision. These standard resections are based on a schematic anatomical subdivision of the liver following the Couinaud segments [IHPBA, 2000].

Tumor Resections

Surgery has been established as the gold standard in tumor therapy, and in recent years, additional localized therapies have been clinically adapted for liver cancer cases for which surgery is not possible. During liver surgery, the part of the liver containing the tumor is removed. This can be performed during open surgery or by laparoscopic intervention. For laparoscopic surgery, specialized instruments and a dedicated camera (laparoscope) are passed into the abdomen through small incisions (cuts). Laparoscopic surgery is also called 'key-hole surgery' or 'minimally invasive surgery'.

There are several risks during surgical resection of tumors, with the most severe risk being liver failure. Two major risk factors include insufficient volume of the remnant liver after surgery as well as deficient health of the remaining liver tissue. The latter can result from pre-existing liver diseases such as steatosis (fatty liver degeneration), cholestasis (bile duct occlusion), fibrosis/cirrhosis, or reduced blood flow hampered by the resection.

In the following, we will use different terms of 'liver volume'. The overall amount of liver mass including tumors will be called *anatomical volume* or *liver volume*. The amount of liver parenchyma without tumors will be called *tumor-free volume.* The liver volume without tumors and without perfusion deficits (e.g., outflow obstruction after resection) will be called functional volume.

In case of metastases in an otherwise healthy organ, a functional remnant liver volume of 25%-30% of the tumor-free volume before surgery is sufficient. This remnant volume has to be higher for diseased organs where the liver tissue is malfunctioning, and the exact amount of minimum volume necessary is difficult to predict in these cases.

To minimize tumor recurrence (i.e. cancer regrowth after surgery), a margin of healthy tissue surrounding the tumor, the *safety margin*, has to be removed with the cancer. The macroscopically and histologically complete tumor removal (so-called *R0 resection*) is the most important factor for long-term survival [Altendorf-Hofmann and Scheele, 2003]. For example, if macroscopically visible tumor portions remain in the liver (*R2 resection*), or if cancer cells are found in the margin of the resected liver part microscopically (*R1 resection*), the risk of a recurrent tumor increases significantly. Therefore, the resection should be performed by transecting tissue with a certain distance from the tumor, e.g., 10mm for metastases. But resecting a tumor in this way is a challenging procedure because the tumor is not visible from outside, and the real distance from the current resection to the tumor may be unknown during the intervention. Furthermore, when removing the tumor with a safety margin, all vessels in this area will be truncated, leading to unperfused or undrained liver regions with additional functional impairment and risks for the patient.

The two competing goals of obtaining a broad safety margin around the tumor while saving sufficient functional liver volume in the challenging presence of the vessels complex anatomy motivated the development of patient-specific, computer-assisted planning tools (see Section 2.2.5 and Section 3.2).

2.2.3 Living Donor Liver Transplantation

History

Compared to tumor resections, the surgical domain of liver transplantation is an emerging discipline. The first attempt of a liver transplantation in men was performed 1963 by Thomas Starzl [Starzl et al., 1963]. However, the patient died during the operation. Five years later, Starzl reported the first successful series of seven liver transplantations [Starzl et al., 1968a, Starzl et al., 1968b]. Significant improvements in long-term survival could be achieved after introduction of new immunosuppressants and optimized preservation techniques [Calne et al., 1979, Calne et al., 1981, Iwatsuki et al., 1988]. When the US *National Institutes of Health Consensus Conference* considered liver transplantation as an accepted therapy in end-stage liver disease in 1983, the patient waiting list for liver organs increased rapidly [Clavien and Breitenstein, 2010]. The related shortage of available donor organs, and especially that of pediatric livers, stimulated the development of new techniques such as reduced-size liver and split-liver transplantations [Pichlmayr et al., 1988, Broelsch et al., 1988, Starzl and Demetris, 1990]. In split-liver transplantations, the cadaveric liver is divided for transplantation of both parts into different recipients. Pichlmayer invented this type of transplantation in 1988 while working at the Medical School in Hannover [Pichlmayr et al., 1988].

With the first split of a living donor organ and transplantation of a left lateral lobe into a 4½-year-old child in 1988, Raia started the era of living donor liver transplantation [Raia et al., 1989]. This first LDLT was followed by a left lobe graft donation from a Japanese mother to her son in Brisbane [Strong et al., 1990]. In the following years, the technique was refined by a number of surgeons worldwide, e.g. [Mori et al., 1992]. Broelsch reported the first series of patients from Chicago in 1991, and performed the first LDLT in Europe [Broelsch et al., 1991].

LDLT Worldwide

In Asia, LDLT was adopted rapidly because cadaveric liver donation did almost not exist. In June 1990, surgeons at the Kyoto University performed the first successful LDLT in Japan [Ozawa et al., 1992], followed by transplantations in Hong Kong in 1993 [Yeung et al., 1994] and Korea and Taiwan in 1994 [Lee et al., 1996, Chen et al., 1996]. The first live liver graft for an adult recipient was transplanted by the Makuuchi group in Japan in 1993 [Hashikura et al., 1994].

By 2002, the five major Asian liver transplant centers[1] had performed 1508 LDLTs including 766 ALDLTs [Lo, 2003]. Of these centers, the team of Prof. Koichi Tanaka and colleagues from the Kyoto University had the most experience [Chen et al., 2003], cf. Figure 10.

The 1508 LDLTs in the five major centers in Asia compare to 1652 cases in all American transplant centers [OPTN, 2012] and to 488 LDLTs in the Eurotransplant region [Eurotransplant, 2012] in the same period. Since 2002, the numbers of adult LDLT have declined rapidly in the USA and Europe due to the increased public awareness of the possibility of donor death. As of 2009, the highest LDLT numbers in Europe were performed in Germany (60), Spain (29), United Kingdom (25), and Belgium (23) [NewsletterTransplant, 2010]. In Asia, however, where cadaveric grafts are very rare, the demand for LDLT has continued and the numbers are still increasing. An overview of LDLT data with the five biggest centers in Asia and North America and their numbers are listed in Table I. LDLT numbers for different regions and countries of the year 2009 and accumulated for the years until 2009 are given in Table II.

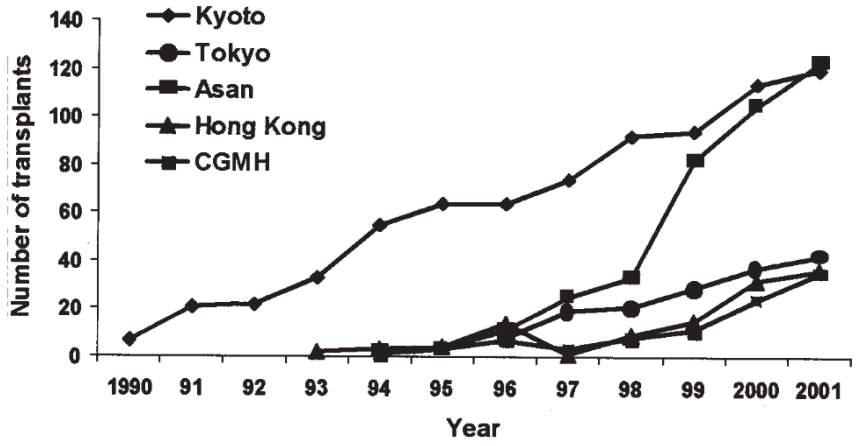

Figure 10: Annual numbers of LDLTs performed in the first twelve years in the major five Asian centers [Chen et al., 2003]. Asan: Asan Medical Center, Seoul; CGMH: Chang Gung Memorial Hospital, Kaohsiung.

[1]Kyoto University Hospital, Kyoto; Asan Medical Center, Seoul; University of Tokyo, Tokyo; University of Hong Kong Medical Center, Hong Kong; and Chang Gung Memorial Hospital, Kaohsiung

TABLE I
LDLT NUMBERS FOR SELECTED TRANSPLANTATION CENTERS IN ASIA AND NORTH AMERICA

Transplantation Center	LDLTs in 2009	Accumulated LDLTs 2005 - 2009
Asan Medical Center, Seoul	290	~1300
Chang Gung Memorial Hospital, Kaohsiung	107	~370
Kyoto University Hospital	70	~400
University of Hong Kong Medical Center	39	~240
University of Tokyo	~24	~130
Lahey Clinic, Burlington	24	125
University of Pittsburgh	13	108
New York Presbyterian	17	61
University of California, San Francisco Medical Center	9	57
New York Mount Sinai	3	47

Sources: Organ Procurement and Transplantation Network [OPTN, 2012] and LDLT Congress, Hong Kong 2010 [ALDLT, 2010].

TABLE II
LDLT NUMBERS FOR DIFFERENT REGIONS

Region	LDLTs in 2009	Accumulated LDLTs until 2009	Time Period
Japan	~470	5659	1990-2009
Korea	718	4878	1994-2009
USA	219	4004	1989-2009
Eurotransplant Countries	98	1374	1991-2009
Taiwan	Unknown	~1200	1994-2009
India	~320	~1060	1994-2009

Sources: Organ Procurement and Transplantation Network [OPTN, 2012], LDLT Congress, Hong Kong 2010 [ALDLT, 2010], and Eurotransplant (Austria, Belgium, Croatia, Germany, Luxembourg, the Netherlands and Slovenia) [Eurotransplant, 2012]

Surgical Technique

In LDLT, the liver of a voluntary healthy donor is divided into the graft for the recipient and the donor's remnant liver. The donation of the left lateral lobe to a pediatric recipient is now an established transplantation procedure and typically requires no computer-assisted planning due to noncritical functional remnant liver volume. In contrast, ALDLT is highly challenging because the donor liver must be divided in the middle of the right liver lobe near the middle hepatic vein (Figure 11). The remaining functional volumes of the two liver parts have to be sufficient for the healthy donor as well as for the diseased recipient. This is difficult to achieve, especially in cases in which the recipient's weight and related hepatic demand is much higher than that of the donor (e.g., a small woman wants to donate to her tall husband). It is now generally accepted that the minimal remnant liver volume for a safe donor operation should be 35% of the original liver volume [Hwang et al., 2006, Asakuma et al., 2007, Taner et al., 2008] or at least 30% when there is no risk of venous congestion (e.g., when the MHV is retained with the remnant liver) [Fan et al., 2011]. The recipient demand is higher due to the pre-existing disease and health condition, and the original liver volume cannot be used to estimate the functional demand due to volumetric alterations of the diseased organ. As a compromise, formulas based on the estimated standard liver volume (ESLV, cf. Section 1.1) are used to compute the required minimal demand of the recipient. Typically, 40% of the ESLV volume or 1.0% of the recipient's body weight is generally believed to suffice for survival [Asakuma et al., 2007, Fan et al., 2011].

The Dilemma of the Middle Hepatic Vein

The major surgical challenge in ALDLT is the resection of the donor liver near the middle hepatic vein. Since the introduction of ALDLT, it has been discussed whether the MHV should be included in the liver graft or retained in the healthy, voluntary donor. Independent of right- or left-lobe donation, tributaries of the middle hepatic vein will be truncated in one of the hemilivers, potentially leading to reduced outflow und insufficient hepatic function in the critical situation directly after the transplantation. In small remnants or grafts, this could eventually lead to organ failure [Fan et al., 2011, Radtke et al., 2007a]. Therefore, it is essential in ALDLT to evaluate the individual donor liver anatomy and related territorial functional volumes as well as to virtually plan the intervention to account for all risks.

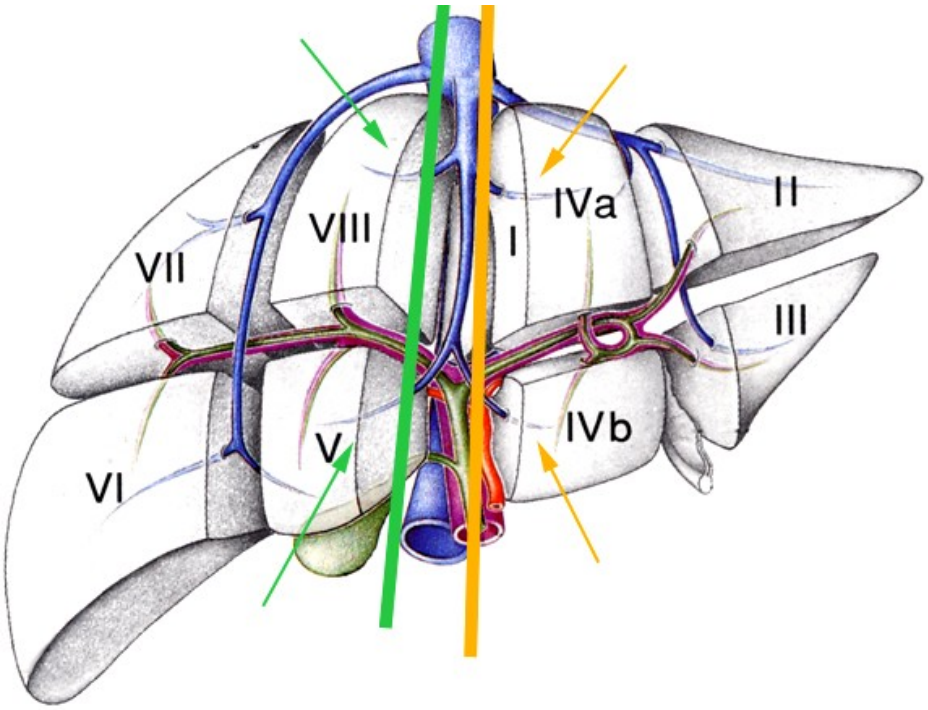

Figure 11: Typical donor liver resection for ALDLT. The resection on one side of the MHV will lead to truncation of tributaries of the middle hepatic vein, either on the right side (green resection line) with the risk of outflow obstruction in the territory 5 and 8 (green arrows) or on the left side (orange line) with territory 4a and 4b at risk of venous congestion (orange arrows). Modified from http://www.rbk.de/.

2.2.4 Thermal Ablations and Other Therapies

Today, surgical resection of primary cancer and solitary metastases is the gold standard for tumor treatment in the liver. However, out of more than 5 million cases of liver cancer per year worldwide, only 5-30% are suitable for surgical resection depending on the selection criteria [Forner et al., 2012]. In patients ineligible for surgical resection due to the tumor number or location or their general condition, local treatment forms such as radio-frequency ablation (RFA) have become increasingly clinically used [Salhab and Canelo, 2011]. RFA is a therapy that locally destroys tissue by heating it above 50ºC, where tissue (both tumor and normal) is destroyed due to thermally induced coagulation of cellular proteins. The first promising investigations on thermal ablation of tumors have been performed in the 1990s, and RFA has since become a widely used approach for the treatment of primary cancer and metastasis in the liver.

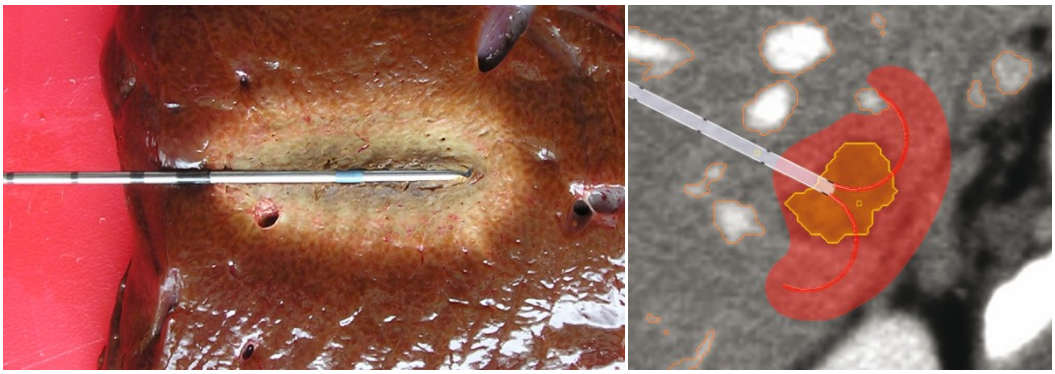

Figure 12: Two types of radiofrequency probes and ablation zones. The needle shape applicator generates an ellipsoid-shaped lesion (Left, image courtesy Celon AG, Berlin). The parachute-like device (right image) opens after needle positioning and creates a larger mushroom-like destruction area [Rieder et al., 2011].

RFA Technique

During an RFA procedure, an applicator containing electrodes is inserted into the tumor and connected to an electric generator, which causes the local flow of an alternating electric current through the tissue. Because the tissue resists the electric current, heat develops and leads to thermal destruction of the cells in the vicinity of the probe (Figure 12). Alternative thermal ablation approaches heat tumor cells by laser irradiation, microwaves or highly focused ultrasound, but clinically, RFA has so far been the most widely used approach [Shimada et al., 2009].

For thermal ablation, the remaining functional liver volume is typically no major risk factor. Instead, computer-assistance in ablation focuses on optimally positioning the applicator(s) and determining the minimal energy necessary for complete tumor destruction. In numerical simulations of the intervention, heat sink effects induced by the blood flow in nearby vessels are important because they decrease the effective coagulation area. The related risk of insufficient tumor destruction and tumor recurrence can be mathematically estimated before the intervention and consequently avoided by adaptating RFA parameters and optimization of applicator position or number [Kroeger et al., 2010b, Schumann et al., 2010, Rieder et al., 2011], see also Section 3.2.3. To support the positioning, first approaches utilizing navigation systems have been developed [Peterhans, 2010, Wood et al., 2010]. Here, the liver segmentation result or landmarks extracted therefrom are often used for initial registration between the three-dimensional virtual organ model and the real liver in the intervention room.

Other Therapies

Other therapies for which the liver model and computer-assistance may play a role in the future are portal vein embolisation, local chemotherapy and radioembolisation. Portal vein embolisation is performed in patients with multiple metastases located in one liver lobe or hemiliver, but with insufficient remnant liver volume after resection. By occluding dedicated portal vein branches in the affected liver area, the blood supply is reduced selectively and the regenerative power of the organ induces growth of the other side. After three to four weeks, the future remnant liver becomes larger and the cancerous liver part can be resected [Shimada et al., 2009]. The liver segmentation can be used to determine the optimal time point for surgery, when the future remnant liver is sufficiently large and before the distributed growth factors induce the development of new metastases.

For local chemotherapy and radioembolisation, the drug or radiation dose that is locally applied via an arterial catheter can be estimated with the help of liver segmentation. The selectively applied dose can be optimized by computing supplied territories and the related regional tumor load. Currently, this is not a routine procedure but performed reliably for hemilivers or portal vein territories in clinical studies. In the future, imaging with higher spatial resolution may enable the segmentation of finer arterial branches including the tumor supplying vessels. The segmentation of these vascular structures together with the liver segmentation may enable computing related arterial liver territories and volumes for locally adapted dose application and planning selective access paths.

Further therapies for primary liver tumors or metastasis include chemotherapy, ethanol injection, transplantation, and ablation by irreversible electroporation. Detailed overviews are given in recent papers about HCCs [Clark et al., 2005, Forner et al., 2012, Salhab and Canelo, 2011], liver metastases [Shimada et al., 2009] and minimally invasive therapies [Rempp et al., 2011].

2.2.5 Computer-Assistance for Hepatic Interventions

Hepatic interventions can be supported by software in many ways for different purposes. The following list shows important tasks for computer-assistance sorted by application time (before, during, or after the intervention):

- Preoperative planning with
    - exploration of 3D anatomy
    - computation of local territories and volumes
    - virtual resection
    - volume estimation for the future remnant liver
    - risk analysis for obstructed vascular supply or drainage (computation of functional volume)
    - distance computation between resection plans and risk structures

    - modeling of thermal ablations
    - optimization of access path (biopsy, ablation)
    - optimization for positioning of single or multiple instruments
    - planning of radiotherapy and optimal dose

- Intraoperative support or monitoring by
    - guided placement of instruments (e.g. biopsy needles and ablation probes)
    - navigated surgery (tracking of instruments and combined visualization of 3D model, real organ, and intraoperative imaging)
    - overlaying the camera view with planning data in laparascopic interventions
    - tracking of patient movements (e.g. breathing) for accurate targeting in radiotherapy

- Postinterventional control by
    - comparing tumors and ablation lesions
    - volume computation after PVE
    - combining follow-up data for regeneration studies
    - follow-up evaluation of a multistep therapy (e.g. tumor growth or shrinkage)

- Training and teaching in medical education.

Because this thesis focuses on liver segmentation that is performed typically in the planning step, we will discuss this preoperative computer-assistance in more details. The result from a liver segmentation mask is utilized also in the other tasks in similar ways. Recent overviews for the other applications are given by different authors, e.g., for intraoperative support and navigated surgery [Peterhans, 2010], for ablation simulation, monitoring and postoperative control [Schumann et al., 2010, Wood et al., 2010], for the application of tumor segmentation in software assisted therapy follow-up [de Hoop et al., 2009, Moltz et al., 2009], and for teaching and training in laparoscopic surgery [Gurusamy et al., 2008]. Examples for teaching tools of liver anatomy and surgery can be found in [Crossingham et al., 2009, Hoehne et al., 2003].

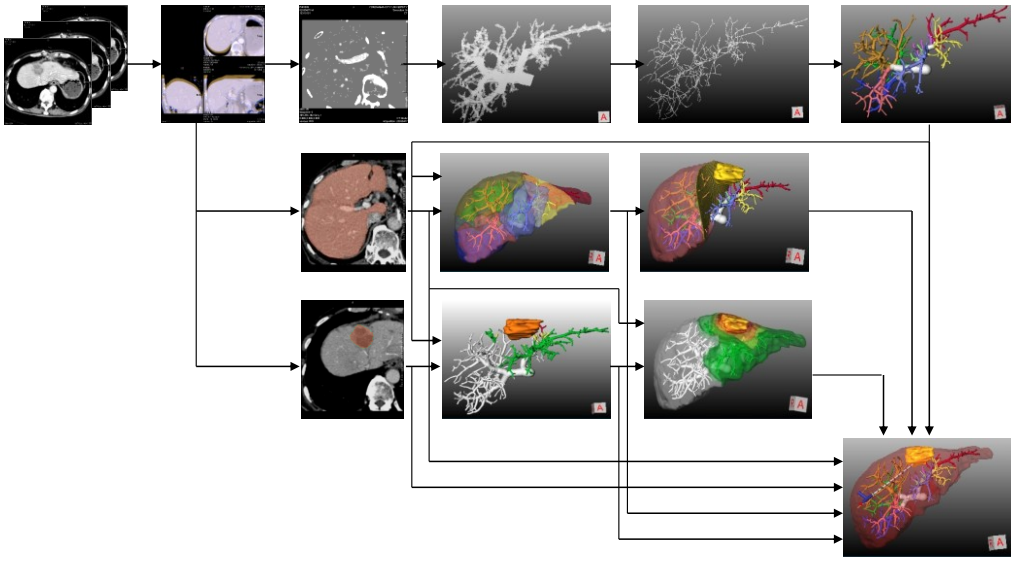

Figure 13: Image processing steps in computer-assisted analysis of liver data as performed at Fraunhofer MEVIS. Top row (from left to right): data import, selection of phases and region of interest, preprocessing for contrast enhancement, vascular segmentation, skeletonization of vessel trees, vascular analysis and hierarchical subdivision. Second row: liver segmentation, computation of vascular territories, virtual resection. Third row: tumor segmentation, tumor-related risk analysis, territories at risk. Lower row: potential application of the patient-individual model for RFA treatment.

Data Acquisition for Preoperative Planning

The decision about a hepatic intervention relies on the detailed knowledge about the individual liver anatomy and pathologies that can be extracted from contrast-enhanced CT or MRI data. During contrast-enhanced image acquisition, contrast media is injected, and reaches the liver artery first, then reaches the portal vein system, and finally leaves the organ via the hepatic vein system. Typically, two to four datasets are acquired sequentially, highlighting in the optimal case only one of the vascular systems in each time point. Imaging of bile ducts requires specific contrast agents that are secreted actively by the hepatocytes and excreted via the biliary system or the combination with magnetic resonance cholangiopancreatography (MRCP) based on a T_2-weighted MRI sequence.

Image Analysis

To analyze radiological data, several image processing steps are performed in the MeVis software assistant Liver Analyzer, (former HepaVision) [Bourquain et al., 2002, Schenk et al., 1999], see also Section 3.2. Research prototypes from other groups or commercial systems, described in the next section, typically include a subset of these steps.

The single image processing tasks are as follows (and illustrated in Figure 13):

1) Registration of different image phases
2) Preprocessing for denoising and contrast enhancement [Schenk et al., 2007, Selle et al., 2002]
3) Segmentation of the liver (see sections 2.1 and 3.1)
4) Segmentation of tumors [Moltz et al., 2009, Schwier et al., 2011]
5) Segmentation and analysis of vascular structures [Selle et al., 2002]
6) Computation of vascular territories [Selle et al., 2002]
7) Virtual resection [Konrad-Verse et al., 2004]
8) Risk analysis [Schenk et al., 2008b, Selle et al., 2000].

Software Applications and Distant Service

The MeVis group started in 1992 as the first group world-wide to investigate computer-assisted 3D reconstruction of hepatic vascular systems and the risk analysis for liver interventions. Research on functional vascular territories and tumor safety margins finally led to certified software assistants for liver surgery planning. The first image analysis procedure developed in this area was the segmentation of vascular structures from CT data published in 1993 [Leppek et al., 1993, Zahlten et al., 1995]. The initial liver segmentation was based on the watershed algorithm and required downscaling the data and subsequent upscaling of the result due to the relative high memory requirements for that time [Schenk et al., 1999, Schindewolf and Peitgen, 2000, Schindewolf et al., 1999]. The live wire algorithm replaced this segmentation method in 2000, which was later replaced by the extended approach presented in this work. The developed live wire method for liver segmentation is still used in daily routine, 12 years after the first implementation.

HepaVision, the first comprehensive liver software application, included all basic image analysis steps and was developed at MeVis in 1999 [Schenk et al., 1999] (for details see Section 3.2.1). A change in the operating system (from Unix to Windows) and significant changes in the underlying MeVisLab platform in 2001 led to a redesign and separation of image analysis and final result visualization, and to the development of the new software assistants HepaVision2 and the Liver Intervention Planner [Bourquain et al., 2002, Preim et al., 2001b]. The visualization step of HepaVision was extended with dedicated interaction techniques that allow virtual resection planning, distance measurements and a more flexible presentation of results [Hahn et al., 2001, Preim et al., 2001a, Preim et al., 2001b, Preim et al., 2002]. Within the SIMPL research project (2002 to 2004), a distant service for image analysis and risk analysis in liver surgery planning was established and evaluated [Hennemuth et al., 2006]. Using secure Internet connections, CT images from hospitals worldwide are sent to MeVis. Risk analysis and preoperative planning are performed, and results, including 3D visualizations, anatomical or functional volumes, and movies are sent back to the hospital. More than

6000 data sets have been evaluated for surgical planning, in research projects and in the distant service that has been commercially available from MeVis Medical Solutions since 2005 [MDS, 2012].

Analyzing risk and planning LDLT began in 1998 together with Prof. Karl J. Oldhafer at the Medical School Hannover and was intensified later at the University Hospital Essen [Hoegemann et al., 1999, Oldhafer et al., 1999, Radtke et al., 2007b, Radtke et al., 2010]. The MeVis computer-assistance for LDLT was also used in other medical centers, but the breakthrough for this technique was a meeting with Dr. Yasuhiro Fujimoto and Prof. Koichi Tanaka from the Kyoto University in October 2012. Prof. Tanaka realized the potential of our risk analysis for the middle hepatic vein, insisted having the information available for every ALDLT from this time point on, and propagated the method in the transplantation society [Bourquain et al., 2003, Asakuma et al., 2007]. This cooperation was the starting point for the worldwide-recognized MeVis risk analysis for LDLT and basis for an increasing number of clinical partners in research and customers of the distant service [Schenk et al., 2009].

Other research groups have been investigating liver surgery planning, navigation, and training. Examples include the Division of Medical and Biological Informatics at the German Cancer Research Center in Heidelberg, the Zuse Institute Berlin, the Research Institute against Digestive Cancer (IRCAD) in Strasbourg, the Institute of Imaging Science at the Vanderbilt University, the ARTORG center at the University Bern, and the Department of Simulation and Graphics at the University of Magdeburg. Some of these institutions have also begun to develop commercial software applications and companies that support liver interventions. The demand for computer-assistance before and during liver interventions can be recognized in the increasing number of commercial products, such as Mint Liver by mint medical (Heidelberg, Germany), Scout Liver and Explorer Liver by Pathfinder Therapeutics (Nashville, USA), IQQA-Liver by EDDA (Princeton, USA and Shanghai, China), and CAS-One by Cascination (Bern, Switzerland).

3 Overview Own Work

Nothing in life is to be feared, it is only to be understood.
Now is the time to understand more, so that we may fear less.
Marie Curie

3.1 Liver Segmentation

The liver segmentation approach that will be presented in this chapter, allows for the semi-automatic extraction of the organ in little time and with a user-defined quality, from a rough contouring to most accurate contours for high-risk surgery.

The starting point at the time of the algorithm development in 1999 was the demand for a high-quality segmentation approach for clinical use. The method was to overcome the time requirements of the labor-intensive manual contour delineation but also avoid the typical and significant errors of automatic or 3D algorithms. Because automatic approaches did not achieve the quality required for high-risk surgery and required much computation and memory, a semi-automatic approach was chosen. The concept was to use the user knowledge directly during the segmentation process on 2D images and to reduce the overall number of contours interactively drawn by a contour interpolation method. Besides several optimizations of the basic algorithm, two different modes for contour correction and another mode for MRI data were implemented. The chapter concludes with an extensive evaluation applied to more than 2000 data sets.

3.1.1 The Concept

The basic ideas of the developed approach are to

1) use the user knowledge about the object properties and

2) accelerate the interactive process of contour delineation while maintaining the high quality.

For the first purpose, the live wire approach is perfect, because the knowledge about the boundary and image properties of the liver can be translated into parameters of the algorithm, and the user directly controls the segmentation process by steering the algorithm to the correct boundary points, e.g., when the automatic process fails to find the correct contour segment.

The second step of interpolation aims to reduce the required interaction time by discarding the interaction with a number of image slices and by generating the remaining contours automatically. For this purpose, the shape-based interpolation was chosen, because it is a fast method able to deal with topological changes. For example, it can transform several contours on one slice into one contour on the

next slice. The last steps of automated and interactive contour correction allow optimizing the overall result.

3.1.2 Live Wire

We will shortly resume the fundamental ideas of the live wire method: the two-dimensional image is transformed into a directed, weighted graph. Vertices of the graph represent image pixels while edges connecting neighboring pixels in two directions. The edges are weighted with local cost functions that are typically a weighted sum of different gradient functions and the Laplace function. In our implementation, a boundary cost function was added to consider the gray values at the object outline. After calculating the cost graph, the user starts the segmentation by setting a first seed point on the boundary and moving the mouse along the outline of the object. Shortest paths – those with lowest accumulated costs – from the seed to at least the current mouse position are computed using Dijkstra's algorithm [Dijkstra, 1959]. The live wire path snaps to the boundary while the user moves the mouse over the image. This is achieved by a real-time computation of the path with lowest costs from the last seed point to the current mouse position. A new seed point has to be set before the path starts to deviate from the desired contour. New shortest paths are computed from the new seed point, and the procedure is repeated. A final closure leads to a controlled and piecewise optimal segmentation result.

The implementation of our live wire approach was provided with the additional concepts of boundary snapping and data-driven cooling to automatically generate seed points [Barrett and Mortensen, 1996, Mortensen and Barrett, 1995]. Boundary snapping moves the user-defined seeds to a pixel position with high gradient or low local costs, whereas cooling automatically generates new seeds when the contour does not change for a predefined amount of time or number of user interactions. Both concepts introduce a form of automation that reduces the direct control. Experience with the image data showed that the impact of these two features was limited, while the correction of erroneous seeds was annoying and time-consuming. Therefore, the methods were not used in the final daily routine.

Instead, the developed algorithm extends and optimizes the basic approach with the following features:

- **Refinement of the contour**
  The original live wire algorithm takes a 4-neighborhood into account for cost and path computation. The resulting path shows a step-wise appearance. By extending the four directly connected pixels with the pixels in the diagonal neighborhood, the live wire contour results in a much smother shape. This decision for 8-neighborhood led to an update of the cost function, which now requires additional definitions for diagonal connections. The cost function was therefore extended by both a length factor and by orientation-dependent costs to specify and optimize the resulting live wire path further.

The increased computational effort for the larger neighborhood was compensated by improvements in the basic implementation, described later.

- **Computational acceleration**
  One of the time-critical steps during computation of shortest paths represents sorting the list of pixels with undetermined final path. By restricting the local costs between two image pixels to integer values with an upper bound of the maximal local costs, the required time can be reduced significantly by using a bucket list for sorting [Cherkassky et al., 1994]. Although the maximal cost value under all paths is unknown, the length of this bucket list can be delimited. Because paths are considered in ascending costs, and the new maximum will be below the current cost plus the maximum of local costs C, the bucket list can be implemented as a cycle of length C. In this way, the computational time for sorting can be reduced significantly. Similar approaches can be found in [Stalling and Hege, 1996, Falcao et al., 2000].

- **Locally restricted cost computation**
  The computation of paths between the last seed point and the current mouse position does not require the computation of minimal paths for all image pixels. Because of positive costs and sorting undermined paths with increasing costs, computing of paths to the current mouse position can be finished when all direct neighbors of this position have been considered for path computation. We further limit this cost computation by restricting the image area for path finding, only considering pixels within a given distance of the contours of the previously segmented image slice. This approach limits computation and avoids boundaries with similar gradient or cost values, especially for larger images. An example is illustrated in Figure 14. Details of the locally restricted costs and implementation are given in [Schenk et al., 2001a].

- **Dedicated cost functions for the liver**
  In our implementation, the user can select different gradient functions, the Laplace function, and an object boundary function and weigh them according to their relevance for the desired boundary. For every cost function, a preset of mean and standard deviation defines a Gaussian-distributed value weighting. In case of the special boundary function, the parameters are defined separately for values inside and outside of the object and combined in the boundary function.
  For liver segmentation, we used the combination of a directed gradient function similar to the Sobel edge detection filter [Falcao et al., 1998] and the directed boundary function. Parameters for both functions (weights, mean, and deviation) were determined experimentally for the venous CT phase as well as for the arterial phase.

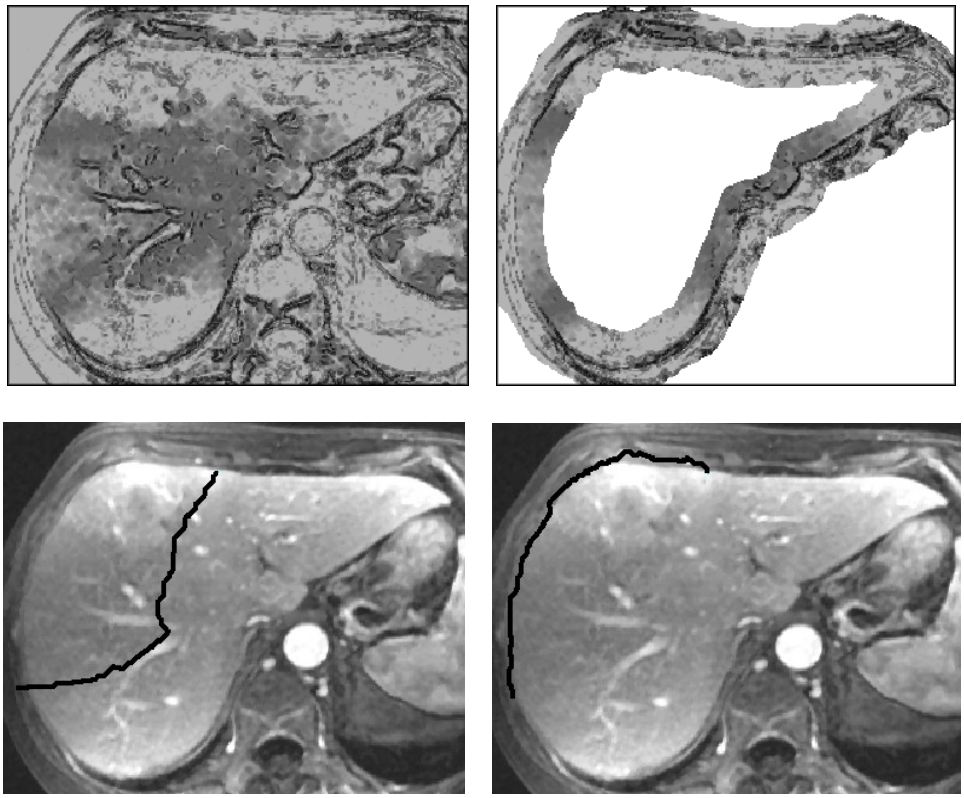

Figure 14: Globally and locally restricted costs. The computation time for the cost function can be reduced by restricting the relevant region (upper row, global costs left, locally restricted costs on the right). Furthermore, it also improves the live wire contour by avoiding erroneous short cuts (lower row, live wire contour based on global costs left, based on locally restricted costs on the left).

- **Learning cost parameters**
  The user can directly set or change the parameters of the cost function. Whereas the relevance or weight of a single cost feature can be judged by inspecting the respective cost image (cf. Figure 14), the parameter values of each single cost feature are difficult to determine. A learning algorithm allows automatic identification of these values based on the evaluation of one or more existing contours. The user can define these contours as manual or live wire contours.

- **Locally adapted cost parameters**
  Motivated by the demand for liver segmentation in MRI data, the global learning approach was refined. Considering the typical inhomogeneity in MR images (cf. Figure 14), a locally adapted learning method seemed more appropriate than global cost parameter learning. Because the properties of the image at the object boundaries are similar to neighboring slices, local parameter learning was implemented.

Using the coherence between the desired and the nearest adjacent contours, the contour and image information on the related slice is taken as reference for the current image. The reference contour is divided into segments for each cost feature, and cost feature parameters are learned for each segment. Partitioning of the reference contour is implemented as an iterative method, merging very small contour segments into larger units while keeping the sum of all cost feature deviations minimal. The merging step is repeated until a given minimal number of contour segments is reached. Additional merging for short segments was implemented and applied to avoid segments shorter than a given minimal length.
Finally, the indices of the contour segments for every cost feature are propagated based on distances from the reference contour onto the image and define a label image with indices for feature-specific regions. During path computation, this label image is used to compute the locally adapted costs and minimal live wire path. Details of the implementation are given in [Schenk et al., 2001a].

- **Manual drawing in the live wire mode**
  For difficult image areas where no real liver boundary is recognizable or where the live wire algorithm snaps to the wrong edges, parts of the contour can be drawn manually. For this purpose, the user keeps the mouse pressed while following the user-estimated organ boundary. Internally, all mouse positions will be collected and combined to a polygon that is part of the final contour. This mode avoids multiple mouse clicks of the live wire approach and accelerates the definition of the contour in areas where the liver boundary has to be estimated by the user.

3.1.3 The Combination with Shape-Based Interpolation

At the time of development, only one live wire approach for the segmentation of 3D objects in images stacks had been published [Falcao and Udupa, 1997]. This approach by Falcao was based on the projection of interactively defined live wire contours onto orthogonal cross-sections through the volumetric image and repeated live wire application between the intersection points. With this algorithm, additional user interaction was required to follow the topology of objects with complex shapes. For instance, stacks of images for which the object could be represented by two contours each had to be separated from image stacks with more or less object outlines in a slice.

In contrast, we aimed to ease the user workflow by avoiding specific user interaction in cases of topological changes. A method that allows for such a contour interpolation is the shape-based interpolation [Raya and Udupa, 1990]. It consists of several steps, illustrated in Figure 15 and described in the following. First, a binary scene is generated from a given object contour. Subsequently, the distance to

this boundary is mapped into a new gray-level scene with positive distance values inside and negative distance values outside the object (shown as absolute values in Figure 15). In the third step, the distance images are interpolated with a conventional gray-level interpolation technique such as linear interpolation. The interpolated gray-level scenes are converted back to a binary contour image by identifying the zero-crossings.To compute the distance transformation, a version of the city-block distance is often employed due to its short computation time [Raya and Udupa, 1990]. We implemented two consecutive chamfering processes [Borgefors, 1986, Herman et al., 1992] realized with 3×3-kernel operations. This chamfering method leads to more accurate results because this transformation better approximates the Euclidean distance [Borgefors, 1986]. After the initial shape-based interpolation, the zero-crossings of the distance image define the boundary points of the new contours. To obtain real contour paths, these zero-crossing pixels have to be sorted and arranged. The correct ordering of these boundary points and the identification and separation of more than one contour proved to be a challenging task. For this purpose, we developed a dedicated path-search algorithm [Schenk et al., 2000].

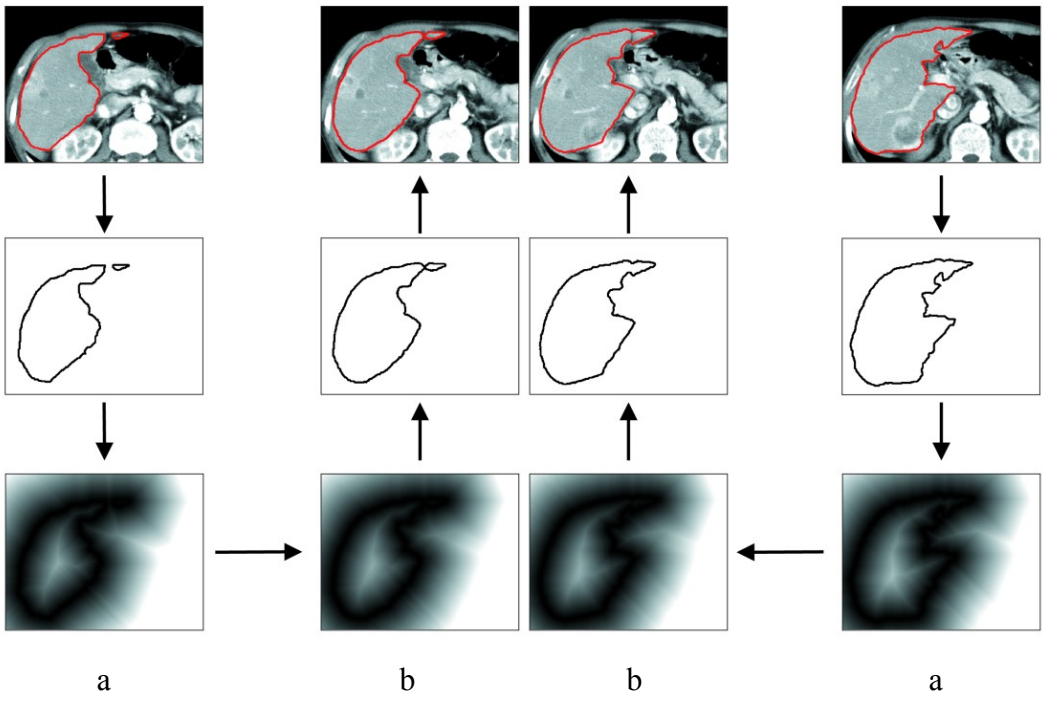

Figure 15: Shape-based interpolation: User-defined contours in CT images (a, top row) are converted to binary scenes (a, middle row). Distance images are computed from these binary images and interpolated for the intermediated image slices (bottom row). From the interpolated distance images, the new contours for the intermediate images are computed automatically (b, middle and upper row).

The same boundary sorting algorithm can be employed to transform a binary mask into a dedicated contour representation. This method allows computing boundary contours from the result of a region-based segmentation approach (realized as the module Region2Contour in MeVisLab [MeVisLab, 2012]).

The combination of live wire and shape-based interpolation is illustrated in Figure 16. The user starts with the live wire algorithm on individually selected slices. If contours on at least two slices are available, all contours on slices in between can be computed using shape-based interpolation. During this process, the user is free to apply one of two methods: live wire and shape-based interpolation in an alternating fashion or in a two-stage approach interactive contour tracing on a larger number of slices with subsequent interpolation. The only restriction is that the first and the last slices of the object of interest are required to be segmented interactively with the live wire algorithm.

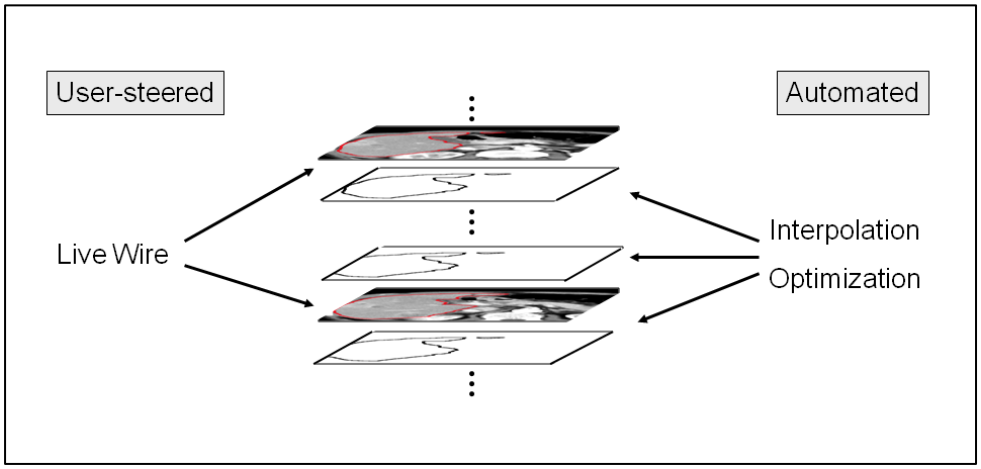

Figure 16: Combination of live wire and shape-based interpolation: User-steered segmentation of selected slices followed by automatic interpolation and optimization of the intermediate contours.

Optimization of Interpolated Contours

Shape-based interpolation is based solely on the geometry of contours and considers no image information. Therefore, interpolated contours may not fit to the desired organ boundary in all images. To correct these contours automatically, an optimization step was developed. The underlying idea was to adapt the new contours by employing the live wire algorithm and to recalculate contour segments as optimal cost paths between seed points. For this purpose, seed points have to be generated for the interpolated contours.

Our method copies the seed points from the two adjacent user-defined contours onto the interpolated contour. For every user-defined seed point, the nearest point on the contour path is determined. If two points are closer than a given minimal distance, they are merged into one central seed point. For instance, using user-

defined seeds instead of equally distributed seeds along the interpolated contour is reasonable, because these points represent the user knowledge and were typically defined in regions of high curvature or weak edges.

After seed point creation, the live wire algorithm is started for each seed point to determine the minimal cost path to the next seed point. In this way, live wire segments are computed automatically, iteratively leading to new optimized contours.

In the implementation, contours are labeled with their construction algorithm, e.g., ‘live wire’ and ‘interpolation’. Thus, the interpolated contours can be detected, and the optimization can be applied selectively. However, the user can also start the optimization for all contours to adapt the contours after a change in the cost function parameters.

3.1.4 Correction Techniques

To allow a user-friendly correction of object contours, two modes were implemented. The first mode is based on the live wire paradigm; the second is an intuitive form of manual contour correction.

With the live wire mode, seed points can be added to a contour, moved to another position, or can be removed completely. All affected contour paths are updated by computing them as live wire paths between the adjacent seed points in real-time. The whole contour can be updated in an automated way, where all contour paths between seed points can be recomputed after interpolation or after a change of the cost function. The correction mode based on live wire is very intuitive and leads to satisfying results in short time whenever the liver boundary values correspond with the current cost function.

For the manual correction mode, the user can draw a boundary line across the existing contour. The outer two intersecting points of the new line with an existing contour are determined. The new boundary between the intersecting points replaces the shorter part of the old contour between these points. In this way, an additional bow outside the object is added to the object and a short cut line inside the object decreases the segmented region. This method reflects user expectations and thus is very intuitive.

3.1.5 Evaluation

Several papers compared live wire segmentation with manual contour tracing and showed the high reproducibility and timesavings for different objects [Barrett and Mortensen, 1996, Barrett and Mortensen, 1997, Falcao et al., 1998]. Our evaluation focused on the application of live wire and shape-based interpolation for liver segmentation in particular. Three studies were performed in different years: an initial evaluation with the first version of live wire and shape-based interpolation

in the year 2000 [Schenk et al., 2000], a clinical study at the Medical School Hannover from 1999 to 2000 [Frericks et al., 2004a], and a large retrospective evaluation on more than 2000 data sets from research projects between 2005 and 2011 that was performed recently [Schenk and Peitgen, 2012]. In all evaluations, the final liver masks were compared to the results of the combined approach of live wire and shape-based interpolation and evaluated with respect to accuracy and time requirements. In particular, the studies investigated the following issues:

Accuracy

- How much do interpolated contours differ from user-defined live wire contours?
- How many image slices with interpolated contours had to be corrected?
- How large are inter- and intraobserver variability in liver segmentation?
- How does the approach compare with other segmentation approaches?
- What is the impact of automatic optimization of contours?

Time Requirements

- How much time does a full accurate liver segmentation need?
- How fast is the combined approach?
- How much time is invested for controlling segmentation results and interactive correction?
- How much time does interpolation save compared to live wire segmentation?
- Is the segmentation time correlated to the number of slices, or does it take longer to segment liver with pathologies than without?

Evaluation Data and Methods

For the first study, five liver CT scans for tumor diagnosis from three different hospitals were evaluated. The images had 512×512 pixels in plane and consisted of 34-41 slices with a distance of 4mm (n=4) or 86 slices with a distance of 2mm (n=1). Three users segmented the images with live wire on all slices and times were recorded. The interactively segmented slices were reduced to data sets with slice distances of 8, 12 and 16mm and the omitted intermediate slices were automatically calculated with both shape-based interpolation and with the automatic optimization approach. Intraobserver variations and volume errors as well as time differences were computed.

In the clinical study in the Medical School Hannover, 56 potential donors for LDLT were scanned by computed tomography and analyzed by radiologists between 1999 and 2002 using the first version of HepaVision. The data had a slice thickness of 2mm, and the pixel size ranged between 0.63mm and 0.88mm. The organ contours were delineated by live wire on every fifth CT image, and all in-

termediate contours were calculated automatically by shape-based interpolation. Interpolated contours were corrected interactively using the live-wire correction method. The number of slices to be corrected and the time needed for overall liver segmentation was recorded.

Between the years of initial algorithm development and the last evaluation, the slice thickness in abdominal CT data has decreased from about 4mm to 0.75-1.0mm (see Figure 17). This means the overall number of images to be segmented has tremendously increased (from about 40 images in the year 1999 to more than 200 slices nowadays) potentiating the benefit of our interpolation approach.

The most recent, retrospective study included more than 2000 CT data sets of livers both with tumors (49.1%) and without (50.9%). The images were reconstructed with a maximum slice thickness of 3mm and averaged 1.16mm. The majority of images (69.2%) were high-resolution scans with 1mm slice thickness or less (Figure 17). The liver segmentation was performed with the methods described in Section 3.1, and the order of live wire, interpolation, and correction was not restricted. Users could repeat interpolation, change the cost function, or correct contours between the other steps. Time was recorded for the overall segmentation including correction steps. Segmentations with a sequential order of live wire, interpolation, and subsequent correction allow comparing the initial results of live wire and interpolation alone (*LWI segmentation*) and the final segmentation after correction. The intermediate LWI results were available for a subgroup of 1516 cases. The final liver segmentation, regarded as our ground truth (*GT segmentation*), was compared to the result of the LWI segmentation for different error measures and time demand.

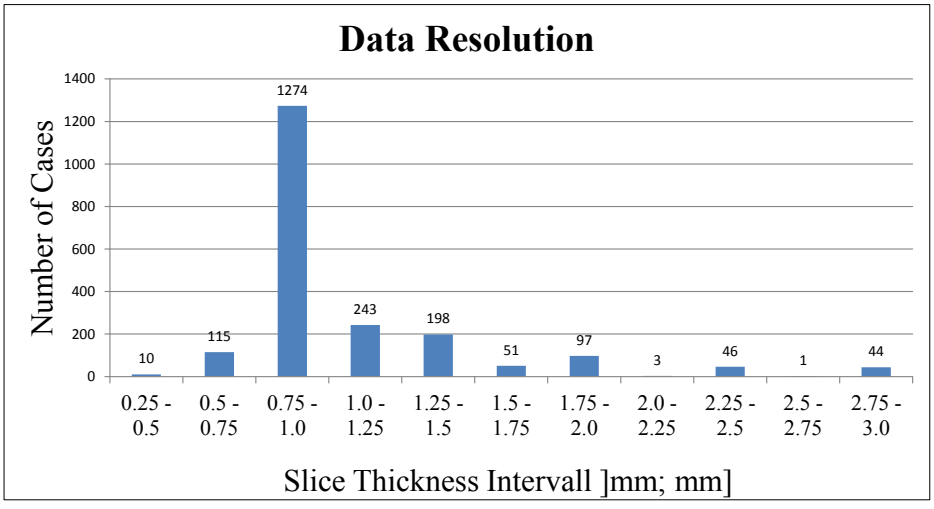

Figure 17: Resolution of evaluation data in terms of slice thickness. The majority of cases are high-resolution images with a slice thickness between 0.75 and 1.0mm.

Results

The first study showed that the segmentation result by leaving out contours on images in a distance of 8mm and automatically computing the missing contours by interpolation leads to errors in the magnitude of the intraobserver variability. Reducing the interaction time further and interpolating contours between 12mm distant slices, lead to slightly increased error rates that could be compensated in most cases by the automatic optimization step. In conclusion, more than 50% and about 90% (for the 2mm data set) of interaction time could be saved with the shape-based interpolation if deviations in the order of the inter-user variability were tolerated. Further details of the study results are given in [Schenk et al., 2000].

In the second, clinical study, the liver segmentation performed by the radiologists required 10 minutes on average, and 17% of the automatically interpolated contours were corrected interactively. Errors were based on partial inclusion of neighboring structures, and the correction took only a few seconds in each case [Frericks et al., 2004a].

The main result of the third, large study showed that the initial approach of live wire and interpolation is already highly accurate, with less than 1% volume overlap error and less than 1mm average surface distance when comparing the final and initial segmentation masks. The semi-automatic initial segmentation required about 15 minutes on average for the overall routine data and 12 minutes in the intraobserver study. The control and correction steps took an average of 11 additional minutes, more than 40 % of the overall segmentation time.

Regarding accuracy, relative small differences were found between the final ground truth segmentation and the initial live wire segmentation including interpolation (Tables III and IV). The absolute volume deviation was 0.33 % (5 ml) of the GT volume, and the mean volume overlap error accounts for less than 1 % of GT liver volume. The mean surface distance was below 0.2mm on average for the absolute distances and below 10mm for the maximal distances. Volume differences and surface distance were smaller for the lesion-free organs than for livers with lesions (Table III).

The overall time for liver segmentation including the control and correction step averaged 24.7 minutes (Table V). The initial LWI segmentation required 15.5 minutes on average and was 1.6 minutes faster for lesion-free livers, which were also generally smaller (1350 ml versus 1556 ml, see Table IV). The control and correction step was almost identical in time requirements for the two liver groups (11.7 and 11.9 minutes).

Intraobserver deviations were in the magnitude of 2.8 % of liver volume, and interobserver differences were larger but still below 4 % of liver volume, confirming

the results of the first study. Further results of the study are given in [Schenk and Peitgen, 2012].

TABLE III
COMPARISON LWI AND GT SEGMENTATION: ERROR MEASURES

	VOE [%]	RVD [%]	ASD [mm]	RMS [mm]	MSD [mm]
All Livers (n=1516)					
Mean	0.77	0.33	0.18	0.66	9.67
Std Deviation	0.94	0.60	0.31	0.86	6.70
Lesion-free Livers (n=736)					
Mean	0.62	0.25	0.14	0.58	9.10
Std Deviation	0.74	0.45	0.27	0.82	6.69
Lesion Livers (n=780)					
Mean	0.92	0.40	0.21	0.74	10.22
Std Deviation	1.09	0.71	0.35	0.90	6.66

Abbreviations: VOE: Volume Overlap Error, RVD: Relative absolute Volume Difference, ASD: Average Symmetric surface Distance, RMS: Root Mean Square symmetric surface distance, MSD: Maximum Symmetric surface Distance (Details in [van Ginneken et al., 2007, Schenk and Peitgen, 2012])

TABLE IV
COMPARISON BETWEEN GT AND LWI SEGMENTATION: VOLUMES AND TIME REQUIREMENTS

	All Livers (n=329)		**Lesion-free Livers** (n=84)		**Lesion Livers** (n=245)	
	GT	LWI	GT	LWI	GT	LWI
Volume [ml]						
Mean	1504	1499	1350	1346	1556	1552
Std Deviation	*512*	*512*	*345*	*344*	*550*	*549*
Time [min]						
Mean	27.3	15.5	26.0	14.3	27.8	15.9
Std Deviation	*14.3*	*9.4*	*12.0*	*7.9*	*14.9*	*9.8*

TABLE V
LIVER VOLUMES AND OVERALL SEGMENTATION TIME OF GT SEGMENTATION

	All Livers	**Lesion-free Livers**	**Lesion Livers**
Volume [ml]	(n=2082)	(n=1059)	(n=1023)
Mean	1499	1356	1647
Std Deviation	*505*	*337*	*598*
Time [min]	(n=1606)	(n=873)	(n=733)
Mean	24.7	23.9	26.6
Std Deviation	*13.5*	*11.5*	*15.4*

3.1.6 Discussion

The liver is a challenging organ to segment, and a correction step is necessary to achieve an accurate liver shape in most data sets. Control and correction takes time, especially when it has to be performed on a large number of image slices. Therefore, directly using an interactive user-controlled approach from the first segmentation step is a consequent conclusion for reliable and accurate results. It also prevents user frustration when automatic results differ significantly from the expectations and cannot be corrected easily.

3.1.7 Summary

For planning critical liver interventions, an accurate liver segmentation approach is mandatory. Automatic methods are not able to achieve the required accuracy reliably for the large variety of organ shapes and image properties. Therefore, an interactive liver segmentation approach based on live wire and shape-based interpolation was developed. We improved the user-steered live wire approach in terms of accuracy and reduced the computation time by optimizing data structures and algorithm and restricting the computation area to a local minimum. Dedicated costs for specific organs and locally adapted cost functions were developed for clinical applications. The idea of combining the two-dimensional live wire approach with shape-based interpolations can be seen as one of the first approaches to combine shape and gray-value algorithms, allowing for a significant reduction of interaction effort and time. To allow for final contour correction, two intuitive correction modes were developed and implemented. The evaluation studies showed that the liver segmentation can be performed by our approach in 10-30 minutes and that the combination of live wire and interpolation alone is already highly accurate compared to the corrected, final segmentation. The correction step accounted for more than 40% of the overall segmentation time and remains an important step in liver segmentation for most data sets when highly accurate results are required.

> **Publications**: The initial combined approach of live wire and shape-based interpolation was presented in a talk on the MICCAI conference in 2000 and published in [Schenk et al., 2000]. This paper presented the algorithm, the automatic optimization of contours, and the first evaluation. The extensions with local cost computations and locally adapted costs and further algorithmic improvements were introduced and discussed on the SPIE conference [Schenk et al., 2001a] and the BVM meeting in 2001 [Schenk et al., 2001b]. The clinical evaluation was performed by B. Frericks and colleagues from the Medical School Hannover and published in [Frericks et al., 2004a]. Recently, we eval-

uated the results of our liver segmentation approach on more than 2000 data sets [Schenk and Peitgen, 2012].

The approach of live wire and shape-based interpolation is part of a commercial tool for contouring in medical data.

3.2 Computer-Assistance for Liver Interventions

"If you think you are too small to make a difference,
try sleeping with a mosquito."
Dalai Lama XIV

This chapter describes four contributions in different areas of computer-assistance for liver interventions. The developments and results were achieved between 1998 and 2012. In Section 3.2.1, we will introduce the first comprehensive software assistant for liver surgery planning. Several image processing steps are necessary to create an individual 3D liver model including all relevant intrahepatic structures. The development of a software assistant combining all steps and providing an optimal workflow for clinicians is a demanding task. The step from the planning into the interventional situation poses another challenge, and we present pioneering work in this area in Section 3.2.2. Further work focused on the modeling of thermal ablations in the liver and the development of a measurement tool for the evaluation of vascular heat sink effects described in the third section. The chapter is concluded by recent developments on an interactive risk analysis application allowing for the immediate assessment of a virtual resection's quality in terms of a new resection score. The achievements described in this chapter are part of the broad topic of computer-assistance for liver interventions. A more general survey of this topic can be found in our overview papers [Schenk et al., 2008b, Schenk et al., 2011].

3.2.1 The First Comprehensive Liver Application

In 1998, only a few algorithms supported the analysis of abdominal images. The MEVIS research institute was the first group worldwide to develop an entire pipeline for vascular analysis and preoperative liver surgery planning. For the full analysis of a liver case in the year 1998, at least ten single steps had to be performed by the user:

1) Data import

   Several import options were necessary since the ACR/NEMA standard 3.0, now known as DICOM, was released in 1993 but was not yet adopted by all scanner vendors.

2) Definition of the liver region

   After inspecting the different CT phases, the image area encompassing the liver was defined by the user to reduce the data amount and computation time for the following steps. It was realized by interactive drawing of rectangles in the different viewer directions.

3) Liver segmentation.

   Initially, the global and interactive watershed algorithm was used for this step and required downscaling the data before segmentation and subsequent upscaling of the liver mask to reduce the required memory and com-

putation time for the algorithm [Schindewolf and Peitgen, 2000]. An editing step allowed correcting results. These four steps were later replaced by our live wire approach.

4) Tumor segmentation

   Lesions could be extracted using the watershed approach in case of homogenous tumors or had to be manually drawn on the 2D images slices.

5) Vascular preprocessing

   A pipeline of several filter algorithms was used to reduce noise and to enhance the contrast between vessels and liver tissue.

6) Vessel segmentation

   Vascular systems were extracted by global region-growing that stored all results in a hierarchical data structure allowing for subsequent interactive real-time adjustment of the threshold [Selle et al., 2002].

7) Vascular skeletonization

   In this step, centerlines and local vessel radii were computed and the segmentation result was transferred into a dedicated graph data structure.

8) Vascular analysis

   Vascular systems could be separated and interactively subdivided hierarchically by clicking on single branches, subtrees, or complete trees to define the basis for computating local supply or drainage.

9) Computation of vascular territories

   According to supply or drainage, local territories according to the supply or drainage were computed based on the liver mask and the subdivision of a vascular system.

10) Visualization

    A 2D and 3D viewer allowed selective display of relevant structures, rotation and zooming objects, and different types of volume visualization (see Figure 18).

All algorithms were implemented as separate image processing networks in IlabMed [Schenk et al., 1999], a predecessor of the MeVisLab research and development platform [MeVisLab, 2012]. Each step required loading data and explicitely saving results. Several parameters had to be entered by the user into single IlabMed module interfaces, and sometimes the same parameters, such as voxel size, had to be provided in several image analysis steps.

In 1998, there was a high demand for a comprehensive application with a convenient workflow that included all steps of data analysis and a subsequent visualization and mean of exploring results. Parameters that could be derived from the im-

age data should be determined automatically, and the exchange of information and data between the single steps should be highly automated.

Such a comprehensive liver application, the first HepaVision, was developed in 1998 by a joint project of the liver team at MeVis (including the author) [Schenk et al., 1999]. We developed and implemented the global workflow including template classes for the exchange of data and parameters, a consistent graphical user interface (GUI) for all single steps, and templates for the HTML help files. The important information for each patient case was transferred between the steps in an XML file that included image and algorithmic parameters, file names, results of volume measurements, visualization parameters, and other data. The application including GUI and workflow, was implemented in APrIL, an object-oriented *Application Programming Interface Language* developed at MeVis. The first HepaVision application was used in clinical research projects at the Medical School Hannover and at the University Hospital Magdeburg. Images of the liver segmentation and the visualization step are shown in Figure 18.

In 2001, changing the operating system from Unix to Windows and significant modifications in the underlying MeVisLab platform led to redesigning the application. The image analysis steps were separated from the final visualization step, and two new software assistants were developed. In the new planning assistant HepaVision2, the GUI was optimized, and additional steps for virtual resection and risk analysis were included in the following years [Bourquain et al., 2002, Konrad-Verse et al., 2004, Schenk et al., 2008b]. Although switching operating systems resulted in several modifications, the basic application concepts developed for the first HepaVision version were adopted and are still in use in the current application, including the workflow concept, the global layout, and the XML data exchange.

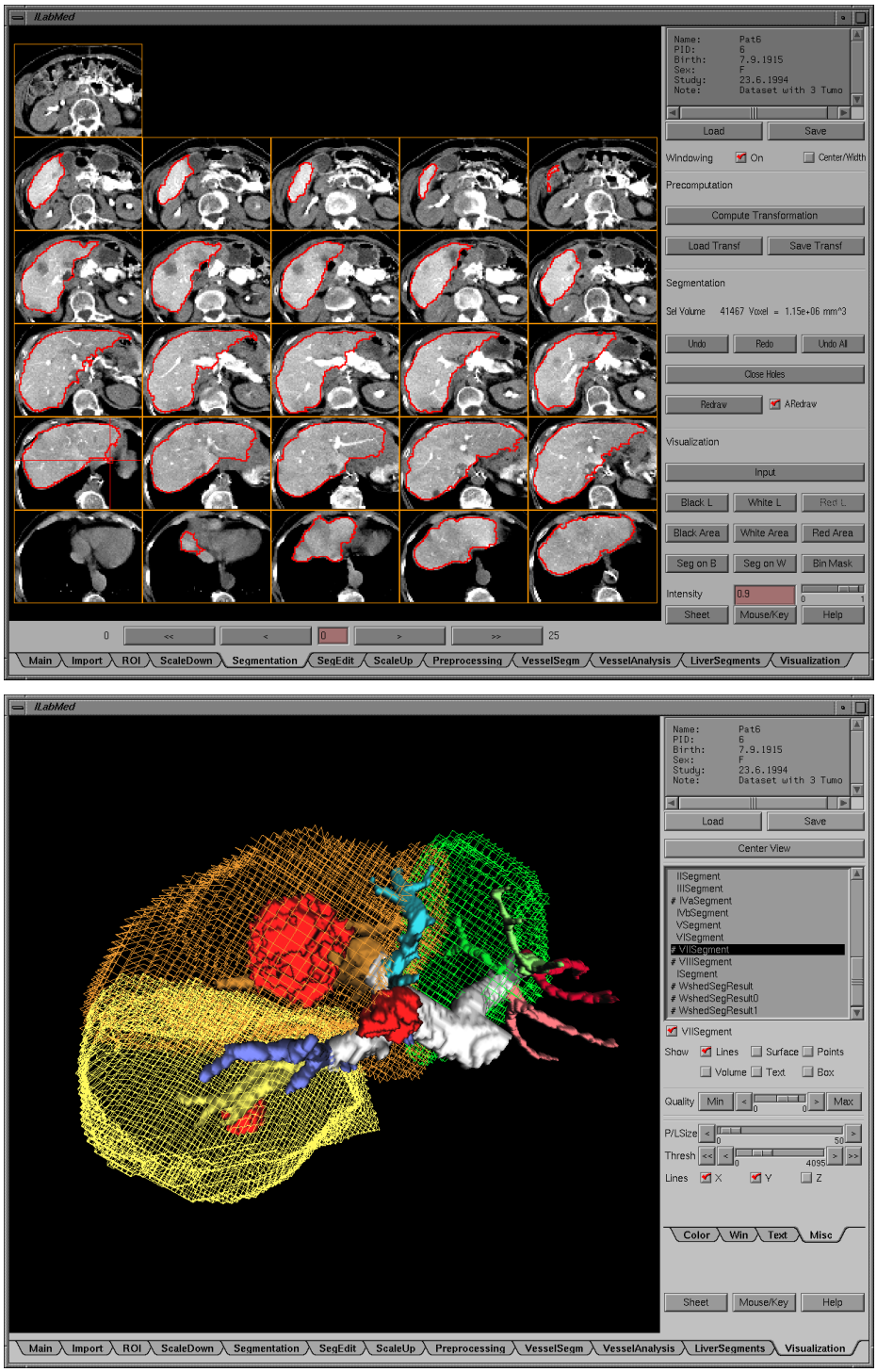

Figure 18: The first version of HepaVision developed in 1998 shown with the first watershed-based liver segmentation step (top) and the visualization step (bottom). In the lower window area, every single step of the application could be selected via a tab. The right border shows the GUI elements of the single step including the information panel, load and save buttons (upper area), step-specific fields (middle), and the help buttons (below).

3.2.2 Integration of Planning Data into Liver Laparoscopy

The first tools and and applications for computer-assistance in liver surgery planning were available in the beginning of the 21st century, but the transfer of this information into the intervention room, especially for abdominal surgery, was rarely investigated. In 2002, there were only few applications to provide planning information during the intervention and these mainly focused on neurosurgery. In liver surgery, matching the virtual liver model with the real organ was typically performed in the surgeon's mind. Few publications have presented feasibility studies for liver registration using organ phantoms or initial trials in open liver surgery [Herline et al., 1999, Vetter et al., 2002]. For minimally invasive liver interventions such as laparoscopic surgery, there was no published approach combining computer-assisted planning and hepatic interventions.

To assist laparoscopic surgery, we collaborated with the University Erlangen-Nürnberg computer graphics group. This group had developed an augmented reality system that projected the 3D planning data into the real laparoscopic video stream [Scheuering, 2003]. The system had been evaluated in five minimally invasive interventions, but during these tests, no preoperative planning information was included. The first integration of planning results was performed in a collaborative work in a minimally invasive intervention in a swine in 2002 [Scheuering et al., 2003].

For this evaluation, a routine abdominal CT of the animal liver was performed at the University Hospital Klinikum rechts der Isar in Munich. The anatomical structures were segmented with the HepaVision assistant, described in Section 3.2.1 [Schenk et al., 1999]. Due to the smaller structures in the animal and breathing artifacts, only the organ and the larger vascular structures (portal vein and hepatic vein) could be segmented. The augmented reality system was calibrated before intervention and rigid registration was performed using anatomical landmarks and four fiducial markers placed onto the body surface before CT acquisition. The virtual 3D liver anatomy was directly projected into the laparoscopic camera view. The display of the vessel system and the liver was utilized for trocar and needle placement (see Figure 19). For interventional assistance, an electromagnetic tracking system was applied and the sensor of the augmented reality system was fixed to the laparoscopic camera. The technical details of the navigation system, that is not part of this thesis, are described in [Scheuering, 2003].

The first trial to combine the individual liver anatomy and planning data with a navigation system for laparoscopic interventions in 2002 established the principal application of such a navigated intervention. Registration accuracy was limited due to the use of external landmarks and hardware limitations. Several improvements in hardware and software have been conducted since our first trial, improving accuracy and workflow for navigated open and minimally invasive liver surgery [Hansen et al., 2010b, Peterhans, 2010, Nicolau et al., 2011].

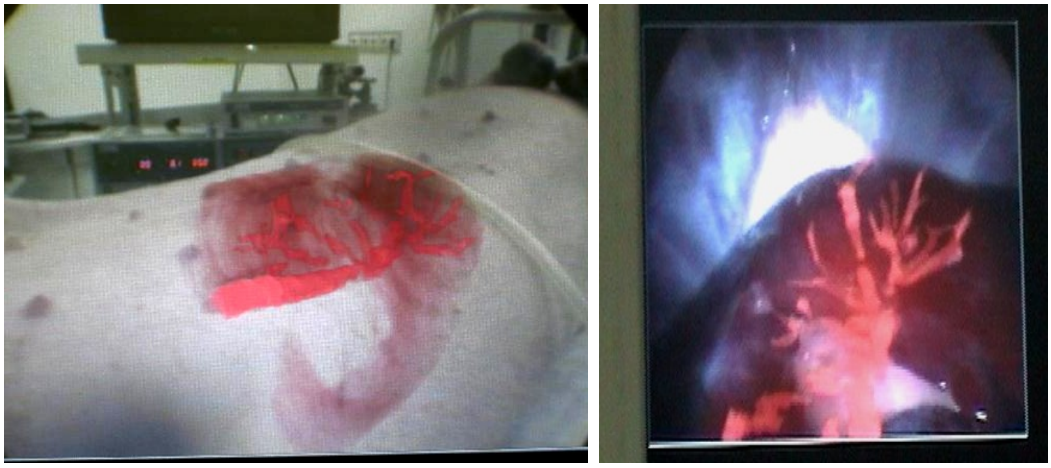

Figure 19: Integration of 3D planning data into the laparoscopic camera view in the year 2002. Left: The individual liver shape and portal vein of the swine are displayed in the view of the endoscope camera to support needle and trocar placement. Right: The laparoscopic view shows the real animal's liver inside the body cavity (red-brown structure lower half) combined with simple 3D renderings of the individual vascular structures extracted from CT data (bright red).

3.2.3 Measuring Cooling Effects in Thermal Ablation

Radiofrequency and other thermal ablation procedures are increasingly being used as an alternative therapy to liver resection. However, local recurrence after ablation of liver tumors in the proximity of major vessels was found, including a 36.5% recurrence rate for liver metastases after RFA [Mulier et al., 2005]. The main cause of recurrence is the cooling effect of adjacent liver vessels, which remove heat and thus preventing neighbored cells to reach adequate temperatures for destruction. Since thermal ablation is a minimally invasive technique, it is difficult to monitor the amount of tumor destruction during the treatment, and intraprocedural monitoring options in the daily clinical routine are limited. These factors motivated the development of computer-assistance for the planning and assessment of ablation procedures.

Fraunhofer MEVIS developed the first prototype to support thermal ablation procedures as early as 2002. In an interdisciplinary project with surgeons and radiologists of Campus Benjamin Franklin at the Charité and physicists of the institute LMTB in Berlin, we combined the individual 3D reconstruction of the patient's liver from radiological data [Schenk et al., 1999, Bourquain et al., 2002] with a numerical simulation of laser-induced thermotherapy (LITT) [Roggan et al., 2001]. The resulting software assistant allowed for the probe placement in 2D and 3D under consideration of the tumor location and the patient's liver vessel structures imported from the planning tool. A subsequent LITT simulation including the computation of vascular cooling effects allowed assessing tumor destruction

under different ablation parameters [Littmann et al., 2003a, Lehmann et al., 2003]. In a clinical study with six pigs, LITT lesions were induced in the neighborhood of major hepatic vessels in vivo. After explantation, the livers were cut into 2mm slices perpendicular to the probe axis and digitally photographed. The volumes of the simulated lesions and the real lesions (computed from manually drawn contours on the photographs) were compared. The analysis showed good correlation with a sensitivity of 0.90 and a specifity of 0.86. Details of the study and the results are given in [Lehmann et al., 2011].

The analysis of the heat sink effect in LITT lesions showed an important phenomen: cooling by the portal triad (portal vein, artery and bile duct) was much stronger than that of the hepatic veins. Lesions influenced by the cooling of the portal field were *flattened* on the vessel side in all 28 cases, while hepatic veins indented the lesion (*indentation*) by their heat sink effect in 31 cases, or were even encased by the ablation zone (*inclusion*, 6 lesions) [Frericks et al., 2008]. Figure 20 illustrates the different heat sink effects.

The observation of this important effect, which should be considered when ablating a lesion near a larger vessel, motivated the development of a measurement tool for additional, more detailed analyses. The developed software application allowed quantifying the size and shape of thermal lesions in digital photographs, for a characterization of the heat sink effect by angle measurements and detailed quantification of the vessel surrounding area [Schenk et al., 2008a].

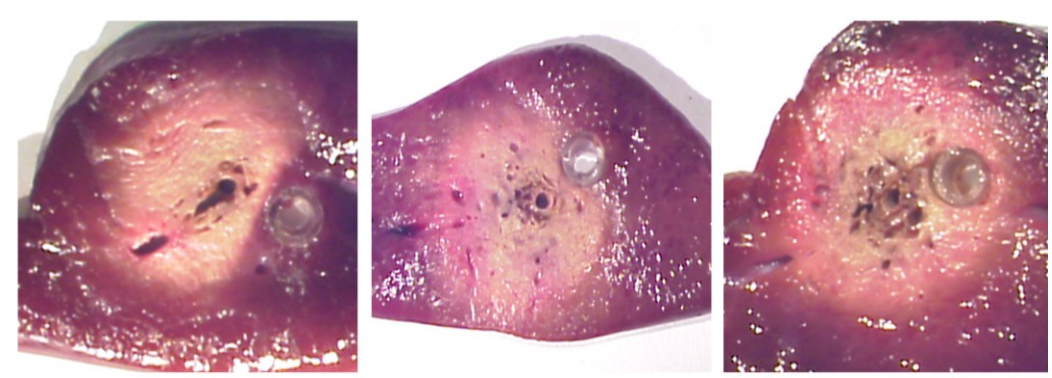

Figure 20: Different types of heat sink effects in RFA analyzed in an ex-vivo experiment with pig livers. Heat is induced from the RFA applicator position (small ring centrally in each image) induces heat, and the liver parenchyma coagulated (yellow to bright red tissue). The vascular cooling effect simulated by perfused glass tubes (larger ring) differs depending on factors such as distance between cylinder diameter, distance to applicator and flow velocity. *Flattened* lesions (left) resulted from a stronger cooling effect than the *indented* lesions (middle), whereas the cooling of *included* real or simulated vessels was weak during ablation (right). Images courtesy of B.F. Frericks and K. Lehmann, Charité Berlin.

After the initial LITT project, further research focused on RFA, following the clinical trend towards this ablation method. Here, different blood flow parameters were evaluated for their cooling effects during ablation. In an ex-situ study, vascular structures were simulated by glass tubes with different diameter and varying distances to the applicator. Blood circulation was simulated by internal water and different flow velocities were achieved with an attached pump. Our measurement tool was applied to more than 400 lesions and the lesion deformation defined by the expert on digital photographs was compared to the automatic characterization of the software. The agreement with the expert definition was above 96% for indented and flatted lesions and 100% for lesion with vessel inclusions [Schenk et al., 2008a].

The evaluation of the cooling effect for the different study parameters showed the following results [Lehmann et al., 2009]: The distance between applicator and vessel model (5mm and 10mm) appeared to be the most important parameter with strong differences between the two distances. The vessel diameter (5, 8, and 10mm) showed a trend towards increased cooling with larger diameter, but the differences were not significant in the study. Lesions at 5mm applicator-to-vessel distance showed local cooling effect with a radial reduction of 50.6% on the vessel side independent of the flow volume. We found no significant differences between six different flow volumes (between 250 and 1,800 ml/min) covering the range that can be measured in hepatic blood vessels. The results support the conclusion that the blood flow rate in the measured range has essentially no influence on the ablation result.

This study and the more recent joint projects with the clinical partners from the Charité, Benjamin Franklin, were dedicated to RFA. A new numerical simulation of the ablation was investigated by Fraunhofer MEVIS and considered three biophysical RFA processes: First, the delivery of energy to the tissue via the alternating electric current, second, the generation of heat, its diffusion, and the cooling through blood flow and perfusion, and third, the denaturation of proteins in the tissue cells by the heat [Preusser et al., 2005]. Mathematical models consisting of partial differential equations, integral equations, and algebraic equations describe these biophysical processes. Details of the numerical implementation and parameter identification are given in [Kroeger et al., 2006, Paetz et al., 2009, Tiesler, 2011]. The numerical simulation is embedded in MeVis SAFIR, a software assistant that supports ablation planning and comparing lesion, numerical simulation, and postinterventional data.

Recent developments to support ablation procedures were performed by the *Modeling and Simulation* group at Fraunhofer MeVis and include the optimization of applicator position to consider lesion size, shape, and the cooling effect of nearby vessels [Altrogge et al., 2007, Kroeger et al., 2010b, Altrogge et al., 2012] and anatomical constraints [Haase et al., 2012], a fast estimation of the ablation zone for interactive use [Kroeger et al., 2010a, Rieder et al., 2011], and the postopera-

tive assessment after registration of pre- and post-interventional CT data [Rieder et al., 2010, Rieder et al., 2012]. An overview of algorithms and related approaches for computer-assistance in radiofrequency ablation for liver tumors was given in [Schumann et al., 2010].

3.2.4 Interactive Risk Analysis for Liver Surgery

As described in Section 3.2.1, risk analysis for liver surgery is performed stepwise. After segmenting liver and vessels, the vascular territories were computed, followed by a virtual resection using liver and vessel visualizations. Finally, the resection plan was combined with the vascular territories, and the risk of truncated vessel branches with the related perfusion impairments was quantified and visualized. Due to this stepwise procedure, the user was forced to define and modify the virtual resection without any direct feedback about the perfusion-related risks induced by the current cutting line. Thus, a resection had to be determined based on the user's experience and expertise, or by repeating of virtual resection and risk analysis. To improve this procedure and to allow directly risk-related resections the so-called *interactive risk analysis* was developed. This application provides interactive definition and modification of a virtual resection including feedback about the risks of the resection plan almost in real-time.

The development of the interactive risk analysis was challenging for two reasons. First, the risk factors for a resection had to be defined to allow quantitative measurements. Second, the enormous amount of information included in different data structures had to be converted into a form that enables fast access and updates with every modification of the resection. The following risk factors were defined and integrated into the computation of a global resection score:

- Remnant volume
- Safety margin
- Supplied volume of the remnant
- Drained volume of the remnant
- Resection surface area
- Curvature of the resection surface

The single risk scores were normalized to values between 0 and 1 according to predefined boundary values, e.g. a minimal remnant volume of 30% of total liver volume is set to a score of 0. The overall resection score was computed as a weighted sum of the individual risk scores. Predefined boundary values and weights for the single risk factors were determined after discussions with liver surgeons, leading to different default values for HCCs and liver metastases. Both our previous experience in surgical planning and interviews with the surgeons yielded that an individual parametrization of risk factors remains necessary for users and for individual patients with pre-existing liver disease. Parameters for the

single risk factor and the computation of the resection score were presented in [Demedts et al., 2010]. The application GUI is shown in Figure 21.

The implementation of the new resection tool required the development of a new data structure that could quickly compute all single risk factors and the overall resection score. A 3D byte array was implemented that stored the precomputed, pixel-based risk information, such as portal and hepatic vein branch relations and tumor distance, and provides the flags for fast updating resection-related risks as the current supply and drainage status of each single image voxel. For implementation details see [Demedts, 2010].

The interactive risk analysis has been evaluated in a small user study with two radiological technicians at MeVis who are experts in resection planning. The resection line was first defined using the existing virtual resection tool [Konrad-Verse et al., 2004] and several days later, with the new interactive risk analysis application. The two resection proposals for each patient were compared in terms of quality (measured by the resection score) and time.

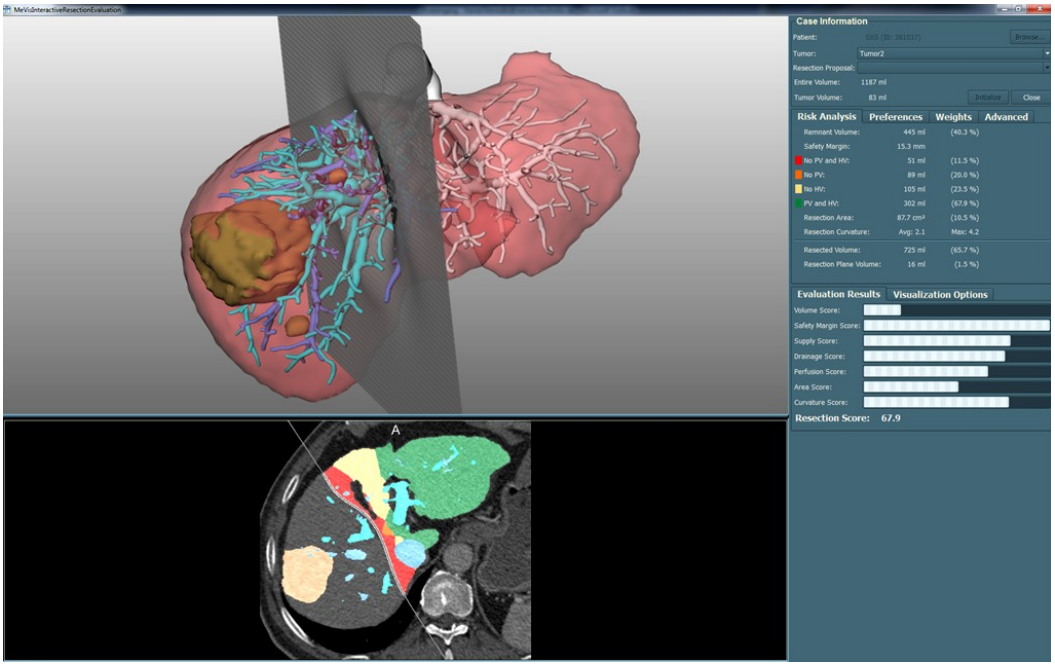

Figure 21: Snapshot of the *Interactive Risk Analysis* application with a preliminary GUI. In the 3D viewer (upper left) and 2D viewer (lower left) the resection line can be defined and modified. On the right side of the GUI, the user can choose presetting or individual parameters for the risk factors (such as minimal remnant volume). Risk values for the current resection were given in absolute values and as scores between 0 and 100, visualized as white bars. The risk areas for perfusion are displayed as colored overlay in the 2D viewer: full perfused (safe) remnant tissue in green, outflow obstructed areas in yellow, and regions without supply and drainage in red. In this case, a hemihepatectomy right including the red areas would improve the resection score but the user had to check for the drainage of territory 4 (yellow) that is at risk with the current resection line.

The evaluation showed that the quality improved and led to more accurate safety margins with the new tool at the cost of slightly increased time requirements. Due to the presentation of additional risk information and the demand to find an optimal resection, the users took more time than with the conventional approach. A clinical evaluation with further user groups (such as surgeons) is asubject of future research.

A second motivation for developing a risk function was automatic creation of optimal resection proposals. Manually defined or automatically initialized resections have to be optimized with respect to a quality function. For the interactive risk analysis, we developed the resection score as a first version of such a quality function. Parallel to this work, a first approach for the determination of automated resection proposals for standard and local resections had been developed [Hansen et al., 2010a]. The combination of these two approaches is the starting point for the automated creation of optimal resection proposals in a future project.

3.2.5 Summary

The first attempts to support hepatic interventions by software, were characterized by technically demanding tools and a workflow that was not dedicated for clinical use. Our first liver application that included the necessary basic steps for the analysis of abdominal CT data and the planning of liver surgery was the first comprehensive tool for clinical use. A second important step, the transfer from the individual liver model into the real interventional situation was tested on an animal and shown in 2002. The organ and vascular structures were extracted from CT data and overlaid as volume renderings in the endoscopic camera view during the intervention. Our approach was the first published navigated abdominal laparoscopy to combine individual 3D planning data and an augmented reality system.
Further work focused on computer-assistance for thermal ablations, for which cooling effects of the vascular structures can reduce the coagulation zone and lead to incomplete tumor destruction. Numerical models and dedicated algorithms to support ablation planning and postoperative lesion assessment have been developed and integrated into a software assistant. In research projects with clinical partners from the Charité Berlin, the methods were discussed, tested, and evaluated. To quantify heat sink effects in ex-situ studies, a measurement tool was developed to assess the size and shape of a lesion and to quantify the influence of vascular cooling.

> **Publications**: The software assistant HepaVision was presented at the congress of the German Radiological Society and during a talk at BVM in 1999 [Schenk et al., 1999]. We performed the first application of 3D planning information for abdominal laparascopy with Michael Scheuering and co-workers, and the work was presented at SPIE in

San Diego [Scheuering et al., 2003]. Subsequent developments in computer-assistance for liver surgery at MeVis up to 2007 were given in a comprehensive overview [Schenk et al., 2008b], and recent work was summarized in a special issue of IEEE Pulse for image-guided therapies [Schenk et al., 2011].

Developments to support thermal ablation planning began with a joint project with clinical partners from the Charité and LMTB in Berlin. The first prototype was implemented by Arne Littmann using dedicated visualization techniques [Preim et al., 2003]. It was presented in 2003 at BVM [Littmann et al., 2003b] and by our clinical partners at CURAC [Lehmann et al., 2003]. The software was evaluated in animal studies by Bernd Frericks, Kai Lehman, and Charité co-workers [Lehmann et al., 2008, Frericks et al., 2008, Lehmann et al., 2011]. The measurement tool for the quantification of cooling effects in thermal lesions was implemented together with Andreas Weihusen and was later extended by Christian Rieder. The tool was evaluated on 400 ex-vivo lesions [Schenk et al., 2008a] and used to quantify heat sink effects in RFA lesion in an ex-vivo study [Lehmann et al., 2009]. Numerical RFA modeling developed in this project [Kroeger et al., 2010a] was later extended by members of the Modeling and Simulation group at Fraunhofer MEVIS.

The interactive risk analysis was implemented by Daniel Demedts during his master thesis (supervised by the author) [Demedts, 2010]. The software was evaluated in an in-house study, and the algorithm and results were presented at CURAC [Demedts et al., 2010].

3.3 Adult Living Donor Liver Transplantation

MAN: Hello. Can we have your liver?
MR. BROWN: My what?
MAN: Your liver. It's a large, eh, glandular organ in your abdomen.
MAN: You know, it's, -- it's reddish-brown. It's sort of ,--
MR. BROWN: Yeah, yeah, I know what it is, but... I'm using it, eh.
...
Monty Python's Meaning of Life,
Live Organ Transplant, 1983

For surgeons, the main considerations during preoperative planning for ALDLT include:

- Precise prediction of anatomical and functional volumes of both graft and remnant livers
- Deciding whether to use the right or left hemiliver as a graft
- Including the MHV in the graft or retaining it in the remnant liver
- The appropriate type of venous outflow reconstruction.

To support these decisions, there are two major issues for computer-assistance for ALDLT planning: first, the precise segmentation and visualization of the individual vascular liver anatomy including anomalies, and second, a virtual resection planning tool for computing vascular territories, areas of potential outflow obstruction and related volumes in both remnant and graft livers.

3.3.1 Vascular Anatomy and Risks

For ALDLT, the liver is divided centrally, typically partitioning the portal vein near its main bifurcation and following the main course of the hepatic vein from the confluence to the gall bladder fossa, as illustrated in Figure 11.

Common anomalies of the **portal vein** are trifurcations with an incidence of 11% (see example in Figure 22), and H-shaped main ramifications found in about 10% of individuals [Koc et al., 2007]. Although these variants are important for the surgeon to know, they do not contraindicate donation [Fan et al., 2011]. Further important variants of the PV are branches that cross the resection line, e.g., territory 5 or 8 portal veins that arise from the left main branch of the portal vein.

For the **hepatic vein** system, existing inferior veins arising directly from the inferior vena cava (cf. Figure 22) should be known to the surgeon in right graft donation, because these veins are resected and have to be reconnected in the recipient if they drain a relevant territory. Radtke showed that the incidence of inferior veins in donor livers was about 50% in Western donors [Radtke et al., 2006b], and Bourquain and Hindennach found that the volume drained by theses veins is different in Western and Eastern individuals [Hindennach et al., 2006]. The dilemma of the MHV for ALDLT and the related outflow obstruction (see sections 2.2.3 and 3.3.2) is a major issue for preoperative planning. Venous outflow obstruction

can lead to compromised function and reduced local regeneration. In cases with limited functional liver volume, such impairment is frequently associated with the small-for-size syndrome (SFSS), a serious clinical complication that may lead to liver failure [Radtke et al., 2011, Tanaka and Ogura, 2004]. A topic of ongoing discussion includes whether to retain the MHV in the donor remnant to expose the healthy voluntary person to no additional risks or to include the MHV in the graft to guarantee a full functionally organ for the diseased recipient. The decision is often based on the surgeon's preference, but recently there has been a trend towards computer-assisted decision making to include MHV risk analysis (see next section).

The **hepatic artery** (HA) is a vessel structure with several variants that may be a risk factor in ALDLT. For example, in one of our studies with the Medical School Hannover, arterial variants were found in about 40% of potential donors [Frericks et al., 2004b]. Critical arteries are those that cross the resection line, e.g., arteries that supply territory 4. These arteries can originate from different sides, either from right or left but dual supply from both hemilivers is also possible. This inflow must be protected to prevent arterial occlusion and loss of the territory. A second arterial issue is the number of arterial branches supplying the graft that have to be reconnected to the arterial system in the recipient. Two or more arteries may lead to technical difficulties during anastomosis due to smaller diameters with an increasing number of arteries. With decreasing diameter, it is also hardly possible to detect beneficial intrahepatic communications in the radiological images [Fan et al., 2011].

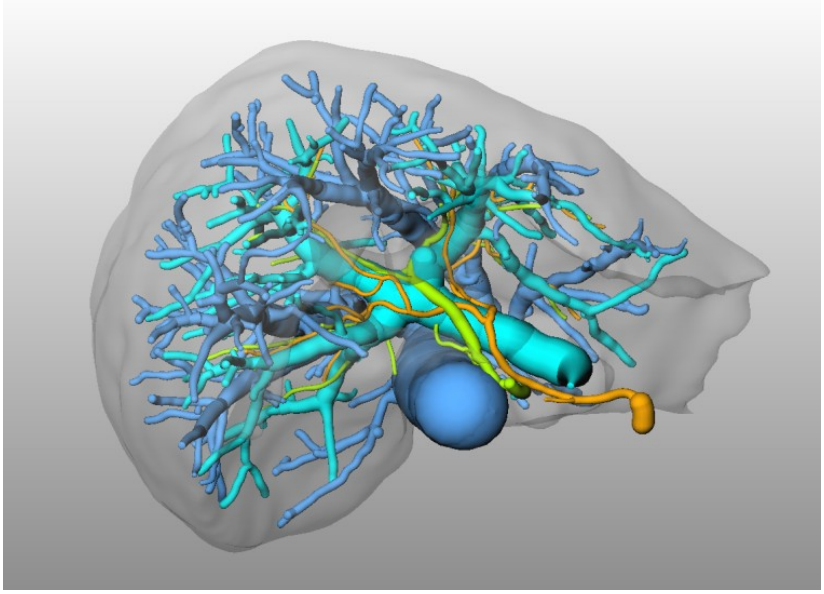

Figure 22: Vascular structures extracted from CT data. Hepatic artery (orange) and bile ducts (green) twine around the portal vein (cyan). The hepatic veins (blue) reach between the branches of the portal vein as the fingers from one hand between the fingers of the other hand. This patient has an inferior vein (small blue branch at the lower image border) and a variant of the portal vein, a trifurcation (image center).

In our first research project for the computer-assisted planning of LDLT with the Medical School Hannover, the CT data had a slice thickness of 2mm in the best cases, limiting the segmentation of finer structures and segmental branches of arteries [Frericks et al., 2004b, Schenk et al., 2002]. The anatomical evaluation of 56 potential donors showed that a region-growing based segmentation of the hepatic arteries including the second-order branches was possible in 46 of 56 cases. With new CT scanner generations, current image resolution has reached a pixel size of 0.75mm or less, and the segmentation of arteries up to segmental level is possible for most donor cases with correct timing during CT acquisition or if bolus tracking is applied.

Bile ducts are the reason for a majority of complications after surgery and transplantation [Fan et al., 2011, Radtke et al., 2008b]. Preoperative imaging of these small vessel structures requires an additional contrast agent for CT, which can cause allergic reactions and often prevents use in donors and patients [Fan et al., 2011]. Alternative imaging methods are intraoperative cholangiography performed in most centers for bile duct visualization during intervention, endoscopic retrograde cholangiopancreatography (ERCP) with a high complication rate, or MRCP, which typically shows only the main bifurcation due to the low spatial resolution. Recently, the combination of hepatocyte specific contrast agents with high resolution MRI sequences was introduced [Asbach et al., 2008]. Image acquisition requires dedicated radiological techniques and is therefore an issue of current research (see Section 0). A summary of methods for bile duct imaging including our results on MRI data is given in [Ketelsen et al., 2008]. In our research project with the University Hospital Essen, the anatomy of bile ducts in donors was studied in detail to develp a classification of hilar and segmental biliary anatomy [Radtke et al., 2008b, Radtke et al., 2008a, Radtke et al., 2009].

In our first ALDLT study, begun in 1998 with the Medical School Hannover, 27 of the 56 potential donors were excluded from LDLT based on the results of the preoperative evaluation [Frericks et al., 2004b]. For only one case was a vascular variation (of the HA) the reason for the exclusion, while in all other cases, the donors were excluded due to inadequate functional volume of the remaining liver or the liver graft. A similar distribution in the exclusion criteria was found in our study with the University Hospital Essen, which was part of the *Optimization of Living Related Liver Transplantation* clinical research group. Here, 73% of potential donors (99 of 135) were excluded from donation, the majority (96 donors) due to insufficient functional liver volume [Radtke et al., 2006a]. Both observations show the importance of the second criterion, the functional liver volume.

In conclusion, anatomical variations typically do no prevent donation, but are very important before surgery when choosing an adequate resection strategy and avoiding complications. The main exclusion criteria, the functional remnant or graft volume, will be discussed in the next section.

3.3.2 Liver Volume and Outflow Obstruction

A remaining liver volume of 35% for healthy donor remnants and a graft providing 40% of the ESLV calculated by formulas, or 1.0% of the body weight of the recipient, is believed to be safe for ALDLT [Asakuma et al., 2007, Fan et al., 2011]. The risks when these volumes cannot be met are the small-for-size syndrome and the loss of the graft or liver failure in the donor [Kiuchi et al., 1999]. Thus, preoperative estimation of graft and remnant volumes is mandatory for ALDLT.

Unfortunately, the overall volume of the partial livers is not sufficient to consider all risks. Due to resection near the MHV in ALDLT, branches of this vein are truncated and the drainage and related liver function may be further decreased. The anatomical background for this risk of venous congestion is induced by the mismatch of portal vein territories (PVT) and hepatic vein territories (HVT): The boundaries of PVT typically do not run parallel to the borders of the HVT (see Figure 23 and Figure 24). An exception is the borderline between left lateral territories (PVT 2 and 3) and the large right liver lobe that are anatomically more separated (cf. Section 2.2.1). When planning an ALDLT resection, the inflow is considered first, and, thus, the cutting line typically follows the boundaries of the PVTs. In doing so, HVT and related HV branches will be truncated, resulting in an area of outflow obstruction. On the other hand, following the course of the HVT for resection cannot solve this problem because it will cause even more severe problems of insufficient inflow.

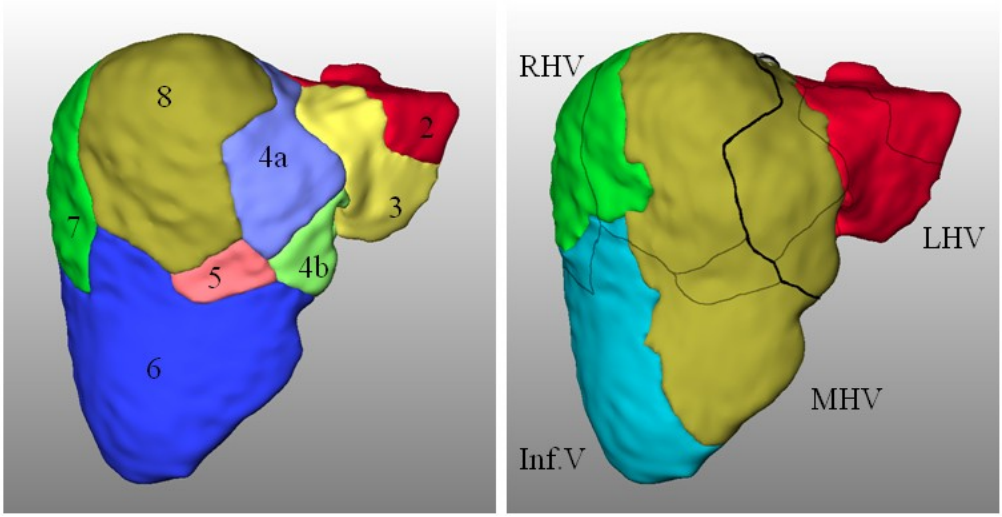

Figure 23: Mismatch between portal vein territories and hepatic vein territories. The images show the PVTs (left) and the HVTs (right) with dark lines illustrating the PVT boundaries and the mismatch between the territories. The black line in the middle of the MHV territory indicates the border between right and left hemilivers (defined by the PVT 1-4 and 5-8 respectively), and thus the zone where the donor liver will be typically divided.

With the software assistant HepaVision, our clinical partners in Hannover and Essen retrospectively evaluated the data of donor livers for which a SFSS in the recipient led to graft loss and for which the patients had to be retransplanted (three patients in both institutions). In Hannover, no venous reconstruction of MHV tributaries in the graft was performed in the very early cases. In all donor livers, the area drained by truncated MHV branches was at least 20% of the graft volume (20%, 29%, 41%) [Frericks et al., 2006]. In Essen, three of the first 23 recipients in a preliminary study, for which the MHV was not included in the graft, sustained a SFSS with liver failure. In these cases, the area of venous congestion estimated by the software was 36% and higher (36%, 38%, 39%) [Radtke et al., 2010].

The importance for the early postoperative phase after the transplantation was also shown by our clinical partners in Nagoya. Kamei and colleagues compared preoperatively computed anatomical and functional graft volumes with postoperative liver function parameters and concluded that only the functional (non-congested) graft volume correlates to early graft function [Kamei et al., 2007].

The territories of potential outflow obstruction can be computed by combining the virtual remnant or graft with the MHV territories computed by the methods described in Section 2.2.3 and Section 3.2.1 [Bourquain et al., 2003, Schenk et al., 2007]. Depending on the decision whether the MHV will remain in the remnant liver or will be included in the graft, these risk territories are located on the right or left side of the donor liver (see Figure 24).

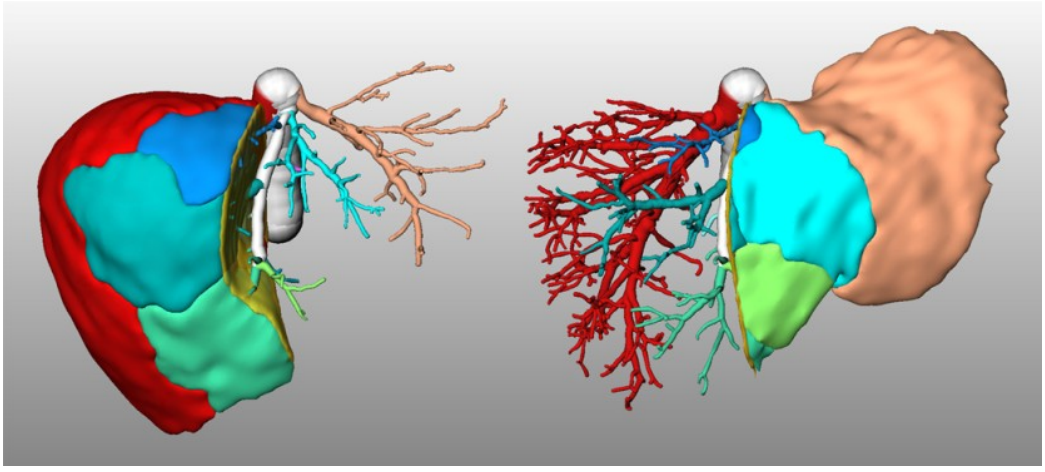

Figure 24: Risk analysis for ALDLT for two variants of virtual resections. The left image shows a right lobe graft. With this resection the MHV will be retained with the remnant (left hemiliver) and three branches of the MHV will be transected. The dependent territories (blue, cyan, green) are at risk of insufficient drainage and will decrease the postoperative graft function when not anastomosed in the recipient. The right image illustrates the remnant liver when the MHV is included in the graft. The related risk analysis shows small regions with potential outflow obstruction (green territories) and a safe territory of a separate vein branch draining segment 4a (cyan). In this example, the MHV was included in the graft (right variant).

The potential to compute the risk of venous congestion in ALDLT with the algorithms developed by MeVis was immediately recognized by Prof. Koichi Tanaka and his team in October 2002 when the two groups first met. Prof. Tanaka, the leading LDLT surgeon at that time, used the method for every ALDLT thereafter. The fundamental change in ALDLT planning at the Kyoto University was described in [Asakuma et al., 2007]:

> *'Before the introduction of 3D-CT volumetry, MHV regional volume was subjectively and qualitatively estimated using conventional 2D-CT. Thus, the issue of potential congestion remained unresolved. With the introduction of 3D-CT simulation with MeVis software, however, the situation has changed dramatically. When this software was first developed, the major aim was to carry out portal vein volumetry. As the team at Kyoto University Hospital was dealing with the problem of right-lobe graft congestion in LDLT at that time, we proposed that this software be used for regional hepatic venous volumetry; our team and the MeVis group then collaborated on this project. Regional volumetry enables us to objectively assess graft selection by introducing an algorithm based on the concept of hepatic dominancy. Using this method, it is easy to objectively select the type of right-lobe graft needed. With step-by-step improvement of the software, it is possible for us to not only evaluate regional venous volumetry but also to visualize hepatic venous construction. This information benefits the surgeon by enabling preoperative prediction of the kinds of vessels that are likely to appear at the parenchymal transection line.'*

The only other group that developed an approach for the computation of outflow obstructed territories in ALDLT in those early years was the team of Prof. Sung-Gyu Lee at the Asan Medical Center in Seoul. Based on manual delineation of MHV territories in 2D CT images slices by an expert, they estimated the venous congestion for right lobe grafts [Hwang et al., 2006].

On the basis of our risk analysis for ALDLT, the transplantation centers in Kyoto and Essen were able to develop new decision algorithms for ALDLT. With these algorithms, surgeons decide whether the MHV will be included in the right lobe graft (Figure 25) [Asakuma et al., 2007], or if MHV tributaries have to be reconstructed [Radtke et al., 2010]. Furthermore, the 3D analyses enabled the development of a new dominancy concept for hepatic veins with respect to the whole liver and to the right and left hemilivers [Radtke et al., 2005, Radtke et al., 2006b, Asakuma et al., 2007].

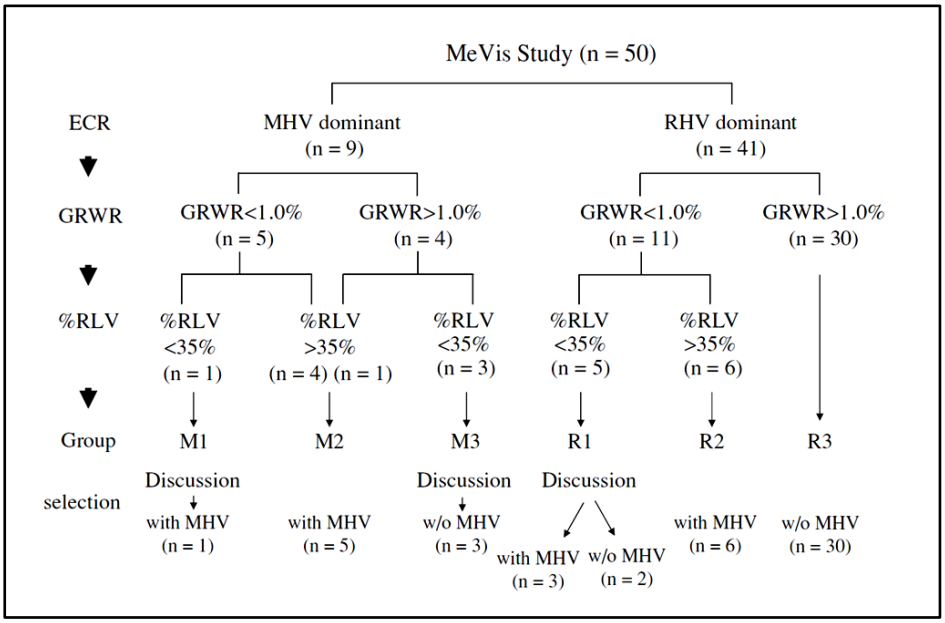

Figure 25: Decision tree about MHV inclusion in right graft donation in ALDLT developed at the University Hospital Kyoto [Asakuma et al., 2007]. Depending on three criteria, the decision to include the MHV in the graft or keep it with the remnant liver is made: 1) the amount of estimated congested volume in territories 5 and 8 (ECR), 2) the graft-to-recipient weight ratio (GRWR), and 3) the remnant liver volume ratio of the total donor liver volume (%RLV). Grafts are defined to be 'MHV dominant' if the estimated congestion ratio (ECR) is above 40% of the graft volume, otherwise it is a 'RHV dominant' graft.

3.3.3 Liver Regeneration in Donor and Recipient

In 2002, Maema found that right lobe grafts with partial outflow disturbances are associated with latent disadvantages in postoperative liver volume regeneration [Maema et al., 2002]. At that time, there was no systematic morphologic regeneration study assessing the individual local liver growth and quantitatively comparing it to areas with outflow obstruction. Furthermore, the growth of vascular structures after resection was not investigated, although the postoperative vascular situation could be an important factor for the patient and thus influencing the surgical strategy. We investigated these and related issues in a liver regeneration project together with the University Hospital Essen by studying the hepatic growth in donors and recipients after ALDLT.

In our study, preoperative abdominal CT images of the donor were acquired and both donor and recipient were scheduled to be scanned at day 7 to 10, as well as three, six, and twelve months after surgery. These scans where performed if the patient condition and compliance allowed.

Algorithms to register the different time phases and an application to evaluate local growth in tissue and vessels were developed [Hindennach et al., 2007, Lohe, 2007, Metzen et al., 2009]. Automatic tree matching algorithms were developed but could not successfully register the growing vessels with different image positions in the follow-up data, changing length and thickness, and a varying number of bifurcations depending on image quality and contrast. Therefore, we interactively transferred the classification for PV and HV systems interactively from one time to the next after application of a rigid registration (Figure 27). Later, a landmark-based registration approach was developed, matching the data by a non-rigid transformation and allowing for a more exact alignment of vascular branches. We utilized this method to combine the area of potential venous congestion with the PV territories in the remnant and computed the estimated ratio of outflow obstruction for each territory and the local regeneration rate (illustrated in Figure 26).

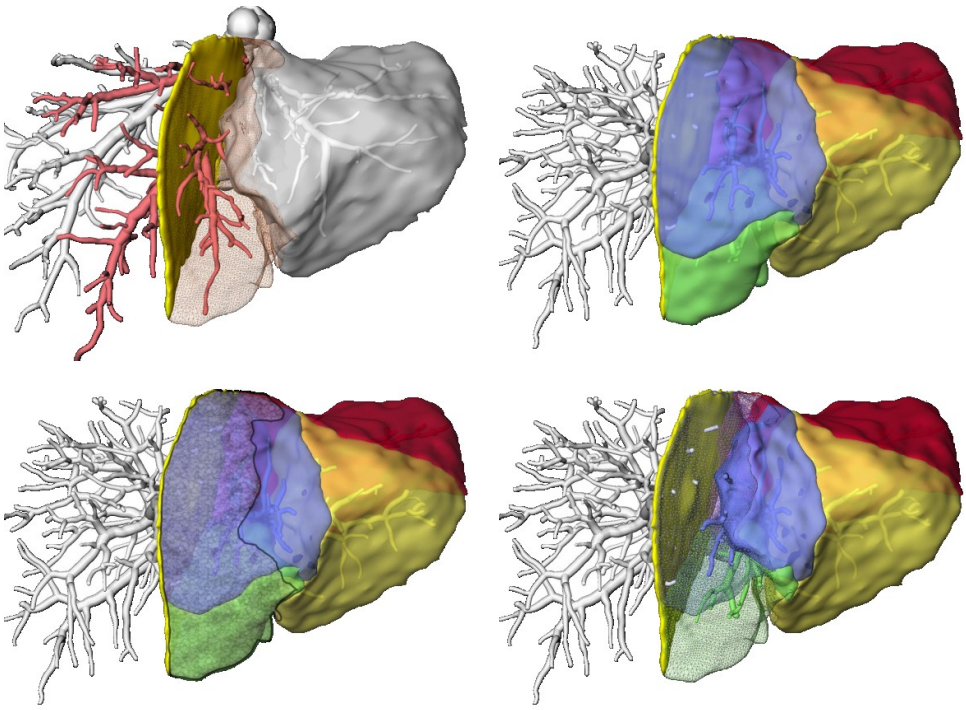

Figure 26: Determination of local outflow obstruction in PV territories. The analysis of preoperative drainage (upper left), shown here with HV, resection line (yellow), LHV territories (white), and truncated MHV territories (light red), is combined with the portal vein segments (upper right). Subsequently, the ratio of potential outflow obstruction in each segment can be computed (lower left) and the outflow obstruction in the single PV territories can be visualized (lower right).

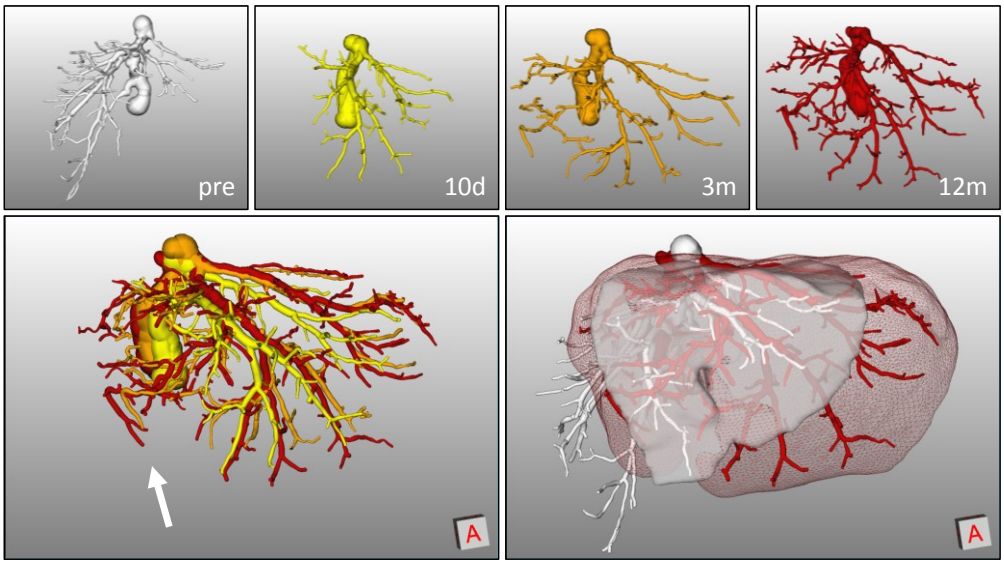

Figure 27: Registration of vascular structures from different time points during regeneration. The upper row shows the HV extracted from the preoperative scan, day 10, tree months, and twelve months after surgery (from left to right). In this donor, collaterals can be found in CT data three and twelve months after transplantation but not in the first postoperative scan (missing yellow branches in the lower left image, arrow). The lower row shows registered postoperative vessels (left) and a comparison of the remnant surface before operation (white) and twelve month after operation (red), illustrating the growth and organ rotation in the abdomen (right).

The CT scans of 25 donors and eight recipients could be evaluated at all time points. We analyzed all single time points (cf. Section 2.2.5 and Section 3.2.1), matched the data of the different time points by registration and compared the growth of the liver with respect to several issues. The main results of the evaluation were [Schenk et al., 2009]:

- **Overall growth of the remnant and graft liver**
  The organ growth measured on the basis of CT data differs between grafts and remnant livers (Figure 28). In the donors, almost double the remnant volume within the first three postoperative months could be observed, from 34% to 77% of total liver volume. After one year, the donor remnant livers reached 86.5% of the original tissue amount (cf. Figure 29). In the recipients, the maximal volume in the postoperative course was found at the first time point of our follow-up data. Due to the inflammatory processes and the swelling of the implanted organ, this volume represents more than the liver regeneration. At the following time points, the liver volume decreases again. The majority of volume growth in donors and recipients was found in the first few days after surgery.

- **Local remnant growth in relation to the MHV**
  The overall volume of remnant livers, including the MHV after 12 months was comparable to the volume of livers without this draining vein. At the first time point, the growths of hemilivers without MHV were not much different from those that included the vein when normalized to the initial remnant volume. Afterwards, the remnants with retained MHV showed a minor advantage, which equalized until almost full recovery after twelve months. Our study data was very limited with only four remnants including the full MHV drainage, but similar result were found by other groups [Scatton et al., 2004, Zappa et al., 2009].
  The left lateral territories (2 and 3), which were not impaired by the resection, showed increased growth compared to that of territory 4 for all cases, and this difference was larger when the MHV was not retained with the remnant liver. This result leads to the conclusion that territories 2 and 3 are able to adjust the reduced growth of territory 4.

- **Local growth and outflow obstruction**
  Using the methods described above, we evaluated the local growth of territory 4 with different outflow obstruction rates in the regions of territory 4a and 4b. The results showed that the ratio of outflow obstruction is negatively correlated to the local regeneration. It also demonstrated the successful surgical strategy to maintain the outflow of territory 4a by preserving smaller and median hepatic veins arising from the MHV or LHV and draining this territory. Territories 4b, typically with a bad prognosis of high congestion rate, showed very low regeneration rates and disappearing in some cases (cf. Figure 30).

- **Development of collaterals**
  In our study, we found no collaterals in the donor remnant between truncated branches of the MHV and the LHV in the first CT data after transplantation, but these collaterals were clearly visible in 60% of donors after three months and in the later images. The remnants with collateral formation had a higher rate of outflow obstruction than those without collaterals (31.3% ± 8.1% versus 20.7% ± 8.9%).
  In 13 of the 21 remnants without MHV, revascularization of territory 4b veins was detectable in CT images three months after surgery. The collaterals were connected to a retained MHV4a branch, to LHV4a branches, or to branches of the LHV originally draining only the left lateral lobe before surgery. Example cases with collateral formation are illustrated in Figure 29 and Figure 31.

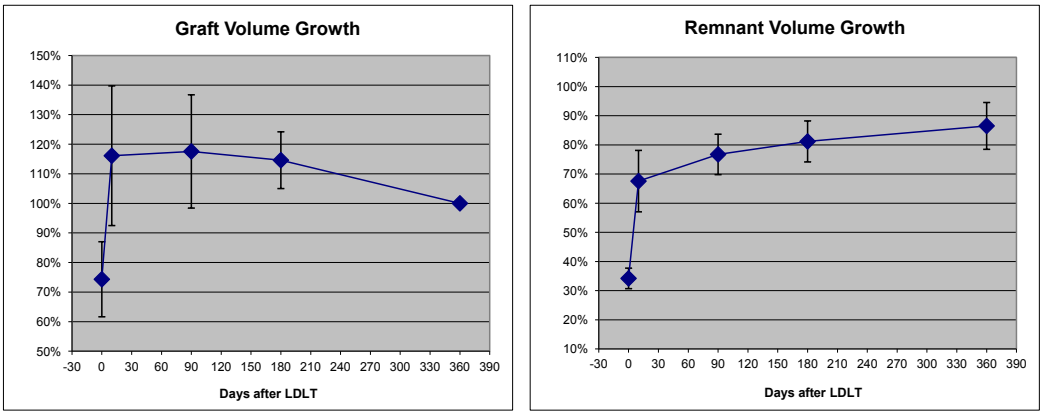

Figure 28: Regeneration in recipient and donor. The curves show the growth of graft livers in eight recipients (left) and the growth of remnant livers in 21 donors (right). Grafts were normalized to the volume after 12 months due to the unknown original liver volume in the recipient. The curves show the initial high increase of regeneration and swelling that is more prominent in the recipients due to immune reaction and inflammatory processes.

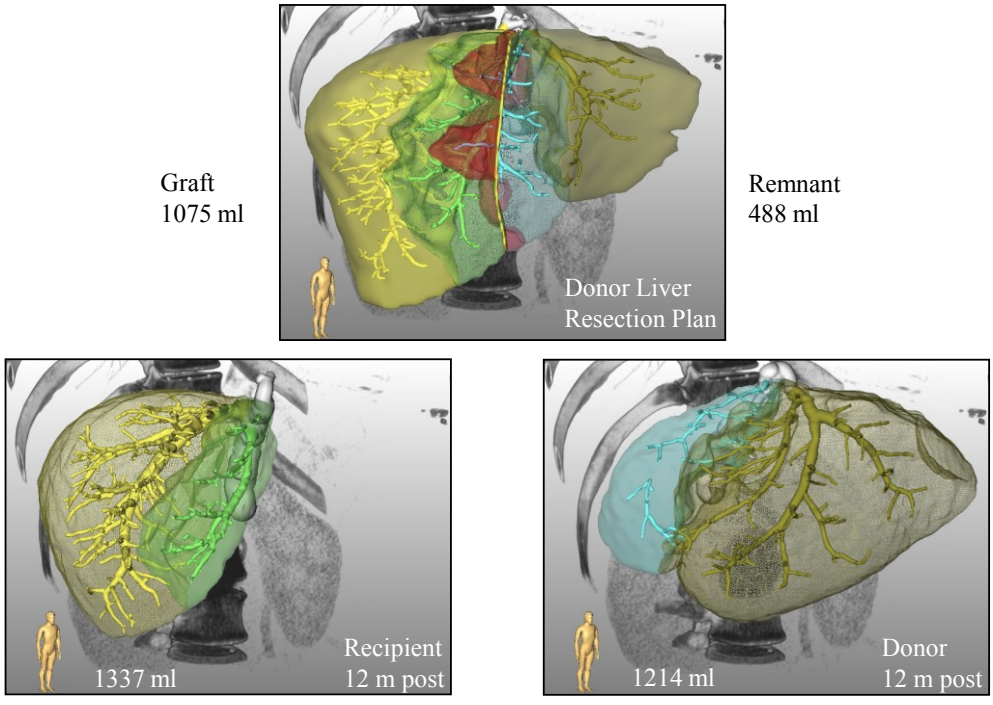

Figure 29: Regeneration in recipient and donor. The preoperative donor liver (upper row) is divided near the MHV (resection line in yellow) with an estimated graft volume of 1075 ml and a remnant liver volume of 488 ml. The graft growths within twelve months to 1337 ml, while the small remnant liver regenerates to 1214 ml. Collaterals can be seen in this donor liver (lower left image, between cyan and dark yellow branches).

Our results show that venous congestion in territories with truncated hepatic vein branches leads to reduced local regeneration. Those areas have a growth deficit which is partially compensated by increased growth of the uncongested remnant region. Collaterals between truncated MHV veins and intact neighboring veins were not visible in the first scans and seem to develop over the first days and weeks after surgery. This results contradicts the hypothesis that pre-existing communication between hepatic veins exists that will prevent venous congestion. In ultrasound examinations, such connections can be found in some patients, but they are small and cannot take over the MHV drainage immediately after occlusion of the vein [Fan et al., 2011]. For example, the first study of Kaneko and colleagues [Kaneko et al., 2000] found that the flow signal in the veins of territory 5 and 8 of a right lobe graft without MHV was obvious no earlier than postoperative day six after implantation. In 2005, the same group showed, that five of 28 MHV tributaries (territory 5 and 8 veins) were connected to the RHV on the first post-OP day, and ten further collaterals were found between post-OP days 2 and 7, while the remaining 50% of all connecting veins were later detected, after the first week [Kaneko et al., 2005]. In conclusion, single intrahepatic venous collateral develop but cannot compensate the outflow obstruction in the critical first postoperative days.

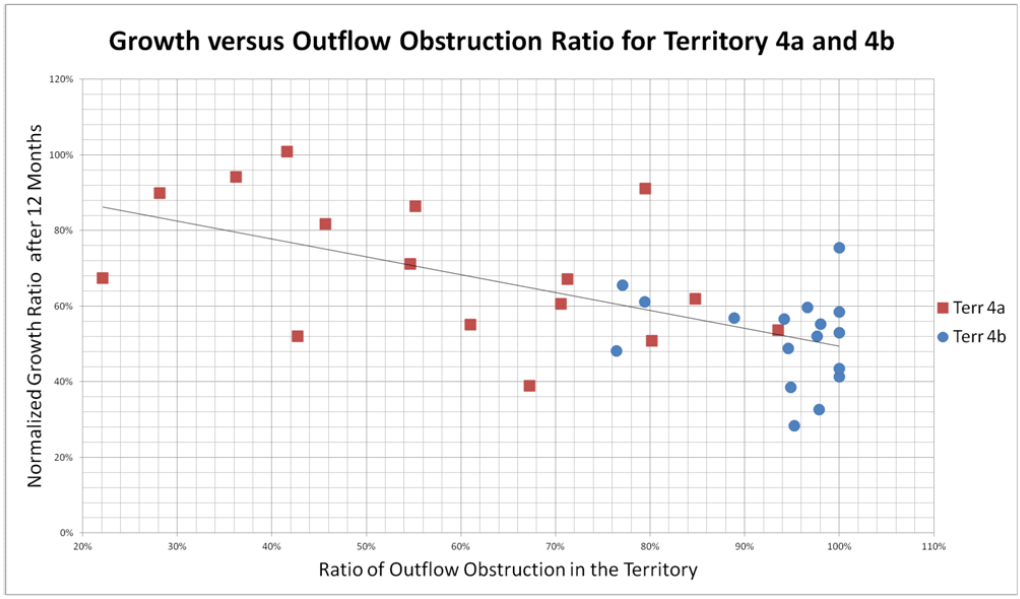

Figure 30: Growth of territories 4a and 4b in donor remnants twelve months after surgery in relation to the ratio of outflow obstruction. The growth is normalized with respect to the preoperative remnant ratio of the territory, showing that almost all territories 4a and 4b grow less than the left lateral lobe (ratio < 100%). Territory 4b typically has a higher percentage of outflow obstruction, which is related to the surgical technique of including most of the MHV in the graft but trying to maintain the drainage of segment 4a. There is an overall tendency for reduced volume regeneration of territories with a higher rate of outflow obstruction.

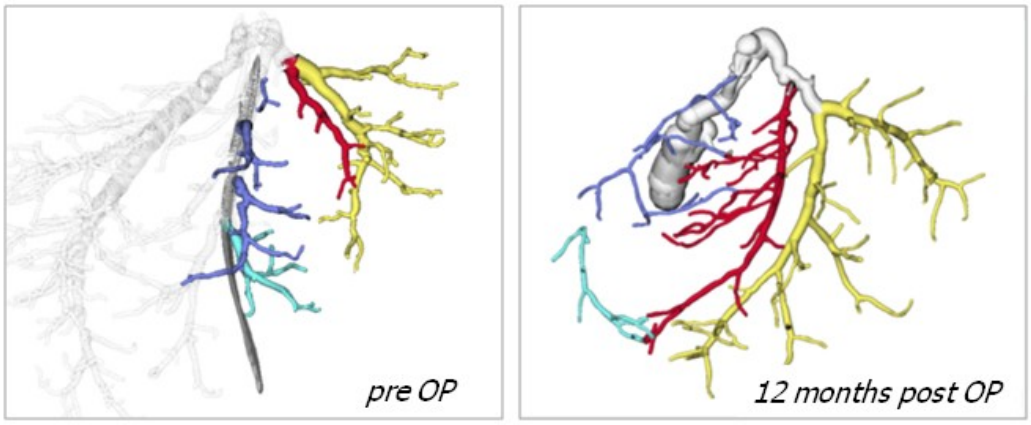

Figure 31: Development of collaterals in a donor remnant liver. The resection line follows the course of the MHV that is included in the graft. As a result, tributaries of the MHV have to be transected (blue and cyan in preoperative image, left). A large part of this remnant liver was outflow obstructed and collaterals were found in this donor liver, connecting tributaries of territory 4 (cyan) with hepatic veins of territory 3 (red).

3.3.4 Influence of Outflow Obstruction on Regeneration

In the critical first postoperative days after surgery, human studies cannot assess the outflow obstruction process with collateral formation and its impact on perfusion, function, and regeneration. Therefore, we performed an animal study with clinical partners at the University Hospital Essen as project of the *Optimization of Living Related Liver Transplantation* clinical research group.

The livers of rodents (e.g., rat, mouse, and woodchuck) consist of four major lobes, with two larger lobes (left lateral and median) and two smaller lobes (right and caudate). The median lobe has a dual inflow and three draining veins and thus shares the basic vascular situation of the human liver. With a ligation of the right vein of the median lobe (RMHV), an outflow problem similar to the situation of the MHV transection in ALDLT can be created. In our study with rats, this congestion model was combined with a resection of about 50% of the rodent's liver mass to induce liver regeneration and to mimic the clinical situation after ALDLT (for details of the surgical technique see [Dahmen et al., 2008a, Dahmen et al., 2008b]).

Microcirculation, functional parameters derived from histological data, and blood values were studied for the evaluation. The microcirculation was assessed by orthogonal polarizations spectroscopy (OPS) [Dirsch et al., 2008] in different areas of the median lobe, in the outflow-obstructed zone (OZ), the normal zone (NZ) and in the border zone (BZ). Measurements were taken during surgery and on postoperative days 1, 2, and 7. At the same time points, probes from the different

zones were taken from sacrificed animals, and several parameters regarding regeneration, necrosis, and vascularization were assessed by histological evaluation.

In the project, software for the automatic calculation of the proliferation index (PI) was developed. The PI reflects regeneration activity and is computed as the ratio of proliferating (dividing) hepatocytes to all hepatocytes. The nuclei of the proliferating cells can be identified by immunohistological staining with 5-bromo-2-deoxyuridine (BrdU). The approach for PI computation consists of a processing pipeline of smoothing, automated thresholding, a search for objects with certain size and shape followed by a Hough transform to detect overlapping nuclei [Ivanovska et al., 2008]. The algorithm was further improved by a step that is able to detect vascular structures [Ivanovska et al., 2010]. Different smoothing filters were evaluated and compared to a manually defined ground truth [Ivanovska, 2009].
Later, a more general approach based on machine-learning classifiers was developed and is currently used to evaluate histological whole-slide data [Homeyer et al., 2011]. This method is more flexible and better suited for the high variability in histological data related to different staining intensities, slice thickness, and other variations of the laboratory routine.

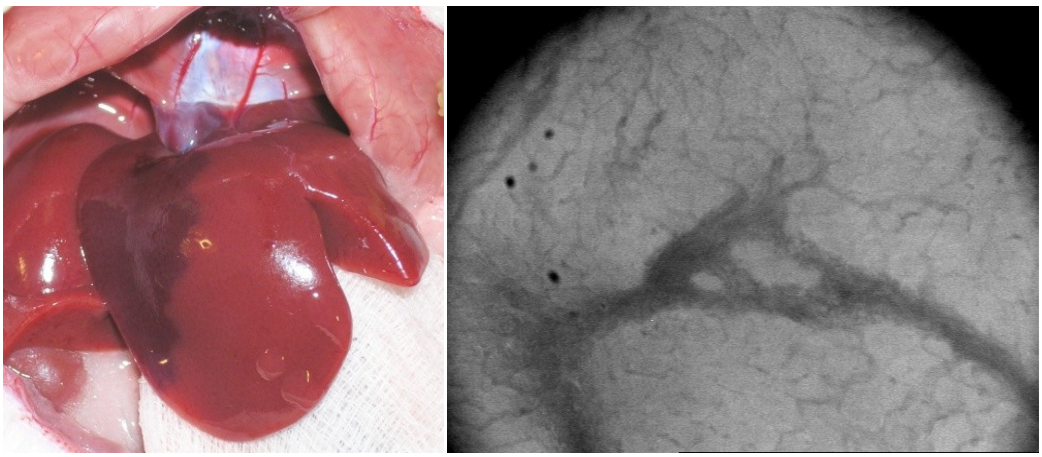

Figure 32: The median lobe of a rat liver on the macroscopic level (left) and microcirculation in the border zone between obstructed and normal zones visualized by OPS (Right). The outflow obstructed area in the median lobe after ligation of the RMHV is clearly visible as dark red area. The visualization of microcirculation on day 7 after surgery shows a vascular canal in the border zone (image center) surrounded by sinusoids of normal diameter. Images courtesy of U. Dahmen and O. Dirsch, Friedrich-Schiller-University Jena.

The observations in the rat study included [Dirsch et al., 2008]:

- On the macroscopic level, the OZ was clearly visible after surgical occlusion of the RMHV (Figure 32). On days 1 and 2 the OZ was still recognizable but no macroscopic sign of outflow obstruction was detected on day 7.
- The microcirculation measurements with OPS showed that there was no blood flow in the OZ after ligation. On days 1 and 2, the blood flow velocity increased in all zones, and sinusoids in OZ and BZ were highly dilated, especially in the BZ. By day 7, both sinusoidal diameters and flow velocity decreased and showed almost normal values. Single highly dilated sinusoids were visible in the BZ on day 7 (Figure 32). The histological findings showed that some of these canals were connected to central veins.
- The ligation of the RMHV caused necrosis in the OZ with about 25% of affected tissue. The necrotic areas were visible in histological data from days 1 and 2 and disappeared on day 7.
- In serial sections, no vascular structure corresponding to the theory of preexisting shunt vessels connecting larger veins was found.
- Liver regeneration measured by PI was highly increased in the NZ and in the BZ, but only single proliferating cells were found in the OZ, indicating a severe reduction of liver function. On day 2, the PI increased slightly in the OZ and decreased in the normal and border zone. Almost no proliferation was detected in all zones on day 7.
- Vascular markers (Laminin, van Willebrandt Factor) were observed in the dilated sinusoids on days 1 and 2, more than twice the number of positive cells in the OZ than in the NZ. Later, the sinusoidal canals in the BZ showed positive staining, while the number of laminin-positive cells was in a similar range in NZ and OZ.

In conclusion, sinusoids at the border between venous congestion and the normal zone were dilated and remodeled to vascular canals serving as communication (collaterals) between the areas. Furthermore, we observed necrosis and decreased cell regeneration in the critical early postoperative phase in the outflow-obstructed areas.

Because the time directly after surgery is crucial for the development of the potentially lethal small-for-size syndrome, excluding the potentially congested territories from the functional liver mass seems to be the logical consequence for the preoperative risk analysis.

3.3.5 MRI Data for Risk Analysis and Surgical Planning

Surgery planning for LDLT is usually performed on the basis of CT data. For the evaluation of the healthy and mostly younger donors, it is desirable to avoid the radiation dose and to plan using MRI data. For this purpose, we developed and adapted existing image analysis methods for MRI data and performed a study with new imaging sequences and a hepatocyte-specific contrast agent. In our study, CT and MRI data from donors were available, and the results of the image analysis could be compared.

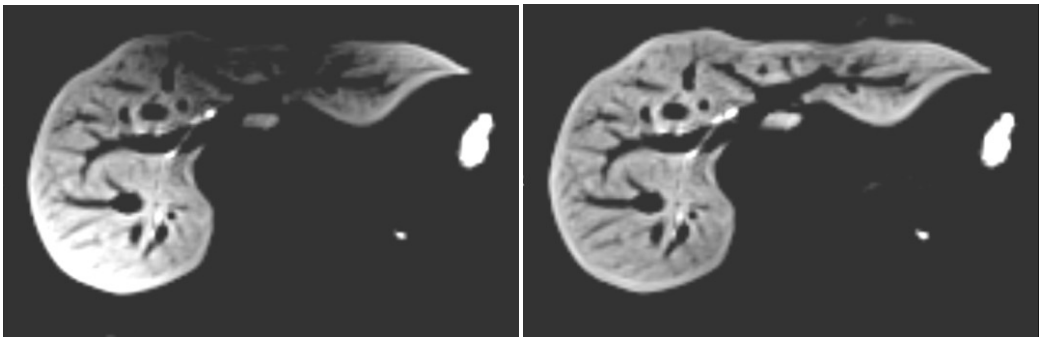

Figure 33: Elimination of inhomogeneities in MRI data: Original slice of a T1 weighted abdominal MRI with Gd-EOB-DTPA as contrast agent (left) and same image slice after application of the correction filter N3 with identical contrast and brightness parameters (right).

Typical challenges for image analysis and surgical planning with MRI data include inhomogeneities and artifacts in the images and lower resolution when compared to CT. MRI resolution in abdominal data is limited, because the liver is scanned during breath-holding and the MR acquisition takes more time than a CT scan. With a 3T scanner and routine breath-holding sequences, one 3D liver volume with a resolution of 1.5×1.5×3.0mm can now be acquired in 10-12 seconds.

In our studies, the MR acquisition involved the administration of the liver specific contrast agent Gadoxetic acid (Gd-EOB-DTPA), which is partially taken up by the hepatocytes and excreted via the bile ducts. The dynamic image sequence shows first enhancing arteries followed by enhancement of the portal veins. In the venous phase, the hepatocyes have taken up so much of the contrast agent that the liver parenchyma shows the same enhancement as the hepatic veins. After 20 to 30 minutes the maximal tissue enhancement is reached, and in this *late* or *hepatocyte-specific phase* the vascular structures appear dark compared to the bright parenchyma. The excretion of the contrast agent via the bile ducts leads to enhancement of this vessel structure in the late phase and later images and enables the segmentation of this structure (Figure 3 and Figure 33). For image processing, the images were filtered using a statistical approach to eliminate the inhomogeneities typically found in MR images [Schenk et al., 2007, Sled et al., 1998]. Liver segmentation of portal and hepatic veins was performed on the late phase of the con-

trast-enhanced images (Figure 33). For liver segmentation, our contour-based approach with live-wire and shape-based interpolation was applied. Intrahepatic vascular structures were segmented by applying the same region-growing method as for CT data, but with inverse thresholding [Selle et al., 2002]. Portal and hepatic veins were separated interactively, and smaller vessels were added by manual drawing when necessary. The following steps of tree labeling and territory computation were performed with the same algorithms that were applied to CT data.

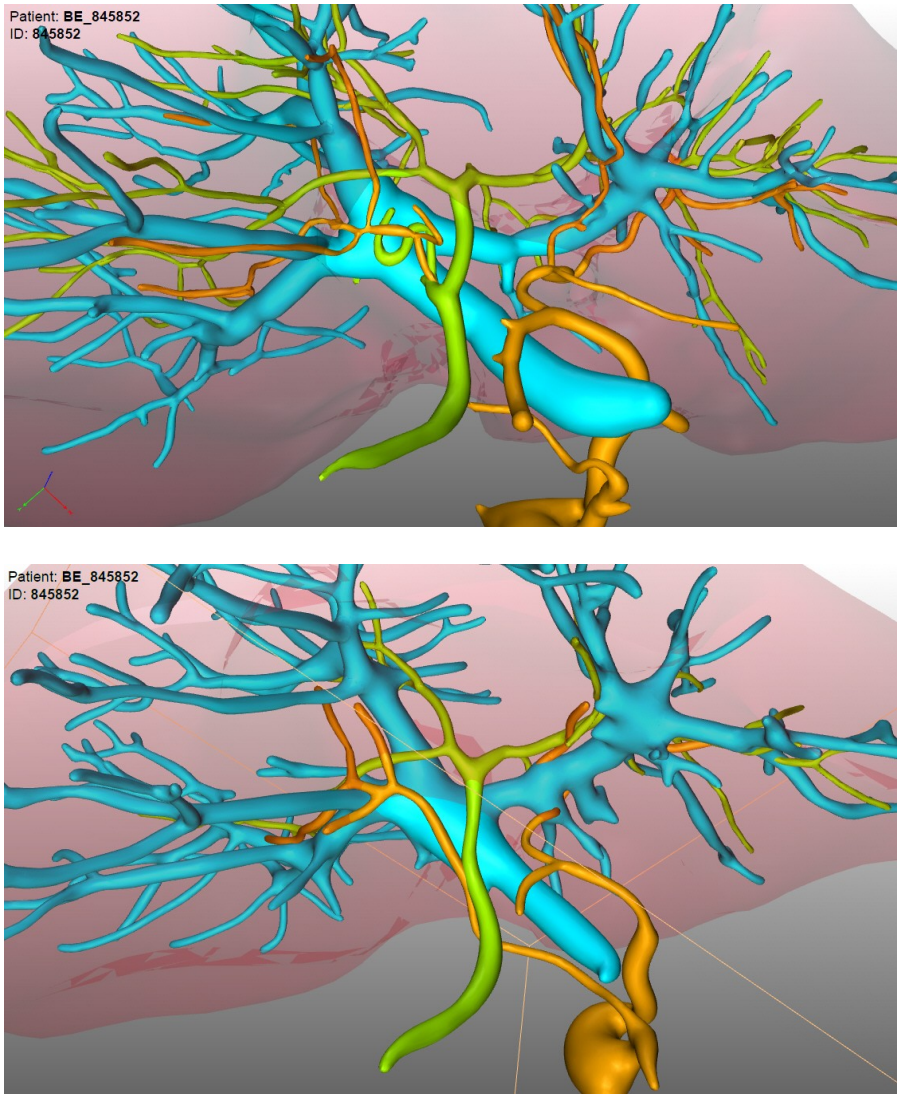

Figure 34: Vascular structures extracted from CT (top) and MRI (below) data of the same donor candidate. The topology of portal vein (cyan), hepatic artery (orange) and bile ducts (green) is comparable with a few more details visible in the CT-based results.

Two evaluation studies were performed, one with our clinical partners in Essen, and the other with radiologists and surgeons from the University Hospital in Tübingen. A first study on 20 potential donors who underwent both CT and MR imaging was performed in Essen in 2006 and 2007. The CT data showed enhanced hepatic vessels and bile ducts after sequential injection of a biliary and conventional iodinated contrast agent, as published in [Schroeder et al., 2006]. The CT and MRI data was analyzed with the methods described in Section 2.2.5 and above.

The study showed that the liver volumes of MRI- and CT-based analyses deviate in the magnitude of 5%, with larger volumes from the MRI data. The level of hierarchy for PV and HV extracted from MRI data was comparable to CT and sufficient for LDLT planning (cf. Figure 34). The territorial volumes for the portal vein showed a difference between MRI and CT data of 1.1% of CT liver volume on average with a standard deviation 0.3%. Volume differences in the HV territories were 1.4% (standard deviation 0.8%). Imaging of BD and HA was not sufficient for most patients in this study related to the slice thickness of 2mm. Details of the study results are given in [Schenk et al., 2007].

The second evaluation involved potential candidates for LDLT scanned following a newly developed MRI protocol with almost isotropic image resolution of 1mm for the late phase [Asbach et al., 2008, Mangold et al., 2012]. So far, only a few donor candidates have been examined with both CT and MRI. The analysis and evaluation of the first two data sets showed that the volumetric deviations were slightly smaller than in the first study [Schenk et al., 2010]. More importantly, the quality of hepatic arteries and bile ducts increased, almost reaching the same anatomical details as the structures extracted from CT data. According to the surgeon, the quality for these cases was sufficient for resection planning. Future research includes optimizing the MRI protocol and the analysis methods, and evaluating more data sets.

In conclusion, the applicability of MRI data for donor evaluation and LDLT planning depends on imaging protocols and requires a data resolution of 1.5mm or better and optimal timing of the arterial phase. MRI is a highly promising future modality because it allows evaluating other aspects of liver perfusion and the condition of abdominal tissue. This includes the local assessment of liver function in terms of contrast media uptake and excretion [Nilsson et al., 2009, Nilsson et al., 2010], as well as examining disease-related fat and iron content [Hu et al., 2012, Sirlin and Reeder, 2010].

3.3.6 Summary

The application of liver segmentation and software assistants to ALDLT is manifold. We presented preoperative planning based on CT and MRI data, liver regeneration in human donors and animals, and the influence of outflow obstruction on perfusion and collateral formation. The developed algorithms and applications assist the surgeon during preoperative planning by providing important information about vascular anomalies and predicting the anatomical and functional volumes for both graft and remnant livers. Liver regions with a high risk of developing venous congestion are estimated by combining the territories of MHV branches with a virtual resection for ALDLT. We evaluated the consequences of venous congestion in the postoperative course in human and animal livers. The studies showed that outflow obstruction reduces local liver regeneration, and that communicating veins that could resolve the outflow problem were not pre-existing, but instead develop from dilated sinusoids in a continuous process. The retrospective 3D analysis of patients with SFSS and liver graft loss after ALDLT uncover large territories of truncated MHV branches that had not been surgically reconnected in earlier years. The negative correlation of outflow obstruction and regeneration as well as the delayed development of collaterals lead to the conclusion that the exclusion of potentially congested territories from the functional liver mass seems to be the logical consequence for preoperative risk analysis.

Recent work focuses on transferring the planning procedure from CT to MRI data to avoid the radiation dose for healthy donors and to enable additional functional evaluations. An initial study comparing CT and MRI analyses from potential donors showed that portal and hepatic veins can be extracted from MR images in sufficient quality, but further research was needed for hepatic artery and bile ducts. Most recent MRI sequences and improved protocols have shown promising results, even for arteries and bile ducts, increasing optimism that MRI can be a sole imaging modality for ALDLT planning.

> **Publications**: The application of liver segmentation, vascular analysis, planning, and risk analysis to LDLT were performed together with several clinical partners and evaluated in joint projects. With clinicians from the Medical School Hannover, we planned and evaluated the first ALDLTs in 1998. The methods and software application were presented at BVM 2001 and received the first prize for the best poster and software demonstration [Schenk et al., 2001b]. The clinical evaluations were published by Bernd Frericks and co-workers [Frericks et al., 2004b, Frericks et al., 2006]. Vascular analysis, volumetric evaluations, and regeneration studies were performed in projects with the University Hospital Essen. The 3D analyses in donors enabled studies on anatomical variations of liver vessels [Radtke et al., 2008b, Radtke et al., 2008a, Radtke et al., 2009], the development of a new

dominancy concept [Radtke et al., 2005, Radtke et al., 2006b] and a decision algorithm for the surgical strategy [Radtke et al., 2011].
Work concerning human liver regeneration was partially presented at the congress of the International Liver Transplantation Society (ILTS) in 2007 and 2009, and at the German Transplant Congress in 2008 and published in [Schenk et al., 2009]. The work was supported by algorithms implemented by Milo Hindennach [Hindennach et al., 2007] and Jan Metzen (co-supervised by the author) [Metzen, 2006, Metzen et al., 2009].
Animal experiments for the regeneration studies in rodents were performed by Uta Dahmen, Olaf Dirsch, and co-workers at the University Hospital Essen [Dahmen et al., 2008a, Dahmen et al., 2008b, Dirsch et al., 2008]. The algorithm for automated computation of the regeneration ratio was implemented by Tetyana Ivanovska, who was supervised by the author in parts of her thesis [Ivanovska et al., 2008, Ivanovska et al., 2010, Ivanovska, 2009].
The research about the ability of MRI to serve as the sole imaging modality for LDLT was performed in joint projects with the University Hospital Essen and with the University Hospital Tübingen. The first comparison of vessels and territories for potential donors was presented at CARS [Schenk et al., 2007]. The initial results based on new MRI sequences were introduced during a talk at ILTS [Schenk et al., 2010], and the related bile duct visualizations were published in [Ketelsen et al., 2008].

4 Summary and Outlook

"One never notices what has been done; one can only see what remains to be done."
Marie Curie

This thesis presents a newly developed method of liver segmentation and its integration into dedicated software assistants for hepatic interventions. New insight about the early postoperative liver function and regeneration could be gained in joint projects with clinicians by applying our algorithms and prototypes and evaluating the outflow-obstruction process after liver resection.

In high-risk surgeries, such as extended hemihepatectomies for adult living donor liver transplantation, or resections of diseased organs, the remaining liver function is a major concern for the survival of the organ and the patient. To guarantee reliable prediction of the functional reserve, the liver volume and the liver segmentation have to be accurate. The first part of the thesis describes the developed liver segmentation approach and subsequent evaluation. The intuitive user-steered approach enables obtaining precise segmentation results. To achieve this aim, the live wire method was extended and optimized in terms of computational speed and accuracy. In combination with shape-based interpolation, the interaction effort was reduced while maintaining high quality. Two correction methods enable the user to finally optimize the liver contours. Default parameters and a learning method were implemented to avoid technical parameterization that may be challenging for clinical users. Three studies and the wide application to patient data in the last twelve years have demonstrated the performance of the algorithm. An extensive evaluation on more than 2000 data sets showed that our semi-automatic approach of live wire and shape-based interpolation alone already leads to satisfying results, and that the time and effort for control and correction should be considered when comparing liver segmentation approaches.

The second part of the thesis focuses on the development of clinical prototypes and their application to liver interventions. In 1999, the first comprehensive software assistant for liver surgery was developed. The application included ten image processing steps and a final visualization to explore all results. In later versions and updates of the software assistant, the basic concepts of the first prototype were maintained. The results of the 3D analysis achieved by the prototype were transferred into the intervention room three years later. Through collaborative work, we demonstrated the integration of abdominal planning data into the laparoscopic camera view. In this successful first example of liver laparoscopy including previously segmented vascular structures overlaid onto the endoscopic view.

In joint projects with clinicians, we investigated the heat sink effect of liver vessels in thermal ablation procedures. The 3D reconstruction of the individual liver and its vascular systems was combined with a numerical simulation of thermal ablation. A measurement tool was developed to assist the evaluation of ablation lesions in ex-situ and in-vivo studies. Our results showed good agreement between expert and automated classification, significantly different cooling effects of portal vein and hepatic vein, and a minor impact of vessel flow velocity and diameter on the extend of the heat sink effect.

Risk analysis for liver surgery combines vascular territories and tumor safety margins with different virtual resection plans to determine an optimal surgical strategy. We improved the existing iterative approach with a new interactive risk analysis with immediate user feedback during modifications of the virtual resection. For this purpose, a new risk score was developed to quantify different risk factors. This score may serve as a quality measure for user-independent optimization of resection proposals in the future.

In the third part of the thesis we focused on computer-assistance in the context of adult living donor liver transplantation. Here, methods and applications for preoperative planning, registering follow-up data after transplantation, and assessing regeneration in humans and animals were developed and utilized. In close cooperation with our clinical partners, we investigated the influence of outflow obstruction on regeneration in the critical early postoperative phase and in the first year after surgery. Our studies showed that although venous collaterals develop in the first days and weeks and take over the drainage of the obstructed areas in the long term, perfusion and regeneration in these regions are highly impaired directly after surgery. In conclusion, the related preoperative risk analysis that excludes the obstructed volume from the functional liver volume seems justified.

The thesis provides a substantial contribution to the accurate determination of anatomical and functional liver volumes. Starting with the technical development of an intuitive liver segmentation approach and the integration into a comprehensive software assistant for surgical planning, further research focused on the clinical issues of outflow obstruction and the relevance of this impairment to regeneration and risk analysis. Most recent investigations into the analysis of MRI data provide the option to include global and local liver function parameters into the risk analysis and to further improve liver surgery planning.

Future developments in liver segmentation will focus on intuitive and fast correction methods. Due to the described challenges in extracting the liver from radiological data, this step will still be required in clinical routine and is essential to achieve accurate volumes for high-risk surgery. Besides the more general aim to improve single image processing steps in the software assistants by developing

highly efficient methods and intuitive workflows, the computation of optimal resection proposal based on a resection score as developed in this thesis will be investigated. Regardinig clinical application, the use of mobile devices and cloud-based medical data exchange and computing will transform existing hospital workflows. The integration of software assistance for preoperative planning, risk analysis and interventional support in this changing clinical environment will play an important role in future projects.

5 Publications - Liver Segmentation

5.1 Efficient Semiautomatic Segmentation of 3D Objects in Medical Images

Andrea Schenk, Guido Prause, and Heinz-Otto Peitgen

Presented during a talk at MICCAI 2000 and published in S.L. Delp, A.M. DiGioia, and B. Jaramaz (Eds.): MICCAI 2000, LNCS 1935, pp. 186–195.

Copyright 2000 Springer. Reprinted with permission.

Efficient Semiautomatic Segmentation of 3D Objects in Medical Images

Andrea Schenk, Guido Prause, and Heinz-Otto Peitgen

MeVis – Center for Medical Diagnostic Systems and Visualization
Universitaetsallee 29, 28359 Bremen, Germany
{schenk,prause,peitgen}@mevis.de

Abstract. We present a fast and accurate tool for semiautomatic segmentation of volumetric medical images based on the live wire algorithm, shape-based interpolation and a new optimization method.
While the user-steered live wire algorithm represents an efficient, precise and reproducible method for interactive segmentation of selected two-dimensional images, the shape-based interpolation allows the automatic approximation of contours on slices between user-defined boundaries. The combination of both methods leads to accurate segmentations with significantly reduced user interaction time. Moreover, the subsequent automated optimization of the interpolated object contours results in a better segmentation quality or can be used to extend the distances between user-segmented images and for a further reduction of interaction time.
Experiments were carried out on hepatic computer tomographies from three different clinics. The results of the segmentation of liver parenchyma have shown that the user interaction time can be reduced more than 60% by the combination of shape-based interpolation and our optimization method with volume deviations in the magnitude of inter-user differences.

1 Introduction

Fully automated segmentation is still an unsolved problem for most applications in medical imaging due to the wide variety of image modalities, object properties and biological variability. On the other hand the most general approach, manual contour tracing, is time-consuming, inaccurate and unacceptable for large three-dimensional data sets.

To overcome these problems, a lot of work has been invested in semiautomatic segmentation methods. A popular group attracting considerable attention over the last years are the two-dimensional active contour models or *snakes* introduced by Kass et al. [1]. These algorithms try to minimize an energy functional based on contour deformation and external image forces. For initialization an approximation of the object boundary is required which is usually drawn manually by the user or in some cases is generated from a priori knowledge. However, active contours are sensitive to the settings of their numerous parameters and the quality of the initial contour which limits their applicability to medical images in the clinical routine.

S.L. Delp, A.M. DiGioia, and B. Jaramaz (Eds.): MICCAI 2000, LNCS 1935, pp. 186–195, 2000.
© Springer-Verlag Berlin Heidelberg 2000

Another promising approach to interactive boundary detection in two-dimensional images is the *live wire* algorithm, also known as *intelligent scissors*, which was first introduced in 1992 [4,5]. With live wire the segmentation process is directly steered by the user who has immediate control over the automatically suggested object contours. The contours are found as minimal paths with respect to a cost function similar to the external energy function of active contours.

Semiautomatic segmentation of three-dimensional objects in volumetric medical images is often based on two-dimensional methods which is prohibitive when each slice needs to be segmented in a larger data set. Although snakes have a direct three-dimensional extension introduced as *balloons* [2] the propagation of an initial two-dimensional snake over the slices and subsequent adjustment is preferred in most applications for reasons of robustness and practicability. For live wire only one approach for segmentation of three-dimensional images has been published so far [3] based on the projection of few interactively defined contours onto orthogonal cross-sections through the volumetric image. With this approach it is difficult to keep track of the topology of complex shaped objects without major user interaction.

The goal of our work was to extend the two-dimensional live wire algorithm to an efficient and easy to use approach for semiautomatic segmentation of three-dimensional objects in medical images. This is achieved by reducing the number of interactively segmented slices and automatic calculation of all missing intermediate contours by an optimized interpolation method which is robust to topological changes. The resulting approach is validated in five hepatic CT scans from three different clinical sites.

2 Methods

2.1 Live Wire

The live wire algorithm is a user-steered segmentation method for two-dimensional images based on the calculation of minimal cost paths by dynamic programming [6] or Dijkstra's graph search algorithm [7]. Several modifications of the basic approach including quality studies have been published [8,9,10,11], proving the high accuracy, efficiency, and reproducibility of the algorithm.

The version of live wire we use in our approach is comparable to the algorithm in [11] and we resume the fundamental ideas of this method. The two-dimensional image is transformed into a directed and weighted graph. Vertices of the graph represent image pixels while edges connect neighboring pixels in two directions. The edges are weighted with local cost functions, related to the external image forces of active contours. The cost function used in our implementation is a weighted sum of different gradient functions, the Laplacian function and the gray values at the object boundary.

After the calculation of the cost graph the user starts with the segmentation by setting a first seed point on the boundary and moving the mouse along the outline of the object. Shortest paths – in the sense of paths with lowest accumulated costs – from the seed to at least the current mouse position are computed

using Dijkstra's algorithm. Computation and display of the resulting live wire boundary segment is achieved in real-time even on larger images. The live wire path snaps to the boundary while the user moves the mouse over the image and a new seed point has to be set before the path starts to deviate from the desired contour. New shortest paths are computed from the new seed point and the procedure is repeated. A final closing leads to a controlled and piece-wise optimal segmentation result.

Our live wire approach is provided with the additional concepts of boundary snapping, data-driven cooling for automated generation of seed points and learning of cost function parameters [6,8].

2.2 Shape-Based Interpolation

Interpolation techniques [12] are used for many applications in medical imaging, e.g. image generation, resampling and visualization. They can be broadly divided into two categories: scene-based and object-based interpolation. While scene-based techniques determine the interpolated values directly from the intensities of the given image, object-based interpolation uses additional information about the objects in the image.

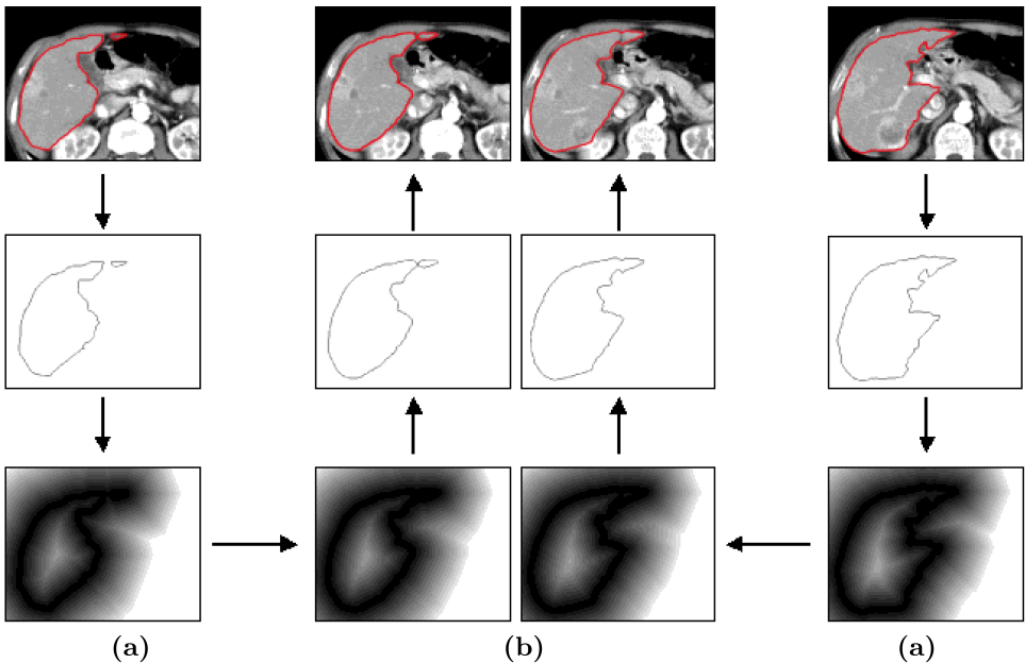

Fig. 1. Shape-based interpolation: **(a)** user-defined contour in CT images (top), binary scenes (middle), distance images (bottom); **(b)** interpolated distance images (bottom), binary scenes (middle), interpolated contours in CT images (top).

The *shape-based interpolation* method we use in our approach is the first object-based interpolation approach published in the literature [13] and it interpolates between binary images of a three-dimensional data set.

Shape-based interpolation consists of the steps illustrated in Figure 1. In the first step a binary scene is generated from a given object contour. Subsequently, the distance to this boundary is mapped into a new gray-level scene with positive distance values inside and negative distance values outside the object (shown as absolute values in Figure 1). In the third step the distance images are interpolated employing a conventional gray-level interpolation technique such as linear or higher-order interpolation. The interpolated gray-level scenes are converted back to a binary contour image by identifying the zero-crossings.

The distance transformation can be calculated efficiently with a version of the city-block distance [13] or, as in our implementation, with two consecutive chamfering processes [14,15] realized with 3×3-kernel operations. The chamfering method leads to more accurate results since this transformation is a better approximation of the Euclidean distance.

2.3 Combination of Live Wire and Interpolation

For the segmentation of volumetric objects we have combined the user-steered two-dimensional live wire segmentation and the fully-automated shape-based interpolation. The user starts with the live wire algorithm on individually selected slices. If contours on at least two slices are available, all contours on slices in between can be computed utilizing the shape-based interpolation.

The user has free choice of applying the two methods: either live wire and shape-based interpolation in an alternating fashion, or – in a two-stage approach – interactive contour tracing first and interpolation subsequently. The only restriction is that the first and the last slice of the object of interest must be segmented interactively with the live wire algorithm.

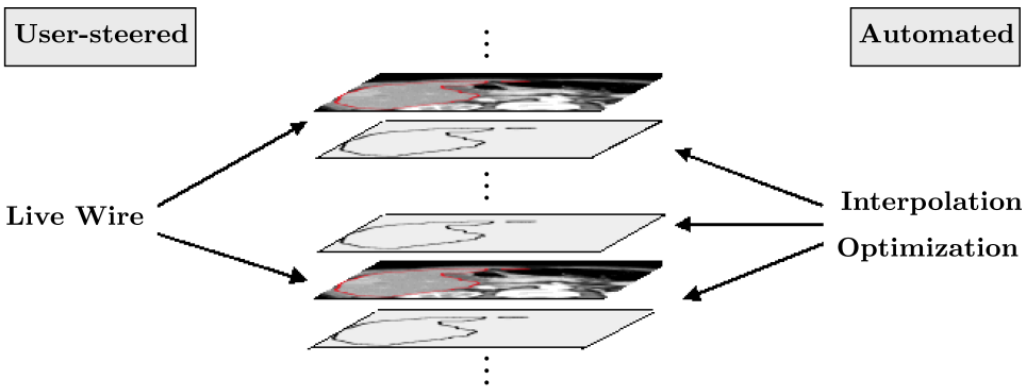

Fig. 2. Combined segmentation scheme: User-steered segmentation of selected slices followed by automatic interpolation and optimization of the intermediate contours.

If the variations of the object boundary between user-selected slices are significant, the interpolation result can be unsatisfying. In this case there is a need for interactive or automatic optimization methods which can be also used for further reduction of the number of interactively segmented image slices.

2.4 Optimization of Interpolated Contours

For the optimization of the interpolated contours we use the basic method of the live wire algorithm and recalculate contour segments as optimal cost paths between seed points with Dijkstra's algorithm.

After the shape-based interpolation the zero-crossings of the interpolated distance images define the boundary points of the new contours. To bring these points into the correct order and to identify separate contours we apply a path search algorithm. Starting with a first contour point (e.g. lower right) we follow neighboring pixels in counterclockwise direction (Figure 3a) until the first point is reached again. The algorithm is repeated until all boundary points are assigned to a contour path and it is provided with a backtracking method to deal with cases of contours connected by a single pixel line (Figure 3b).

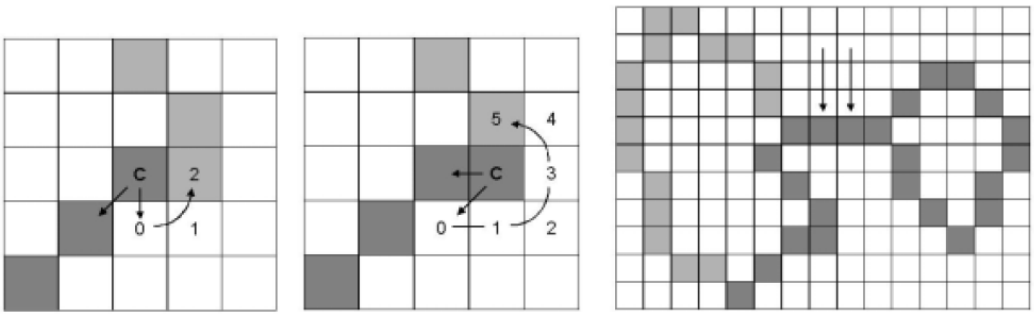

Fig. 3. Tracing the contour in the zero-crossings (gray) of the interpolated distance images. **a)** From the current pixel C of the marked path (dark gray) the next contour point is found as first (light gray) neighbor in counterclockwise direction (numbers describe the search order in the 8-neighborhood). **b)** If two boundaries are connected via a single pixel line a backtracking algorithm separates the single contours and deletes the connecting pixels (arrows).

To establish a basis for the minimal path search, the seed points from the two adjacent user-defined contours are projected onto the slices with interpolated boundaries. For every user-defined seed point the nearest point on the boundary path is determined. If two points are closer together than a given minimal distance they are merged to one central seed point. The utilization of the user-defined instead of e.g. equally distributed seeds along the contour is suggestive, since these points represent the knowledge of the user in regions of high curvature or weak edges.

The automatic contour optimization starts on all interpolated slices with the calculation of the cost matrix. Based on this data structure and the approximated seed points all contour segments linking two seeds are computed as minimal cost paths.

In the interactive optimization mode the user moves, deletes or inserts new seed points and the piece-wise optimal paths concerning these seeds are recomputed and displayed in real-time.

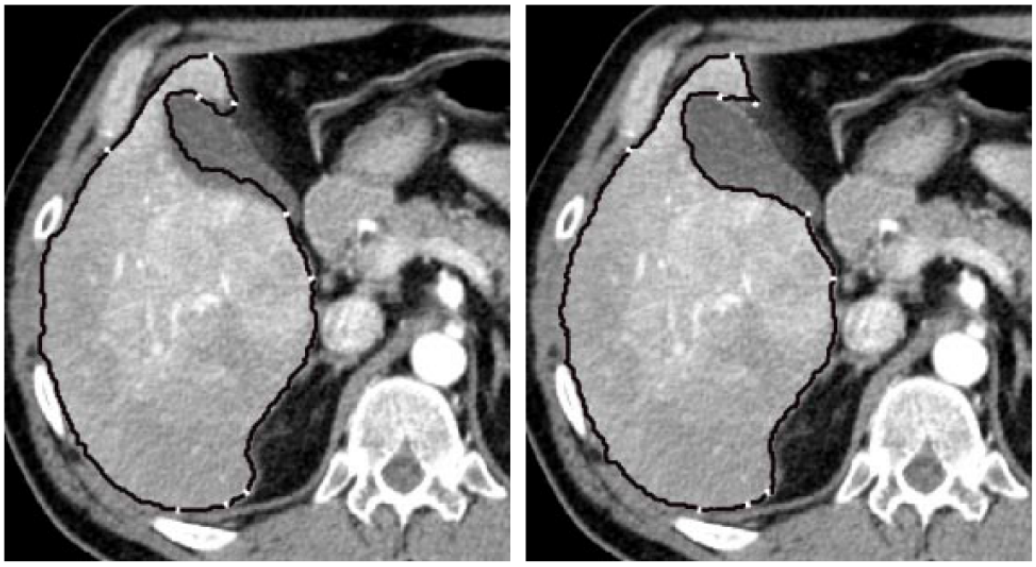

(a) **(b)**

Fig. 4. Liver CT with segmented parenchyma: **a)** Image with shape-based interpolated contour and approximated seed points from the two adjacent user-defined slices; larger deviations occur at the gall bladder (dark gray) **b)** contour after automated optimization.

3 Experiments and Results

Our approach has been successfully applied to CT and MR images of the liver and the lung for interactive segmentation of the parenchyma. It is part of an ongoing clinical project for the approximation of patient-specific organ segments and preoperative planning of surgery [17,18]. Compared with the other image processing steps of this project the segmentation is the most time-consuming part.

The test presented here was designed to quantify the volumetric deviations that have to be expected when the interactive segmentation is reduced and gradually replaced by automated interpolation. For the experiment we used five diagnostic liver CT data sets (I1-I5) from three different hospitals. The underlying examinations are helical CTs during arterial portography (CTAP) (I1-I4)

and one biphasic spiral CT scan (I5, data set from the portal venous phase). All images have 512×512 pixels in plane and consist of 34–41 (I1-I4) or 86 (I5) slices with a distance of 4 mm (I1-I4) or 2 mm (I5). Three users segmented the liver parenchyma with the live wire algorithm on all slices and the time needed for the segmentation was recorded. For one image slice an average time of 6-11 seconds and 4-6 seed points were needed depending on the user. The cost function used for the test was identical for all images and was based on a Sobel-like gradient function (feature f_5 in [10] extended to 8-neighborhood) and the gray values at the object border with relative weights of 0.45 and 0.55, respectively. Parameters for both functions (mean and deviation) were determined experimentally.

Table 1. Results for the test images: inter-user variability, volume deviation for the SBI and OPT interpolation methods and saved interaction time (in %).

	Inter-user	**Automated interpolations**		**Saved**
	variability	**SBI**	**SBI+OPT**	**interaction time**
Image 1	1.68			
8 mm		1.24	0.79	51.0
12 mm		2.03	1.20	65.5
16 mm		3.20	1.95	72.7
Image 2	3.47			
8 mm		2.28	1.83	47.4
12 mm		2.70	1.65	62.3
16 mm		5.70	4.35	72.8
Image 3	1.43			
8 mm		1.57	1.19	51.9
12 mm		2.87	1.98	65.3
16 mm		3.81	2.69	75.0
Image 4	1.24			
8 mm		1.34	1.17	50.1
12 mm		1.89	1.30	67.5
16 mm		2.50	1.92	75.2
Image 5	1.26			
8 mm		1.91	1.85	74.5
12 mm		2.20	1.67	82.9
16 mm		3.17	2.30	86.5

The interactively segmented slices were reduced to data sets with slice distances of 8, 12 and 16 mm and the omitted intermediate slices were automatically calculated with shape-based interpolation (SBI) and, additionally, with the cost-based optimization described above (OPT).

We defined the user-dependent reference volumes as the results of the interactive segmentation on all slices. The differences between two reference volumes

(inter-user variability) or between an interpolated volume and its reference volume were calculated with the formula

$$1 - \frac{2|V_i \cap V_j|}{|V_i| + |V_j|}, \qquad i \neq j,$$

which is equal to 1 minus the similarity index [16]. These relative volume differences were averaged over the three users and listed as inter-user variability, respectively volume deviations for the automated interpolations in Table 1.

The results for the sequences I1-I4 show that we can save more than 50% of interaction time with the shape-based interpolation alone if we tolerate deviations in the order of the inter-user variability. Moreover, we can use the optimization method (OPT) for a further reduction of the differences (up to one half) or for further savings of user interaction time.

With an optimized interpolation (SBI + OPT) between all 12 mm slices we have comparable deviations to the SBI method for 8mm slices, but interaction time savings of approximately 66% instead of 50%. The interpolation on the 16 mm distant slices lead to deviations of 2.5-5.7%. With automated optimization these results can be improved, but the inter-user variability can only be reached with manual corrections which require extra interaction time.

With the biphasic image sequence I5 we achieved similar results to those of I1-I4, but due to the smaller slice distance higher savings of interaction time. The interpolation leads to higher deviations compared to those of the other four images, which is also caused by more than twice the number of intermediate slices. Here we have for example a volume deviation of 1.67% and interaction time savings of 82.9% with the shape-based interpolation and automated optimization on 12 mm distant slices (set of every sixth slice) compared to the interactive segmentation on all slices.

If the user verifies the automatically generated contours, the supported manual optimization can be used for further improvements. Corrections of the SBI + OPT results on few slices where the automatically determined lowest cost paths considerably deviate from the object boundary (Figure 5, right), usually lead to a significant reduction of the volume differences.

4 Conclusions

In this paper we presented a new approach for the semiautomatic segmentation of three-dimensional objects in medical images. The combination of the live wire algorithm and shape-based interpolation builds an effective and accurate segmentation tool which we extended by an automated optimization method.

The live wire algorithm provides direct control to the user, is easy to use and offers high flexibility regarding image modalities and segmentation objects. For the segmentation of three-dimensional objects we combined this slice-based method with shape-based interpolation, leading to a significant reduction of interaction time compared to the segmentation on all slices. The applicability

Fig. 5. Surface rendering of the user-segmented volume in image I1 (left), deviations between this volume and the 12mm SBI volume (middle), deviations for 12mm SBI + OPT (right).

of this combination depends on the properties of the object contours, it is less appropriate for strongly undulated boundaries (e.g. white/gray matter in the brain), but a good choice for structures with a more regular surface (e.g. liver, lung). The shape-based interpolation is especially suited for image sequences with a large number of image slices like multi-slice CTs.

We showed in experiments with five hepatic CTs that we can considerably improve the interpolation results or decrease – with constant level of accuracy – the number of user-segmented slices with an automatic optimization method based on the ideas of the live wire algorithm. In the validation we have used equal distances for the interactively segmented images, but we expect even better results with slices individually selected by the experienced user who rates the boundary changes during the segmentation process and specifies the images for contour interpolation.

While the shape-based interpolation and the path-finding algorithm can be calculated efficiently in a few seconds for all interpolated slices, the automated optimization requires more computational time primarily due to the calculation of the cost graph on every interpolated image. Therefore one focus in our current work is the local restriction of cost computation.

Further improvements regarding the accuracy of the interpolated contours can be expected from a better adjustment of the approximated seed points to the underlying image data.

Acknowledgments

The computer tomographies were provided by the Klinikum der Medizinischen Hochschule Hannover, Staedtische Krankenanstalten Krefeld and Klinikum Hof. We would like also to thank D. Boehm, Dr. B. Preim, Dr. R. Rascher-Friesenhausen and Dr. D. Selle for their support in this project.

References

1. M. Kass, A. Witkin, and D. Terzopoulos. Snakes: active contour models. *International Journal of Computer Vision* 1(4), pp. 321–331, 1988.
2. D. Terzopoulos, A. Witkin, and M. Kass. Constraints on deformable models: Recovering 3D shape and nonrigid motion. *Artificial Intelligence* 36(1), pp. 91–123, 1988.
3. A. X. Falcao and J. K. Udupa. Segmentation of 3D objects using live-wire. In *SPIE on Medical Imaging*, vol. 3034, pp. 191–198, Newport Beach, CA. 1997
4. E. N. Mortensen, B. S. Morse, W. A. Barrett, and J. K. Udupa. Adaptive boundary detection using live-wire two-dimensional dynamic programming. In *IEEE Computers in Cardiology*, pp. 635–638, Durham, North Carolina, IEEE Computer Society Press, 1992.
5. J. K. Udupa, S. Samarasekera, and W. A. Barrett. Boundary detection via dynamic programming. In *Visualization in Biomedical Computing '92*, Chapel Hill, North Carolina, pp. 33–39, 1992.
6. E. N. Mortensen and W. A. Barrett. Intelligent scissors for image composition. In *Computer Graphics (SIGGRAPH '95)*, Los Angeles, CA, pp. 191–198, 1995.
7. D. Stalling and H.-C. Hege. Intelligent scissors for medical image segmentation. In *Digitale Bildverarbeitung fuer die Medizin*, Freiburg, Germany, pp. 32–36, 1996.
8. W. A. Barrett and E. N. Mortensen. Fast, accurate and reproducible live-wire boundary extraction. In *Visualization in Biomedical Computing*, Hamburg, Germany, pp. 183–192, 1996.
9. W. A. Barrett and E. N. Mortensen. Interactive live-wire boundary extraction. *Medical Image Analysis* 1(4), pp. 331–341, 1997.
10. A. X. Falcao, J. K. Udupa, S. Samarasekera, S. Sharma, B. E. Hirsch, and R. A. Lotufo. User-steered image segmentation paradigms: Live-wire and live-lane. *Graphical Models and Image Processing* 60(4), pp. 223–260, 1998.
11. A. X. Falcao, K. Jayaram, J. K. Udupa, and Miyazawa F. K. An ultra-fast user-steered image segmentation paradigm: Live-wire-on-the-fly. In *SPIE on Medical Imaging*, vol. 3661, Newport Beach, CA, pp. 184–191, 1999.
12. T. M. Lehmann, C. Goenner, and K. Spitzer. Survey: Interpolation methods in medical image processing. *IEEE Transactions on Medical Imaging* 18(11), pp. 1049–1075, 1999.
13. S. P. Raya and J. K. Udupa. Shape-based interpolation of multidimensional objects. *IEEE Transactions on Medical Imaging* 9(1), pp. 32–42, 1990.
14. G. T. Herman, J. Zheng, and Bucholtz C. A. Shape-based interpolation. *IEEE Computer Graphics and Applications* 12(3), pp. 69–79, 1992.
15. G. Borgefors. Distance Transformations in Arbitrary Directions. *Computer Vision, Graphics and Image Processing* 27(3), pp. 321–345, 1984.
16. A. P. Zijdenbos, B. M. Dawant, R. A. Margolin, and A. C. Palmer. Morphometric Analysis of White Matter Lesions in MR Images: Method and Validation. *IEEE Transactions on Medical imaging* 13(4), pp. 716–724, 1994.
17. D. Selle, T. Schindewolf, C. J. G. Evertsz, and H.-O. Peitgen. Quantitative analysis of CT liver images. In *Computer-Aided Diagnosis in Medical Imaging*, Chicago, pp. 435–444, Elsevier, 1999.
18. B. Preim, D. Selle, W. Spindler, K. J. Oldhafer, H.-O. Peitgen. Interaction Techniques and Vessel Analysis for Preoperative Planning in Liver Surgery. In *Medical Image Computing and Computer-Assisted Intervention – MICCAI 2000* (this volume).

5.2 Local Cost Computation for Efficient Segmentation of 3D Objects with Live Wire

Andrea Schenk, Guido Prause, and Heinz-Otto Peitgen.

Presented at SPIE Medical Imaging 2001 and published in M. Sonka, K.M. Hanson (Eds.), Proceedings of SPIE 2001,Vol. 4322, pp.1357-1364.

Copyright 2001 Society of Photo Optical Instrumentation Engineers. Reprinted with permission.

Local Cost Computation for Efficient Segmentation of 3D Objects with Live Wire

Andrea Schenk, Guido Prause and Heinz-Otto Peitgen

MeVis – Center for Medical Diagnostic Systems and Visualization
Universitaetsallee 29, 28359 Bremen, Germany

ABSTRACT

We present an approach for the optimization of the live wire algorithm applied to 3D medical images. Our method restricts the computation of the cost function to relevant areas and considers regionally specific properties of the object boundary. As a consequence, precise contours can be obtained in reduced computation and interaction time. For the calculation of the cost function on the current image slice, the nearest contour on an adjacent slice is taken as reference. The reference contour is divided into local segments and the image pixels are classified into regions with respect to their distance to the contour segments. The size of these regions is controlled by a given maximum distance. Cost function parameters are learned separately from every local contour segment of the reference slice and define the cost function for the respective region on the current slice. We used the local cost computation for the interactive definition of object contours, as well as for the optimization of interpolated contours between user-defined contours. Applied to CT and MR data of the liver, our method showed considerable advantages over the conventional algorithm based on a global cost function, particularly for objects with inhomogeneities or with different surrounding tissue.

Keywords: image segmentation, boundary detection, interactive segmentation, 3D segmentation, interpolation, local cost computation

1. INTRODUCTION

The segmentation of 3D objects is an important step in medical image processing. Segmentation results are the basis for many other subsequent processes like morphological and functional quantification or surface shaded displays in a 3D visualization. Fully automatic segmentation methods are highly desirable but still an unsolved problem for most applications in medical imaging due to the wide variety of image modalities, object properties and biological variability. On the other hand, the most general approach, manual contour tracing, is time-consuming, inaccurate and unacceptable for large three-dimensional data sets.

A reasonable compromise between fully automated and manual segmentation are interactive and semiautomatic methods. A new approach for interactive boundary detection, the *live wire* algorithm, has been introduced in 1992 by Mortensen and Udupa.[1,2] The segmentation process of this method is directly steered by the user who has immediate control over automatically suggested contours between interactively placed contour points. Object contours are found as minimal paths between those points in real-time and with respect to a cost function similar to the external energy function of active contour models.[3]

In this paper we present an approach for the efficient segmentation of 3D objects in medical volume data on the basis of the live wire algorithm. We developed methods for the optimization of the underlying cost computation and for the interpolation of contours between user-defined contours. The information we gain from one or more user-defined contours is the basis for the optimization of the cost computation. We use the information about the image region of the reference contour and local image properties at contour pixels for the segmentation on a neighboring slice.

The position and shape information gives us the possibility to restrict the cost computation on the neighboring slices to relevant areas. The computation time saved by this restriction is beneficial for the interactive process and also accelerates the optimization of interpolated contours, an approach we proposed recently.[4] The second goal of our work is the reduction of the necessary user interaction by improving the underlying cost function. This is achieved

Email: andrea.schenk@mevis.de, URL: www.mevis.de

by replacing the global cost parameters by locally adapted characteristics. Both extensions of the live wire algorithm make the segmentation method faster, more robust and thus applicable to a larger variety of medical images and objects of interest.

2. METHODS

2.1. Interactive Segmentation with Live Wire

The live wire algorithm is a user-steered segmentation method for two-dimensional images based on the calculation of minimal cost paths by dynamic programming[5] or Dijkstra's graph search algorithm.[6] Several modifications of the basic approach including quality studies have been published, proving the high accuracy, efficiency, and reproducibility of the algorithm.[7–12]

The first step of the live wire method is the transformation of a two-dimensional image into a directed and weighted cost graph. Vertices of the graph represent image pixels while edges connect neighboring pixels in two directions. The edges are weighted by the costs for the directed connection between one pixel and the respective neighbor. The costs are computed as a weighted sum of different cost features like gradient functions, the Laplacian function and the gray values at the object boundary. Every feature is defined by parameters like mean value and deviation, expected at the desired contour. Examples for these global cost features and parameters are given by Falcao et al.[10] as well as by Mortensen and Barrett.[11]

After the computation of the cost graph the user starts the segmentation by setting a first seed point on the boundary and moving the mouse along the outline of the object of interest. Shortest paths – in the sense of paths with lowest accumulated costs – from the seed to at least the current mouse position are computed using Dijkstra's algorithm. Computation and display of the resulting live wire boundary segment is achieved in real-time even on larger images (512 x 512 pixels). The live wire path snaps to the boundary while the user moves the mouse over the image and a new seed point has to be set before the path starts to deviate from the desired contour. New shortest paths are computed from the new seed point and the procedure is repeated. A final closing leads to a controlled and piece-wise optimal segmentation result.

2.2. Local Cost Computation

2.2.1. Locally restricted cost computation

The aim of the local restriction of cost computation is a speed-up of the computation time by a reduction of the image area where costs are calculated. We define a relevant region on the current slice as a tube-like area around a contour copied from the nearest adjacent slice. The pixels of this region are identified with the help of a distance transform. All pixels which are less distant than a given maximal distance are marked as relevant. The distance transform used in our approach, is an integer-based transformation proposed by Herman et al.[13] in 1992, an extension of the basic algorithm introduced by Borgefors.[14] The distances are calculated efficiently with two consecutive chamfering processes realized with 3×3-kernel operations. Since we use this method in our approach not only for the locally restricted cost computation but also for other purposes, we repeat the main ideas of the algorithm.

A distance image in the size of an image slice is created and initialized with a large positive value inside and a large negative value outside the object. The contour pixels, representing the inner border of the object, are assigned

Figure 1. Templates and directions of the chamfering process used for the efficient calculation of an integer approximation to the Euclidean distance. The left template is applied row by row, top to bottom and a left to right ordering within the rows, the second template from bottom to top and from right to left.

with +5, neighboring pixels outside the object (4-neighborhood) with -5. (To avoid separate edge treatment, a temporary additional one pixel wide border around the image with the large negative value is proposed.)

Now the two chamfer templates given in Fig. 1 are applied, the values of the image are updated first with the left and then with the right template. Both template operations change the pixels in a row by row fashion, the left template from top to bottom and from left to right, the right template from bottom to top with a right to left ordering within the rows (Fig. 1).

During this process the pixel in the center of the template is always the pixel in question. If it has the value +5 or -5 from the initialization, the pixel is left unaltered. If the sign of the central pixel is positive, then we add for each non-empty template pixel the value of the image pixel to the covering template pixel. The value of the central pixel is replaced by the smallest of these sums. If the pixel in the template center is negative, we subtract from each non-empty template pixel the value of the underlying image pixel. The largest of these differences is the new value of the central pixel. The second chamfering process is performed with the right template from Fig. 1 following the same rules. If only positive distances from the contour are required, the process can be simplified. In this case, the pixels next to the contour are initialized with +5 instead of -5 and the case for a negative value of the central pixel can be omitted.

On the basis of the resulting distance image, the costs for a connection between two neighboring pixels are calculated. If the distance is larger than a given maximum distance, the cost value is set to a maximum cost value and otherwise the costs are calculated with the given cost function parameters. Depending on the size of the contour and the given maximal distance, the time for the cost computation can be reduced significantly.

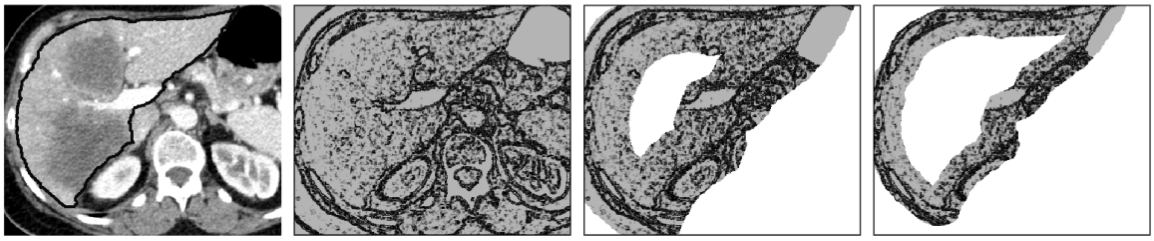

(a) **(b)** **(c)** **(d)**

Figure 2. **(a)** CT of the liver with reference contour. **(b)** Global cost image of the next slice (shown is the minimum cost value of all (8-neighborhood) connections from one pixel to its neighbors). **(c)** Locally reduced cost image, the saved computation time is about 44%. **(d)** Locally reduced cost image with a reduction of computation time of approximately 67%.

2.2.2. Locally adapted cost computation

The idea of locally adapted costs in our approach is based on the assumption that the properties of the image at the object boundaries are similar on neighbored slices. Therefore, we exploit the coherence between the image slices and consider the contour on the nearest adjacent slice as a reference for the current image. Cost feature parameters are learned from this reference contour and form the basis for the cost computation of the current image slice. Considering the inhomogeneities and different surrounding tissues we found in several images (e.g. MRT), a locally adapted learning seems to be more appropriate than a global learning.

In our approach, we divide the reference contour into local segments and derive the cost feature parameters separately for every contour segment. The regions on the current slice where these local parameters are applied, comprise the pixels with the smallest distance to the respective segment of the reference contour.

The algorithm that identifies the pixels of every segment region works as follows. First an index image is created and every contour segment is assigned a unique index number. From these contour pixels the indices are propagated over the image with the help of the distance transformation described in Sect. 2.2.1. While the templates used in this process are shifted over the image, the indices are updated simultaneously to the distance values. Utilizing the distance transformation for index propagation we can also restrict the index regions by a given maximum distance. Thus we perform the preparatory work for the locally adapted and restricted cost computation at once.

(a) **(b)** **(c)**

Figure 3. **(a)** MRT with reference contour **(b)** Index image with eight equally spaced and locally restricted regions used for all cost features. **(c)** Index image for the inner gray-value feature with regions locally adapted to this cost feature.

A prerequisite for the definition of indexed regions is the partitioning of the reference contour into segments. This can be performed in the simplest way by dividing the contour into equally spaced contour fragments containing the same number of pixels. As a consequence, local parameters for the different cost features are learned for the same local regions. Furthermore, this approach does not take into account the changes of the single cost feature properties occuring at the contour path. For example, a border between two segments usually does not reflect a change in the gradient magnitude.

Due to the limitations of the simple method we developed a more elaborate approach, where the reference contour is divided into segments, individually for every cost feature and depending on the particular feature characteristic at the contour pixels. Thus a respective index image is calculated for every feature representing a locally adapted partitioning of the image. The aim of the feature-specific subdivision of the contour is the determination of a given number of segments, each with a relative small cost value deviation. For example, every segment computed for the gradient feature should contain contour pixel with similar gradient values.

For this purpose we used a fast method inspired by the procedure of region merging. Initially every contour pixel of the reference contour represents a single segment. The mean of this segment is the cost feature value at this pixel, while the deviation is zero. A second list comprises the mean and deviations for all possible segments, built of the initial segments and the respective neighboring segment. This list is ordered with ascending deviation. Now the neighbors with the lowest deviation are merged, forming a new segment in the first list. The second list is updated, new mean and deviations are computed for this segment and the two adjacent neighboring segments.

The merging step is repeated until a given minimal number of contour segments is reached. An additional merging for short segments during this process can be used to avoid segments smaller than a minimal length. The indices of the contour segments are finally propagated over the image and define one index image with feature-specific index regions. For every cost feature such an index image is computed and for all local contour segments parameters are learned separately from the reference contour.

On the current slice the costs from every pixel to its neighbors are calculated for all cost feature depending on the pixel index and the respective local feature parameters. The weighted sum of all feature costs results in the costs for the current image and is used for the subsequent path computation.

2.3. Shape-Based Interpolation

The aim of our approach is the efficient segmentation of 3D objects in medical data. Since the live wire algorithm initially was designed for the segmentation on two-dimensional images, we developed a method to reduce the number of interactively segmented slices and to calculate all missing contours automatically.[4] The method we use for this automatic step is the *shape-based interpolation*[15] which is illustrated in Fig. 4.

In the first step a binary scene is generated from a given object contour. Subsequently, the distance to this boundary is mapped into a new gray-level scene with positive distance values inside and negative distance values outside the

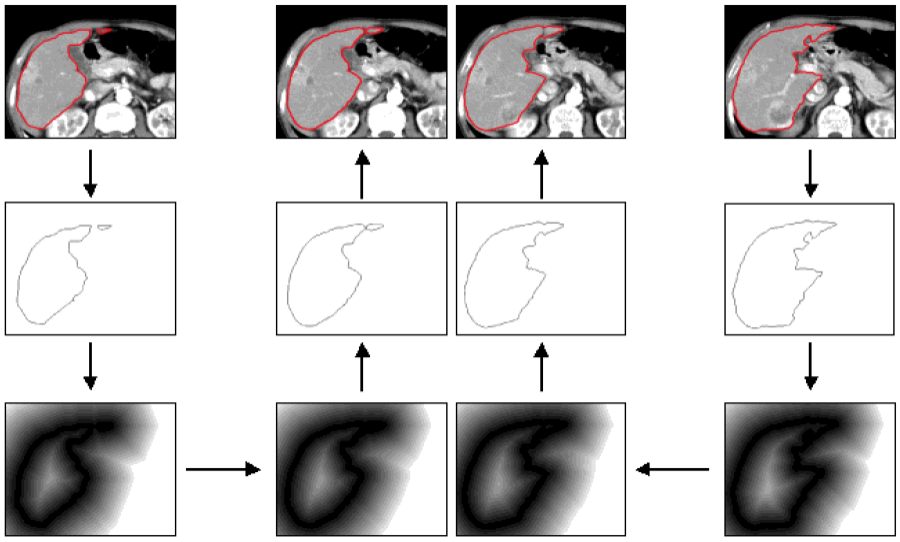

Figure 4. Shape-based interpolation: **(a)** user-defined contour in CT images (top), binary scenes (middle), distance images (bottom); **(b)** interpolated distance images (bottom), binary scenes (middle), interpolated contours in CT images (top).

object (shown as absolute values in Fig. 4). In the third step the distance images are interpolated employing a conventional gray-level interpolation technique such as linear or higher-order interpolation. The interpolated gray-level scenes are converted back to a binary contour image by identifying the zero-crossings. The distance transformation is again efficiently calculated with the chamfering process described in Sect. 2.2.1.

The user has free choice of applying the two methods: either live wire and shape-based interpolation in an alternating fashion, or – in a two-stage approach – interactive contour tracing first and interpolation subsequently. The only restriction is that the first and the last slice of the object of interest must be segmented interactively with the live wire algorithm.

2.4. Optimization of Interpolated Contours

For the optimization of interpolated contours we use the basic method of the live wire algorithm and recalculate contour segments as optimal cost paths between seed points with Dijkstra's algorithm, an approach we proposed recently.[4] After the shape-based interpolation the zero-crossings of the interpolated distance images define the boundary points of the new contours. These points are brought into the correct order and separate contours are identified. A basis for the minimal path search is built from the seed points of the two adjacent user-defined contours.[4]

The next step of the contour optimization is the calculation of the cost graph. Knowing the distance between the interpolated and the adjacent contours, the cost computation can be reduced to relevant, locally restricted areas. The distance values of the shape-based interpolation are directly used for the test against the tolerated distance, a second distance transformation is not required. Based on the reduced cost graph and the approximated seed points all contour segments linking two seeds are computed as minimal cost paths.

3. EXPERIMENTS AND RESULTS

Our approach has been successfully applied to CT and MR images for the segmentation of the liver parenchyma, the gall bladder, the lung and other structures. It is part of an ongoing clinical project for the approximation of patient-specific organ segments and preoperative planning of surgery.[16–18] A test for the quantification of the volumetric

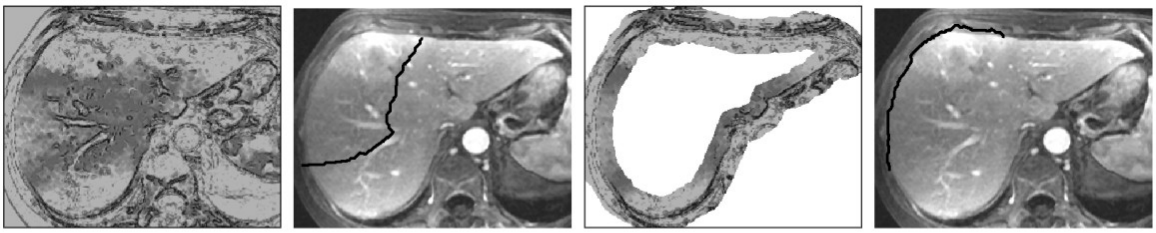

(a) (b) (c) (d)

Figure 5. **(a)** Global cost function for the liver parenchyma. **(b)** Live wire path between two contour points, computed from the cost function in (a). The path was misled by the vessel structure in the middle of the liver parenchyma. **(c)** Locally restricted cost function, calculated in significantly reduced computation time. **(d)** Live wire path based on the cost function in (c) following the boundary of the liver.

deviations that have to be expected when the interactive segmentation is reduced and gradually replaced by the automated interpolation and subsequent optimization was designed. The test showed that the user interaction can be reduced by more than 60 % compared to the segmentation with live wire on all slices when deviations in the magnitude of the inter-user differences were accepted.[4]

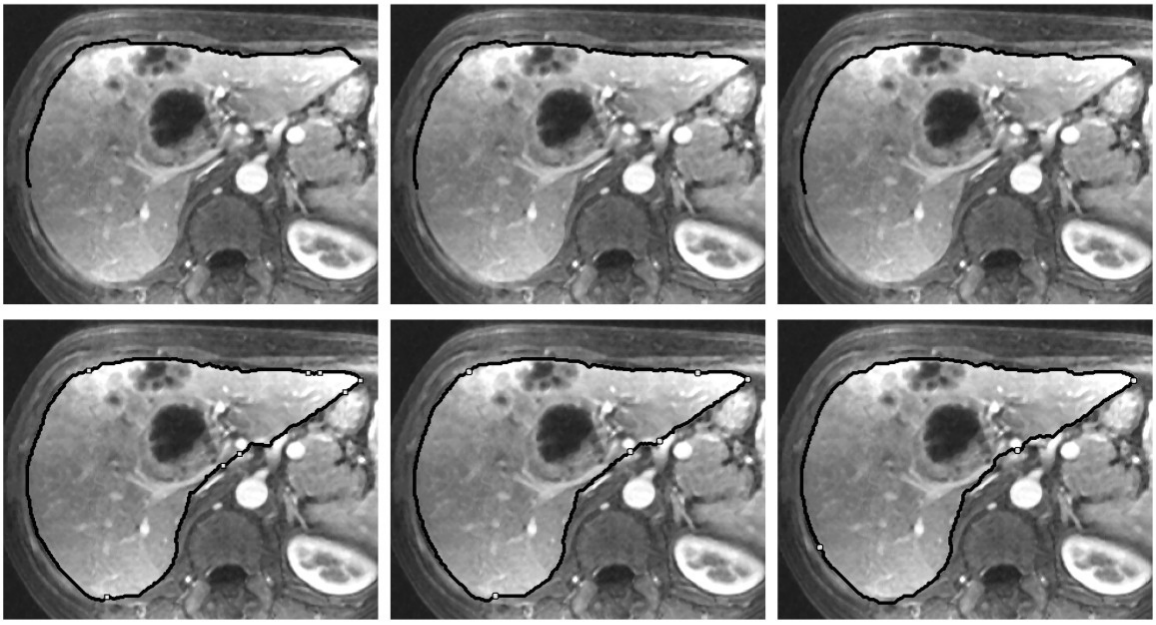

(a) (b) (c)

Figure 6. Liver MRT with live wire paths. The paths are calculated based on **(a)** global costs, **(b)** local costs with parameters learned on equally spaced contour segments, **(c)** locally adapted costs learned from a cost feature specific partitioning of the reference contour. The images of the first row show a path between two contour points based on the particular cost function. In the second row an acceptable segmentation of the liver parenchyma was achieved with a varying number of seed points. For the method in (a) were 8, for (b) 6 and for (c) 3 seeds required.

Experiments with the locally restricted cost computation have been performed, showing the acceleration of computation time. Depending on the size of the contour and the given maximal distance, this time is reduced considerably. In particular, the saved computation time is beneficial for the automatic optimization of interpolated contours where more than one slice is processed. Moreover, if image pixels with low costs are found in the image, misleading the live wire path to a wrong direction, an improvement can be achieved by the locally restricted cost computation. If the unwanted pixels are more distant from the reference contour than the given maximal distance, the unfavored path will not appear due to the maximal cost given to this image area (Fig. 5).

First experiments with the locally adapted cost computation showed the advantages of this method, particularly for the segmentation of objects in MRT data. In these images the brightness is often not equally distributed, so that the gradient, gray values and other properties vary along the object boundaries. Compared to a global cost function the locally adapted and feature-specific costs represent a more suitable basis for the computation of live wire paths. Utilizing the simple approach of equally spaced contour segments the number of needed seed points for the interactive segmentation was reduced considerably. With the locally adapted and feature-specific partitioning of the reference contour the segmentation process was even more simplified, the number of necessary seed points even less (Fig. 6). The savings of interactively places seed points together with the better adapted live wire paths make the user-steered segmentation more efficient and robust.

4. CONCLUSION AND FUTURE WORK

In this paper we presented an extension of the live wire algorithm for the semiautomatic segmentation of three-dimensional objects in medical images. The combination of the live wire algorithm and shape-based interpolation with subsequent optimization builds an effective and accurate segmentation tool. The additional methods of local cost computation, we presented in this paper, make the algorithm more robust and applicable to a larger variety of objects and image modalities.

With the local cost computation, the required computation time as well as the interaction time was reduced. The computational time was shortened because the number of pixels to consider was decreased considerably. The use of locally adapted cost feature parameters improved the cost function and thus the live wire paths. As a result, the number of interactively placed seed points and therefore the interaction time was reduced.

We applied the local restriction of cost computation to the optimization of automatically interpolated contours. The speed-up of the automatic optimization step led to a better acceptance in the clinical routine. The utilization of the locally adapted cost computation for the optimization is part of our ongoing work. For this approach different methods are possible and part of our studies.

Another focus in our current work is laid on statistical methods for the partitioning of the reference contour depending on the local cost feature properties. A test on all possible subdivisions of the contour would lead to the optimal solution, but is too time-consuming. Thus the aim of our research is a fast method with nearly optimal results. Additionally, we focus on the automatic determination of the number of contour segments that are used for the locally adapted cost computation.

Acknowledgments

This work was supported by a grant of the City of Bremen. We would like to thank Prof. M. Galanski, Dr. F. Caldarone and Dr. G. Stamm, Department of Diagnostic Radiology, Medical School Hannover, Prof. J. Debatin, Department of Diagnostic Radiology, University Hospital Essen and Dr. E. Vielhauer, Hospital Hof, for their support and the provided data.

REFERENCES

1. E. N. Mortensen, B. S. Morse, W. A. Barrett, and J. K. Udupa. Adaptive boundary detection using live-wire two-dimensional dynamic programming. In *IEEE Computers in Cardiology*, pp. 635–638, Durham, North Carolina, IEEE Computer Society Press, 1992.
2. J. K. Udupa, S. Samarasekera, and W. A. Barrett. Boundary detection via dynamic programming. In *Visualization in Biomedical Computing '92*, Chapel Hill, North Carolina, pp. 33–39, 1992.
3. M. Kass, A. Witkin, and D. Terzopoulos. Snakes: active contour models. *International Journal of Computer Vision* 1(4), pp. 321–331, 1988.

4. A. Schenk, G. Prause, H.-O. Peitgen. Efficient semiautomatic segmentation of 3D objects in medical images. *Medical Image Computing and Computer-Assisted Intervention – MICCAI 2000*, Springer, pp. 186–195, 2000.
5. E. N. Mortensen and W. A. Barrett. Intelligent scissors for image composition. In *Computer Graphics (SIGGRAPH '95)*, Los Angeles, CA, pp. 191–198, 1995.
6. A. X. Falcao and J. K. Udupa. Segmentation of 3D objects using live-wire. In *SPIE on Medical Imaging*, vol. 3034, pp. 191–198, Newport Beach, CA. 1997
7. W. A. Barrett and E. N. Mortensen. Fast, accurate and reproducible live-wire boundary extraction. In *Visualization in Biomedical Computing*, Hamburg, Germany, pp. 183–192, 1996.
8. D. Stalling and H.-C. Hege. Intelligent scissors for medical image segmentation. In *Digitale Bildverarbeitung fuer die Medizin*, Freiburg, Germany, pp. 32–36, 1996.
9. W. A. Barrett and E. N. Mortensen. Interactive live-wire boundary extraction. *Medical Image Analysis* 1(4), pp. 331–341, 1997.
10. A. X. Falcao, J. K. Udupa, S. Samarasekera, S. Sharma, B. E. Hirsch, and R. A. Lotufo. User-steered image segmentation paradigms: Live-wire and live-lane. *Graphical Models and Image Processing* 60(4), pp. 223–260, 1998.
11. E. N. Mortensen and W. A. Barrett. Interactive Segmentation with Intelligent Scissors. *Graphical Models and Image Processing* 60(5), pp. 349–384, 1998.
12. A. X. Falcao, K. Jayaram, J. K. Udupa, and Miyazawa F. K. An ultra-fast user-steered image segmentation paradigm: Live-wire-on-the-fly. In *SPIE on Medical Imaging*, vol. 3661, Newport Beach, CA, pp. 184–191, 1999.
13. G. T. Herman, J. Zheng, and Bucholtz C. A. Shape-based interpolation. *IEEE Computer Graphics and Applications* 12(3), pp. 69–79, 1992.
14. G. Borgefors. Distance Transformations in Arbitrary Directions. *Computer Vision, Graphics and Image Processing* 27(3), pp. 321–345, 1984.
15. S. P. Raya and J. K. Udupa. Shape-based interpolation of multidimensional objects. *IEEE Transactions on Medical Imaging* 9(1), pp. 32–42, 1990.
16. D. Selle, T. Schindewolf, C. J. G. Evertsz, and H.-O. Peitgen. Quantitative analysis of CT liver images. *Computer-Aided Diagnosis in Medical Imaging*, Chicago, Elsevier, pp. 435–444, 1999.
17. D. Selle, W. Spindler, A. Schenk, B. Preim, D. Böhm, K. J. Oldhafer, M. Galanski, J. H. D. Fasel, K. J. Klose, and H.-O. Peitgen. Computerized models minimize surgical risk. *Diagnostic Imaging Europe*, 12/2000, pp. 16–20, 2000.
18. B. Preim, D. Selle, W. Spindler, K. J. Oldhafer, and H.-O. Peitgen. Interaction techniques and vessel analysis for preoperative planning in liver surgery. In *Medical Image Computing and Computer-Assisted Intervention – MICCAI 2000*, Springer, pp. 608–617, 2000.

5.3 Accurate Liver Segmentation with Live Wire and Interpolation: Evaluation on 2000 Computed Tomographies

Andrea Schenk and Heinz-Otto Peitgen

Submitted 2012.

Accurate Liver Segmentation with Live Wire and Interpolation: Evaluation on 2000 Computed Tomographies

Andrea Schenk and Heinz-Otto Peitgen

***Abstract*—. For the planning of critical liver interventions, an accurate liver segmentation approach is mandatory. Automatic methods are not able to achieve the required accuracy reliably for all datasets. Interactive but more time-consuming algorithms can obtain better results. In this paper, we present a semi-automatic approach of live wire and shape-based interpolation with two additional semi-automatic modes for correction.**

The methods were applied and retrospectively evaluated on more than 2000 abdominal computed tomography data sets from different scanners and hospitals worldwide. In the evaluation, results from live wire and interpolation alone were compared with the final corrected segmentation mask in terms of accuracy and time requirements. An intra- and interobserver study on a subset of data sets complements the evaluation.

Our results show that the initial approach of live wire and interpolation is already highly accurate, with less than 1% volume overlap error and less than 1 mm average surface distance when comparing the final and initial segmentation masks. The semi-automatic initial segmentation required about 15.5 minutes on average for the overall routine data and 11.9 minutes in the intraobserver study. The control and correction step took an average of 11.4 additional minutes.

The evaluation demonstrated that our semi-automatic approach of live wire and shape-based interpolation results in already accurate results and that the control and correction step should be taken into account when comparing liver segmentation approaches.

***Index Terms*—Computed Tomography, Liver, Segmentation, Surgical Planning**

I. Introduction

Liver segmentation is the prerequisite for many clinical applications such as the planning of hepatic surgery, tumor load computation, and therapy monitoring [1], [2], [3] The applications have different demands for accuracy, and the clinical routine often limits the available interaction time. Thus, dedicated image processing techniques or different parameters for liver segmentation approaches are needed.

The challenges for good liver segmentation are manifold: several other organs and structures with similar density values are in the neighborhood of or adjacent to the liver, including the heart, spleen, diaphragm, and pancreas. Furthermore, the liver parenchyma often appears inhomogeneous in the images due to liver diseases, such as cirrhosis, or can have technical reasons, e.g., field inhomogeneities from magnetic resonance (MR) imaging. Intrahepatic structures with different gray values also hamper the segmentation process. Typical examples include vessels enhanced by contrast agent, hypointense bile ducts in computed tomography (CT) data, and lesions with different appearances and locations. Whereas the mentioned difficulties present problems for methods focusing on gray values, the wide variability of the liver shape prevents the general success of shape-based approaches. As shown by the MICCAI liver segmentation challenge, the most successful automatic liver segmentation methods are combinations of both segmentation paradigms [4], [5], [6].

The remnant liver volume is one of the most important criteria in the decision for a hepatic therapy. It can determine resectability and is relevant when the optimal intervention strategy is sought under different options, e.g., open hepatectomy with different resection extent or minimally invasive interventions such as thermal ablations.

When analyzing the results of liver segmentations, the acceptable error must be determined. In the continued MICCAI web contest, the results of the three best automatic algorithms show mean volume overlap errors of the ten test data sets between 6 % and 8.5 % and an average error of 24 % over all algorithms (http://www.sliver07.org/). In the MICCAI live contest, where the teams had to segment ten other data sets within three hours, the results were even less convincing. The three best automatic approaches showed volume overlap errors between 8.4 % and 14.6 %, while the best interactive approaches had error rates of 7.1% to 8.1 %. The standard deviations of the three best methods were about 4 % for the automatic segmentations and about 2.4 % for the interactive segmentations with the latter showing better consistency related to the direct user control [6].

A volume overlap error of 10 % in a mean liver volume of 1500 ml accounts for about 150 ml of erroneously segmented parenchyma. In cases of critical oncologic surgery, this volume typically exceeds the limit of 5-10 %, at which time a decision about resectability has to be made. Thus, for high-risk surgery, we propose liver segmentation that is as exact as

A. Schenk is with Fraunhofer MEVIS, Universitaetsallee 29, 28359 Bremen, Germany (corresponding author: phone: +49 421 218 59279; fax: +49 421 218 98 59279; e-mail: andrea.schenk@mevis.fraunhofer.de). H.-O. Peitgen is also with Fraunhofer MEVIS, Universitaetsallee 29, 28359 Bremen, Germany (e-mail: peitgen@mevis.fraunhofer.de)

possible.

The liver segmentation approach presented in this paper is dedicated to achieving accurate liver contours in a short time. Therefore, our method includes user knowledge from the beginning, aids the required interaction, and enables the immediate control and correction of results. We first introduce our basic semi-automatic approach combining the live wire algorithm and a shape-based interpolation method and subsequently describe two additionally implemented correction modes. The evaluation was performed on more than 2000 CT data sets to study volumes and times and compare the basic approach of live wire and interpolation alone with the final segmentation result. An inter- and intraobserver study on ten data sets completes the evaluation. In the final section, we will discuss the most important evaluation results, review errors related to liver segmentation, and conclude with future issues for the correction task in liver segmentation.

II. Methods

The presented liver segmentation approach consists of three basic modules: the interactive segmentation with the live wire method, a contour interpolation algorithm, and the contour correction methods. A preliminary version combining live wire and interpolation was presented at the MICCAI [7]. The three steps are typically processed in a sequential way, but they can also be used in a free, user–defined order with additional parameter adjustment and automated optimization, see Fig. 1. In the following, each algorithm will be described.

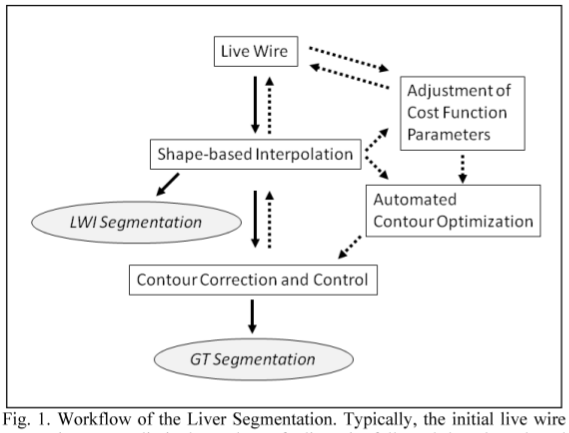

Fig. 1. Workflow of the Liver Segmentation. Typically, the initial live wire contouring on a limited number of slices is followed by shape-based interpolation and a final manual correction and control of contours (continuous arrows). The user is free to use the optional methods of adapting the cost function parameters, automated optimization of contours, or to use more than a single iteration of live wire and interpolation (right boxes, dotted arrows). The intermediate result (LWI Segmentation) represents the segmentation after a straightforward workflow of live wire and one interpolation step, while our ground truth (GT segmentation) is the final result after all user interaction.

A. Live Wire for Liver Segmentation

The live wire algorithm was introduced in 1992 [8], [9] and is a user-steered segmentation method for two-dimensional images based on the calculation of minimal cost paths by a graph search method such as Dijkstra's algorithm [10]. We will shortly review the fundamental ideas of this method; details can be found in Falcao [11].

The two-dimensional image is transformed into a directed, weighted graph. Vertices of the graph represent image pixels, while edges connecting neighboring pixels in two directions. The edges are weighted with local cost functions. After calculating the cost graph, the user starts segmenting by setting a first seed point on the boundary and moving the mouse or some other drawing device along the outline of the object. Shortest paths – those with lowest accumulated costs – from the seed to at least the current mouse position are computed using Dijkstra's algorithm. The live wire path snaps to the boundary while the user moves the mouse over the image. This is achieved by a real-time computation of the path with lowest costs from the last seed point to the current mouse position. A new seed point has to be set before the path starts to deviate from the desired contour. New shortest paths are computed from the new seed point, and the procedure is repeated. A final closure leads to a controlled and piecewise optimal segmentation result.

In our implementation, costs are computed for an 8-neighborhood allowing for diagonal connections between image pixels in contrast to the 4-neighborhood of the original live wire algorithm. The costs for diagonal connections are subdivided by their increased length to avoid discrimination of straight pixel paths. The cost function is a weighted sum of different gradient functions, the Laplacian function, and the gray values at the object boundary. For every cost function, a preset of mean and standard deviation defines a Gaussian-distributed value weighting. In the case of our boundary function, the parameters are defined separately for values inside and outside the object and then combined [7].

One time-critical step during computation of shortest paths is sorting the list of pixels with undetermined final path. By restricting the local costs between two image pixels to integer values with an upper bound of the maximal local costs, the required time can be reduced significantly by using a so-called bucket list for sorting [12]. Although the maximal cost value under all paths is unknown, the length of this bucket list can be limited. Because paths are considered in ascending costs and the new maximum will be below the current cost plus the maximum of local costs C, the bucket list can be implemented as a cycle of length C. In this way, the computational time for sorting can be reduced from $O(n \log n)$ to $O(n)$, where n represents the number of nodes in the graph, i.e., pixels in the image. A similar approach was published by Stalling and Hege [13] and later by Falcao [14].

In our implementation, the parameters of the cost function can be directly set and changed by the user. Whereas the relevance or weight of a single cost feature can be judged by inspecting the respective cost image, the parameter values of each single cost feature are difficult to determine. A learning algorithm allows automatically identifying these values based

on the evaluation of one or more existing contours. The user can define these contours either manually or as live wire paths.

For difficult image areas where no real liver boundary is available or where the live wire algorithm snaps to the wrong edges, parts of the contour can be drawn manually. For this purpose, the user keeps the mouse pressed while following the user-estimated organ boundary. Internally, all mouse positions will be collected and combined to a polygon that is part of the final contour. This mode avoids multiple mouse clicks of the live wire approach and accelerates the definition of the contour in areas where the liver boundary has to be estimated by the user.

Our live wire algorithm with shape-based interpolation is implemented as a module in the research and development platform MeVisLab, and the basic tool is available in the free version (http://www.mevislab.de).

B. Shape-based Interpolation and Automated Generation of new Live Wire Contours

Interpolation techniques are widely used in medical image processing, for tasks such as resampling, registration, and visualization. These techniques can be divided into two broad categories: scene-based and object-based interpolation. Whereas scene-based techniques determine the interpolated values directly from the intensities of the given image, object-based interpolation uses additional information about the objects in the image. The shape-based interpolation algorithm in our approach is an object-based interpolation method that interpolates between binary images of a three-dimensional data set [15].

The shape-based interpolation algorithm we use for contour interpolations consists of the following steps. First, a binary scene is generated from a given object contour. Subsequently, the distance to this boundary is mapped onto a new gray-level scene with positive distance values inside and negative distance values outside the object. In the third step, the distance images are interpolated with a conventional gray-level interpolation technique such as linear interpolation. The interpolated gray-level scenes are converted back to a binary contour image by identifying the zero crossings.

To compute the distance transformation, a version of the city-block distance is often employed [15]. We implemented two consecutive chamfering processes realized with 3x3-kernel operations [16], [17]. This chamfering method leads to more accurate results because this transformation is a better approximation of the Euclidean distance [17].

After the shape-based interpolation, the zero-crossings of the interpolated distance images define the boundary points of the new contours. To arrange these points into the correct order and to identify single contours, we developed a dedicated path search algorithm [7].

C. Automatic Optimization and Manual Correction Modes

Shape-based interpolation is based solely on the geometry of contours and takes no image information into account. Therefore, interpolated contours may not fit to the desired organ boundary in all image slices. To correct these contours automatically or with the help of the user, an optimization step was developed [7].

The underlying idea was to adapt the new contours by employing the live wire algorithm and to recalculate contour segments as optimal cost paths between the seed points. Our method copies the seed points from the two adjacent user-defined contours onto the interpolated contour. For every user-defined seed point, the nearest point on the contour path is determined. If two points are closer than a given minimal distance, they are merged into one central seed point. The use of the user-defined seeds instead of equally distributed seeds along the interpolated contour, for instance, is reasonable, because these points represent the knowledge of the user and were defined in regions of high curvature or weak edges.

After seed point creation, the live wire algorithm is started for each seed point to determine the minimal-cost path to the next seed point. Live wire segments are computed automatically, leading in an iterative fashion to new optimized contours.

Two modes of manual contour correction are offered in our implementation. The first mode is based on the live wire paradigm; the second is an intuitive form of manual contour correction.

With the live wire mode, seed points can be added to a contour, moved to a different position, or removed. All affected contour paths are updated by computing them as live wire paths between the adjacent seed points in real-time. The whole contour can be updated in an automated way, where all contour paths between seed points can be recomputed after interpolation or after a change of the cost function.

In manual correction mode, the user can draw a boundary line across the existing contour. The two outer intersecting points of the new line with an existing contour are determined. The new boundary between the intersecting points replaces the shorter part of the old contour between these points. An additional bow outside the object is added to the object, and a shortcut line inside the object decreases the segmented region. This intuitive method reflects the user expectations.

D. Type of Image Data

Most image analysis approaches are dedicated to contrast-enhanced CT data utilizing the portal venous or venous phase. Few approaches have been developed for magnetic resonance (MR) data in recent years [18], [19].

Our algorithm can be applied to data from both imaging modalities, but computed tomography images are favored due to their higher spatial resolution. Resolution and slice thickness have shown to be important factors for several aspects of surgical planning, such as the detection of small arteries and bile ducts as well as the accurate segmentation of tumors. Therefore, we will present the evaluation of our approach on abdominal CT data sets.

III. DATA

Our approach has been used for liver segmentation in

research projects and for a commercial surgical planning service. For 2082 data sets available from different research projects from 2004 to 2011, we retrospectively evaluated the segmentation results in terms of volumes and time requirements. When intermediate results were available, we compared the segmentation based on live wire and shape-based interpolation (*LWI segmentation*) with the final or ground truth segmentation (*GT segmentation*).

The data sets were acquired on different scanners and sent from different hospitals worldwide. In most cases, the images were analyzed to plan tumor resections and living donor liver transplantations (LDLT), but the data also includes regenerating livers after surgery. These organs, as well as the livers for LDLT planning, are lesion-free organs (n=1059, 50.9 %) that are healthy in most cases. The lesion cases include livers with metastases, hepatocellular carcinomas, cholangiocarcinomas, and other malignant or benign tumors (n=1023, 49.1 %).

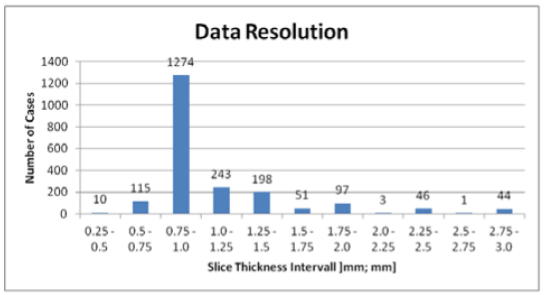

Fig. 2. Resolution of evaluation data in terms of slice thickness.
The majority of cases are high-resolution images with a slice thickness of 1.0 mm or less.

The liver was typically segmented on the portal venous or venous phase of contrast-enhanced CT image series. Data sets used for evaluation were images with a slice thickness of 3.0 mm or less. Of all images, only 190 cases (9.1 %) show a slice thickness of more than 2.0 mm. The images of 452 data sets (21.7 %) are between 1.0 mm and 2.0 mm thick, whereas the majority of images, 1440 cases (69.2 %), are high-resolution data sets with a slice thickness of 1.0 mm and less. Mean slice thickness for all images was 1.16 mm (standard deviation 0.46 mm; min 0.4 mm; max 3.0 mm), with a mean in-plane resolution of 0.69 mm (dev 0.11 mm; min 0.33 mm; max 1.76 mm). The distribution of the slice thickness for the evaluation data is given in Fig. 2. The number of image slices that include the organ and on which the segmentation had to be performed is related to the slice thickness. In our study data, the average liver spanned 161 axial image slices (18.7 cm).

IV. Evaluation

The data sets were analyzed by radiological technical assistants and other radiological or technical experts with more than 5 years experience in abdominal image analysis. The results were verified by a physician or second expert and corrected until consensus was achieved. The liver segmentation was performed with the methods described above. Liver lesions were included in the segmentation mask, but extrahepatic vessels such as the vena cava and the hilar parts of the portal vein are not part of the organ mask. Because the order of live wire, interpolation, and correction was not restricted, users could repeat interpolation, change the cost function, or correct contours between the other steps. Only data sets with a sequential order of live wire, interpolation, and subsequent correction allow for a comparison of the initial results of live wire and interpolation and the final segmentation after correction. The intermediate segmentation results, the *LWI segmentations,* were available for a subgroup of 1516 cases. The final liver segmentation, regarded as our ground truth (*GT segmentation*), was compared to the result of the LWI segmentation.

The evaluation of the required overall segmentation time was possible for a subgroup of 1606 data sets due to later implementation for time logging. Time comparisons between LWI and GT were available when the user applied the sequential order of segmentation steps and when the time for the intermediate result was available (implemented recently, n=329 data sets).

To assess the typical error magnitude between different users and repeated segmentations of the same user, we performed an additional inter- and intraobserver study on a subset of 10 datasets, consisting of 5 lesion-free organs and 5 livers with lesions.

A. Volumetric and Surface Distance Evaluation

To compare the results of GT and LWI segmentation, the volumes of these segmentations were computed as V_{GT} and V_{LWI}. The differences of the segmentation results were measured by different metrics:

- **VOE [%]**, the volume overlap error defined as

$$VOE = (1.0 - \frac{V_{GT} \cap V_{LWI}}{V_{GT} \cup V_{LWI}}) \cdot 100 \,. \quad (2)$$

- **RVD [%]**, the relative absolute volume difference:

$$RVD = \frac{V_{LWI} - V_{GT}}{V_{GT}} \cdot 100 \,. \quad (3)$$

- **ASD [mm]**, the average symmetric surface distance, defined as the average of the absolute distances between border voxels of the two segmentation masks. For each border voxel, defined as a voxel with at least one background voxel in an 18-neighborhood, the minimum of all Euclidean distances to the border voxels of the other segmentation mask is computed. The ASD is computed as the average of all absolute distance values.

- **RMS [mm]**, the root-mean-square symmetric surface distance. This measure is similar to the previous

measure, but stores the squared distances between the two sets of border voxels. After averaging the squared values, the root is extracted to give the symmetric RMS surface distance.

- **MSD [mm]**, the maximum symmetric surface distance, is defined as the RMS, but instead of the average, the maximum of all voxel distances is computed.

The metrics given above have been used in the MICCAI liver segmentation challenge [6] and allow for comparisons with other methods.

B. Time Evaluation

The overall time for segmentation, control, and correction of results was documented for 1606 cases. Times were evaluated for lesion-free organs and livers including lesions separately. For a subset of images, the intermediate segmentation mask and the time required for this first step of live wire and interpolation was available (n=329). These times will be compared to the overall segmentation time.

The times were recorded during routine surgical analysis procedures and are sometimes interrupted by colleagues, lunch breaks, or other events. To control these breaks, the time recording was stopped automatically when the images slice did not change or when the mouse was not moved for more than 20 seconds and was restarted with renewed user interaction. The pause time was then subtracted from the overall time. Idle times below the limit of 20 seconds were not taken into account and may increase the overall segmentation times to a limited extent.

C. Inter- and Intraobserver Evaluation

Two experienced users segmented the livers of 10 data sets twice with an interval of at least two weeks between the segmentations. The 10 data sets include 5 lesion-free livers and 5 livers with tumors randomly selected from the evaluation data.

The users were told to segment using live wire, interpolation, and correction, in that order, to enable the comparison of not only the final segmentations but also the LWI segmentations. Evaluations were performed in terms of volumes, distances, and time requirements.

V. Results

A. Volumetric and Surface Distance Evaluation

The mean liver volume of all segmented organs was 1.50 l with a standard deviation of 0.51 l. Livers including lesions are generally larger than the lesion-free organs (1.65 l versus 1.35 l) due to the additional tumor volume load. The number of organs with a volume above 2 l is also much higher in the lesion-liver group. Details of the organ volume distribution for the two groups are given in Fig. 3.

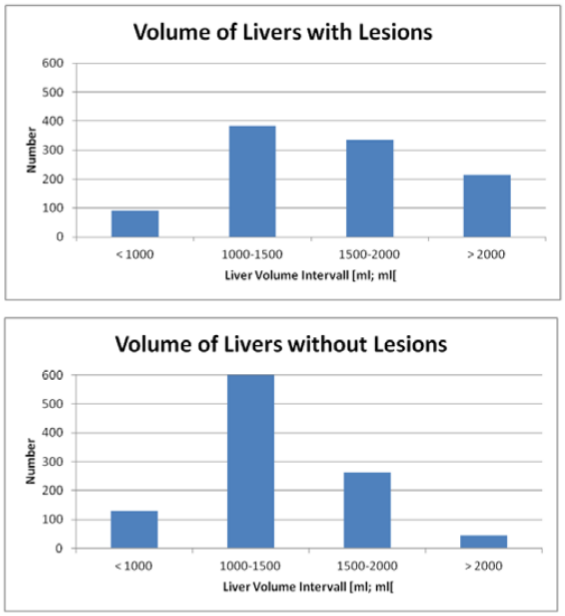

Fig. 3. Distribution of liver volumes in the evaluation data of 2082 data sets. In the upper diagram, volumes of organs without lesions, e.g., from live liver donors or regeneration studies, are shown (n= 1059). The lower diagram with the volume distribution of livers including lesions, e.g., metastases or primary liver tumors (n=1023) illustrates that this group includes a high number of large organs. The increased volume is related to the additional tumor volume load in these organs.

The comparison of the final ground truth segmentation and the initial live wire segmentation including interpolation showed relative small differences (Tables I and II). The absolute volume deviation was 0.33 % (5 ml) of the GT volume, and the mean volume overlap error accounts for less than 1 % of GT liver volume. The mean surface distance was below 0.2 mm on average of all absolute distances (ASD) and below 10 mm for the maximal distance. The maximal surface distance found in all data sets between the LWI and the GT liver mask was 47 mm. Volume differences and surface distance were smaller for the lesion-free organs than for livers with lesions (Table I).

TABLE I
COMPARISON LWI AND GT SEGMENTATION: ERROR MEASURES

	VOE [%]	RVD [%]	ASD [mm]	RMS [mm]	MSD [mm]
All Livers (n=1516)					
Mean	0.77	0.33	0.18	0.66	9.67
Std Deviation	0.94	0.60	0.31	0.86	6.70
Lesion-free Livers (n=736)					
Mean	0.62	0.25	0.14	0.58	9.10
Std Deviation	0.74	0.45	0.27	0.82	6.69
Lesion Livers (n=780)					
Mean	0.92	0.40	0.21	0.74	10.22
Std Deviation	1.09	0.71	0.35	0.90	6.66

B. Time Evaluation

The overall time for liver segmentation including the control and correction step averaged 24.7 minutes with 23.9 minutes for lesion-free organs and 26.6 minutes for organs with lesions (Table III). The values for livers for which LWI segmentation and time information was available were slightly higher (27.3, 26.0 and 27.8 minutes, see Table II). The reason may be the increased number of segmented and controlled image slices related to the decreased slice thickness for the subgroup of this more recent data. The slice thickness was 1.13 mm for the livers in Table II versus 1.16 mm for the organs in Table III.

The comparison of times required for the initial LWI segmentation and the final GT segmentation is given in Table II. For all livers, the LWI segmentation was completed in an average of 15.5 minutes, while the control and correction step accounted for additional 11.8 minutes or 43.2 % of the overall segmentation time. The initial LWI segmentation was 1.6 minutes faster for lesion-free livers, which were also generally smaller (1350 ml versus 1556 ml in this sub-study, see Table II). The control and correction step was almost identical in time requirements for the two liver groups (11.7 and 11.9 minutes). The standard deviation in all time measurements was higher for organs with lesions.

TABLE II
COMPARISON BETWEEN LWI AND GT SEGMENTATION: VOLUMES AND TIME REQUIREMENTS

	All Livers (n=329)		**Lesion-free Livers** (n=84)		**Lesion Livers** (n=245)	
	GT	LWI	GT	LWI	GT	LWI
Volume [ml]						
Mean	1504	1499	1350	1346	1556	1552
Std Deviation	*512*	*512*	*345*	*344*	*550*	*549*
Time [min]						
Mean	27.3	15.5	26.0	14.3	27.8	15.9
Std Deviation	*14.3*	*9.4*	*12.0*	*7.9*	*14.9*	*9.8*

TABLE III
LIVER VOLUMES AND OVERALL SEGMENTATION TIME FOR GT SEGMENTATION

	All Livers	**Lesion-free Livers**	**Lesion Livers**
Volume [ml]	(n=2082)	(n=1059)	(n=1023)
Mean	1499	1356	1647
Std Deviation	*505*	*337*	*598*
Time [min]	(n=1606)	(n=873)	(n=733)
Mean	24.7	23.9	26.6
Std Deviation	*13.5*	*11.5*	*15.4*

C. Inter- and Intraobserver Variability

The ten data sets for this sub-study were selected randomly. Differences in the mean organ volumes can be found by comparing the data to the global study data. In the sub-study, the mean liver volume of all organs is smaller than in the global study, and the lesion-free livers are larger than the organs with lesion. This contradicts the trend in the global study (Tables III and IV). The segmentation times were also higher for the lesion-free organs, corresponding to the larger organ size in this study data.

The overall segmentation time was shorter than in the global study (Table IV). This effect may be related to the fact that these livers are on average smaller, or the users may have segmented the organs in this dedicated sub-study faster than during routine analysis.

Intraobserver deviations were in the magnitude of 2.8 % of liver volume, 0.5 mm in average surface distance, and 9.4 mm in maximal surface distance. Interobserver deviations were larger but still below 4 % of liver volume, below 0.5 mm average surface distance, and about 10 mm maximal surface distance. Further volume and surface distance measures of the intra- and interobserver comparison are given in Table V.

TABLE IV
INTRA- AND INTEROBSERVER EVALUATION: LIVER VOLUMES AND SEGMENTATION TIMES

	All Livers (n=10)	**Lesion-free Livers** (n=5)	**Lesion Livers** (n=5)
Volume [ml]			
Mean	1411	1517	1304
Std Deviation	*251*	*173*	*288*
Overall Time [min]			
Mean	18.4	19.3	16.3
Std Deviation	*4.4*	*5.9*	*6.3*
LWI Time [min]			
Mean	11.9	12.3	10.8
Std Deviation	*3.6*	*3.9*	*4.9*

TABLE V
INTRA- AND INTEROBSERVER EVALUATION: VOLUME AND SURFACE DEVIATIONS

	VOE [%]	RVD [%]	ASD [mm]	RMS [mm]	MSD [mm]
All Livers (n=10)					
Intraobs Mean	2.81	0.74	0.44	0.76	9.43
Interobs Mean	3.30	1.00	0.53	0.95	13.49
Lesion-free Livers (n=5)					
Intraobs Mean	3.25	1.15	0.49	0.84	10.42
Interobs Mean	3.81	1.39	0.60	1.07	14.18
Liver incl. Lesions (n=5)					
Intraobs Mean	2.37	0.33	0.40	0.69	8.44
Interobs Mean	2.78	0.61	0.47	0.83	12.80

VI. DISCUSSION

We presented an interactive segmentation approach based on live wire and shape-based interpolation. Algorithms and subsequent correction were used for accurate liver segmentation in high-resolution data and evaluated on more than 2000 CT data sets. The segmentation time required for the initial LWI algorithm was about 15 minutes, whereas additional 12 minutes were spent for control and correction of results. Remarkably, the intermediate liver mask was corrected for less than 1 % of liver volume, and the average surface

distance between initial and final segmentation averaged less than 0.2 mm over all data sets. These differences show that the initial LWI segmentations were already very accurate, especially when compared to automatic approaches and their typical differences to the ground truth segmentation. Here, volume overlap errors in the magnitude of 10% are common, and an error of 6 -7 % represents a very good result, even for interactive approaches [6].

One point of criticism in our evaluation may be that both the initial algorithm and one of the correction modes use the same segmentation approach of live wire and may cause the small deviations, but only about 20 % of image slices were interactively segmented with live wire while 80 % of liver images held interpolated contours. Furthermore, the second correction method allows for a freehand mode independent of live wire. Other evaluations including more than 10 ground truth data sets also do not use manually drawn contours, instead using the segmentation results of semiautomatic approaches followed by manual correction. The most popular example is the MICCAI challenge, for which the ground truth livers were based on a slice-wise intensity-based region growing followed by expert corrections [20]. The results of our approach, the “Mevis liver segmentations” have also been used by other groups as ground truth segmentation in their evaluation [21], [22].

Comparing the segmentation times of lesion-free livers and organs with lesions, the segmentation time of lesion-free livers was about 10% faster than in the other group. The main cause is the smaller size of those organs and the fewer slices that have to be segmented. This corresponds to the intraobserver study data with larger lesion-free livers resulting in a higher time demand compared to organs with lesions. Another reason may be the location of lesions at the liver surface, leading to different gradient and boundary values than typically used for liver segmentation. As a consequence, the live wire path does not always snap to the aimed outline, and a more time-consuming interaction with an increased number of live wire seeds or an intermediate manual contouring may be necessary. Compared to automatic approaches, lesions at the organ surface or in liver regions with lower enhancement do not influence our user-steered approach greatly. For automatic algorithms, those data sets are highly challenging and often

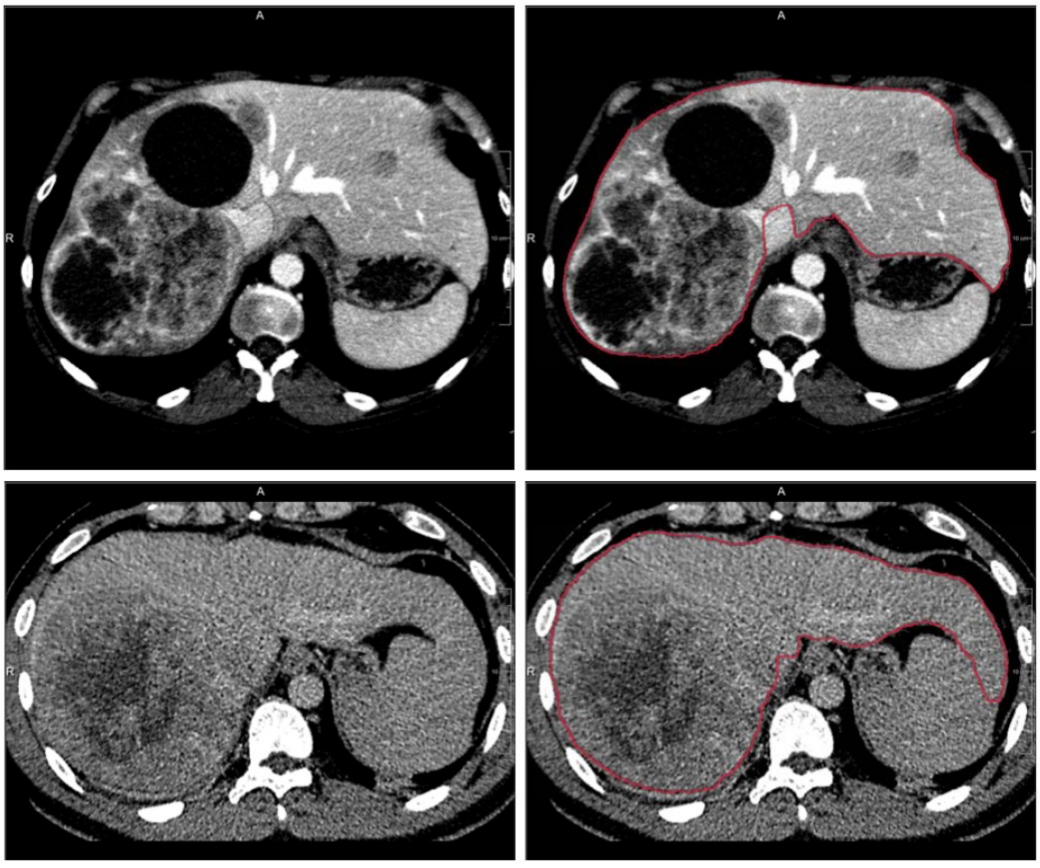

Fig. 4. Examples of liver data sets that are challenging for automatic segmentation approaches (original data left, boundary of liver segmentation right, red).Top: Liver with several metastases and a cystic lesion (central); the tumor mass enlarges the liver and shifts the left lobe to the right body cavity. Buttom: The data shows a cirrhotic liver with a hepatocellular cancer (primary liver tumor) in low-contrast enhanced and noisy data. The organ extends to the left body part and touches the spleen, an organ with similar density as the liver.

lead to complete segmentation failure.

When discussing the errors in liver segmentation and how they could be corrected for clinical applicability, three questions arise:

1) What is an acceptable segmentation error?
2) How can the segmentation error be measured to reflect the required correction effort?
3) What correction methods are appropriate to correct certain types of errors?

The acceptable error for liver segmentation depends on the clinical application. As a first volume estimation for all potential donors in LDLT or for the preparation of a tumor resection with enough remaining tissue, the exact liver volume may be of minor importance and allow for errors in the magnitude of 10% of liver volume or more. In high-risk surgery planning cases, the segmentation error should be as small as possible. Our strategy to achieve an accurate result is also based on the fact that several other error sources accompany the way from CT-based liver segmentation to the estimation of remaining liver function after a hepatic intervention. Typically, the demand of organ tissue is described and intraoperatively measured as weight. For example, in living donor liver transplantation, the criteria of minimal graft weight to recipient's body weight ratio (GRBWR) has to be fulfilled [23], [24]. For the GRBWR, the preoperatively segmented liver volume value is typically converted into an identical weight value, assuming a density of 1.0 ml/g for liver tissue. In a study with 16 donors, Lemke et al. found that the mean liver tissue density was approximately 12 % higher than suspected and that substantial interindividual variations of density occurred [25]. Animal studies also showed that the volume of perfused livers (as in CT data) was 13 % and even up to 33% higher than the volume of the non-perfused organs [26], [27]. Typically there is no way to avoid the first error source of varying density because a biopsy of liver tissue is not a standard procedure before liver resections and gives only local information. The second error of vascular volume is considered by subtracting a fixed percentage of volume or by applying a simple linear formula to compute the liver weight [26], [28]. Other error sources are related to partial volume effects, changes of the liver size caused by alimentary effects, varying liver volumes in different CT phases, and difference between the virtual and real resection when computing remnant liver volumes [25], [29], [30].

If we conclude that an accurate liver segmentation is desirable, how can the segmentation quality be measured? Most evaluations, including our study, use the typical error measures such as volume overlap and surface distances between the results of the evaluated approach and existing ground truth segmentations. Unfortunately, these error measures can only partially determine how easy and fast correcting those deviations would be. For example, a volume error of 7% can be caused by a single leakage into a neighboring organ and corrected easily with a sophisticated 3D correction tool. The neighboring organ can be roundish, like the heart, which will lead to larger surface distances than the leakage into parts of the intestine located near the liver surface. The same volume error may also be caused by diaphragm inclusion and multiple smaller metastases located at the liver surface, which may require extensive and time-consuming user interaction for correction. The difficulty in deriving the correction effort from the error measures shows that evaluation should include the correction of segmentation errors as a final step. In our evaluation data, the users have applied the correction modes even for small errors to achieve a satisfying result. The time spent for this step was about 12 minutes. If we consider an inspection time of 1-2 seconds per image slices, the control of all 2D images requires about 160-320 seconds in a typical dataset of about 160 liver slices. The remaining 6-9 minutes were still spent on the slice-based correction. Most of our segmentation errors were small-to-moderate deviations at the liver boundary, which are difficult to correct automatically.

An alternative to error measures, or in studies where no ground truth segmentation is available, may be a rating by radiological experts, but this includes the risk of subjective judgment [31]. Only a few groups worldwide have focused on dedicated correction methods for segmentation in medical data. In most cases, some kind of manual correction on 2D images is applied, e.g., cutting or adding parts of the segmentation mask by drawing an intersection line or curve at the boundary [32]. The same type of manual correction is applied in 3D, in most cases on the basis of deformable 3D meshes [33], [34], [35]. A typical example of correcting the segmentation result is presented by Silva, who modifies the mask by removing and adding voxels in 3D by a spherical brush with a user-defined radius [36]. However, 3D correction tools are not intuitive, and these surface-based correction methods can result in strange modifications, as shown in the same paper. Another recent approach has been developed by Heckel based on user-defined correct boundary paths in one image slice, live-wire extrapolation on neighbored slices, and morphological postprocessing [37]. However, in the area where automatic approaches fail and corrections are necessary, the boundary information often is low and, thus, is challenging for image-based approaches, especially when those are applied to low-contrast or noisy images (example images are given in Fig. 4)

In summary, the liver is a challenging organ to segment, and a correction step is necessary to achieve an accurate liver shape in many data sets. Control and correction takes time, especially when it has to be performed on a large number of image slices. Therefore, directly using an interactive user-controlled approach from the first segmentation step is a consequent conclusion for reliable and accurate results. It also prevents user frustration when automatic results differ significantly from the expectations and cannot be corrected easily.

ACKNOWLEDGMENT

We would like to thank all clinical partners for data contribution, valuable discussions, and continuous support.

Without our MEVIS team and their great experience in the analyses of donor and patient data, this study would not have been possible. We express our gratitude for thorough image processing and medical advice. Finally, we thank Longuan Chen for helpful scripting, Olaf Klinghammer for database support, and Guido Prause and David Black for careful review of the manuscript.

REFERENCES

[1] H. Lang, A. Radtke, M. Hindennach, T. Schroeder, N. R. Frühauf, M. Malagó, H. Bourquain, H.-O. Peitgen, K. J. Oldhafer, and C. E. Broelsch, "Impact of virtual tumor resection and computer-assisted risk analysis on operation planning and intraoperative strategy in major hepatic resection." *Arch Surg*, vol. 140, no. 7, pp. 629–38; discussion 638, Jul 2005.

[2] A. Radtke, G. C. Sotiropoulos, S. Nadalin, E. P. Molmenti, T. Schroeder, H. Lang, F. Saner, C. Valentin-Gamazo, A. Frilling, A. Schenk, C. E. Broelsch, and M. Malagó, "Preoperative volume prediction in adult living donor liver transplantation: how much can we rely on it?" *Am J Transplant*, vol. 7, no. 3, pp. 672–679, Mar 2007.

[3] S. Nadalin, G. Testa, M. Malagó, M. Beste, A. Frilling, T. Schroeder, C. Jochum, G. Gerken, and C. E. Broelsch, "Volumetric and functional recovery of the liver after right hepatectomy for living donation." *Liver Transpl*, vol. 10, no. 8, pp. 1024–1029, Aug 2004.

[4] L. Ruskó, G. Bekes, G. Németh, and M. Fidrich, "Fully automatic liver segmentation for contrast-enhanced ct images," in *MICCAI Workshop on 3D Segmentation in the Clinic: A Grand Challenge*, 2007, pp. 143–150.

[5] D. Kainmueller, T. Lange, and H. Lamecker, "Shape constrained automatic segmentation of the liver based on a heuristic intensity model," in *Proc MICCAI 2007 Workshop: 3D Segmentation in the Clinic-A Grand Challenge*, 2007, pp. 109–116.

[6] T. Heimann, B. van Ginneken, M. Styner, Y. Arzhaeva, V. Aurich, C. Bauer, A. Beck, C. Becker, R. Beichel, G. Bekes, F. Bello, G. K. Binnig, H. Bischof, A. Bornik, P. Cashman, Y. Chi, A. Cordova, B. M. Dawant, M. Fidrich, J. D. Furst, D. Furukawa, L. Grenacher, J. Hornegger, D. Kainmüller, R. Kitney, H. Kobatake, H. Lamecker, T. Lange, J. Lee, B. Lennon, R. Li, S. Li, H.-P. Meinzer, G. Németh, D. S. Raicu, A.-M. Rau, E. M. van Rikxoort, M. Rousson, L. Ruskó, K. A. Saddi, G. Schmidt, D. Seghers, A. Shimizu, P. Slagmolen, E. Sorantin, G. Soza, R. Susomboon, J. M. Waite, A. Wimmer, and I. Wolf, "Comparison and evaluation of methods for liver segmentation from ct datasets," *IEEE Trans. Med. Imaging*, vol. 28, no. 8, pp. 1251–1265, 2009.

[7] A. Schenk, G. Prause, and H.-O. Peitgen, "Efficient semiautomatic segmentation of 3d objects in medical images," in *Medical Image Computing and Computer-Assisted Intervention*. Berlin: Springer, 2000, pp. 186–195.

[8] E. N. Mortensen, B. Morse, W. A. Barrett, and J. K. Udupa, "Adaptive boundary detection using live-wire two-dimensional dynamic programming," in *IEEE Computers in Cardiology*, R. Werner, Ed. Durham, North Carolina, USA: IEEE Computer Society Press, 1992, pp. 635–638.

[9] J. K. Udupa, S. Samarasekera, and W. A. Barrett, "Boundary detection via dynamic programming," in *Visualization in Biomedical Computing '92*, Chapel Hill, North Carolina, 1992, pp. 33–39.

[10] E. W. Dijkstra, "A note on two problems in connexion with graphs," *Numerische Mathematik*, vol. 1, pp. 269–271, 1959, 10.1007/BF01386390.

[11] A. X. Falcao, J. K. Udupa, S. Samarasekera, S. Sharma, and B. E. Hirsch, "User-steered image segmentation paradigms: Live-wire and live-lane," *Graphical Models and Image Processing*, vol. 60, no. 4, pp. 223–260, 1998.

[12] B. V. Cherkassky, A. V. Goldberg, and T. Radzik, "Shortest paths algorithms: Theory and experimental evaluation," in *SODA*, 1994, pp. 516–525.

[13] D. Stalling and H.-C. Hege, "Intelligent scissors for medical image segmentation," in *Digitale Bildverarbeitung für die Medizin*, Freiburg, Germany, 1996, pp. 32–36.

[14] A. X. Falcão, J. K. Udupa, and F. K. Miyazawa, "An ultra-fast user-steered image segementation paradigm: Live-wire-on-the-fly," *IEEE Trans. Med. Imaging*, vol. 19, no. 1, pp. 55–62, 2000.

[15] S. P. Raya and J. K. Udupa, "Shape-based interpolation of multidimensional objects," *IEEE Transactions on Medical Imaging*, vol. 9, no. 1, pp. 32–42, 1990.

[16] G. T. Herman, J. Zheng, and B. C. A., "Shape-based interpolation," *IEEE Computer Graphics and Applications*, vol. 12, no. 3, pp. 69–79, 1992.

[17] G. Borgefors, "Distance transformations in digital images," *Computer Vision, Graphics, and Image Processing*, vol. 34, no. 3, pp. 344–371, 1986.

[18] L. Ruskó and G. Bekes, "Liver segmentation for contrast-enhanced mr images using partitioned probabilistic model," *Int. J. Computer Assisted Radiology and Surgery*, vol. 6, no. 1, pp. 13–20, 2011.

[19] O. Gloger, K. D. Toennies, and J.-P. Kuehn, "Fully automatic liver volumetry using 3d level set segmentation for differentiated liver tissue types in multiple contrast mr datasets," in *SCIA*, ser. Lecture Notes in Computer Science, A. Heyden and F. Kahl, Eds., vol. 6688. Springer, May 2011, pp. 512–523.

[20] B. van Ginneken, T. Heimann, and M. Styner, "3d segmentation in the clinic: A grand challenge," in *MICCAI 2007 Workshop Proceedings: 3D Segmentation in the Clinic - A Grand Challenge*, v. G. B. Heimann T, Styner M, Ed., 2007, pp. 7–15.

[21] R. Pohle, M. Hinz, K. D. Tönnies, G. Stamm, and T. Pohle, "Schnelle, interaktive segmentierung medizinischer 3d-datensätze durch anwendung der image-foresting-transformation in zwei verschiedenen auflösungsstufen," in *Bildverarbeitung für die Medizin*, ser. CEUR Workshop Proceedings, M. Meiler, D. Saupe, F. Kruggel, H. Handels, and T. M. Lehmann, Eds., vol. 56. Springer, 2002, pp. 189–192.

[22] S. Li, J. M. Waite, B. T. Lennon, J. D. Stefansic, R. Li, and B. M. Dawant, "Development of preoperative liver and vascular system segmentation and modeling tool for image-guided surgery and surgical planning," in *Society of Photo-Optical Instrumentation Engineers (SPIE) Conference Series*, ser. Society of Photo-Optical Instrumentation Engineers (SPIE) Conference Series, vol. 6918, Apr. 2008.

[23] N. Habib and K. Tanaka, "Living-related liver transplantation in adult recipients: a hypothesis." *Clin Transplant*, vol. 9, no. 1, pp. 31–34, Feb 1995.

[24] C. M. Lo, S. T. Fan, C. L. Liu, J. K. Chan, B. K. Lam, G. K. Lau, W. I. Wei, and J. Wong, "Minimum graft size for successful living donor liver transplantation." *Transplantation*, vol. 68, no. 8, pp. 1112–1116, Oct 1999.

[25] A.-J. Lemke, M. J. Brinkmann, T. Schott, S. M. Niehues, U. Settmacher, P. Neuhaus, and R. Felix, "Living donor right liver lobes: preoperative ct volumetric measurement for calculation of intraoperative weight and volume." *Radiology*, vol. 240, no. 3, pp. 736–742, Sep 2006.

[26] S. M. Niehues, J. K. Unger, M. Malinowski, J. Neymeyer, B. Hamm, and M. Stockmann, "Liver volume measurement: reason of the difference between in vivo ct-volumetry and intraoperative ex vivo determination and how to cope it." *Eur J Med Res*, vol. 15, no. 8, pp. 345–350, Aug 2010.

[27] B. B. J. Frericks, T. Kiene, G. Stamm, H. Shin, and M. Galanski, "[ct-based liver volumetry in a porcine model: impact on clinical volumetry prior to living donated liver transplantation]." *Rofo*, vol. 176, no. 2, pp. 252–257, Feb 2004.

[28] S. Hwang, S. G. Lee, K. H. Kim, K. M. Park, C. S. Ahn, D. B. Moon, C. W. Chu, Y. J. Lee, and P. C. Min, "Correlation of blood-free graft weight and volumetric graft volume by an analysis of blood content in living donor liver grafts." *Transplant Proc*, vol. 34, no. 8, pp. 3293–3294, Dec 2002.

[29] A. Radtke, G. Sotiropoulos, S. Nadalin, E. Molmenti, T. Schroeder, H. Lang, F. Saner, C. Valentin-Gamazo, A. Frilling, A. Schenk, C. Broelsch, and M. Malago, "Preoperative volume prediction in adult living donor liver transplantation: How much can we rely on it?" *Am J Transplant*, vol. 7, no. 3, pp. 175–185, 2007.

[30] L. Hermoye, I. Laamari-Azjal, Z. Cao, L. Annet, J. Lerut, and B. Dawant, "Liver segmentation in living liver transplant donors: comparison of semiautomatic and manual methods," *Radiology*, vol. 234, no. 1, pp. 171–178, 2005.

[31] L. Ruskó, G. Bekes, and M. Fidrich, "Automatic segmentation of the liver from multi- and single-phase contrast-enhanced ct images." *Med Image Anal*, vol. 13, no. 6, pp. 871–882, Dec 2009.

[32] L. Gao, D. G. Heath, B. S. Kuszyk, and E. K. Fishman, “engAutomatic liver segmentation technique for three-dimensional visualization of ct data.” *engRadiology*, vol. 201, no. 2, pp. 359–364, Nov 1996.
[33] Y. Kang, K. Engelke, and W. A. Kalender, “Interactive 3d editing tools for image segmentation,” *Medical Image Analysis*, vol. 8, no. 1, pp. 35–46, 2004.
[34] A. Bornik, R. Beichel, and D. Schmalstieg, “Interactive editing of segmented volumetric datasets in a hybrid 2d/3d virtual environment,” in *VRST*, 2006, pp. 197–206.
[35] T. Schwarz, T. Heimann, R. Tetzlaff, A. Rau, I. Wolf, and H. Meinzer, “Interactive surface correction for 3d shape based segmentation,” in *Proc. SPIE Int. Soc. Opt. Eng.*, vol. 6914, 2008, p. 691430.
[36] S. S. Silva, B. S. Santos, J. Madeira, A. Silva, and A. Silva, “A 3d tool for left ventricle segmentation editing.” in *ICIAR*, ser. International Conference on Image Analysis and Recognition Image Analysis and Recognition, 2010, pp. 79–88.
[37] F. Heckel, J.-H. Moltz, V. Dicken, B. Geisler, H.-C. Bauknecht, M. Fabel, S. Meier, and H.-O. Peitgen, “3D contour based local manual correction of liver segmentations in CT scans,” in *International Journal of Computer Assisted Radiology and Surgery*, vol. 4, no. 1. Springer, 2009, pp. 45–46.

6 Publications - Computer-Assistance for Liver Surgery

6.1 ILabMed workstation – A Development Platform for Radiological Applications

Andrea Schenk, Jens Breitenborn, Dirk Selle, Thomas Schindewolf, Dominik Böhm, Wolf Spindler Hartmut Jürgens, Heinz-Otto Peitgen

Presented during a talk at the German congress Bildverarbeitung für die Medizin 1999 and published in H. Evers, G. Glombitza, T. Lehmann, and H.-P. Meinzer (Eds.), Proceedings of BVM 1999, pp. 238 – 242.

Copyright 1999 Springer. Reprinted with permission.

ILabMed-Workstation - Eine Entwicklungsumgebung für radiologische Anwendungen

A. Schenk, J. Breitenborn, D. Selle, T. Schindewolf, D. Böhm,
W. Spindler, H. Jürgens, H.-O. Peitgen

MeVis - Centrum für Medizinische Diagnosesysteme und Visualisierung
Universitätsallee 29, 28359 Bremen
Email: andrea.schenk@mevis.de

Zusammenfassung. Die *ILabMed-Workstation* ist eine Entwicklungsumgebung für die medizinische Bildverarbeitung. Basierend auf einer großen Anzahl an Bildverarbeitungsalgorithmen können verschiedenste radiologische Probleme gelöst werden. Das System kann in einfacher Weise um neue Algorithmen erweitert und die individuellen Problemlösungen können mit einer Bedienoberfläche versehen werden. Dies wird in der neu entwickelten Programmiersprache *APrIL* durchgeführt, die durch eine interpretierte Ausführung kurze Entwicklungszyklen ermöglicht.
Die ILabMed-Workstation wird am Centrum für Medizinische Diagnosesysteme und Visualisierung zur Entwicklung von radiologischen Anwendungsprojekten u.a. im Bereich der präoperativen Planung der Leberchirurgie eingesetzt.

Schlüsselwörter: Entwicklungsumgebung, Computer Assisted Surgery, Software Engineering, Gefäßerkennung, Visualisierung

1 Einleitung

In den letzten Jahren hat der Einsatz der computerunterstützten Bildverarbeitung in der Medizin eine immer größere Bedeutung erlangt. Gleichzeitig nehmen die Komplexität der Algorithmen und der Bedienungsaufwand zur Lösung der vielfältigen medizinischen Fragestellungen zu.

Ein modulares Bildverarbeitungssystem, das Teilaufgaben in einzelnen Komponenten realisiert, die sich entsprechend der speziellen Problematik kombinieren und erweitern lassen, stellt ein geeignetes flexibles Konzept zur Entwicklung medizinischer Anwendungsprogramme dar. Dieses System bietet idealerweise auch eine Möglichkeit zum Bau graphischer Benutzungsschnittstellen an, um den Bedienkomfort zu erhöhen und um Akzeptanzprobleme bei der Verwendung im klinischen Alltag zu verringern.

Die *ILabMed-Workstation* ist ein Bildverarbeitungssystem, das dieses Konzept realisiert und den Entwicklungsprozeß, angefangen von der Programmierung neuer Bildverarbeitungsalgorithmen über deren Verknüpfung mit weiteren sogenannten *Operatoren* in Bildverarbeitungsnetzwerken bis hin zur Erstellung von leicht bedienbaren Benutzungsoberflächen, unterstützt.

2 Die ILabMed-Workstation

Die Basisplattform der ILabMed-Workstation wird seit 1993 am Centrum für Medizinische Diagnosesysteme und Visualisierung auf Silicon Graphics Workstations entwickelt, und eine erste Version wurde 1995 auf dem 3. Freiburger Workshop vorgestellt [1]. Seitdem ist das System kontinuierlich weitergeführt und verbessert worden. Im folgenden werden die bisherigen Komponenten zusammengefaßt und die neuesten Entwicklungen präsentiert.

2.1 Die Systemkomponenten

Die ILabMed-Workstation stellt mehr als 200 Bildverarbeitungsalgorithmen, Datei-Operationen und Visualisierungswerkzeuge zur Verfügung. Diese lassen sich innerhalb einer graphischen Oberfläche interaktiv zu Bildverarbeitungsnetzwerken verknüpfen.

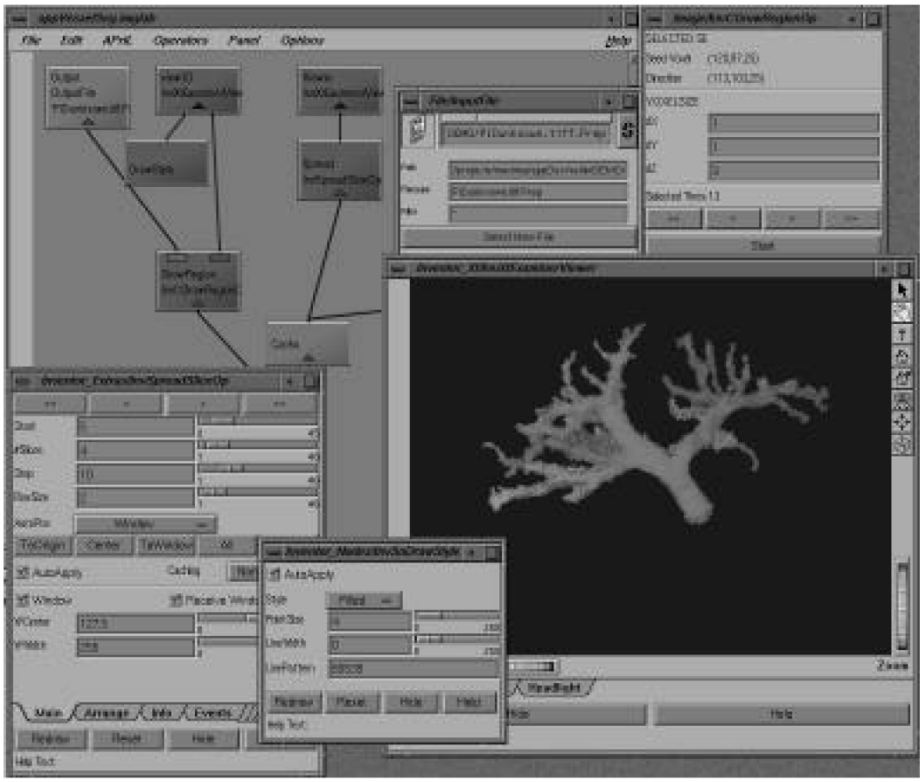

Abb. 1. Ein Bildverarbeitungsnetzwerk mit Operatoren und deren Schnittstellen

Weitere problemspezifische Algorithmen lassen sich innerhalb der Entwicklungsumgebung mit der neu entwickelten Programmiersprache APrIL oder auch in C++ implementieren und integrieren.

Bei komplexen Problemen enthalten die Bildverarbeitungsnetzwerke eine große Anzahl an Operatoren, deren eigene vielfältige Parameter auf separaten Benutzungsschnittstellen kontrolliert werden. Dies kann die Bedienung aufwendig machen und erfordert neben der Kenntnis des Datenflusses auch die Übersicht über die Lage der Bedienfelder (Abb. 1).

Innerhalb der ILabMed-Workstation kann diese Komplexität reduziert werden, indem in der Programmiersprache APrIL ein einziges Benutzungsinterface implementiert wird. Dazu können sowohl die schon vorhandenen Bedienelemente der benutzten Operatoren kopiert als auch neue Oberflächenelemente hinzugefügt werden. Auf diese Weise können zahlreiche Parameter vorbelegt werden und erscheinen ebenso wie andere nicht benötigte Bedienfelder nicht mehr auf der dann übersichtlichen und benutzerfreundlichen Oberfläche (Abb. 2).

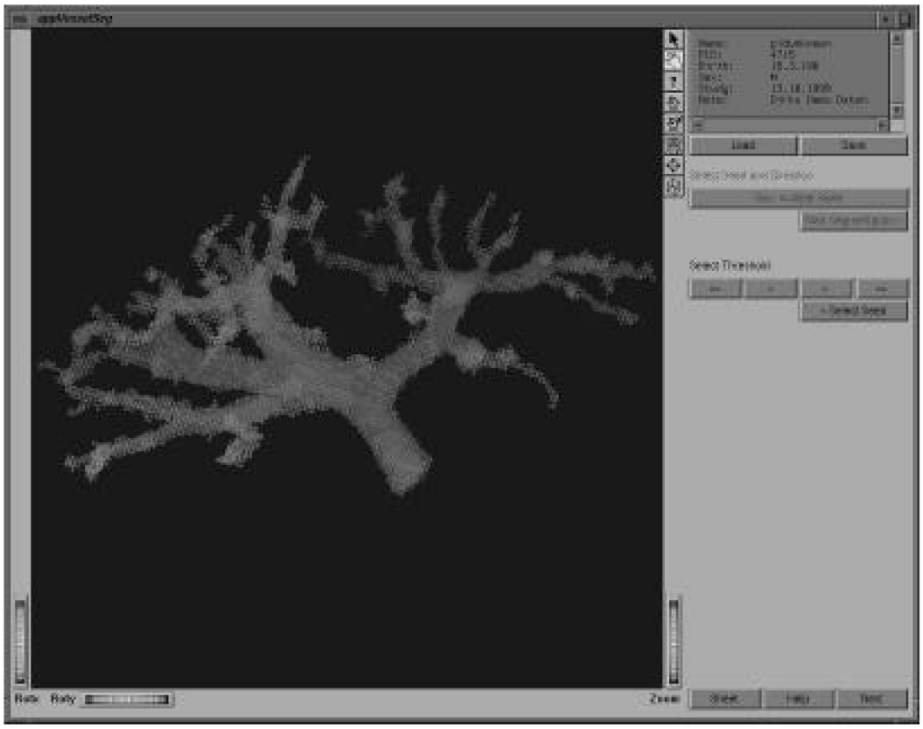

Abb. 2. Benutzerfreundliche Bedienoberfläche zum Netzwerk von Abb. 1

Eine zusätzliche Hilfestellung und Führung durch die Applikation erlaubt ein HTML-Browser. In diesem Fenster können sowohl Hilfetexte angezeigt als auch einzelne oder komplexe Bedienschritte über HTML-Links ausgelöst werden. Damit ergibt sich die Möglichkeit, die Applikation um ein interaktives Demonstrations- bzw. Lernprogramm zu erweitern.

Soll speziell eine größere, aus mehreren sequentiellen Arbeitsschritten bestehende Applikation aufgebaut werden, läßt sich auch der Workflow mit Hilfe von APrIL steuern. Dies ermöglicht eine genaue Kontrolle des Datenflusses und einen besseren Anwendungskomfort.

2.2 Die Programmiersprache APrIL

Eines der Hauptwerkzeuge der ILabMed-Workstation ist die neu entwickelte, objektorientierte Programmiersprache APrIL (Application Programming Interface Language). Sie stellt mit ihrer C++ ähnlichen Syntax und zahlreichen an den Applikationsbau angepaßten Methoden ein schnell erlernbares und mächtiges Hilfsmittel zur Implementierung von Bildverarbeitungsalgorithmen und zur Erstellung von graphischen Benutzungsschnittstellen dar. Durch die Ausführung des APrIL-Codes in einem interpretierten Modus reduziert sich die benötigte Zeit der Entwicklungszyklen. Innerhalb der ILabMed-Workstation wird dieser Modus durch die automatische Generierung von C++ Sourcen, Header- und Makefiles ergänzt und ermöglicht so die abschließende Kompilierung. Alternativ kann die Implementierung auch direkt in C++ erfolgen.

3 Das Anwendungsbeispiel HepaVision

HepaVision ist ein komplexes Anwendungssystem zur präoperativen Planung in der Leberchirurgie. Es beruht auf Algorithmen, die im Centrum für Medizinische Diagnosesysteme und Visualisierung entwickelt wurden [2, 3] und beinhaltet alle Schritte, die zur Segmenteinteilung der Leber und zur Volumetrie von Leber und Tumoren nötig sind.
Im einzelnen sind dies die Komponenten

Datei-Import	Laden von Daten über eine DICOM-Schnittstelle und Einlesen von ACR-Nema, Tiff und anderen Dateiformaten
Region of Interest	Ansicht der Daten in drei Raumrichtungen und Auswahl einer ROI
Segmentierung	Halbautomatische Segmentation von Objekten im zwei- oder dreidimensionalen Datensatz
Volumetrie	Berechnung der Volumina von Leber und Tumoren mit Hilfe der Wasserscheidentransformation [4]

Gefäßanalyse	Auf Skelettierung beruhende Auswertung des Gefäßsystems der Leber
Segmenteinteilung	Modellbasierte Bestimmung der Lebersegmente und deren farbliche Markierung
Visualisierung	Objektbasierende Graphik mit 3D-Rendering und Surface-Shaded-Displays.

Realisiert wurde die Applikation innerhalb der ILabMed-Workstation durch mehrere Bildverarbeitungsnetzwerke und eine in APrIL programmierte Benutzungsschnittstelle. Ebenfalls in APrIL wurde der die einzelnen Teilschritte verbindende Workflow umgesetzt, der u.a. die automatische Weitergabe von Informationen des aktuellen Datensatzes möglich macht.

4 Zusammenfassung

Die ILabMed-Workstation ermöglicht nur mit Kenntnis der C++ ähnlichen Programmiersprache APrIL eine schnelle Entwicklung von neuen Bildverarbeitungsalgorithmen und Benutzungsschnittstellen für Applikationsprototypen. Mit diesen neuen Tools und der Bildverarbeitungsbasis, die die ILabMed-Workstation bietet, lassen sich auch sehr spezielle radiologische Fragestellungen bearbeiten und erfüllen somit den Wunsch nach einem umfassenden Werkzeug für die medizinische Bildverarbeitung.

Literatur

1. T. Netsch, S. Dachwitz, H. Jürgens: ILab - Eine interaktive Programmierumgebung für die medizinische Bildverarbeitung. Digitale Bildverarbeitung in der Medizin, Tagungsband zum 3. Freiburger Workshop, 1995, S. 1-7.
2. C.J.G. Evertsz, H. Jürgens, H.-O. Peitgen, D. Selle, W. Spindler, C. Zahlten, K.-J. Klose, R. Leppek: Segmenteinteilung der Leber: Operationsplanung, Therapieüberwachung und Anatomie. Mathematik - Schlüsseltechnologie für die Zukunft, Verbundprojekte zwischen Universität und Industrie. K.-H. Hoffmann, W. Jäger, T. Lohmann, H.Schunck (Hrsg.). Springer Verlag, Berlin 1997, S.421-434.
3. D. Selle, T. Schindewolf, C.J.G. Evertsz, H.-O. Peitgen: Quantitative Analysis of CT Liver Images. Proc. First International Workshop on Computer-Aided Diagnosis. Chicago, Illinois, September 20-23, 1998 (in press).
4. S. Wegner, D. Stalling, H.C. Hege, H. Oswald, E. Fleck: Die 3D-Wasserscheidentransformation auf Graphebene - eine Anwendung für die Hyperthermieplanung. Digitale Bildverarbeitung in der Medizin. Tagungsband zum 5. Freiburger Workshop, 1997, S. 31-36.

6.2 Intraoperative Augmented Reality for Minimally Invasive Liver Interventions

Michael Scheuering, Andrea Schenk, Armin Schneider, Bernhard Preim, Guenther Greiner

Presented at SPIE in 2003 and published in Proc. of SPIE Medical Imaging, vol 5029, pp. 407-417.

Copyright 2003 Society of Photo Optical Instrumentation Engineers. Reprinted with permission.

Intraoperative Augmented Reality for Minimally Invasive Liver Interventions

Michael Scheuering[1], Andrea Schenk[2], Armin Schneider[3], Bernhard Preim[2], Günther Greiner[1]

[1]Computer Graphics Group, University of Erlangen-Nuremberg,
Am Weichselgarten 9, 91058 Erlangen, Germany
[2]MeVis - Center for Medical Diagnostic Systems and Visualization,
Universitaetsallee 29, 28359 Bremen, Germany
[3] Institute MITI, TU Munich, Trogerstrasse 26, 81675 Munich, Germany

ABSTRACT

Minimally invasive liver interventions demand a lot of experience due to the limited access to the field of operation. In particular, the correct placement of the trocar and the navigation within the patient's body are hampered. In this work, we present an intraoperative augmented reality system (IARS) that directly projects preoperatively planned information and structures extracted from CT data, onto the real laparoscopic video images. Our system consists of a preoperative planning tool for liver surgery and an intraoperative real time visualization component. The planning software takes into account the individual anatomy of the intrahepatic vessels and determines the vascular territories. Methods for fast segmentation of the liver parenchyma, of the intrahepatic vessels and of liver lesions are provided. In addition, very efficient algorithms for skeletonization and vascular analysis allowing the approximation of patient-individual liver vascular territories are included. The intraoperative visualization is based on a standard graphics adapter for hardware accelerated high performance direct volume rendering. The preoperative CT data is rigidly registered to the patient position by the use of fiducials that are attached to the patient's body, and anatomical landmarks in combination with an electro-magnetic navigation system. Our system was evaluated in vivo during a minimally invasive intervention simulation in a swine under anesthesia.

Keywords: Registration, image-guided surgery, direct volume rendering, hardware acceleration, computer assisted surgery

1. INTRODUCTION

The vascular anatomy, in particular the branching patterns of vasculature determines therapeutic decisions and the realization of therapy in the operating room. Therefore, vascular analysis based on volumetric datasets becomes more and more important.

Especially for oncologic resections in liver surgery, the spatial location of tumors and their relation to the main hepatic vessels and the parenchyma is essential. According to the complex anatomy of the liver, preoperative therapy planning and the intervention in the operation room demand a lot of practice to the surgeon. The introduction of a liver planning tool can assist the physician immensely, providing patient-individual analysis and visualization. Thus, it allows a 3D exploration of the patient's liver anatomy, tumor and vascular measurements. Additionally, the shape and the volume of vascular territories can be extracted, based on algorithms that take into account the intrahepatic vascular anatomy.

Although preoperative planning tools for liver surgery can assist the surgeon in an efficient way, a drawback is the lack of presence of planning data in the operation room during the intervention. Therefore, it is the surgeon's task to map the planning results on the intraoperative scene in mind. Especially in the context of minimally invasive procedures, this mapping becomes more complex, since the whole operation field can only be visualized

Further author information: (Send correspondence to M. Scheuering)
Phone: +49.9131.8529923
E-mail: scheuering@cs.fau.de
Web: http://www9.informatik.uni-erlangen.de/Persons/Scheuering

by means of a camera-monitor system. Additionally, the tissue of interest is only accessible via small surgical tools and depth information is completely lost.

A possible assistance for such intervention schemes is provided by *augmented reality systems* (ARS) that allow the projection of 3D information onto the real laparoscopic video streams, which can ease the navigation within the patient's body immensely. Additionally, the provision of preplanned 3D information into the surgeon's view allows to directly make use of the patient-individual liver analysis, which increases the available 3D information of a patient at intervention time.

In our work, we present such an ARS in terms of an image overlay system that directly projects patient-individual information, provided by HepaVision,[1] onto the real laparoscopic video images at real time frame rates. While the surgeon moves the laparoscopic camera, the virtual view including the preplanned 3D information, is adapted automatically.

This work is divided into the following sections. In Section 2 we give an overview of some previous work that is similar to our approach. In Section 3, an overview of our preoperative planning tool for liver analysis and its applied mechanisms and algorithms is presented. The rigid registration between the patient and the visualization system is explained in Section 4, whereas the necessary calibration steps such as lens distortion correction is presented in Section 5. Since the visualization of the presented 3D data has to be performed at real time frame rates, Section 6 introduces the techniques of our algorithms. Afterwards, some results are presented in Section 7. Finally, in Section 8 the work is concluded.

2. PREVIOUS WORK

Image overlay systems often have been used in different medical applications. The first important use was in neurosurgical interventions as proposed by Roberts *et al.*[2] Simple outlines or trajectories in one eyepiece have been overlaid, extracted from the original CT volume. Other systems use standard flat panel liquid crystal displays (LCD), whereas the visualization panel is tracked by an navigation system.[3] Alternatively, head-mounted displays (HMD) like the Varioscope System[4] are applied. For minimally invasive procedures, Fuchs *et al.*[5] developed an expensive 3D laparoscope, consisting of a projector for structured light for depth calculation of the inner organs. The augmentation of the surgeon's view is realized by the use of a tracked HMD. A complete visualization platform for image overlay has been proposed by Shahidi *et al.*,[6] including intraoperative navigation of the surgical tools and OpenGL-based visualization for the image overlays, which is similar to our system. All presented systems apply a rigid body registration in order to match the patient and the visualization system.

There are also systems for non-linear registration between the liver and the preoperative CT in order to assist open liver surgery.[7] Here, the registration is performed by the introduction of Doppler ultrasound and electro-magnetic navigation.

Although all mentioned techniques provide the possibility for image overlay or augmentation, there is a lack of systems for minimally invasive liver interventions that merge the power of intraoperative augmented reality and special purpose preoperative planning results.

3. PREOPERATIVE PLANNING

For therapies in liver tumor treatment, preoperative planning requires detailed knowledge about the patient's anatomy. The spatial relations between pathological and vital structures are essential for estimating the risks of minimally invasive and surgical treatment. For conventional surgery, a resection proposal has to fully enclose the tumors to be removed, whereas main branches of the vascular systems must be preserved. This guarantees that the remaining functional part of the liver is sufficient for the patient's survival. If a surgical resection proves impossible as a result of either a tumors location or the patient's constitution, the destruction of a tumor by minimally invasive interventions or thermal ablations, such as laser-induced thermotherapy (LITT) or radio-frequency ablation (RF), often is a viable alternative. However, profound planning is even more important for minimally invasive therapies than in conventional surgery. On one hand, vascular territories have to be respected as well, while on the other hand, there is a lack of visual control of the ongoing therapy due to limitations of intraoperative imaging. Moreover, minimally invasive strategies require planning of the instruments' trajectories to ensure that major vascular branches are not violated.

The preoperative planning in this project is based on contrast enhanced CT data and consists of several segmentation and image analysis steps:

- Segmentation of the liver
- Segmentation of liver tumors
- Segmentation of hepatic vessels
- Structural analysis of hepatic artery, portal vein and hepatic veins
- Calculation of vascular territories and risk analysis

These steps are all part of the software assistant HepaVision and described in detail in the following subsections.

3.1. Liver Segmentation

The liver is neighbored to other anatomical structures with similar density values (heart, stomach). This causes problems for fully-automatic segmentation approaches and is the reason why in most hospitals the liver boundaries are manually defined by contour tracing. As a compromise between unsuccessfull automatic and time-consuming manual segmentation, we perform the definition of liver contours with a modified live-wire method, a semi-automatic edge-oriented algorithm.[8,9] With live-wire the user starts with selecting a first contour point and moves a pointing device (for example a mouse) to roughly sketch the object's contour. The algorithm relies on a cost-function to calculate an optimal path between the start point and the current position of the pointing device in real-time. The cost-function is a weighted sum considering the magnitude of the gradient, the direction of the gradient and the laplacian zero-crossing. With this approach, a few user-defined contour points lead to a piece-wise optimal user-steered segmentation.

The initial approach has been carefully refined in order to enhance 3D segmentation. For this purpose, we combined live-wire with shape-based interpolation[10] between interactively segmented contours and subsequent optimization. This new approach computes the majority of the contours automatically and therefore reduces the interaction effort.[8,11] Interactive modification of the interpolated contours, however, is still possible. With this approach the user can steer the segmentation process and generate precise results in acceptable time.

3.2. Tumor Segmentation

The segmentation of a liver tumor from CT data requires different tools depending on the type of the lesion. Therefore, more than one tool is offered for this image processing step. While the segmentation of metastasis can be performed in most cases with a simple region-growing or a watershed algorithm, the extraction of hepatocellular carcinoma is more elaborate. For example, after chemoembolisation with Mitomycin and Lipiodol these lesions appear in the data as inhomgenious, hyperdense regions. Here, a modified algorithm based on Fuzzy-Connectedness[12,13] showed promising results. In cases where the automatic or semi-automatic approaches fails, a live-wire or manual delineation tool can be used. For larger lesions, the interpolation method described in the last subsection is applied. The segmentation of tumors at the boundary of the liver is simplified by restricting it to the liver mask, allowing the user to draw the outer contours very roughly.

3.3. Vascular Segmentation

The segmentation of the intrahepatic vessels is a prerequisite for a subsequent geometrical and structural analysis. In a preprocessing step, filter functions for noise reduction (Gaussian, median filter) and for background compensation (Laplace-like filters) are applied to the CT-data.[14] As a result, intrahepatic vessels can be identified and delineated by use of a threshold-based region-growing method. Usually, region-growing segmentation must be repeated with modified thresholds until an appropriate result is found. To accelerate this procedure, we refined it to suggest a threshold automatically.[14] The new algorithm works as follows.

Initially, a seed voxel is selected interactively in the portal vein at the liver hilum. Starting with this seed voxel, the region-based segmentation algorithm iteratively accumulates the 26 adjacent voxels with an intensity

equal to or greater than the intensity θ_{beg} of the seed voxel and keeps them in a list $L(\theta_{beg})$. Using $L(\theta_{beg})$ as new seed voxels, all adjacent voxels with intensities greater or equal $\theta_{beg} - 1$ are collected in a list $L(\theta_{beg} - 1)$. The threshold is further decreased until a given threshold θ_{end} is reached which creates only voxels $L(\theta_{end})$ outside the vascular systems. The automatic threshold selection is based on the observation that the number of voxels $N(\theta)$ is approximately linear decreasing for $\theta = \theta_{opt} \ldots \theta_{beg}$. At θ_{opt} the slope changes considerably because many voxels belonging to the liver tissue are collected for thresholds below θ_{opt}. A suggestion for θ_{opt} can thus be found by calculating an optimal fit of two straight lines for $N(\theta)$. If the suggested threshold is not satisfying it may be adjusted interactively. New segmentation results are displayed immediately using the voxel lists already created.

3.4. Vascular Analysis

The segmentation result is a set of voxels representing the intrahepatic vascular systems. For surgery planning, a further analysis of these voxels is required. This includes geometric measurements of the branches (radius, length), the identification of individual vascular systems and the identification of the ramification pattern (e.g. to determine the main portal subtrees supplying the liver segments).

Depending on the scanning protocol, usually two or more different vascular systems of the liver are enhanced with contrast agent during the scan. Often the portal vein and hepatic veins are affected. Therefore, the scan yields high-intensity voxels for both vascular systems. Due to the limited spatial resolution of the scanned volume data, voxels of different vascular systems are often adjacent to each other such that they are segmented as one object when in reality there is only proximity between the two. We analyze and separate such "forests" of connected vascular systems automatically using graph theoretical methods. In a first step, the voxel-based shape representation of the vessels is transformed into an abstract graph representation, utilizing "skeletonization".[15] The skeleton representation enables a much easier access to the geometry of the branches and to structural information (ramifications).

The separation of vascular systems is based on the model assumption that the cross section of a vascular tree becomes smaller towards the periphery. If two adjacent branches of the vascular tree have strongly different diameters and the branch with larger distance to the tree has the larger diameter then we have a candidate for the separation of the vascular tree. If the automatic vessel separation does not succeed completely, interaction facilities can be used to manually set the root of a vascular system or to identify touching points. The graph representation of the vessels is also the basis for user interactions such as defining the hierarchical structure of trees, subtrees and paths. Furthermore it allows to measure the radius, length or volume of branches.The main branches of the portal vein were identified automatically by determining the 8 most voluminous subtrees, which are assumed to supply the various vascular territories roughly corresponding to Couinaud[16] liver segments.

3.5. Vascular Territories and Risk Analysis

For liver surgery, the knowledge of the shape and volume of the patient's vascular territories is essential to estimate the risk of different resection strategies. Due to the limited spatial resolution only the major branches of the portal vein can be extracted. Referring to the liver, the problem can be described as follows: Assume that L is the set of all voxels in the medical volume data representing the liver. Furthermore, let $B \subset L$ denote the set of voxels belonging to the extracted portal venous tree. B is the union of the main branches or subtrees $B_i \subset B$, $i = 1, ..., n$, which supply the portal venous territories. To determine the vascular territories, we have to find a function which assigns to each liver voxel $\in L$ a territory with number i, provided it is supplied by the branch B_i.

The definition of a realistic function must reflect the probability, that the sprouts of the various incomplete subtrees B_i reach and supply a certain liver voxel. Measures for this 'reachability' can be expressed by a metric. A voxel then is assigned to that branch B_i, which has the shortest distance with respect to a suitable metric. The choice of a metric is difficult since the blood supply is realized by complex branching structures, whose formation process is not fully understood. After carefully evaluating two different metrics[17] we chose the Euclidean distance metric. With respect to the number of voxels assigned correctly, similar results were achieved with both metrics. The Euclidean distance, however, is better suited for the requirements of the clinical routine since it is computationally fast.

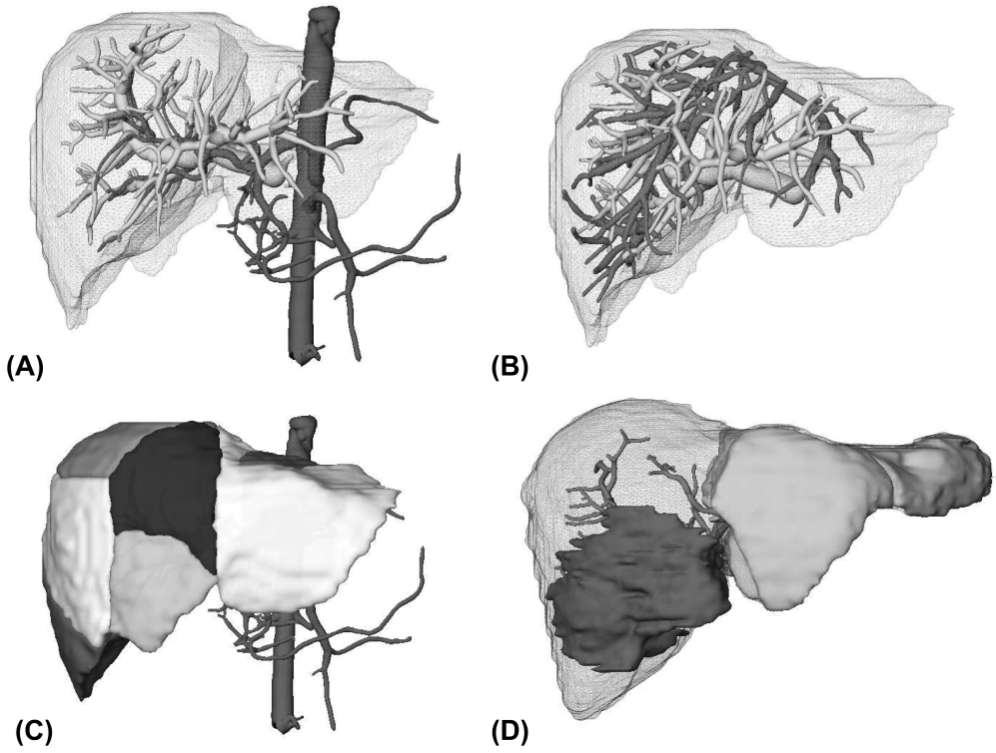

Figure 1. Example images of HepaVision: (A) presents the portal vein and the hepatic artery of a patient's liver. (B) visualizes the portal vein and hepatic veins. (C) shows the vascular territories. (D) presents the portal vein, a large tumor (dark) and the segments being not at risk by insufficient blood supply caused by the planned tumor resection. The dataset (A)-(C) have been provided by the Lahey Clinic Boston and (D) by the Technical University of Munich, Radiology.

In patients with liver tumors a risk analysis is performed. Risk analysis includes the identification of vessels within a safety margin around a tumor and the depending vessels in the periphery. Subsequently, the territory which is supplied by all involved vessels is calculated. This area is highlighted in the visualization and its volume (as absolute value and as percentage of the total liver volume is shown). The quantification and visualization of the parenchyma at risk is a valuable support for the surgical decision about resectability. This procedure is described in detail in.[18]

3.6. Implementation

All necessary image processing steps are performed with ILAB4, a R&D platform for image processing and visualization developed at MeVis. With ILAB4, modules, each representing an image processing task, are combined graphically to create specialized networks that perform a well defined task. By means of a scripting language a graphical user interface (GUI) can easily be composed. The user interface contains only a subset of the control elements available in the underlying image processing modules. These control elements are carefully chosen to reflect the most frequently needed parameters. Thus, the complexity of the underlying image processing networks are hidden from the user. Also, the user is guided through all necessary processing steps by the GUI.

All segmentation results are managed by HepaVision. For this purpose, a data structure has been developed which uses the syntax of the wide-spread XML-format (Extended Markup Language). By choosing XML it is possible to import the results of the planning process into other tools. In each processing step the GUI consists

of two large displays for image data and one region where the control elements are provided. The display regions may be used to display 2D slice data as well a 3D visualization with the usual facilities to control (zoom and rotate) the virtual camera. It is possible to superimpose the segmentation results to the original slice data.

3.7. Clinical Evaluation

In addition to the anatomical validation, our methods have been evaluated in the clinical environment for more than 220 cases until now (at Medical School Hannover, at University Hospital Essen, at the Institute MITI in Munich and others). The system is also used for living donor liver transplantations in the Lahey Clinic Boston and the Kyoto University Hospital.

For the planning of liver resections in patients with liver tumors, the liver, tumors, arteries, portal vein and hepatic veins were extracted from CT-data and visualized in 3D with our software assistant HepaVision. It has been shown that these visualizations allow a suitable interactive planning of liver resections and improve the preparation especially of complex liver resections.[19] Surgeons at Medical School Hannover regularly use the 3D reconstruction and volumetric analysis for the preoperative planning of living donor liver transplantations.[20,21] The vascular anatomy is crucial in the evaluation of potential donors.

For the acceptance in a clinical setting, the time required to carry out the image analysis is important. Using the feedback provided by the clinical partners, HepaVision has been improved significantly over the last four years and migrated from Silicon Graphics Hardware to Windows-based PCs. In this process, the graphical user interface, the facilities to generate visualizations and animation sequences have been enhanced. With the current version, preoperative planning takes an experienced user an hour on average for oncologic cases and 45 minutes for planning of LRLT where tumor segmentation and risk analysis are not relevant. Some results are presented in Figure 1.

4. REGISTRATION

In order to register the patient to the visualization system for generation of the video overlays, which will be described in Section 6, we use plastic fiducial markers that are attached to the patient's body and anatomical landmarks. Since the fiducials have to be identified both on the patient's surface and within the CT volume, we use an electro-magnetic navigation system (Ascension^{TM} miniBird 800, 6 degrees of freedom, with a $8mm \times 8mm \times 18mm$ sensor), but optical tracking (NDI^{TM} Polaris) would also be possible. For realization in the operation room, the sensor of the navigation system is fixed to the laparoscopic camera for image guidance such that a sterile plastic wrapping of the camera during the intervention is possible.

For registration purposes N pairs of points $(p^i_{patient}, p^i_{CT}), i = 1...N$ are collected. Then a rigid body registration by the use of the Singular Value Decomposition[22] (SVD) is applied.

5. CALIBRATION

Modern video-based endoscopes or laparoscopes offer physicians a field of view that is wide angled which is imperative for minimally invasive interventions. Unfortunately, this causes heavy lens distortion effects, mostly of radial and tangential type. In order to guarantee correct video overlays, one has to calculate a projective 3D/2D mapping that maps 3D object points $\mathbf{p}^W_{3D}$, defined in world coordinates, to 2D image points $\mathbf{p}^I_{2D}$, which are defined in the image plane of the camera (notation in homogenous coordinates):

$$\mathbf{p}^I_{2D} = \mathbf{P}^{\in\mathcal{R}^{3\times4}} \cdot \mathbf{T}^{\in\mathcal{R}^{4\times4}} \cdot \mathbf{p}^W_{3D} \tag{1}$$

This requires the determination of a projective matrix $\mathbf{P}^{\in\mathcal{R}^{3\times4}}$, whose elements can be determined by standard camera calibration routines.[23] Object rotation and translation is considered by matrix $\mathbf{T}^{\in\mathcal{R}^{4\times4}}$. In order to apply OpenGL 3D renderings in an efficient way, lens distortion correction has to be considered. Therefore, we implemented a fast hardware accelerated correction method, which divides a video image into $N \times M$ patches. By means of 2D texture mapping, each texture coordinate $\mathbf{t}^i$ is assigned a vertex coordinate $\mathbf{v}^i$ (Figure 2):

$$\mathbf{t}^i = (x, y)^T = F((x', y')^T) = F(\mathbf{v}^i) \tag{2}$$

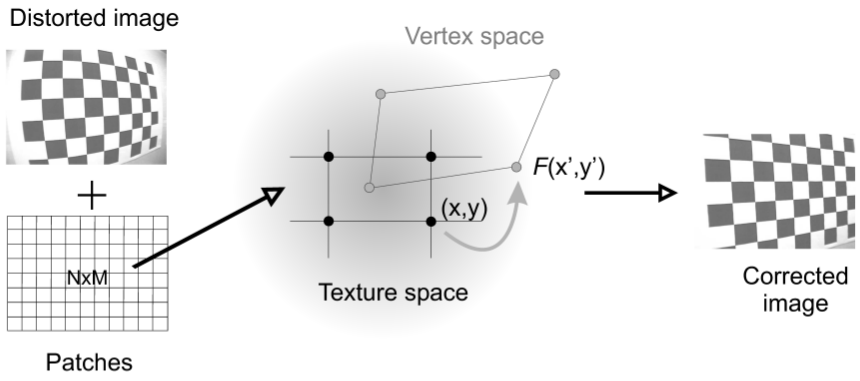

Figure 2. Lens distortion correction by the use of OpenGL hardware acceleration and 2D texture mapping.

The polynomial function F is determined by camera calibration.[23] For $N = M = 32$ patches we achieved high image quality at real time frame rates. Finally, the tip transformation of the tracker's sensor to the optical center of the camera is calculated by a hand-eye calibration procedure.[24]

6. VISUALIZATION

There is a variety of different visualization approaches for scalar volumes in many different applications. Since we want to present 3D volumes, extracted from our preoperative planning tool, in a semitransparent manner in order to enhance depth information, we only apply *direct volume rendering* methods that immediately display the voxel data. Although approaches like standard software *raycasting*[25] provide powerful visualization nowadays, hardware accelerated texture-based techniques based on new graphics adapters have been successfully developed for medical visualization.[26–29]

2D texture-based approaches allow direct volume rendering in terms of object-aligned slices. By changing the viewing direction of more than 90 degrees, a new stack of slices has to be applied, blended in back-to-front order and bilinear interpolation within the slices. The main drawback of such methods is the lack of spatial interpolation. The standard in texture-based approaches in terms of image quality has been provided by Cabral *et al.*[26] utilizing 3D textures and viewport-aligned slices, blended in back-to-front order. Hereby, trilinear interpolation in hardware is responsible for filling in the slicing polygons. On changing the camera view, the polygons have to be recalculated.

By the introduction of *multi-texturing* and a *programmable multi-stage rasterization* hardware, 2D multi-textures are superior to 3D textures in terms of frame performance.[30] Multi-texturing which is defined in recent standard API releases like *DirectX* or *OpenGL*, provide the capability to assign one polygon to several textures within the rendering-pipeline (Figure 3 (A)). In our approach, the resulting attributes of a single fragment (pixel values of geometric primitives) such as color or opacity are determined, using programmable arithmetic operations during rasterization. These operation schemes, such as the *Register Combiners* from NVIDIA^{TM} GeForce cards or the *Fragment Shaders* from ATI^{TM} Radeon allow to completely bypass the standard texturing unit. In combination with multi-textures, trilinear interpolation can be efficiently calculated in hardware (Figure 3 (B)). If S_i and S_{i+1} are two volume slices then the intermediate slice $S_{i+\alpha}$ can be calculated by

$$S_{i+\alpha} = (1 - \alpha) \cdot S_i + \alpha \cdot S_{i+1}. \tag{3}$$

Additionally, programmable multi-stage rasterization allows to introduce for example the *Phong* local illumination model or non-polygonal isosurfaces at high frame rates.[28, 29] Thus, this approach is the visualization system of choice, since high image quality for tumors and vessels at interactive frame performance is requested for image overlay. Additionally, stereo rendering is also applicable in conjunction with standard shutter glasses.

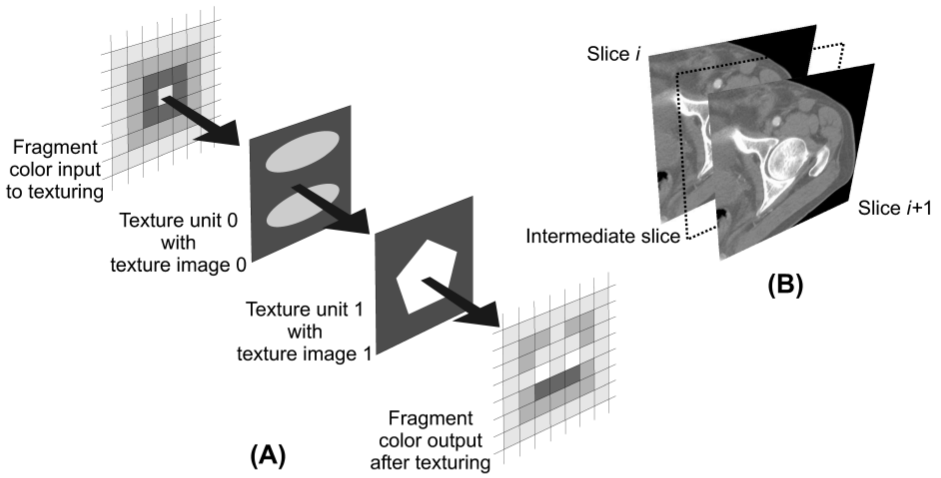

Figure 3. Interpolation of an intermediate volume slice by multi-texturing techniques: A) shows the process of multi-texturing by assigning one polygon several textures, B) intermediate slice interpolation in hardware.

7. RESULTS

Our system was evaluated in vivo during a simulated minimally invasive intervention in a swine. The medical work flow was similar to a liver intervention, which is one possibility to get advantage from the ARS. In our case, a routine abdominal CT of the swine was acquired using contrast agent for enhancement of the vessels. The following preoperative analysis and planning was accomplished within less than one hour, using the techniques presented in Section 3. The resulting anatomical information (liver, portal venous and hepatic venous trees, vascular territories) was used for insertion of the Veress needle in order to generate the pneumoperitoneum (Figure 4 (A)(B)(C)), for trocar placement, and for intraoperative navigation during intervention (Figure 4 (D)). The applied data volume was of dimension $512 \times 512 \times 90$ with 3mm slice thickness at 25 fps (3D video overlay by the use of the multi-texture-based direct volume rendering (Section 6) and lens distortion correction (Section 5)). For rigid registration purposes (Section 4) only four fiducial landmarks are necessary in order to achieve 5mm of overlay accuracy. Since the system has been evaluated in a swine in vivo, the planning procedure, especially the vascular segmentation and analysis was hampered by breathing artifacts during the CT scan. Nevertheless, in real therapy work flows, this does not provide a problematic circumstance.

8. CONCLUSION

Using our high performance volume rendering system based on general purpose hardware, we are capable of augmenting the surgeons laparoscopic view at real time frame rates. In combination with the preoperative liver planning tool, which performs a dedicated liver vascular analysis, an intraoperative fusion of preplanned information and real laparoscopic images is possible. Additionally, for visualization, all combinations of anatomical structures or intervention plans are feasible, depending on the surgeons requests. Moreover, the system is also applicable for many other intervention schemes such as radiofrequency (RF) ablation, percutaneous ethanol injection therapy (PEIT) and hepatic or pancreatic resections. According to the registration error, arising from the soft tissue movement of the liver, one can introduce a method for non-linear registration.[7, 31]

ACKNOWLEDGMENTS

We would like to thank H. Barfuss, C. Rezk-Salama and H. Feussner for fruitful scientific discussions.

REFERENCES

1. H. Bourquain, A. Schenk, F. Link, B. Preim, G. Prause, and H.-O. Peitgen, "Hepavision2: A software assistant for preoperative planning in living-related liver transplantation and oncologic liver surgery," in *Computer Assisted Radiology and Surgery, Proc. CARS*, pp. 341–346, 2002.
2. D. W. Roberts, J. W. Strohbehn, J. F. Hatch, W. Murray, and H. Kettenberger, "A frameless stereotaxic integration of computerized tomographic imaging in the operating microscope," *Journal of Neurosurgery* **65**, pp. 545–549, 1986.
3. M. Blackwell, C. Nikou, A. M. DiGioia, and T. Kanade, "An image overlay system for medical data visualization," in *Proc. Medical Image Analysis (SPIE)*, pp. 67–72, 2000.
4. W. Birkfellner, M. Figl, K. Huber, F. Watzinger, F. Wanschitz, R. Hanel, A. Wagner, D. Rafolt, R. Ewers, and H. Bergmann, "The varioscope ar - a head-mounted operating microscope for augmented reality," in *MICCAI*, pp. 869–877, 2000.
5. H. Fuchs, M. A. Livingston, R. Raskar, D. Colucci, K. Keller, A. State, J. R. Crawford, P. Rademacher, S. H. Drake, and A. A. Meyer, "Augmented reality visualization for laparoscopic surgery," in *MICCAI*, pp. 934–943, 1998.
6. R. Shahidi, B. Wang, M. Epitaux, J. Adler, and G. Steinberg, "Intraoperative video and volumetric image fusion," in *CARS*, 1999.
7. M. Vetter, P. Hassenpflug, I. Wolf, M. Thorn, C. Cárdenas, L. Grenacher, G. M. Richter, W. Lamadé, M. W. Büchler, and H.-P. Meinzer, "Intraoperative Navigation in der Leberchirurgie mittels Navigationshilfen und Verformungsmodellierung," in *Bildverarbeitung für die Medizin 2002*, pp. 73–76, 2002.
8. A. Schenk, G. Prause, and H.-O. Peitgen, "Efficient semiautomatic segmentation of 3d objects in medical images," in *Medical Image Computing and Computer-Assisted Intervention – MICCAI 2000*, **1935**, pp. 186–195, 2000.
9. A. X. Falcao, K. Jayaram, J. K. Udupa, and F. K. Miyazawa, "An ultra-fast user-steered image segmentation paradigm: Live-wire-on-the-fly," in *Medical Imaging: Image Processing, Proc. SPIE* **3661**, pp. 184–191, 1999.
10. S. P. Raya and J. K. Udupa, "Shape-based interpolation of multidimensional objects," *IEEE Transactions on Medical Imaging* **9**(1), pp. 32–42, 1990.
11. A. Schenk, G. Prause, and H.-O. Peitgen, "Local cost computation for efficient segmentation of 3d objects with live wire," in *Medical Imaging: Image Processing, Proc. SPIE* **4322**, pp. 1357–1364, 2001.
12. J. K. Udupa, S. Samarasekera, and W. A. Barrett, "Boundary detection via dynamic programming," in *Visualization in Biomedical Computing '92*, pp. 1087–1091, 1992.
13. A. Schenk, S. Behrens, S. A. Meier, P. Mildenberger, and H.-O. Peitgen, "Segmentierung von Hepatozellulaeren Karzinomen mit Fuzzy-Connectedness," in *Bildverarbeitung für die Medizin*, 2003. to appear.
14. D. Selle, B. Preim, A. Schenk, and H.-O. Peitgen, "Analysis of vasculature for liver surgery planning," *IEEE Transactions on Medical Imaging* **21**(11), 2002. to appear.
15. D. Selle and H.-O. Peitgen, "Analysis of the morphology and structure of vessel systems using skeletonization," in *Medical Imaging: Physiology and Function from Multidimensional Images, Proc. SPIE* **4321**, pp. 271–281, 2001.
16. C. Couinaud, "Le foie. etudes anatomiques et chirurgicales," 1957.
17. J. H. D. Fasel, D. Selle, C. J. G. Evertsz, F. Terrier, and H.-O. Peitgen, "Segmental anatomy of the liver: Poor correlation with CT," *Radiology* **206**, pp. 151–156, 1998.
18. B. Preim, H. Bourquain, K. J. O. D. Selle, and H.-O. Peitgen, "Resection proposals for oncologic liver surgery based on vascular territories," in *Computer Assisted Radiology and Surgery, Proc. CARS*, pp. 353–358, 2002.
19. D. Hoegemann, G. Stamm, H. Shin, K. J. Oldhafer, H. J. Schlitt, D. Selle, and H.-O. Peitgen, "Individuelle Planung leberchirurgischer Eingriffe an einem virtuellen Modell der Leber und ihrer Leitstrukturen," *Radiologe* **40**, pp. 267–273, 1999.
20. D. Hoegemann, G. Stamm, K. J. Oldhafer, D. Selle, T. Schindewolf, and M. Galanski, "Volumetric evaluation and 3d-visualization of the liver before living-related donation," in *Computer Assisted Radiology and Surgery, Proc. CARS*, pp. 249–252, 1999.

21. B. B. J. Frericks, F. C. Caldarone, A. Schenk, D. Selle, B. Preim, H.-O. Peitgen, M. Galanski, B. Nashan, and J. Klempnauer, "New computational methods for the evaluation of living related liver donation," in *American Journal of Transplantation*, **1**, p. 209, 2001.
22. W. H. Press, S. A. Teukolsky, W. T. Vetterling, and B. P. Flannery, *Numerical Recipes in C*, Cambridge University Press, 2nd ed., 1992.
23. R. Tsai, "A versatile camera calibration technique for high-accuracy 3D machine vision metrology using off-the-shelf TV cameras and lenses," *IEEE Journal of Robotics and Automation* **3**, pp. 323–344, 1987.
24. R. Y. Tsai and R. K. Lenz, "A new technique for fully autonomous and efficient 3D robotics hand/eye calibration," *IEE Transactions on Robotics and Automation* **5**(3), pp. 345–358, 1989.
25. P. Lacroute and M. Levoy, "Fast volume rendering using a shear-warp factorization of the viewing transformation," in *Proc. of SIGGRAPH '94*, pp. 451–458, 1994.
26. B. Cabral, N. Cam, and J. Foran, "Accelerated volume rendering and tomographic reconstruction using texture mapping hardware," in *Proc. of 1994 Symposium on Volume Visualization*, pp. 91–98, 1994.
27. R. Westermann and T. Ertl, "Efficiently using graphics hardware in volume rendering applications," in *Proc. of SIGGRAPH, Comp. Graph. Conf. Series*, pp. 169–177, 1998.
28. C. Rezk-Salama, K. Engel, M. Bauer, G. Greiner, and T. Ertl, "Interactive volume rendering on standard PC graphics hardware using multi-textures and multi-stage rasterization," in *Proc. SIGGRAPH/Eurographics Workshop on Graphics Hardware*, pp. 109–118, 2000.
29. C. Rezk-Salama and M. Scheuering, "Multitexturbasierte Visualisierung in der Medizin," in *Bildverarbeitung für die Medizin 2001: Algorithmen, Systeme, Anwendungen*, pp. 137–141, Springer, 2001.
30. C. Rezk-Salama, *Volume rendering techniques for general purpose graphics hardware*. PhD thesis, University of Erlangen-Nuremberg, Computer Graphics Group, 2002.
31. M. Scheuering, C. Rezk-Salama, H. Barfuss, A. Schneider, and G. Greiner, "Augmented reality based on fast deformable 2D-3D registration for image-guided surgery," in *SPIE Medical Imaging*, pp. 436–445, 2002.

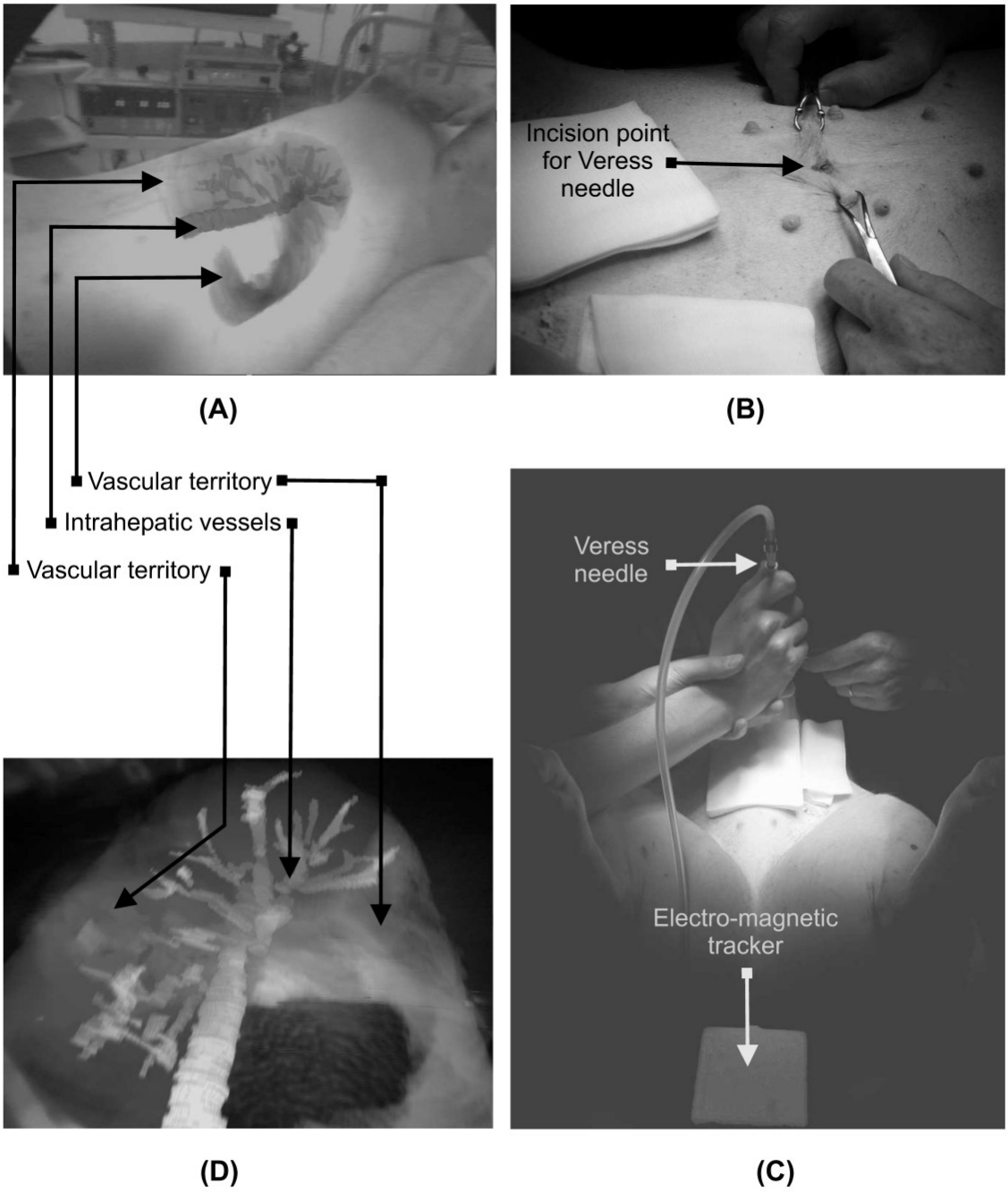

Figure 4. Results of a minimally invasive intervention simulation in a swine: (A) Shows intrahepatic vessels and liver segment overlay for Veress needle insertion. (B) Incision point of the Veress needle according to video overlays. (C) Insertion of the Veress needle for generation of the pneumoperitoneum. (D) Video overlay of a laparoscopic liver image with 3D renderings from our preplanning tool.

6.3 Clinical Relevance of Model Based Computer-Assisted Diagnosis and Therapy

Andea Schenk, Stephan Zidowitz, Holger Bourquain, Milo Hindennach, Christian Hansen, Horst K. Hahn, and Heinz-Otto Peitgen.

Based on a keynote lecture of Professor Heinz-Otto Peitgen at SPIE and published in Maryellen L. Giger and Nico Karssemeijer (eds) Proc. of SPIE Medical Imaging, Computer-Aided Diagnosis 2009, 6915, pp 691502,1-19.

Copyright 2009 Society of Photo Optical Instrumentation Engineers. Reprinted with permission.

Keynote Paper

Clinical relevance of model based computer-assisted diagnosis and therapy

Andrea Schenk*, Stephan Zidowitz, Holger Bourquain, Milo Hindennach, Christian Hansen,
Horst K. Hahn, Heinz-Otto Peitgen
MeVis Research GmbH – Center for Medical Image Computing,
Universitaetsallee 29, 28359 Bremen, Germany

ABSTRACT

The ability to acquire and store radiological images digitally has made this data available to mathematical and scientific methods. With the step from subjective interpretation to reproducible measurements and knowledge, it is also possible to develop and apply models that give additional information which is not directly visible in the data. In this context, it is important to know the characteristics and limitations of each model. Four characteristics assure the clinical relevance of models for computer-assisted diagnosis and therapy: ability of patient individual adaptation, treatment of errors and uncertainty, dynamic behavior, and in-depth evaluation. We demonstrate the development and clinical application of a model in the context of liver surgery. Here, a model for intrahepatic vascular structures is combined with individual, but in the degree of vascular details limited anatomical information from radiological images. As a result, the model allows for a dedicated risk analysis and preoperative planning of oncologic resections as well as for living donor liver transplantations. The clinical relevance of the method was approved in several evaluation studies of our medical partners and more than 2900 complex surgical cases have been analyzed since 2002.

Keywords: Medical image computing, Models, Risk analysis, Computer-assisted diagnosis, Liver surgery

1. INTRODUCTION

The prerequisite of computer aided diagnosis is the silent digital revolution in image based medical diagnosis and therapy. As a result we witness the major new historical phase in the development of radiology as field of science and medicine. The early phase extends from the discovery of X-rays in 1895 to approximately the early 1970s. The second phase begins with the introduction of CT and MRI and certainly continues. The third phase begins some time in the middle 1990s is a on the onset of a complete digitization of all image based and image related processes and aims at software assistants for diagnosis and therapy. Looking back at the first phase it appears almost miraculous at which pace diagnostic breakthrough applications followed one another:

1896:	first angiogram	1902:	first image of brain lesion
	first dental image	1905:	first image of kidney
	first image of in vivo heart	1910:	first contrast agent (Bariumsulfate)
	first image of headan dpelvis	1923:	first image of gall bladder
	first image of thorax	1929:	first heart catheter (Fossmann)
		1956:	Ultra sound

Let's remember that the development of the modern natural and engineering sciences beginning with the heroes such as Galileo, Brahe, Kepler, and Newton have made their steps and jumps based on a critical advancement of measurements. Historically from the point of view of the practitioners, radiology by and large has been an interpreting discipline in which measurements in a controlled scientific manner did not have a place.

*andrea.schenk@mevis.de; phone 49 421 218-7716; fax 49 421 218-2436; www.mevis-research.de

Medical Imaging 2008: Computer-Aided Diagnosis, edited by Maryellen L. Giger, Nico Karssemeijer
Proc. of SPIE Vol. 6915, 691502, (2008) · 1605-7422/08/$18 · doi: 10.1117/12.780270

The complete digitization of all processes now permits us to introduce measurements in obvious and more subtle ways based on image information. And already we witness that image acquisition aims both at providing images for human interpretation and as well as information to be exploited for measurements. In some sense interpretation is replaced by arguable and reproducible knowledge. CAD in the narrow sense but also computer assisted diagnosis in a broader sense start right here and quite like the natural and engineering sciences have shown as in their progress modeling and models become possible and necessary to fully exploit the given information or generate model based new information which exceeds and extends the image information.

It is the position of this invited lecture that along this development we need to rethink the issues of clinical relevance of our contributions and the impact that follows on how we manufacture and provide solutions in the domain of software assistants. Here are our major points and concern that we believe should have a stronger emphasis and which be addressed in our case study:

- Models and modeling in CAD will become increasingly important. Models require a patient individual fit. This in turn requires at times innovative measurements.
- What are the systematic and random errors and uncertainties which pollute the patient individual data and may question the integrity of a model. How sensitive does a model react against the variability and errors in the data? How does one monitor the gain or loss of the suitability of a model?
- Models have to be flexible and must allow for some user interaction and correction. For example extraordinary pathologies may occur or intra-operative findings may be discovered which have to be adequately integrated. Ideally, a model will indicate its limitations and monitor its own integrity.
- Evaluation of models is a particular problem. Classically medicine is accustomed to rely on clinical studies. It appears that here methodologies from the natural sciences have to introduced for supporting validity and evidence, which may result in a cultural clash.

2. THE SENSITIVITY OF RISK

In our case study, we will discuss the risk analysis for tumor resections in the liver. An optimal resection in terms of surgical technique is the so-called R0-resection that guarantees the complete excision of the lesion and a microscopically tumor-free resection margin. On the other hand as much healthy parenchyma as possible should be preserved. Considering the anatomy of the liver, we have to take into account vascular structures in the neighborhood of the tumor. Removing the tumor together with the safety margin from the liver, local vascular structures have to be transected that are supplying or draining a dedicated liver region and thus defining a territory at risk (Fig. 1).

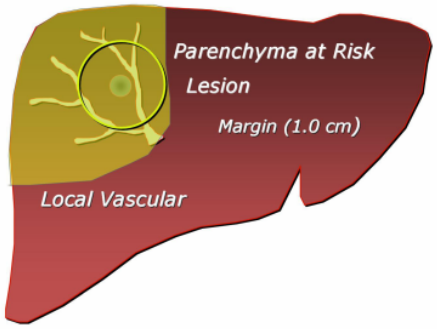

Fig. 1 Schematic drawing of a lesion in the liver surrounded by local vessels. Together with a safety margin of 1cm (circle) vessels have to be transected supplying a part of the liver (yellow), which will have an impaired inflow and are therefore considered as the parenchyma at risk.

The risk distribution can be considered as a function of the vascular systems and the two parameters tumor location and safety margin. Regarding an individual vascular structure as a fixed parameter, then position and margin influence in particular two attributes of the risk territory: First, the size of that region depends on the influence of the transected vessels in terms of supplied or drained parenchyma. Second and much more important for the surgical intervention is the

sensitivity of the territory to small changes of the parameters position and margin. There exist parameter settings with a 'robust' risk where changes that are e.g. in the magnitude of the achievable surgical precision alter the risk territories only to a limited extend. But more interesting and even more difficult to estimate are risk territories with parameters, where small modifications change the risk significantly and thus demand a different resection strategy. Fig. 2 shows two adjacent positions of an artificial tumor in a single vascular system extracted from a corrosion cast of a human liver. The parenchyma at risk is much smaller for the position of the tumor shown in the left while the second position compromises for the largest safety margin the complete right hemiliver. The more sensitive the risk distribution appears at a specific position of a tumor the more important is a risk analysis for this region.

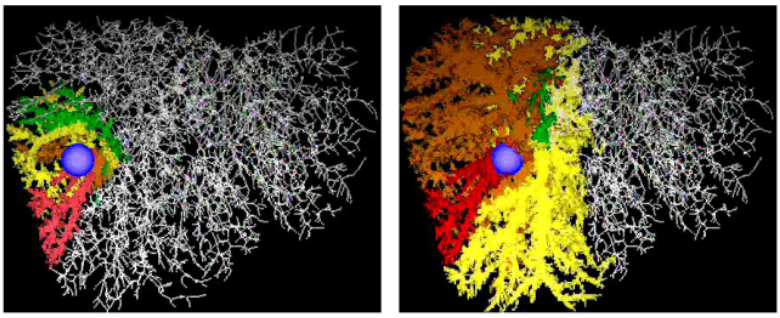

Fig. 2 A sphere as a model for tumor has been placed in the 3D model of a corrosion cast. The different colors of the thick branches indicate which part of the portal venous system would be affected by a resection of the tumor with different safety margins. The position of the tumor influences significantly size and location of the parenchyma at risk and is thus an example for a very sensitive tumor location.

Taking into account the fact that the liver is supplied or drained by four vascular systems, the risk distribution is even more complex. For the final aim of supporting the physician in identifying an optimal resection strategy, also aspects of surgical feasibility have to be considered.

3. LIVER SEGMENTS AND TERRITORIES

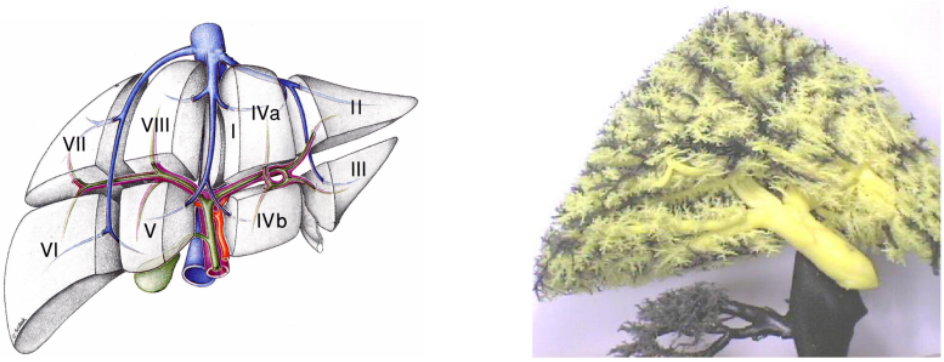

Fig. 3 Liver anatomy. Left: Four vascular systems supply or drain the liver, hepatic artery (red), portal vein (magenta), hepatic vein (blue), and bile ducts (green). Right: Corrosion cast of a human liver with portal vein (yellow) and hepatic vein (black), prepared by Prof. J. Fasel, Geneva, Switzerland.

The vascular anatomy of the liver is complex since four different vascular systems supply and drain the liver: hepatic veins, portal vein, hepatic arteries, and bile ducts (Fig. 3). The latter three vascular systems run almost parallel peripherally and are called the portal triad. Although in the liver hilum where these vessels enter into the liver parenchyma, a great inter-individual variability is present and fixed spatial resolutions of major vascular branches do not exist. In case of high resolution data and sufficient contrast, a separate risk analysis for all systems is possible. For data where the image quality is not sufficient e.g. for extracting smaller but relevant branches of hepatic artery and bile ducts,

the analysis should be performed only for the portal vein as the leading system of the triad while keeping in mind that vascular anomalies have to be assessed separately.

Risk analysis and preoperative planning for liver surgery is based on multi-phase computer tomography (CT) or magnetic resonance imaging (MRI) data with contrast enhanced vascular structures (examples in Fig. 4). The contrast agent passes through hepatic artery, portal vein and hepatic vein and during this time two or three datasets (phases) are acquired showing one or two vascular systems each. The imaging of bile ducts requires a different contrast agent at least for CT images.

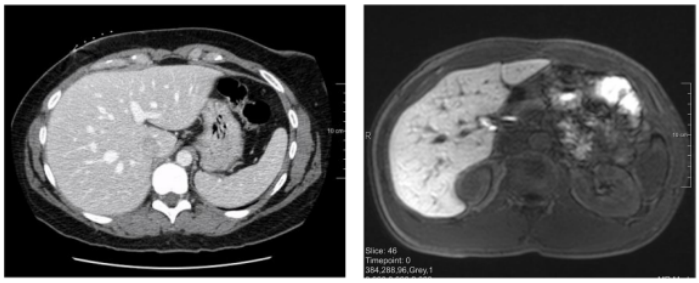

Fig. 4 Cross-sectional slice of a 3D dataset of the abdomen. In the CT image (left) vessels appear bright due to application of contrast agent, while a liver-specific contrast agent in the MRI data brightens the parenchyma (right), thus showing the vessels as dark tubular structures.

3.1 The Couinaud scheme

For a surgeon, it is difficult to mentally construct the 3D structure of vascular systems based on cross-sectional slices of radiological data and to estimate which part of a vessel system would be damaged as a consequence of a surgical intervention. In order to enable surgeons to perform liver resections respecting the vascular anatomy, a schematic model of the liver is employed that was introduced by Couinaud in 1957 long before CT technology was introduced[1]. At this time, a preoperative evaluation of the individual vascular liver anatomy was not possible. Following the Couinaud model, the human liver can be divided into eight segments which are determined according to the main branches of the portal vein and the hepatic veins. A liver segment is supposed to be defined by the supplied territory of a third-order branch of the portal vein with intermediate hepatic veins (Fig. 3). Applying the widespread scheme of Couinaud directly is questionable, since the liver segments do not correspond well to the individual territories (Fig. 5) and do not reflect common anatomical variants, e.g. trifurcations of the portal veins or inferior hepatic right veins draining directly into the inferior caval vein[2-4].

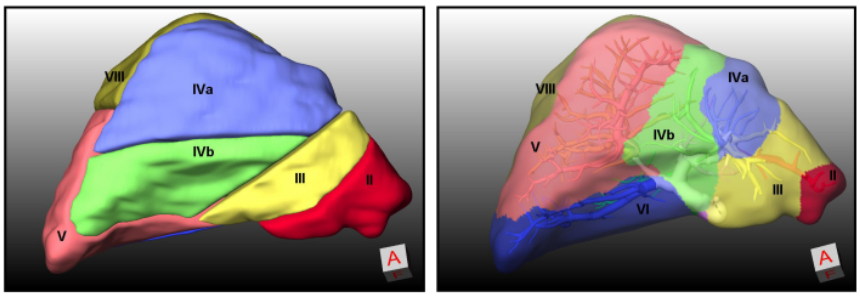

Fig. 5 Comparison of Couinaud segments and approximation of portal venous territories. Segments and territories differ significantly in position and size for this corrosion cast of a human liver.

3.2 Analysis of individual anatomy

The patient-individual risk analysis for a specific surgical intervention is based on the information that can be extracted from abdominal CT or MRI data. Relevant for liver surgery are the intrahepatic vascular systems, the shape and volume of the liver, and for oncologic surgery, the size and position of tumors. The MeVis group started in 1992, as the first group world-wide, with the computer-assisted analysis of branching patterns of hepatic vascular systems and functional vascular units which finally led to software assistants for liver surgery planning[5-9]. For the analysis of radiological data

we perform the following image processing steps: Liver segmentation is achieved with a modified live-wire algorithm, a semi-automatic edge-oriented algorithm as described in Schenk[10,11]. The analysis of vascular systems is described in detail in Selle[12,13] and consists of 1) an image preprocessing step to eliminate in homogeneities within the liver[14,15], 2) segmentation of the vascular structures with a modified region growing algorithm[16,17], 3) determination of the centerlines (skletonization) of this segmentation result, and 4) the hierarchical analysis of the vascular trees[12,18]. From the skeletonized vessels the different vascular systems are separated semi-automatically, and analysis for each of these systems can be performed. The analysis includes identification of the major branches of the portal vein, thus giving an individual classification similar to Couinaud's scheme (Fig. 5 and 6) and a subsequent risk analysis.

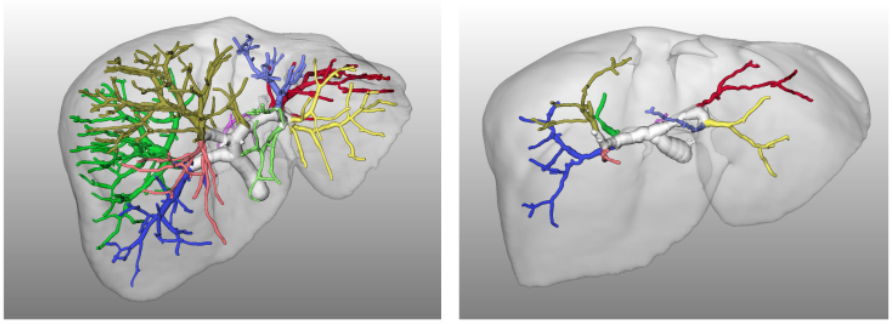

Fig. 6 Portal vein classification and example for different data quality. Analysis of the vascular system with a subdivision similar to Couinaud's scheme. Results for good high-resolution data (left) and low contrast images (right).

Being aware of image quality problems, e.g. anisotropic resolution, low contrast or high image noise, and displacement or compression of vessels by tumors, we focus on robust methods that meet the demands of short runtime and sufficient level of automation. For difficult cases, an additional mode for manual corrections is available.

Assuming that the image data has an excellent quality and spatial resolution comparable to that of a corrosion cast, then a tumor could be directly assigned to a single territory and a risk analysis could be performed directly from the vascular structures. This assumption of optimal data cannot be fulfilled due to the need to avoid excessive radiation exposure in case of CT or with the currently available scanner technique for MRI. As a consequence, there is a demand for an approximation of vascular substructures or liver territories that can be met with model based approaches.

4. LIVER MODELS

Perhaps the most salient contribution of mathematics to medical image analysis consists of models as a basis for extraction of meaningful parameters from the data for speculations about information which is not directly visible in the image data. For risk analysis in liver surgery, we require a model to estimate the assignment of a given position, most notably of a given lesion part, within the liver to a certain subbranch of each vascular system. This can be achieved in two ways, which will be further detailed below: firstly, by modeling the vascular system to the required level of detail, and, secondly, by identifying a suitable assignment function. Under specific assumptions, these two approaches are equivalent in a certain mathematical sense that will not be discussed here.

4.1 Modeling vascular systems

Inspired by the theorems of Hess and Murray on the principle of minimum work in vascular systems[19,20], by the simulations of Meinhardt[21], who derived complex structures, such as trees or networks, from basic cellular mechanisms, i.e., activation, inhibition, and elongation, and based on our own observations[22], we developed a method for constructing realistic vascular systems[23].

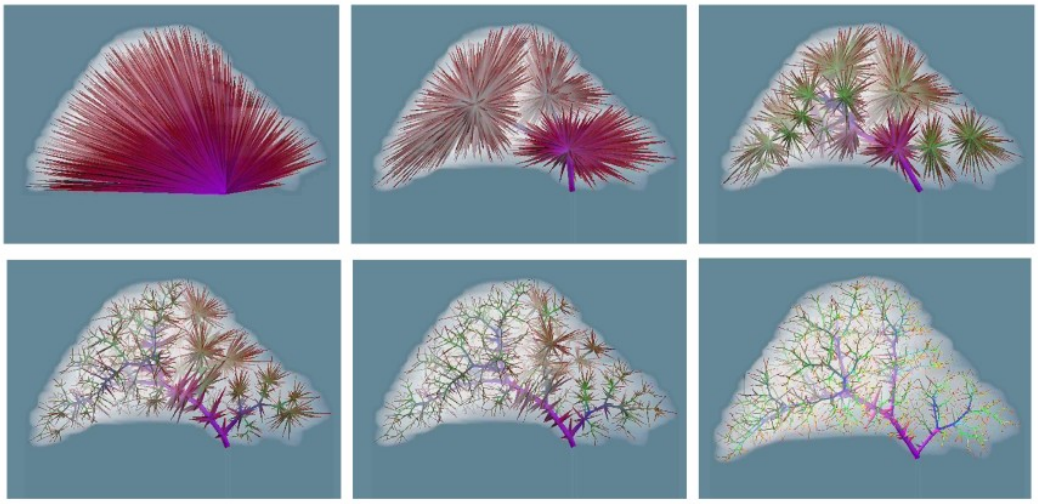

Fig. 7 Result of the constructive optimization model for a portal vein within a predefined liver hull. Starting with a simple configuration where each liver cell is supplied by a straight vessel from the hilum, the vascular system is modified step by step following a mathematical minimization principle for the physical work of blood transport.

Our model is initialized by a complete but overly simple and suboptimal tree that fills an organ at a given resolution using straight tubes. This initial tree is then subject to positional and topological local optimization techniques, as shown in Fig. 7. The boundary conditions for the optimization procedure are given by the position and flow distribution for all vascular end points corresponding to the leaves of the tree, by the position of the vascular hilum corresponding to the tree root, and by the maximum blood pressure available for organ perfusion. Then, according to the Hess-Murray law, optimization can be driven by intravascular volume minimization. Our algorithm is novel in that it implements topological changes corresponding to the subsequent merging and splitting of bifurcations, which have proven essential for the optimization process. For global optimization, we additionally employ a multi-level approach based on iterative pruning[23]. The generated models are found to be similar to real data acquired from corrosion casts of a human liver (cf. Fig. 8).

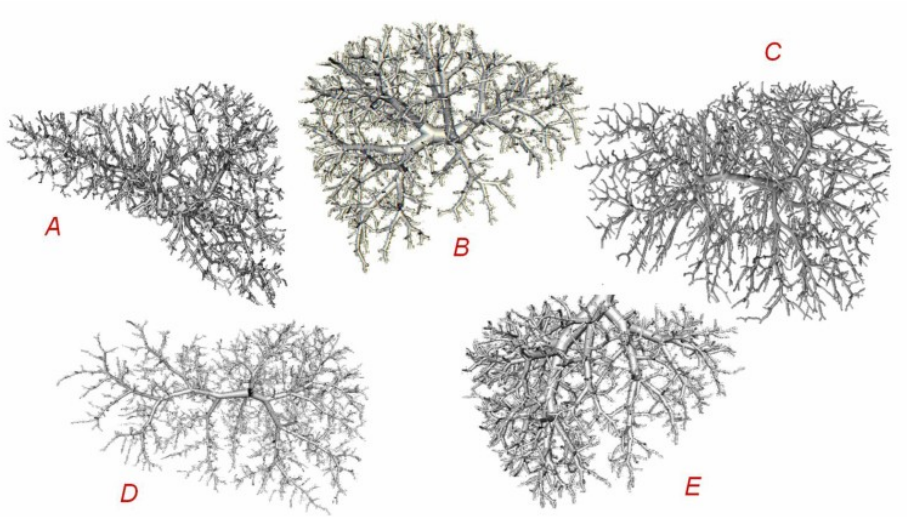

Fig. 8 Vascular systems from corrosion cast of real humans livers (A,C) and from the optimization process of our model within a given liver hull (B,D,E).

4.2 Laplace Model

In this model approach, we are searching for a function assigning each liver cell to one of the branches of a vascular tree. The definition of a realistic function must reflect the probability that the ends of the various incomplete subtrees reach and supply a liver cell. Measures for this "reachability" can be expressed by a metric. A cell then is assigned to that branch which has the shortest distance with respect to a suitable metric. The choice of a metric is difficult since the blood supply is realized by complex branching structures, whose formation process is not fully understood (see Hahn[22] for a discussion).

The use of potential functions was inspired by recent advances in statistical physics dealing with growth models for branching structures known as Laplacian fractals (lightning, viscous fingering, electrochemical deposits, and other deposits driven by diffusion) [24-26]. The Laplace model (cf. Fig. 9) is based on a fundamental equation of physics and offers interesting venues for a scientific understanding of the prediction method. Details of this model and its implementation can be found in Selle[12].

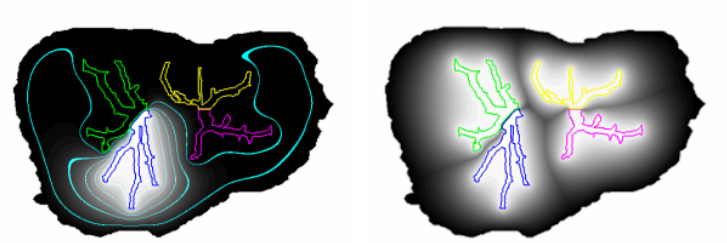

Fig. 9 Laplace Model using a metric based on potentials. Left: The potential for the single branch (blue) is set to 1 (white) and to 0 (black) for the other branches and the region outside the liver. The gray values for the other cells indicate the potential ranging between 0 and 1. Lines indicate surfaces of equal potential. Right: The maximum of the potential functions for all branches reveals the segment boundaries.

4.3 Nearest Neighbor Model

Assuming the most popular distance measure, the Euclidean distance, as metric for the "reachability" measure, we get another model for our assignment problem. The Nearest Neighbor method is conceptually simple and has rather low computational complexity. When comparing the results of the two assignment functions for the eight corrosion casts (cf. section 4.4), the differences for the liver territories are quite small[12,13]. Regarding our problem of liver subdivision, the territories are relatively rough shapes and the deviations are more prominent for smaller structures. Having in mind the medical problem of liver surgery, it is obvious that the differences for the territories are smaller than the achievable surgical precision. Therefore, the computational fast algorithm is utilized for clinical routine.

4.4 Model Evaluation

As an example we will show the anatomical evaluation for the quality of approximated territories. The validation of the methods is based on a study on eight vascular corrosion casts of the human liver[2,12]. High-resolution CT scans of the corrosion casts allow for extracting the portal branches with an accumulated length of about 10–18 m (contrary to in vivo data with a length of only 1–1.5 m). This yields sufficient branching generations for the determination of location and geometry of portal liver territories. For this work, we choose branches that define the segments according to the scheme of Couinaud (Fig. 10, upper left). The gaps between the branches were closed with morphological dilation and erosion operations. Due to the large number of branching generations extracted, the resulting solid portal segments provide a precise approximation of the true anatomical segments.

The derived segments have been compared with liver segments manually specified by anatomists[2]. To simulate the incomplete portal trees obtained from in vivo radiological data, we systematically pruned the trees obtained from the casts (Fig. 10, upper row). Finally, the predictions made for the pruned casts and the exact segment anatomy of the cast were compared to validate the approximation methods. For the validation study, we distinguish three degrees of pruning, covering the different "quality levels" of the portal vein, which are expected to be found in clinical CT data of different quality.

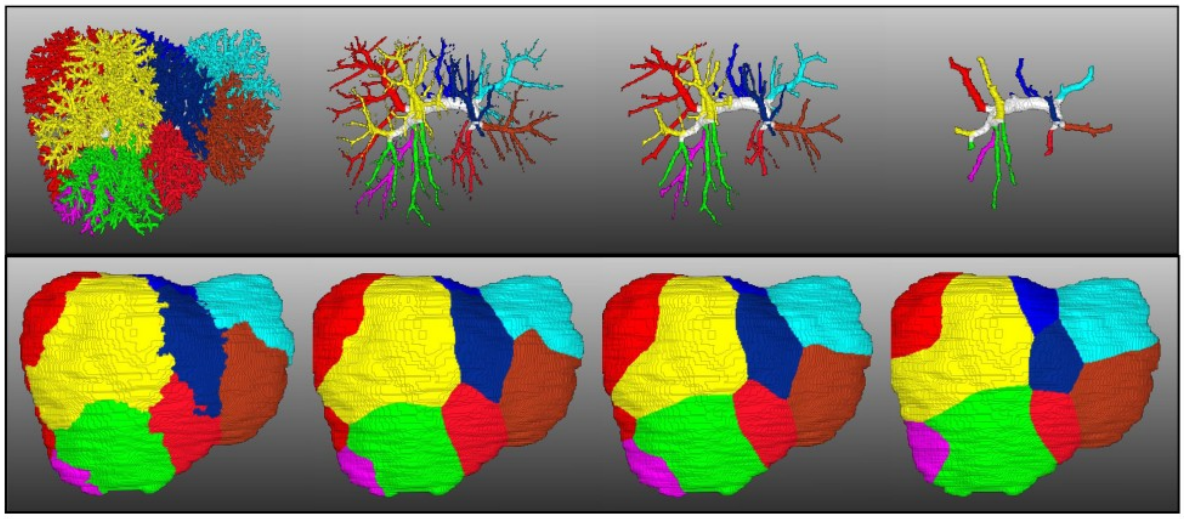

Fig. 10 Rendering of the portal vein obtained from a CT scan of a human liver cast. The main subtrees in the corrosion cast (upper left) are labeled by colors representing the liver segments. The pruned vessels (upper row) simulate the rather incomplete trees obtained from in vivo CT scans. Based on these pruning levels, the liver segments (lower row) are predicted with the Laplace model and compared with the authentic anatomical segments (lower left).

A quantitative evaluation of the accuracy of the approximation methods was carried out by computing the volumetric overlap between the approximated and the authentic segments. The Laplace method predicts the portal segment volumes with accuracy between 80% for the third order branches (Fig. 10, upper right) and 94% for branches that can be extracted in currently optimal multi-detector CT data[12,13].

5. APPLICATION OF MODELS

In the previous chapter we have utilized our model for a subdivision into territories of common supply or drainage. For the application to our initial problem of risk analysis for tumor resections we closer examine the vessels extracted from the images and label all branches and dependent subbranches that are located within a specific safety margin around the lesion. Every labeled branch supplies or drains a dedicated liver region that defines the corresponding risk territory for this vessel, lesion, and safety margin, respectively (Fig. 11). These risk territories provide the basis for subsequent analysis steps and for the final resection proposal. Before proceeding with the actual surgical planning, we will analyze more closely the complex interrelationship of tumor position, safety margin and affected volumes.

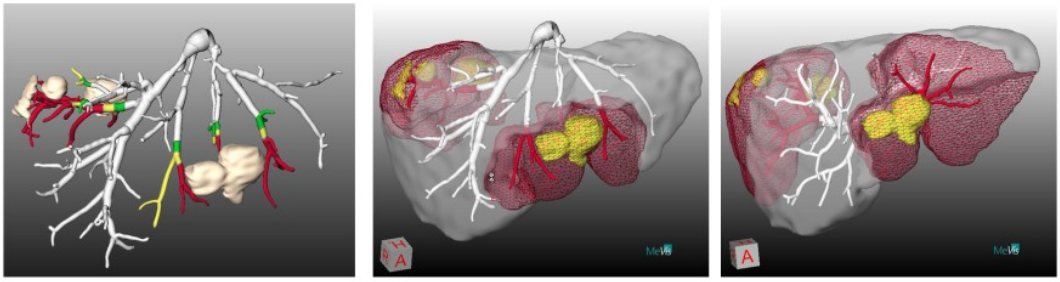

Fig. 11 Risk analysis with multiple metastases. The colored subbranches of the hepatic vein would be affected if the metastasis was resected with a safety margin of 5mm (red), 10mm (yellow) or 15mm (green).Based on the vascular analysis (left) the risk territories are computed for the hepatic veins and a safety margin of 1cm (middle). Risk analysis for the portal vein of the same patient is shown in the right image.

5.1 Combine Risks

The next step would be to combine the risks from each individual vascular system. Before this, we will take a more general view to the relation of safety margin and liver volumes at risk. Following the nearest neighbor model (section 4.3), a Voronoi tessellation of the liver volume according to the centerline voxels of the segmented vascular structure approximates the perfusion or drainage areas. Combining this information with a distance transformation with respect to the tumor boundary and taking the hierarchical dependencies of the vascular tree into account, a "safety map" of the liver can be calculated. This map then encodes the safety margin at which each particular volume will be affected by the tumor. The combined risk of different vascular systems can then be simply computed by assigning each voxel the minimum value of the individual safety maps. The quantification of compromised volume as a function of the safety margin is extracted from these maps by histogram analysis. Fig. 12 exemplifies the interrelation of safety margin and territories at risk for a given tumor position. The discontinuities in the compromised volume curves (Fig. 12 bootom right) correspond to the transection of major vessels, setting the dependent territories at risk. Hence, these curve discontinuities directly correspond to sensitive parameters for the surgical planning: Given that the corresponding safety margin is required to guarantee the R0-resection, the surgeon has to decide, whether the loss of functional volume in this magnitude can be tolerated.

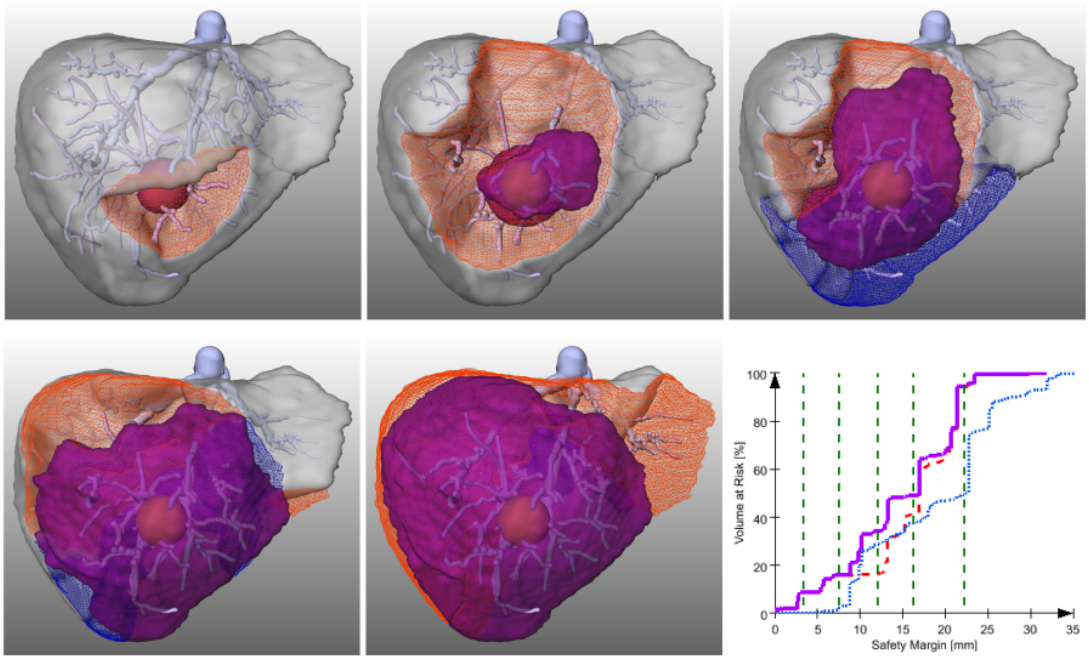

Fig. 12 Risk volumes as function of the safety margin. An artificial spherical tumor and the impaired volumes for hepatic veins only (dark blue), portal veins only (light red) and for both vascular system (purple) with safety margins of 3.4mm, 7.6mm, 12.1mm, 16.3mm, and 22.2mm are visualized. The diagram in the lower left shows the risk volume as a function of the safety margin (dotted: hepatic vein, dashed: portal vein, solid: combined).

5.2 Cascading Risks

Due to the entanglement of the different vascular systems within the liver, it is in general not possible to remove reasonable parts of the liver in such a way that the supply as well as the drainage will completely be ensured for all parts of the remnant. As the risk territories for the different vascular systems do not overlap with each other exactly, the removal of any of these territories will cut off some primarily not affected parts of the other vascular systems, respectively (cf. Fig. 13). Hence, the removal of a primary territory at risk from one vascular tree will in general enlarge the affected volumes induced by the other vascular systems and vice versa. The resulting cascading of risk areas is most prominent for centrally located lesions, but will appear in the peripheral regions as well, where the vascular systems are

more unidirectional. As a consequence, surgical resection planes must be adopted such that as many as possible major vessels are saved. In case of the liver, this is of particular importance for the arterial vessels and bile ducts.

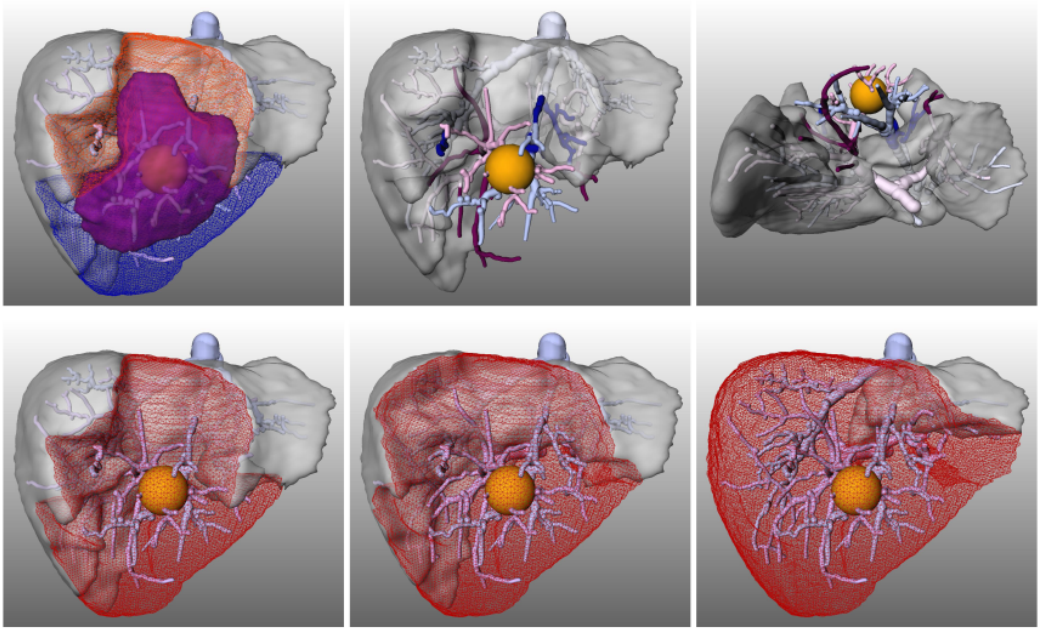

Fig. 13 Cascading of risk territories for an artificial tumor. Upper left: Primary territories at risk for hepatic vein only (dark blue), portal vein only (light red) and for both vascular systems (purple). Upper middle and right: Impairment of vascular systems (light colors: impaired by safety margin, full colors: impaired by collateral risk territory).Lower row: Cascading of risk territories (left to right: primary territories at risk, 1st extension, and 2nd extension).

5.3 Risk maps

As we have discussed in the beginning, the sensitivity of the risk distribution to inaccuracies in tumor localization or intended safety margin reflects the criticality of the succeeding surgical procedure. To give a first guess of the distribution of sensitive and of robust tumor locations in the liver, we conduct a statistical experiment: By placing artificial tumors with an assumed distribution of radii at different locations within the liver, we calculate the probability that a given safety margin will just coincide with the distance to a larger vessel.

For these situations, a small inaccuracy in the resulting surgical procedure will either save or endanger the volume supplied or drained by the vessel in question. Assuming a Poisson distribution with mean size of 3cm for the tumor diameter and a safety margin of 1cm, we get the resulting assessment of sensitivity for a tumor position as shown in Fig. 14. Here ‘robust’ represents a mean value of less than two substantial clashes for a distribution of tumors located at that specific position and ‘very sensitive’ represents more than four substantial clashes. We assume a substantial clash, if more than 5% of the liver volume is in question. These risk distributions are evaluated for portal vein and hepatic veins.

In terms of this new definition, the robust positions are located at the outer regions of the organ with no major vessels, but interestingly also in the very central part of the liver (Fig. 14). In this central region, the nearest affected vessel often leads to a loss of the total liver or of a complete liver lobe, hence the mean number of critical clashes is low – even though a tumor at this position might be inoperable. The most critical positions in terms of uncertainty or inaccuracy are located half way out from the central vessels. In these regions, the segmental structures of both vascular systems interweave each other. The resulting risk maps give a first guess about the locations of tumors, for which a precise planning of the surgical strategy promises the most benefit.

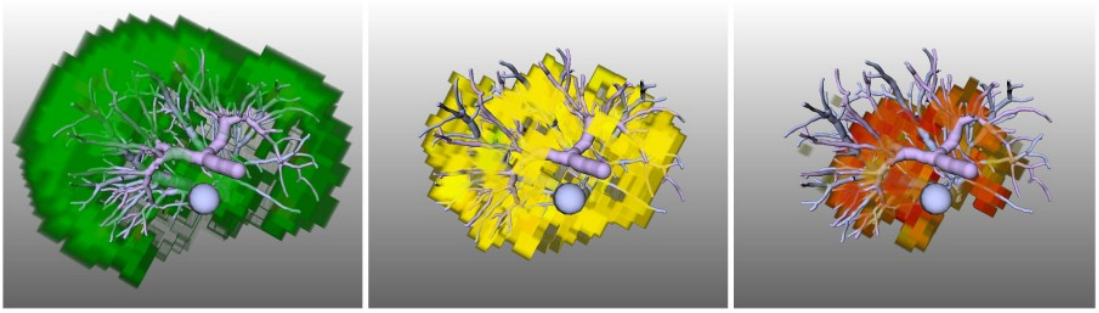

Fig. 14 Sensitivity distribution for tumor positions concerning the stability of risk territories: Each cube represents the statistical mean value of sensitivity of the respective position. The images show positions with different levels of sensitivity, from robust to very sensitive (left to right).

6. RESECTION PLANNING AND ADAPTION

We have analyzed the risk distribution and the influence of the parameters location, margin and vascular system in detail. Now the question arises how can we create an adequate resection proposal for a specific individual patient?

6.1 From risk territories to resection proposals

Based on the risk analysis for a given safety margin that is defined by the surgeon or derived from the margin-volume function (cf. section 5.1) we can compute the risk territories for the portal vein and the hepatic veins (Fig. 15). It is obvious, that the intersection of these territories should be part of the resection proposal as it includes the tumor and represents a region without supply or drainage.

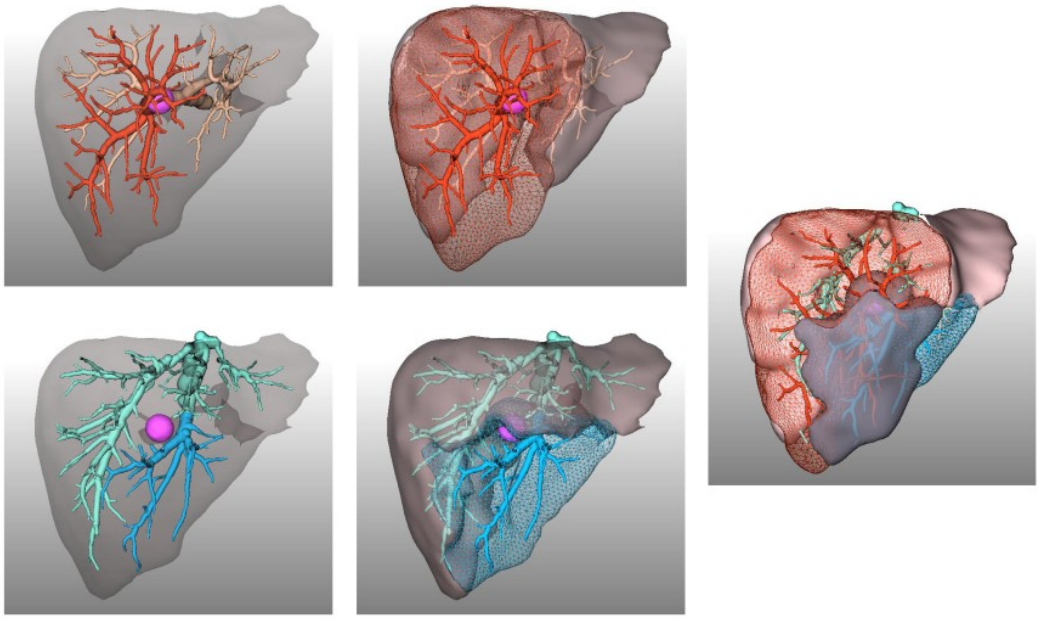

Fig. 15 Risk analysis and territories. A hypothetical spherical tumor has been placed in a clinical dataset. Vessels transected with a given safety margin are marked as darker structures (left) and risk territories are visualized with a mesh surface (middle). Combining the risk analysis for portal vein (upper row) and for hepatic vein (lower row) we get the joint risk territory (right) derived as the union of the two risk territories. The intersection of the portal and the hepatic risk territories contains the tumor and should be part of the resected parenchyma (right, continuous surface).

The first resection proposal that would come into one's mind is the union of the two risk territories. But, as the discussion in section 5.2 has shown, a resection of this area would result in additional impaired liver regions without perfusion or drainage and, thus, the resection proposal should rather be smaller (Fig. 16). In general, the optimal resection plane lies between the intersection and the union of all risk territories.

Our experience and the discussion with our surgical partners have shown that besides the results of the risk analysis several other factors have to be considered for an adequate resection proposal. Some of these factors are 1) maintenance of import supplying vessel branches (hepatic artery and portal vein), 2) access to the tumor 3) minimal resection surface 4) consideration of typical, well experienced resection types (e.g. hemihepatectomy), 5) remaining volume, 6) possibility of anastomoses and reconstruction of vessels, 7) typical surgical approaches for multiple metastases and 8) the option of alternatives such as radiofrequency ablation. Fig. 17 shows a resection proposal that was defined interactively with our software,[27,28] and preserves the large branch of the right hepatic vein that was transected with the automated resection proposal based on the union of risk territories (cf. Fig. 15). In conclusion, it is an ambitious task to create feasible automated resection proposals and unclear if it is even possible for all cases.

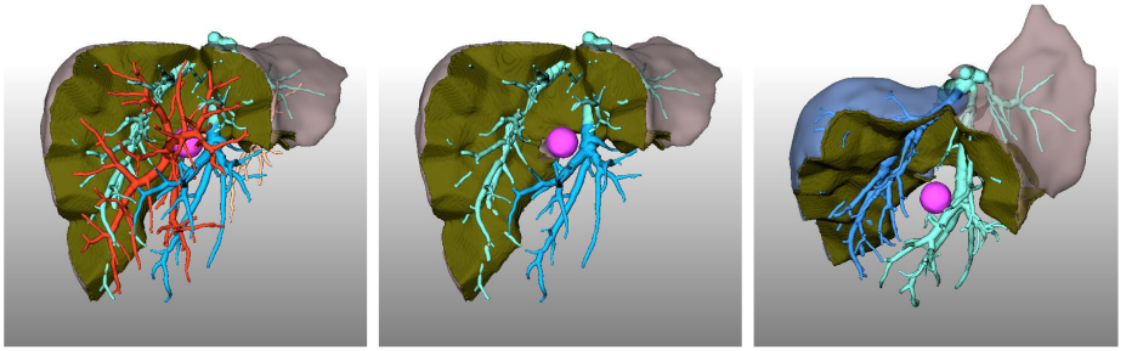

Fig. 16 Automated resection proposal. Using the union of portal vein and hepatic vein risk territories as a resection proposal, would lead to interference of additional vessels. Here, the right hepatic vein would be transected and the rest of the right hemiliver would be without drainage (dark).

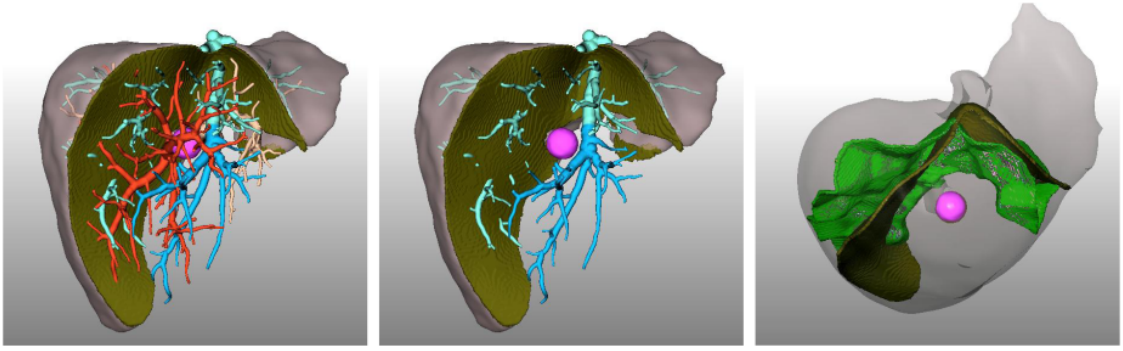

Fig. 17 Interactive resection proposal and comparison. The manually defined resection proposal preserves the main branch of the right hepatic vein (middle) and reflects with its smoothness the surgical practicability. A comparison of the two resection proposals in the cranio-caudal view (right).

6.2 Resection proposals for living donor liver transplantation

In living donor liver transplantation (LDLT) the liver of a voluntary healthy donor is divided into the graft for the recipient and the remnant liver that remains in the donor. In contrast to the donation of the relatively independent left lateral lobe graft for a pediatric recipient, the adult living donor liver transplantation (ALDLT) requires a subdivision of the right liver lobe near the middle hepatic vein (MHV) (Fig. 18). Due to the complex vascular liver anatomy and the

restricted liver volume that has to be sufficient for both the healthy donor and the diseased recipient, a detailed risk analysis is mandatory for this intervention[29].

Each resection proposal in ALDLT is based on the main bifurcation of the portal vein and a subdivision of the liver into right and left portal vein territories. This is caused by the fact that, e.g. for right lobe grafts, the right branch of the portal vein will be anastomosed to the stump of the central portal vein in the recipient. The subdivision still leaves a large degree of freedom for the resection line. Since there are usually no other relevant branches of the portal vein in the central area, the risk analysis is concentrated on the draining MHV. As stated above, one major problem in LDLT is a sufficient volume and more precisely a sufficient 'functional' volume. The required volume for donor and recipient is dependent on size and weight of the person and therefore critically in particular with small donor livers. Territories that depend on transected subbranches of the MHV are at risk of insufficient drainage and postoperative function. Therefore, this volume is subtracted from the graft or respectively from the remnant volume. The resection proposal is not only depending on the functional volume in donor and recipient, but also on the individual surgical strategy of each LDLT center and surgeon. Regarding this strategy, a typical resection can be located directly near the MHV, in a distance of 1-2cm and depending on the assignment of the MHV to graft or recipient on the left or right side of the MHV. Recently, left liver lobes are also considered as grafts in LDLT, changing the resection proposal due to the subdivision of the portal vein at the other, the right side of the bifurcation.

In conclusion, resection proposals for ALDLT are based on a rough subdivision of the portal vein into left and right branch but the final decision if the liver volume is sufficient for donor and recipient and the exact resection proposal is mainly influenced by the risk analysis for the MHV.

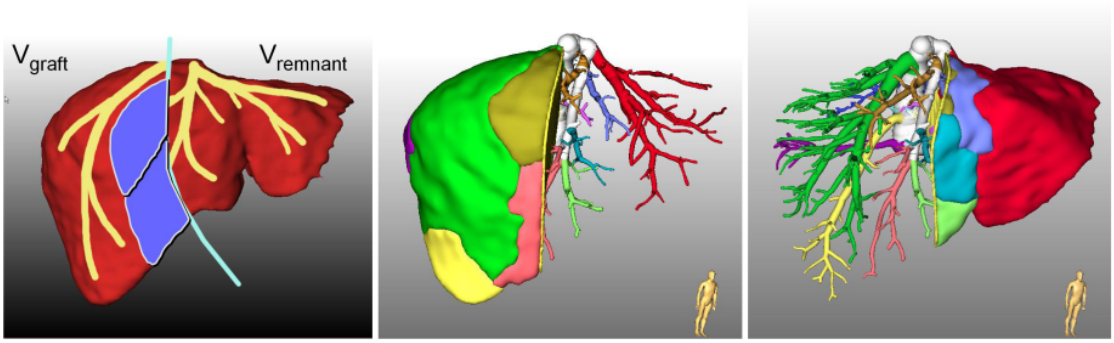

Fig. 18 Risk analysis for adult living donor liver transplantation. Left: With the planned resection two larger branches of the middle hepatic vein (MHV) will be transected. The dependent territories (blue) are at risk of insufficient drainage and postoperative function. The risk analysis for a graft without MHV shows drainage territories that are at risk and therefore potentially reduce the functional graft volume (middle). A risk analysis with a resection proposal procuring the MHV for the graft shows the regions with potential outflow obstruction in the donor (right).

6.3 Intraoperative adaptation of risk assessment

In oncologic liver surgery, additional tumors that were not visible in the preoperative images are often found during the intervention. With such findings, the resection strategy must be updated or completely revised. To provide surgeons with an efficient tool for the quantitative assessment of planning, which is integrated in the workflow of oncologic liver interventions, the planning system is combined with an ultrasound-based navigation system.[30-32] Beside providing means to transfer the preoperative planning onto the patient's situs, the combination of planning and navigation systems allows to determine exact position and size of a new found tumor and transfer these information to the planning system.

For this purpose a registration technique for intraoperative ultrasound images and preoperative planning data is required. We implemented a progressive registration method that is robust, executable in real-time and interactive adaptable. Therefore the surgeon defines a small set of corresponding markers in the preoperative radiologic data and the intraoperative ultrasound images (usually at ramifications). In a first step, an affine transformation is computed in real-time and is applied to the preoperative data. If needed, the surgeon can refine the result in a second step by applying a non-linear registration method.

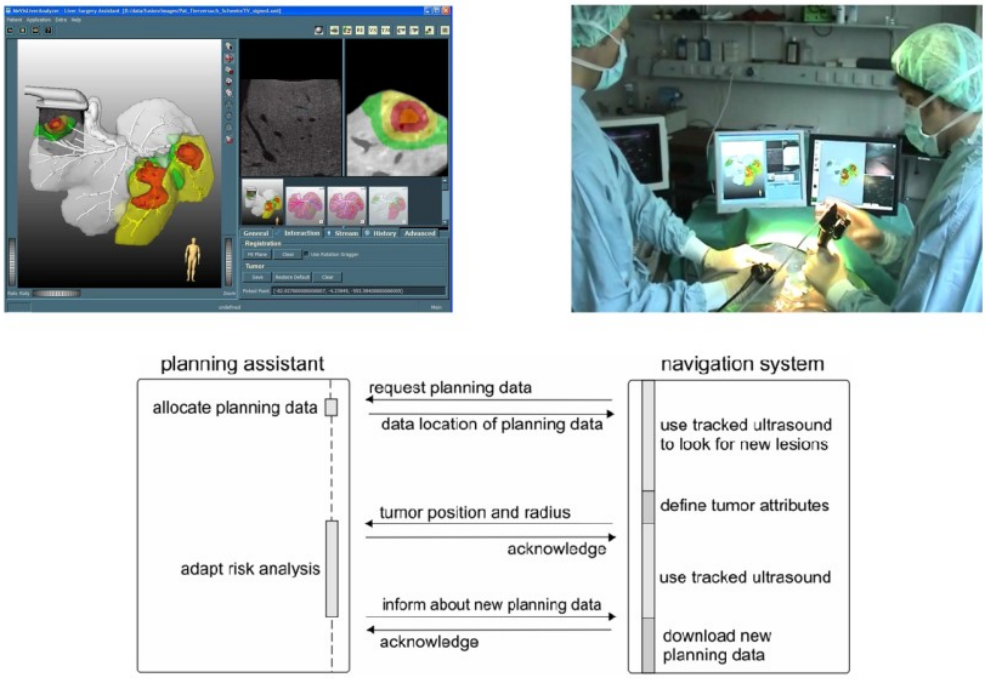

Fig. 19 Intraoperative adaptation of planning. Top left: GUI of the planning system showing the risk analysis for a pig's liver with artificial tumors after applying a risk analysis adaptation. Top right: Preliminary evaluations in the operating room using the planning system (left monitor) and the ultrasound-based navigation system (right monitor) for laparoscopic liver surgery. Bottom: Scheme of data exchange between planning system and navigation system for the intraoperative incorporation of a newly detected tumor.

Tumor size and position are determined by the surgeon who defines the new found tumor directly on the ultrasound image by drawing a circle around the tumor. For simplification, tumors are assumed to be approximately spherical in shape. Once the tumor is added to the planning model a new risk analysis is performed and the results are transferred back to the ultrasound-based navigation system. After a computation time of less than 30 seconds the planning update is visible on the ultrasound screen. Furthermore, it is possible to delete added tumor or change their attributes. Fig. 19 illustrates the XML-based exchange protocol, defined between the planning software and the navigation system.

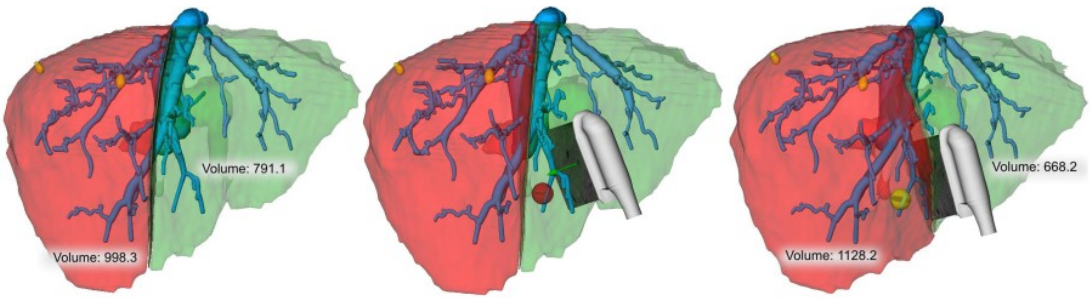

Fig. 20 Left: Preoperatively planned right hepatectomy. The right part of the liver model (red) shows the parenchyma to be resected, while the left part is intended to remain. The yellow nodules represent segmented metastases. Middle: A new resection plane is defined with the ultrasound-based navigation system. The red sphere represents an intraoperative detected tumor. Right: The preoperative resection plane is merged with the resection plane defined intraoperatively and the volume calculation is updated.

Based on the new risk situation the surgeon can define an adapted resection surface interactively by using the navigated ultrasound probe as input device: In order to sculpt an arbitrary shape around newly detected tumors (e.g., a wedge-shaped resection) the surgeon can define a set of planes using the ultrasound plane as reference (cf. Fig. 20). First tests in the operating room confirmed that in case of newly discovered tumors an adaptation of a preoperative risk analysis is a beneficial support for precise liver surgery. The combination of planning system and navigated ultrasound offers a crucial decision support, is easy to use and integrates smoothly into the clinical workflow. The new system provides major support for evidence-based decision making in the surgical theatre and thus improves the safety of the surgical interventions.

Moreover, the availability of planning data directly at operation table calls for the development of special visualization methods supporting the cognitive needs of the surgeons in the surgical workflow. E.g. in case of parallel visualization of ultrasound plane and the 3D planning model, occlusion of the ultrasound by the planning model is an inevitable problem.To address these problems, we define three guiding requirements to ensure clinical applicability[31]:

1. **Diagnostic Usability**: While the whole visualization is presented in a single view, ultrasound information should always be visible, even if it would be occluded by planning data or parts thereof.
2. **Orientation Aid**: Spatial relations between ultrasound plane and planning data should be clearly perceivable without rotating or translating the camera.
3. **Error Identification**: Since recent intraoperative registration methods make a compromise between real-time and error-prone computation, a clear hint to perceive registration errors should be provided.

The main objective of our visualization approach is to provide the surgeon with a focus view on the ultrasound plane and a context view on the planning model in order to ensure diagnostic usability.

To optimize the intraoperative guidance furthermore, the use of non realistic rendering techniques for the condensation of information is of major interest. E.g. the distance to critical structures can be color-coded on planned resection surface to attract the alertness of the surgeon.

7. CLINICAL EVALUATION

A typical clinical evaluation requires a study with a randomized decision of utilizing the results of the risk analysis or not and the subsequent evaluation of clinical criteria, i.e. patient outcome in terms of 5-year-survival, complication rate, tumor recurrence, blood loss and others. There are two reasons why this standard evaluation procedure is not suitable for the software-assisted risk analysis. First, it is ethically not justified to leave out information that helps the physician in decision making and operation planning and second, the clinical criteria of the study depend on multiple factors, e.g. medical history of the patient, degree of liver steatosis, experience of the surgeon, surgical technique that would require from the statistical point of view an enormous, not achievable number of cases for reliable conclusions.

Nevertheless, it is possible to analyze a dedicated aspect for application of the model-based risk analysis. Lang et al showed that with 15 oncologic resections, the surgical strategy was changed in one third of the cases when taking the results of the risk analysis into account[33]. In another study, results of the resection of hilar cholangiocarcinoma with the preoperative analysis were compared to older interventions where the software was not available. Here, the sensitivity, specificity and accuracy of the new methods proved to be significantly higher and even increased the R0-rate from 62.3% before 2002 to 92.9% with our software[34,35]. In a recent case of liver metastases that were treated preoperatively by chemotherapy, one lesion was no longer visible in CT data and not palpable during surgery. Therefore, the resection was performed as one of the first world-wide as navigated surgery and on basis of the risk analysis and planning that was made on a combination of the two CT data sets before and after chemotherapy.[36] In living donor living transplantation, an algorithm for the surgical operability was developed that is based on the results of our risk analysis for the middle hepatic vein[43].

Several other clinical partners have approved the usefulness of the risk analysis and preoperative planning for oncologic surgery[37-42] as well as for living donor liver transplantations[43-55].

8. CONCLUSION

We have presented an example how mathematical models can be applied to a medical problem: the analysis of vascular structures and the approximation of liver territories supplied or drained by them. The evaluation with corrosion casts

showed how the quality of image data influences the correctness of the segment approximation and helps to estimate errors and indicates the robustness of the model. Based on the model, we developed a risk analysis for liver surgery. Discussing miscellaneous aspects of combined risk territories and the difficult transfer from the risk analysis to a clinically useful resection proposal, we showed what problems have to be overcome before a model could be applied in clinical reality.

Our approach provides a new, measurable and objective basis for the assessment of risks in liver surgery and the development of new surgical standards. Since 2002 we have analyzed more than 2900 data sets from more than 95 clinical sites world-wide and transferred our research results into a commercially available service[56]. More than half of the processed cases are related to living donor liver transplantations and more than 1000 data sets were analyzed for oncologic resections. About 250 analyses were performed for surgical interventions of other organs e.g. kidney and lung, and show that our approach is not restricted to the liver but can also be applied to other organs characterized by hierarchical vessel systems.

The application of models to radiological data gives an example how medical image computing can provide a basis for new developments and values for diagnosis and therapy. Essential in this context is the step from subjective interpretation to reproducible quantification. Computer-assistance in medicine is an interesting and valuable field for mathematical and scientific approaches and can be achieved in an intensive interdisciplinary cooperation of mathematicians, scientists and medical experts.

9. ACKNOWLEDGMENTS

Our current liver projects are supported by grants of the German Federal Ministry of Education and Research (FKZ 01IBE03C) and of the German Research Foundation (PE 199/14-3, PE199/15-2, PE199/18-1, and PE199/19-1).

REFERENCES

[1] Couinaud, L. "Le Foie - Etudes anatomiques et chirurgicales", Masson, Paris (1957).

[2] Fasel, J. H. D., Selle, D., Evertsz, C. J. G., Terrier, F., Peitgen, H.O. and Gailloud, P., "Segmental anatomy of the liver: poor correlation with CT," Radiology 206(1), 151-156 (1998).

[3] Radtke, A., Sotiropoulos, G. C., Molmenti, E. P., Nadalin, S., Schroeder, T., Schenk, A., Saner, F., Valentin-Gamazo, C., Dahmen, U., Spasov, L., Broelsch, C. E. and Malago, M., "The influence of accessory right inferior hepatic veins on the venous drainage in right graft living donor liver transplantation," Hepatogastroenterology 53, 479-483 (2006).

[4] Fasel, J. H. D., "Portal venous territories within the human liver: an anatomical reappraisal," Anatomical Record, in press (2008).

[5] Leppek, R., Zahlten, C., Juergens, H., Evertsz, C. J. G., Peitgen, H. O. and Klose, K. J., "In situ visualization of portal vein branching," European Radiology 221 (1993).

[6] Juergens, H., Zahlten, C., Evertsz, C. J. G., Peitgen, H. O., Leppek, R. and Klose, K. J., "3D-Reconstruction of branching blood vessels from CT-data," Digitale Bildverarbeitung in der Medizin (1994).

[7] Zahlten, C., Juergens, H., Evertsz, C.J., Leppek, R., Peitgen, H. O. and Klose, K. J., "Portal vein reconstruction based on topology," Eur J Radiol 19, 96-100 (1995).

[8] Zahlten, C., Juergens, H. and Peitgen, H. O., "Reconstruction of branching blood vessels from CT-data," Visualization in Scientific Computing 41-52 (1995).

[9] Peitgen, H. O., "Rekonstruktion von Gefäßsystemen aus CT-Daten," Therapie-Woche 45(3), 144-148 (1995).

[10] Schenk, A., Prause, G. and Peitgen, H. O., "Efficient semiautomatic segmentation of 3D objects in medical images," Proc. MICCAI, 186-195 (2000).

[11] Schenk, A., Prause, G. and Peitgen, H. O., "Local cost computation for efficient segmentation of 3-D objects with live wire," Proc. SPIE 4322, 1357–1364 (2001).

[12] Selle, D., "Analyse von Gefäßstrukturen in medizinischen Schichtdatensätzen für die computergestützte Operationsplanung," Shaker-Verlag (1999).

[13] Selle, D., Preim, B., Schenk, A. and Peitgen, H. O. "Analysis of vasculature for liver surgical planning," IEEE Trans Med Imaging 21, 1344-1357 (2002).

[14] Sied, J. G., Zijdenbos, A. P. and Evans, A. C. A, "Nonparametric method for automatic correction of intensity nonuniformity in MRI data," IEEE Transactions on Medical Imaging 17, 87-97 (1998).
[15] Zidowitz, S., Drexl, H., Kroeger, T., Preusser, T., Ritter, F., Weihusen, A. and Peitgen, H. O., "Baysian Vessel Extraction for Planning of RF-Ablation," Proc. BVM, 187-191 (2007)
[16] Selle, D., Spindler, W., Preim, B. and Peitgen, H. O., "Mathematical methods in medical imaging: Analysis of vascular structures for liver surgery planning, " Mathematics Unlimited, Springer, Berlin, 1039–1059 (2001).
[17] Hindennach, M., Zidowitz, S., Schenk, A., Bourquain, H. and Peitgen, H. O., "Computer assistance for fast extraction and analysis of intrahepatic vasculature from contrast-enhanced CT-volume data for preoperative planning in liver surgery," Proc. CARS, 451-452 (2007).
[18] Selle, D. and Peitgen, H. O. "Analysis of the morphology and structure of vessel systems using skeletonization," Proc. SPIE 4321, 271–281 (2001).
[19] Hess, W. R., "Das Prinzip des kleinsten Kraftverbrauchs im Dienste hämodynamischer Forschung," Archiv Anat Physiol, 1-62 (1914).
[20] Murray, C. D., "The physiological principle of minimum work. I. The vascular system and the cost of blood volume," Proc Natl Acad Sci 12, 207-214 (1926).
[21] Meinhardt, H., "Morphogenesis of lines and nets," Differentiation 6(2), 117-123 (1976).
[22] Hahn, H. K., Evertsz, C. J. G., Fasel, J. H. D. and Peitgen, H. O., "Fractal properties, segment anatomy, and interdependence of the human portal vein and the hepatic vein in 3D, " Fractals 11 (1), 53–62 (2003)..
[23] Hahn, H. K., Georg, M. and Peitgen, H. O., "Fractal aspects of three-dimensional vascular constructive optimization," Fractals in Biology and Medicine IV, 55-66 (2005).
[24] "Fractals in physics—Proc. Int. Conf. Honouring B. Mandelbrot, " Physica D 38(1–3) (1989).
[25] Evertsz, C. J. G., "Laplacian fractals," Ph.D. dissertation, Univ. Groningen, The Netherlands (1989).
[26] Evertsz, C. J. G., Peitgen, H. O. and Voss, R. F., "Fractal geometry and analysis," The Mandelbrot Festschrift, World Scientific, Curaçao, The Netherlands (1996).
[27] Bourquain, H., Schenk, A., Link, F., Preim, B., Prause, G., and Peitgen, H. O., "HepaVision2: A software assistant for preoperative planning in living-related liver transplantation and oncologic liver surgery," Proc. CARS 341-346 (2002).
[28] Konrad-Verse, O., Preim, B. and Littmann, A., "Virtual Resection with a Deformable Cutting Plane," Proc. Simulation und Visualisierung, 203-214 (2004).
[29] Bourquain, H., Schenk, A. and Peitgen, H. O., "Computer-assisted planning and decision-making in living-donor liver transplantation," In: Tanaka K., Inomata Y., Kaihara S. (eds). Living-donor liver transplantation - Surgical techniques and innovations. Prous Science, Barcelona, 23-28 (2003).
[30] Hansen, C., Schlichting, S., Markert, M., Zidowitz, S., Hindennach, M., Kleemann, M., and Peitgen, H. O., "Intraoperative adaption of preoperative risk analysis for oncologic liver surgery using navigated 2D ultrasound," Proc. CURAC: 155-158 (2007).
[31] Hansen, C., Schlichting, S., Zidowitz, S., Köhn, A., Hindennach, M., Kleemann, M., and Peitgen, H. O., "Intraoperative adaptation and visualization of preoperative risk analyses for oncologic liver surgery," SPIE Medical Imaging, in print (2008).
[32] Hansen, C., Köhn, A., Schlichting, S., Weiler, F., Konrad, O., Zidowitz, S. and Peitgen, H. O., "Intraoperative modification of resection plans for liver surgery," Proc. CARS, in print (2008).
[33] Lang, H., Radtke, A., Hindennach, M., Schroeder, T., Fruhauf, N. R., Malago, M., Bourquain, H., Peitgen, H. O., Oldhafer, K. J., Broelsch, C. E., "Impact of virtual tumor resection and computer-assisted risk analysis on operation planning and intraoperative strategy in major hepatic resection," Arch Surg 140(7), 629-638 (2005).
[34] Endo, I., Shimada, H., Takeda, K., Fujii, Y., Yoshida, K., Morioka, D., Sadatoshi, S., Togo, S., Bourquain, H. and Peitgen, H. O., "Successful duct-to-duct biliary reconstruction after right hemihepatectomy. Operative planning using virtual 3D reconstructed images,".J Gastrointest.Surg 2007, 11, 666-670 (2007).
[35] Endo, I., Shimada, H., Sugita, M., Fujii, Y., Morioka, D., Takeda, K., Sugae, S., Tanaka, K., Togo, S., Bourquain, H. and Peitgen, H. O., "Role of three-dimensional imaging in operative planning for hilar cholangiocarcinoma," Surgery 142(5), 666-75 (2007).
[36] Markert, M., Nowatschin, S., Weber, S., Hansen, C., Zidowitz, S., Bourquain, H., Stavrou, G. A., Oldhafer, K. J., Peitgen, H. O., and Lueth, T.C., "Navigated resection of residual liver tumors that are no longer visible after presurgical chemotherapy," Proc. CARS, in print (2008).

[37] Fuchs, J., Warmann, S. W., Szavay, P., Kirschner, H. J., Schäfer, J. F., Hennemuth, A., Scheel-Walter, H.G., Bourquain, H., Peitgen, H. O., "Three-dimensional visualization and virtual simulation of resections in pediatric solid tumors," .Journal of Pediatric Surgery 40(2), 364–370 (2005).

[38] Lang, H., Radtke, A., Liu, C., Fruhauf, N. R., Peitgen, H. O. and Broelsch, C. E., "Extended left hepatectomy-modified operation planning based on three-dimensional visualization of liver anatomy. Langenbecks," Arch Surg 389(4), 306-310 (2004).

[39] Lang, H., Radtke, A., Liu, C., Sotiropoulos, G. C., Hindennach, M., Schroeder, T., Peitgen, HO. and Broelsch, C. E., "Improved Assessment of Functional Resectability in Repeated Hepatectomy by Computer-assisted Operation Planning.," Hepatogastroenterology 52, 1645-1648 (2005).

[40] Lang, H., Radtke, A., Hindennach, M., Schroeder, T., Bourquain, H., Schenk, A., Oldhafer, K. J., Prause, G., Peitgen, H. O. and Broelsch. C. E., "Virtual hepatic surgery - computer-assisted operation planning on the 3-dimensional reconstructed liver," Z Gastroenterol 45(9), 965-970 (2007).

[41] Lang, H., Broelsch, C. E., Bertona, C. and Bourquain, H., "Extended left hepatectomy with an inferior right liver vein: improved operation planning by 3-D reconstruction and computer-assisted imaging," J Am Coll Surg 205(4), 626-627 (2007).

[42] van Ooijen, P. M. A., Wolf, R., Schenk, A., Rouw, D. B., Slooff, M., Peitgen, H. O. and Oudkerk, M., "Recent Developments in Organ-Selective Reconstruction and Analysis of Multiphase Liver CT," Imaging Decisions 7(1), 37-43 (2003).

[43] Asakuma, M., Fujimoto, Y., Bourquain, H., Uryuhara, K., Hayashi, M., Tanigawa, N., Peitgen, H. O. and Tanaka, K., "Graft selection algorithm based on congestion volume for adult living donor liver transplantation," Am J Transplant 7(7), 1788-1796 (2007).

[44] Frericks, B. B., Kirchhoff, T. D., Shin, H. O., Stamm, G., Merkesdal, S., Abe, T., Schenk, A., Peitgen, H. O., Klempnauer, J., Galanski, M. and Nashan, B., "Preoperative volume calculation of the hepatic venous draining areas with multi-detector row CT in adult living donor liver transplantation: Impact on surgical procedure," Eur Radiol. 16(12), 2803-10 (2006).

[45] Frericks, B. B., Caldarone, F. C., Nashan, B., Savellano, D. H., Stamm, G., Kirchhoff, T. D., Shin, H. O., Schenk, A., Selle, D., Spindler, W., Klempnauer, J., Peitgen, H. O., Galanski, M., "3D CT modeling of hepatic vessel architecture and volume calculation in living donated liver transplantation," Eur Radiol. 14(2), 326-33 (2004).

[46] Harms, J., Bourquain, H., Bartels, M., Peitgen, H. O., Schulz, T., Kahn, T., Hauss, J. and Fangmann, J., "Surgical Impact of Computerized 3D CT-Based Visualizations in Living Donor Liver Transplantation," Surg Technol Int 13, 191-195 (2004).

[47] Hoegemann, D., Stamm, G., Oldhafer, K. J., Selle, D., Schindewolf, T and Galanski, M, "Volumetric evaluation and 3-D visualization of the liver before living-related donation," in Proc. CARS, 249–252 (1999).

[48] Karaliotas, C., Broelsch, C. E., Habib, "Liver and Biliary Tract Surgery: Embryological Anatomy to 3D-imaging and Transplant," Springer, Wien (2007).

[49] Radtke, A., Schroeder, T., Molmenti, E. P., Sotiropoulos, G. C., Nadalin, S., Schenk, A., Malamutmann, E., Saner, F., Valentin-Gamazo, C., Dahmen, U., Lang, H., Peitgen, H. O., Broelsch, C. E., Malago, M., "The territorial belonging of the middle hepatic vein: a troublesome dilemma in adult live donor liver transplantation--anatomical evidence based on virtual 3-dimensional-computed tomography-imaging reconstructions," Eur J Med Res 11, 66-72 (2006).

[50] Radtke, A., Schroeder, T., Sotiropoulos, G. C., Molmenti, E., Schenk, A., Paul, A., Nadalin, S., Lang, H., Saner, F., Peitgen, H. O., Broelsch, C. E. and Malago, M., "Anatomical and physiological classification of hepatic vein dominance applied to liver transplantation," Eur J Med Res 10:187-194 (2005).

[51] Radtke, A., Nadalin, S., Sotiropoulos, G. C., Molmenti, E. P., Schroeder, T., Valentin-Gamazo, C., Lang, H., Bockhorn, M., Peitgen, H. O., Broelsch, C. E. and Malago, M., "Computer-assisted operative planning in adult living donor liver transplantation: A new way to resolve the dilemma of the middle hepatic vein," World Journal of Surgery 31, 175-185 (2007).

[52] Radtke, A., Schroeder, T., Molmenti, E. P., Sotiropoulos, G. C., Schenk, A., Paul, A., Frilling, A., Lang, H., Nadalin, S., Peitgen, H. O., Broelsch, C. E. and Malago, M., "Anatomical and physiological comparison of liver volumes among three frequent types of parenchyma transection in live donor liver transplantation," Hepatogastroenterology 52, 333-338 (2005).

[53] Radtke, A., Nadalin, S., Sotiropoulos, G. C., Molmenti, E. P., Schroeder, T., Schenk, A., Frilling, A., Saner, F. H., Peitgen, H. O., Broelsch, C. E. andMalago, M., "Parenchyma transection in adult live donor liver transplantation:

The virtual dilemma of "where to cut". Experience based on virtual 3-dimensional computed tomography imaging reconstructions," Hepato-Gastroenterology 53, 811-815 (2006).

[54] Radtke, A., Sotiropoulos, G. C., Nadalin, S., Molmenti, E., Schroeder, T., Lang, H., Saner, F., Valentin-Gamazo, C., Frilling, A., Schenk, A., Broelsch, C. E. and Malago, M. "Preoperative Volume Prediction in Adult Living Donor Liver Transplantation: How Much Can We Rely on It? ," Am J Transplant 7(3),175-185 (2007).

[55] Wald, C. and Bourquain, H., "Role of new three-dimensional image analysis techniques in planning of live donor liver transplantation, liver resection, and intervention," J Gastrointest Surg 10(2), 161-165 (2006).

[56] http://mms.mevis.de/Distant_Services.html

6.4 Planning of Image-Guided Interventions in the Liver

Andrea Schenk, Dieter Haemmerich, and Tobias Preusser

Published in IEEE Pulse 2011, 2(5), pp. 48-55.

© 2011 IEEE. Reprinted with permission.

Planning of Image-Guided Interventions in the Liver

By Andrea Schenk, Dieter Haemmerich, and Tobias Preusser

Use of Computer-Aided Treatment Systems

Digital three-dimensional (3-D) imaging modalities, such as computed tomography (CT), magnetic resonance imaging (MRI), and ultrasound imaging, have permitted the development of computer-aided systems for patient-specific treatment planning. Generally in such a system, after image processing of digital image data sets, patient-specific models are developed and can then be employed for planning of the procedure and/or guidance during the procedure. The type of computational model employed varies depending on the specific application but can include geometrical, mechanical (e.g., deformation), and functional models (e.g., blood flow and cardiac electrical activity) as well as tissue interaction (e.g., with radiation, heat, and drugs), among others. Today, computational modeling has found its way into clinical use for treatment planning in a number of image-guided interventions, for example:

- surgical procedures, e.g., neuro and liver surgery
- training for laparoscopy procedures
- dental applications, e.g., implants
- bone fractures and implants
- intensity-modulated radiation therapy (IMRT), where high-energy radiation is focused on cancerous tumors.

Computational treatment planning is particularly useful for either complex new procedures (e.g., IMRT) or complex cases of procedures that have traditionally been used without computational modeling assistance. In the latter, computer-aided platforms may allow treatment of patients who would otherwise have not been candidates for the therapy due to the complexity of the cases as well as provide more consistent treatment results.

In the following, we demonstrate the use of computational modeling for treatment planning of interventional procedures on the example of two clinically used therapies for liver cancer, which are used for both primary tumors (i.e., cancer originating in the liver) as well as metastatic tumors.

Digital Object Identifier 10.1109/MPUL.2011.942605
Date of publication: 11 October 2011

2154-2287/11/$26.00©2011 IEEE

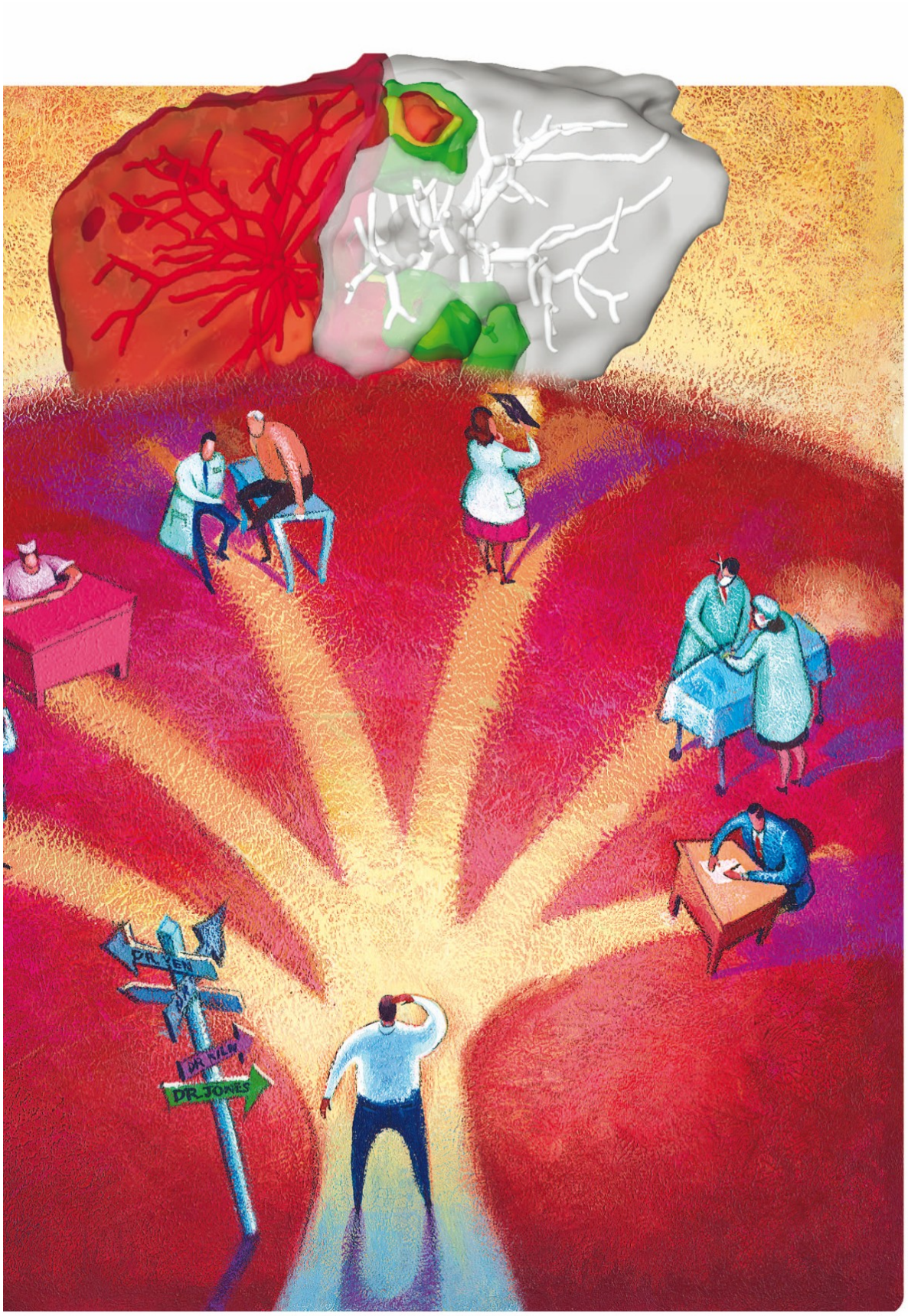

© MASTERSERIES

Liver Cancer Surgery

The treatment options for liver cancer have been limited compared to other cancer types since chemotherapy and radiation therapy used in other cancers are typically not curative due to biological reasons. Surgery historically has been established as the gold standard, and in recent years, additional localized therapies (e.g., thermal tumor ablation, described in more detail later) have been clinically adapted for liver cancer cases where surgery is not possible. During liver surgery the part of the liver containing the tumor is surgically removed (i.e., surgical resection) via different methods that transect liver tissue while limiting bleeding. This can be done during open surgery or by a laparoscopic procedure through small access holes in the patient's skin and with specialized surgical tools. Owing to the high regenerative power of the liver, liver tissue grows back within a couple of months until the liver volume is similar to before surgery.

Computational modeling has found its way into clinical use for treatment planning in a number of image-guided interventions.

There are several risks during surgical resection of tumors, with the most severe risk being liver failure. Two major risk factors include insufficient volume of the remnant liver after surgery as well as deficient health of the remaining liver tissue. The latter can result from preexisting liver diseases, such as steatosis (fatty liver degeneration) or fibrosis/cirrhosis (liver tissue scarring), as well as reduced blood flow, hampered by the resection. In case of a healthy liver, a future remnant liver volume of 25–30% of the functional tumor-free volume before surgery is sufficient. This remnant volume has to be higher for diseased organs and the exact amount of minimum volume necessary is difficult to predict in these cases.

To minimize the chance of tumor recurrence (i.e., cancer regrowth after surgery), a margin of healthy tissue surrounding the tumor (safety margin) has to be removed during resection, typically a rim of 10–15 mm. This safety margin is a critical marker for the success of the surgery, as often there are cancer microsatellites present in the rim surrounding the tumor. For example, if the surgeon cuts into the cancerous tissue or cancer cells are found on the resection surface in pathology, the probability of a recurrent tumor exceeds 90%. Therefore, the resection should be performed by transsecting tissue (e.g., cutting) at a certain distance from the tumor(s). The goal of saving as much healthy liver tissue as possible is conflicting with the aim of a large safety margin around the tumor, especially in the context of keeping the resection procedure simple. To simplify the surgical procedure, 1) the surface area of the resection plane is minimized, 2) access to the tumor is as simple as possible (note that the liver is fixed in the abdomen by several lines of connective tissue), and 3) the number of surgical cuts is minimized (particularly for multiple tumor cases).

A typical strategy while considering these criteria without any patient-specific modeling is followed during a standard liver resection procedure. A standard resection is based on an artificial subdivision of the liver into so-called segments, sectors (usually contain 2–3 segments), and lobes (right and left part of the liver) according to blood supply (Figure 1). A tumor would then be removed together with the segments, sectors, or lobe it is located in. Without support by dedicated software, the division of the liver is roughly estimated via the stack of two-dimensional (2D) radiological images [Figure 1(a)], taking into account the locations of the main branches of portal and hepatic veins (note that liver is, contrary to other organs, primarily supplied by venous blood).

The two competing goals of obtaining a sufficient safety margin around the tumor while saving sufficient volume of functional liver tissue, together with the complexity of the liver vasculature, motivated the development of a patient-specific, computer-assisted planning platform. This system is particularly useful for liver surgery in difficult cases with multiple tumors and/or diseased organs, where achieving sufficient remaining healthy liver volume is challenging.

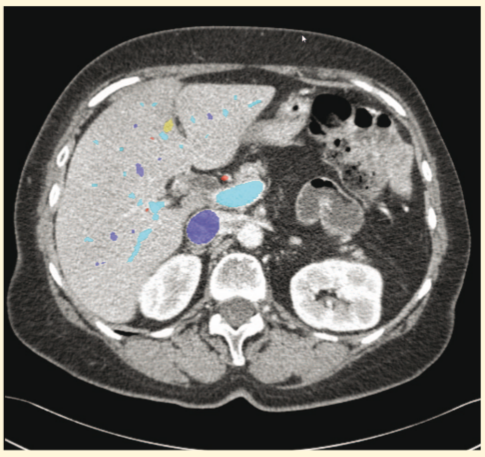

(a)

(b)

FIGURE 1 Patient-specific model of liver anatomy. (a) From CT images, all relevant structures are identified. (b) A 3-D visualization shows the tumors (yellow) in relation to the portal venous system (turquoise), hepatic veins (dark blue), and hepatic artery (red), with transparent liver surface.

Patient-Specific Modeling of Liver Anatomy and Perfusion

Basis for a decision about whether resection is possible and on the specific resection plan is the individual liver anatomy of a patient extracted from contrast-enhanced medical imaging data (typically, CT or MRI data). During contrast-enhanced image acquisition, contrast media is injected as bolus into the blood stream and flows first through the liver arteries, then through the portal vein system, and finally leaves the organ via the hepatic vein system. At different time points, 3-D image data sets are acquired, showing one or two of these vascular structures (depending on which vessel system the contrast agent is located in at the time of imaging). A registration (spatial matching) of the different imaging data sets will thus be the first step for image analysis, guaranteeing for the correct alignment and visualization of all relevant structures after combining the different image data sets in a virtual 3-D model of the patient's organ (Figure 1). Besides the assessment of the vascular anatomy and variations thereof, knowledge about the functional subdivision of the liver regions based on blood supply can support the surgical decision.

The treatment options for liver cancer have been limited compared to other cancer types since chemotherapy and radiation therapy used in other cancers are typically not curative.

For patient-specific planning of liver surgery, a software assistant was developed (HepaVision, Institute for Medical Image Computing and Visualization, Fraunhofer MEVIS) that is described later. This software platform comprises all necessary image processing steps:

- identification (segmentation) of vascular structures based on contrast imaging [1] (see Figure 1)
- extraction of the organ boundaries [2]
- identification (segmentation) of tumor region based on type and imaging modality [3]
- spatial matching of image data sets obtained at different time points (registration)
- division of liver into territories based on blood supply, via algorithmic computation based on distance evaluation from closest vessels of the portal venous liver blood supply [1] (Figure 2).

The subsequent automatic computation of volumes of tumors, (tumor-free) liver, and territories (based on blood supply) allows for an evaluation of surgical resection strategies based on patient-specific anatomy (i.e., treatment plans).

Simulation of Surgery and Risk Analysis

In cases of multiple or large tumors or in diseased organs with a requirement of larger remnant liver volume, a simulation of different resection strategies and patient-specific risk analyses, based on the computational models discussed previously, are used to support the decision on the specific procedure according to the following analysis steps.

In the first step, the distances between tumors and surrounding vascular structures are calculated. For each tumor and for varying extents of safety margin as desired by the surgeon, the tumor volume is virtually enlarged by this margin, and vessel structures within these regions (tumor + margin) are identified. Based on the potentially truncated vascular branches as a consequence of the resection, the tissue depending on (i.e., being supplied or drained by) these vessels is computed (Figure 3). As a result, an assessment of different safety margin extents around the tumor as well as of the hemodynamically safe volume of the future remnant liver can be performed.

The second step in supporting the surgical treatment decision is by interactive evaluation of different resection strategies in the patient's liver model (i.e., performing virtual surgical resections). The resection plane (i.e., plane through which tissue transsection would occur during the procedure) is user defined as follows: The user draws an initial cutting line on the surface of the liver, from which a 3-D

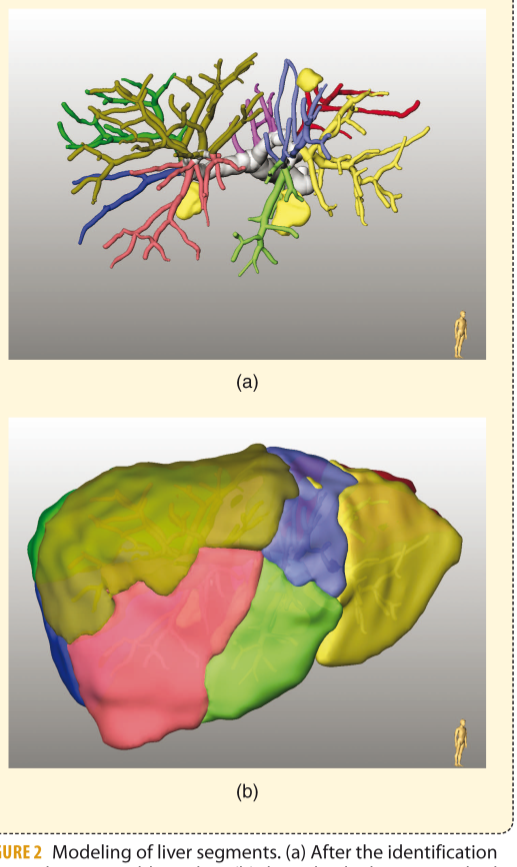

FIGURE 2 Modeling of liver segments. (a) After the identification of portal venous subbranches, (b) the individual anatomical subdivision of the liver based on the portal venous blood supply is computed. It shows the relative position of the tumors and can be used for initial planning of the surgical procedure. Segments are defined such that each individual segment can potentially be surgically removed without affecting blood supply to any other segments.

plane transsecting the liver is computed. This plane can then locally be deformed by the user to adapt to the individual patient anatomy, e.g., to avoid important vessels (Figure 4). Subsequently, truncated vascular branches and shape and volume of the removed tissue as well as of remnant tissue with identification of perfused and nonperfused areas is estimated. The assessment of the volume of the remnant tissue with adequate blood supply and potentially impaired liver tissue (i.e., without blood supply) together with adjustment of the tumor safety margin allows for a patient-specific risk assessment and comparison of different resection strategies.

The described software platform has so far been used for treatment planning in over 5,000 patients around the world, and a clinical study found that the use of this software has resulted in change of the treatment originally proposed by the surgeon (i.e., without the software) in 33% of the cases [4].

(a)

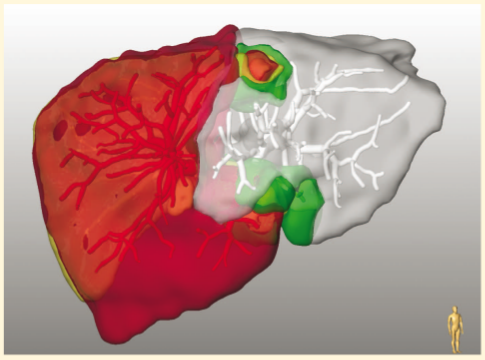

(b)

FIGURE 3 Risk analysis with multiple metastases. Subbranches of the portal vein would be affected during surgery, depending on the safety margin. For support of surgical planning decision, varying safety margins are color coded: 5 mm (red), 10 mm (yellow), or 15 mm (green). (a) Based on the vascular analysis, (b) the risk territories are computed for the portal vein and the different safety margins.

During an RFA procedure, an applicator containing electrodes is inserted into the tumor and connected to an electric generator.

Liver Tumor Ablation

Today, surgical resection of primary cancer and solitary metastases is the gold standard for tumor treatment in the liver. However, out of more than 5 million cases of liver cancer per year, worldwide only 15–30% are suitable for surgical resection. In patients who are not eligible for surgical resection due to the number and location of the tumors or their general condition, local treatment forms such as radio-frequency ablation (RFA) have become increasingly clinically used. RFA is a therapy that locally destroys tissue by heating it to above 50 °C, where tissue (both tumor and normal) is destroyed due to thermally induced coagulation of cellular proteins. The first promising investigations on thermal ablation of tumors have been performed in the 1990s, and RFA has since become a widely used approach for the treatment of primary cancer and metastasis in the liver, and other organs such as lung and bone. During an RFA procedure, an applicator containing electrodes is inserted into the tumor and connected to an electric generator, which causes the local flow of an alternating electric current through the tissue. Since the tissue has resistance to the electric current, heat develops leading to thermal destruction of the cells in the vicinity of the probe. Alternative thermal ablation approaches consider the heating of tumor cells by laser irradiation or microwaves, but clinically, heating via RFA has so far been the most widely used approach.

For successful treatment of the cancer patient, the evolving heat must destroy all tumor cells to ensure that there is no tumor regrowth from surviving cancer cells (recurrence). However, full thermal tumor destruction can be difficult to achieve as the blood flow in medium- and large-sized blood vessels in the vicinity of the RF applicator will remove heat, thus preventing cells close to these vessels to reach adequate temperatures for destruction.

Since RFA is a minimally invasive technique, it is difficult to monitor the amount of tumor destruction during the treatment, and intraprocedural monitoring options in the daily clinical routine are limited. Attempts to monitor the heat development by MRI or ultrasound are still rarely used or in the preclinical development phase. Clinical studies show that RFA is a very promising technique for tumor treatment, and recent clinical studies have found efficacy rates comparable to surgical resection in certain patient populations [10], [11]. Clearly, if RFA could be performed in all tumors with efficacy similar to surgical resection, it would be a true alternative, because it is much less traumatic for the patient with lower morbidity and considerably less expense. However, particularly for RFA of large tumors, clinical studies found high recurrence rates up to 60% [9]. In addition to tumor size, proximity to large vasculature is associated with tumor recurrence due to blood flow mediated cooling described previously.

Software Assistance for RFA

The above expositions motivated the development of computer assistance for the planning and assessment of RFA. The goal was to develop software that allows predicting the outcome of RFA

and interactively planning the optimal placement of the RF applicator. Furthermore, the software platform facilitates evaluation of the treatment quality, i.e., whether the volume of destroyed tissue covers the tumor with a sufficient safety margin (similar to tumor resection described previously, a margin of normal tissue surrounding the tumor needs to be destroyed during RFA to reduce risks of tumor recurrence).

As RFA is often a percutaneous procedure (i.e., performed through a small incision in the skin), medical imaging with MRI, CT, or ultrasound receives an important role throughout the whole process from diagnosis, through treatment planning, guidance during treatment, and for follow-up. During the planning stage, preinterventional image data is used to determine the size and location of the tumor in relation to the blood vessels (i.e., generation of patient-specific geometric 3-D model after identification of tumor and vessels). Moreover, for the planning of the placement of the applicator, it is important to determine vital structures in the vicinity of the organ, which must not be damaged (e.g., heart and colon).

Today, surgical resection of primary cancer and solitary metastases is the gold standard for tumor treatment in the liver.

The main goal of the planning of RFA is to find the best placement of the applicator such that the tumor and a sufficient safety margin around it is destroyed, while taking into account structures that must not be penetrated by the applicator (large blood vessels, diaphragm, and intestines) and that cannot be transversed (ribs and spine). A linear access path must be found from the surface of the body of the patient to the tumor so that the mentioned constraints are fulfilled. Besides these safety constraints, practicability criteria also need to be taken into account: small liver capsule penetration angles, small penetration depth, small angulation of the path to the transversal plane, position and posture of the radiologist for performing the penetration, and so on. Taking into account these criteria and constraints makes RFA planning a constrained multicriteria optimization problem.

Similar to the surgical treatment planning platform described previously, a software assistant for RFA planning was developed at Fraunhofer MEVIS. The software assistant considers multiple cylindrical projections of the relevant criteria along paths starting from a selected target point inside the tumor to all points on the patient's skin. Together with adequate weighing functions, these criteria can be combined to a multicriteria map, the extreme values of which yield access paths of particular good quality. In this initial approach, only a very rough estimation of the volume of coagulated (thermally destroyed) tissue is considered by giving preference to paths, which are parallel to the tumor's main axis.

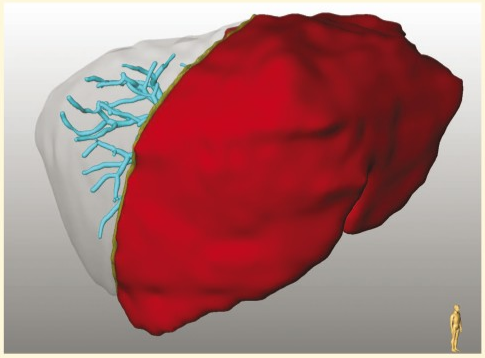

(a)

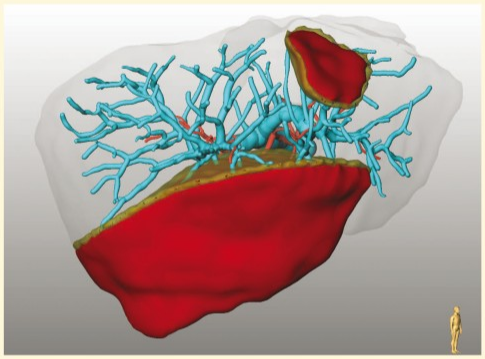

(b)

FIGURE 4 Two potential resection plans in the 3-D model of the patient's liver showing portal vein (turquoise) and hepatic artery vessel systems (red). (a) A single resection plane for simultaneous removal of all tumors (red tissue volume is removed) results in a small remnant liver (shown in transparent) of 30% of the original volume. (b) Performing the procedure by two small (local) resections will leave a remnant volume of 75% but with reduced safety margin for one of the tumors to only 2 mm (right).

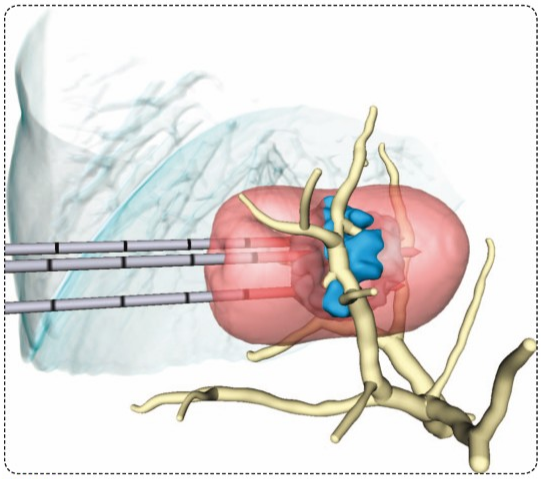

FIGURE 5 The simulated thermal tissue destruction for a configuration with three electrodes is shown. In this case, the lesion (blue, only partly visible) is very close to vascular structures. It is clearly visible how the volume of thermally destroyed tissue (red) is compromised by the cooling blood flow (yellow). The lungs, which lie directly above the liver, are shown in transparent blue. (Reprinted from [12] with permission.)

Mathematical Modeling and Computer Simulation of RFA

To obtain an accurate estimate of the extent of the coagulated volume, a simulation of the biophysical processes must be performed for the given individual data of the patient under treatment. We need to consider three basic biophysical processes: First, the delivery of energy to the tissue via the alternating electric current; second, the generation of heat, its diffusion, and the cooling through blood flow and perfusion; and third, the denaturation of proteins in the tissue cells by the heat. These biophysical processes are described by mathematical models consisting of partial differential equations, integral equations, and algebraic equations. An electrostatic equation describes the electric potential in the tissue depending on the settings of the electric generator. The bioheat-transfer equation models the tissue heating by the electric current, diffusion of heat in the tissue, as well as cooling by blood flow and perfusion. Finally, with the Arrhenius equation we estimate the volume of destroyed tissue based on the temporal evolution of the tissue temperature. The equations of the mathematical models take into account a variety of tissue characteristics such as the electric and thermal conductivity and perfusion. Since these tissue properties depend on the temperature, the equations of the model are nonlinearly coupled [5].

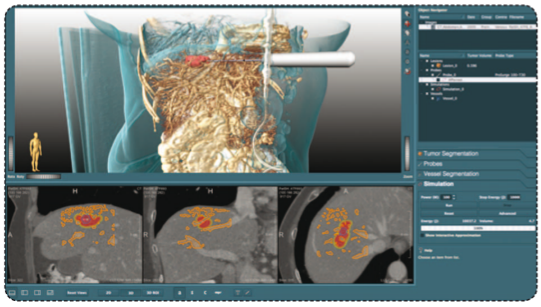

FIGURE 6 A screenshot of the SAFIR Software Assistant of Fraunhofer MEVIS. The graphical user interface shows the classical two-dimensional and 3-D viewers on the left as well as a series of input tabs on the right.

For the patient-specific prediction of the volume of thermal tissue coagulation, this system of equations needs to be solved with the help of numerical computations on the computer considering patient-specific geometry. Using special model simplifications and with additional acceleration via implementation on graphics processors, an interactive and patient-specific prediction of the thermal ablation is achieved [6]. Figure 5 shows the result of a simulation of the thermal tumor destruction during RFA. In this figure, the cooling effects of the blood flow and potential remainder of the tumor close to the vessel become clearly visible.

In Figure 6, a screenshot of the software assistant for interventional radiology (SAFIR) system developed by Fraunhofer MEVIS is shown [7]. The user interface of SAFIR is designed such that it fits optimally into the clinical workflow from therapy planning to therapy assessment. In contrast to the software assistance for surgical resection described previously, the RFA assistant does not require a complete image analysis of the full 3-D data set. Only local information in the vicinity of the tumor is needed, which can be obtained through one-click segmentations of the tumor and blood vessels. The volume visualization shown in Figure 6 displays the local vascular structures in the liver, lungs (above the liver), and RF applicator as well as the estimation of the thermally ablated tissue. The user can move the applicator interactively and thereby explore the risk of therapy failure and unintended damage to sensitive nearby tissues for various placements of the applicator.

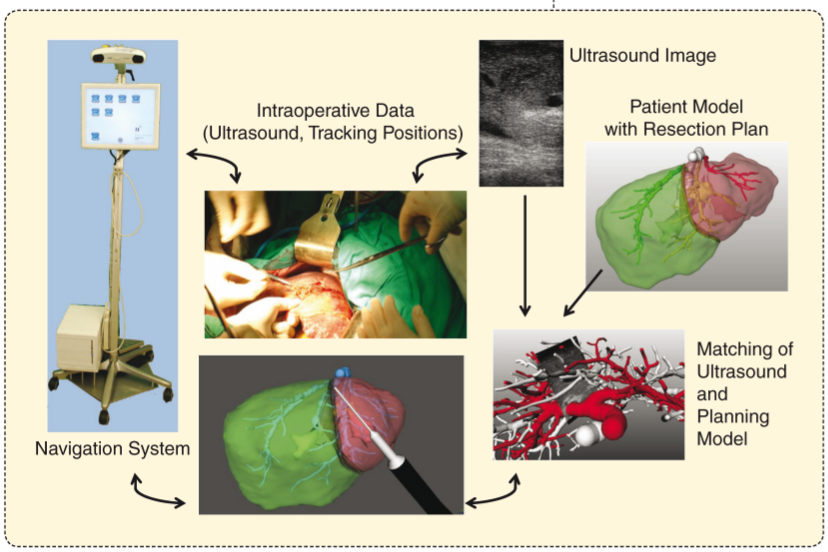

FIGURE 7 Integration of components for navigated surgery. The navigation system (CAScination AG and University of Bern, Switzerland) tracks the position of instruments and the ultrasound transducer in the operating room. The virtual liver model including the resection plan is matched to the ultrasound images based on landmarks and vascular structures. The combination allows for real-time visualization of instruments in the liver model and more accurate implementation of the treatment plan.

In summary, the image processing, modeling, simulation, and optimization of RFA discussed here provide information about the treatment, which is beyond the visual inspection of the patient-specific image data by the attending radiologist. It allows for the interactive exploration of the complex interplay among the heat emerging from the electric current, cooling influence of the blood flow, and therapy constraints posed by other anatomical structures. Settings can be identified in

advance, in which the cooling blood flow or other anatomical structures may pose a limiting factor for therapy success. Thus, we expect that the use of SAFIR will lead to an enhanced quality of the treatment in particular for configurations with large tumors or tumors in the vicinity of large blood vessels. Currently, clinical partners are evaluating the SAFIR prototype.

Future Perspectives

Patient-specific liver models can potentially be used for planning of other interventions in addition to surgery and ablation as presented here, e.g., dosimetry planning for radiation therapies and local delivery of chemotherapy. In the context of liver surgery as well as tumor ablation described previously, the logically next step is the transfer of planning results into the operation room (see Figure 7). Commercially available navigation systems are able to track the position of surgical instruments and imaging devices (e.g., ultrasound transducers) during the intervention and align the real organ with the virtual model [8]. Research projects in surgical navigation focus on the precise matching of the organ, computation of organ movements (e.g., by breathing or surgeon's interaction), and workflow in the operating room. In contrast to established navigation procedures in brain surgery, highly deformable organs such as the liver pose a particular challenge for navigated surgery.

The combination of computer-aided simulation with patient-specific imaging data allows optimization of a treatment plan based on the specific case, while combination of tracking and intraprocedural imaging simplifies the procedure and ensures accurate implementation of the plan. Particularly for complex interventional procedures, further advances in the technologies presented here in the near future will likely facilitate the integration of computer-aided modeling as an instrumental part of planning of image-guided procedures as well as for intraprocedural guidance.

Acknowledgments

The authors thank K.J. Oldhafer from the Asklepios Hospital Hamburg-Barmbek, Y. Wang from the Eastern Hepatobiliary Surgery Hospital in Shanghai, as well as A. Mahnken from the University Clinic Aachen, Germany, for providing the clinical data sets shown in the figures. They also acknowledge the research team and collaborators of Fraunhofer MEVIS, who have contributed to the results shown here. In particular, they acknowledge C. Rieder, D. Ojdanic, C. Hansen, S. Zidowitz, M. Hindennach, and T. Kröger for their support and for providing the images shown in Figures 5–7.

Andrea Schenk (andrea.schenk@mevis.fraunhofer.de) *is with the Fraunhofer Institute for Medical Image Computing MEVIS, Bremen, Germany,* ***Dieter Haemmerich*** *is with the Department of Pediatrics, Medical University of South Carolina, and the Department of Bioengineering, Clemson University, South Carolina, and* ***Tobias Preusser*** *is with the Fraunhofer Institute for Medical Image Computing MEVIS, Bremen, Germany, and School of Engineering and Science, Jacobs University Bremen, Bremen, Germany.*

References

[1] D. Selle and H.-O. Peitgen, "Analysis of the morphology and structure of vessel systems using skeletonization," in *Proc. SPIE*, 2001, vol. 4321, pp. 271–281.

[2] A. Schenk, G. Prause, and H.-O. Peitgen, "Efficient semiautomatic segmentation of 3D objects in medical images," in *Proc. MICCAI* (LNCS 1935). Berlin: Springer-Verlag, 2000, pp. 186–195.

[3] J. H. Moltz, L. Bornemann, J. M. Kuhnigk, V. Dicken, E. Peitgen, S. Meier, H. Bolte, M. Fabel, H. C. Bauknecht, M. Hittinger, A. Kießling, M. Püsken, and H.-O. Peitgen, "Advanced segmentation techniques for lung nodules, liver metastases, and enlarged lymph nodes in CT scans," *IEEE J. Select. Topics Signal Processing*, vol. 3, no. 1, pp. 122–134, 2009.

[4] H. Lang, A. Radtke, M. Hindennach, T. Schroeder, N. R. Frühauf, M. Malago, H. Bourquain, H.-O. Peitgen, K. J. Oldhafer, and C. E. Broelsch, "Impact of virtual tumor resection and computer-assisted risk analysis on operation planning and intraoperative strategy in major hepatic resection," *Arch. Surg.*, vol. 140, no. 7, pp. 629–638, 2005.

[5] T. Kröger, I. Altrogge, T. Preusser, P. L. Pereira, D. Schmidt, A. Weihusen, H.-O. Peitgen, "Numerical simulation of radio frequency ablation with state dependent material parameters in three space dimensions," in *Proc. MICCAI* (LNCS 4191). Berlin: Springer-Verlag, 2006, pp. 380–388.

[6] T. Kröger, T. Pätz, I. Altrogge, A. Schenk, K. S. Lehmann, B. B. Frericks, J.-P. Ritz, H.-O. Peitgen, and T. Preusser, "Fast estimation of the vascular cooling in RFA based on numerical simulation," *Open Biomed. Eng. J.*, vol. 4, pp. 16–26, Feb. 4, 2010.

[7] C. Rieder, M. Schwier, A. Weihusen, S. Zidowitz, and H.-O. Peitgen. "Visualization of risk structures for interactive planning of image guided radiofrequency ablation of liver tumors," in *Proc. SPIE Medical Imaging: Visualization, Image-Guided Procedures, and Modeling*, 2009, pp. 726134.1–726134.9.

[8] M. Peterhans, A. vom Berg, B. Dagin, D. Interbitzin, C. Baur, D. Candinas, and S. Weber, "A navigation system for open liver surgery: design, workflow and first clinical applications," *Int. J. Med. Robotics Comput. Assist. Surg.*, vol. 7, no. 1, pp. 7–16, 2011.

[9] Y. S. Kim, H. Rhim, O. K. Cho, B. H. Koh, and Kim Y, "Intrahepatic recurrence after percutaneous radiofrequency ablation of hepatocellular car-cinoma: Analysis of the pattern and risk factors," *Eur. J. Radiol.*, vol. 59, no. 3, pp. 432–441, 2006.

[10] T. Livraghi, F. Meloni, M. Di Stasi, E. Rolle, L. Solbiati, C. Tinelli, and S. Rossi, "Sustained complete response and complications rates after radiofrequency ablation of very early hepatocellular carcinoma in cirrhosis: Is resection still the treatment of choice?," *Hepatology*, vol. 47, pp. 82–89, Jan. 2008.

[11] A. R. Gillams and W. R. Lees, "Five-year survival in 309 patients with colorectal liver metastases treated with radiofrequency ablation," *Eur. Radiol.*, vol. 19, pp. 1206–1213, May 2009.

[12] T. Preusser and H.-O. Peitgen, "Patient-specific planning for radio-frequency ablation of tumors in the presence of uncertainty," *IT Technol.*, vol. 52, no. 5, pp. 265–271, 2010.

Further Reading

S. Vaezy and V. Zderic, Eds., *Image-Guided Therapy Systems*, 2009.

7 Publications – Adult Living Donor Liver Transplantation

7.1 Evaluation of Vascular Analysis and Volumetry for the Planning of Living Donor Liver Transplantations

Andrea Schenk, Holger Bourquain, Bernd B. Frericks, Franco C. Caldarone, Michael Galanski, Heinz-Otto Peitgen

Presented as poster and software demonstration at the congress Bildverarbeitung für die Medizin 2002 and published in the Proceedings of BVM 2002, pp. 397 – 400.

Copyright 2002 Springer. Reprinted with permission.

The work was awarded the **1st prize** for the best poster and software demonstration.

Evaluierung von Gefäßanalyse und Volumetrie für die Planung von Leberlebendspenden

Andrea Schenk[1], Holger Bourquain[1], Bernd B. Frericks[2], Franco C. Caldarone[2], Michael Galanski[2], Heinz-Otto Peitgen[1]

[1]MeVis – Centrum für Medizinische Diagnosesysteme und Visualisierung
Universitätsallee 29, 28359 Bremen
[2]Medizinische Hochschule Hannover, Abteilung für Diagnostische Radiologie
Carl-Neuberg-Straße 1, 30625 Hannover
Email: andrea.schenk@mevis.de

Zusammenfassung. Vor einer Leberlebendspende ist eine sorgfältige Untersuchung des potenziellen Spenderorgans, sowie eine detaillierte Planung und Risikoabschätzung des Eingriffes notwendig. In diesem Artikel werden Methoden der Gefäßanalyse und Volumetrie vorgestellt, deren Ergebnisse einen wesentlichen Einfluss auf die Spenderauswahl und Planung der Transplantation haben. Zur Evaluierung der Verfahren wurden an der Medizinischen Hochschule Hannover 29 potenzielle Spender präoperativ untersucht und die Resultate der computergestützten Auswertung mit den intraoperativen Befunden verglichen. Sowohl die Gefäßanatomie als auch die Resektatvolumina zeigten eine sehr gute Übereinstimmung bzw. Korrelation.

1 Einleitung

Die Leberlebendspende (Living Donor Liver Transplantation, LDLT), bei der ein gesunder Spender freiwillig einen Teil seiner Leber als Transplantationsorgan einem nahestehenden Patienten zur Verfügung stellt, wurde 1989 erstmals durchgeführt [1]. Während die Zahl der Leichenspenden rückläufig ist, gibt es bei den Leberlebendspenden einen starken Anstieg [2,3]. Zu den Vorteilen dieser Methode zählen die Reduktion der Wartezeit auf ein Spenderorgan, die meist sehr gute Organqualität und die ausreichende Zeit für die Operationsplanung. Jedoch steht diesen Vorteilen die Gefährdung eines gesunden Spenders gegenüber. Nach weltweit ca. 3000 LDLT wird das Risiko des Spenders, den Eingriff nicht zu überleben, mit 0.2-1% und das Risiko von Komplikationen während oder nach der Operation mit über 10% angegeben [4,5]. Daher ist eine sorgfältige Spenderauswahl und präoperative Planung der LDLT essenziell, um Risiken im Vorfeld möglichst genau abzuschätzen. Neben der Berücksichtigung von Laborwerten lassen sich dazu insbesondere durch eine Bildanalyse radiologischer Daten wichtige Informationen gewinnen. Dies beinhaltet die dreidimensionale Darstellung und Analyse der Gefäßanatomie sowie die Abschätzung von Volumina potenzieller Lebertransplantate. Letztere entscheiden vielfach über die Annahme oder Ablehnung eines Spenders, da der verbleibende Organanteil des Spenders und auch das gespendete Resektat für den Empfänger gewisse Mindestvolumina für eine ausreichende Leberfunktion aufweisen müssen.

2 Methode

Im einem Zeitraum von zwei Jahren wurden an der Medizinischen Hochschule Hannover (MHH) 29 potenzielle Spender für die LDLT untersucht. Die in der Routine gewonnenen CT-Aufnahmen (Siemens Somatom Plus 4, Kollimation 3-7mm, Pitch 1.5-1.7, 140 kV und 206 mA, 512x512 Matrix, Rekonstruktionsintervall 2mm) wurden mit der Software HepaVision jeweils von dem zuständigen Radiologen analysiert und mit dem Transplantationsteam diskutiert.
Die Auswertung der Bilddaten beinhaltet im wesentlichen die Analyse der Gefäßsysteme der potenziellen Spenderleber und eine Volumetrie möglicher als Spenderorgan geeigneter Anteile des Organs.

2.1 Gefäßanatomie der Leber

Nach einer speziellen Vorverarbeitung zur Unterdrückung von Rauschen und Dichtevariationen werden die kontrastierten Gefäße mit einem weiterentwickelten Region-Growing segmentiert. Bei Bedarf kann der automatisch vorgeschlagene Schwellwert in Echtzeit verändert und so das Ergebnis benutzergesteuert angepasst werden. Anschließend werden die Gefäßstrukturen skelettiert und in einer Graphstruktur gespeichert. Mittels einer Graphanalyse können automatisch Gefäßbäume (portalvenös, venös) voneinander getrennt werden, mit der zusätzlichen Möglichkeit sowohl ganze Gefäßäste oder Teilbäume als auch einzelne Voxel interaktiv einem Versorgungsgebiet zuzuordnen [6].
Für die LDLT ist neben Anomalien der portalvenösen Versorgung (wie z. B. einer Trifurkation) das Vorkommen, die Lage und Größe von akzessorischen Lebervenen relevant. Diese werden ab einem Durchmesser von 5mm erhalten und mit der unteren Hohlvene des Empfängers anastomosiert. Daher sind in der neuesten Version der Software neben der Darstellung aller anatomischen Strukturen der Leber Vermessungswerkzeuge in die dreidimensionale Visualisierung integriert.

2.2 Volumina der Leberresektate

Eine Voraussetzung für die Volumetrie von Versorgungsgebieten der Leber ist die Segmentierung des Leberparenchyms. Dies geschieht in HepaVision mit einer speziell für diese Fragestellung angepassten Weiterentwicklung des Live-Wire-Verfahrens. Um die Segmentierung mit dieser schichtbasierten Methode für das dreidimensionale Organ zu beschleunigen, wurde das Verfahren mit einer Interpolation von Konturen und einer nachfolgenden Optimierung kombiniert [7].
Die Analyse der Gefäßhierarchie des portalvenösen Systems erlaubt es, das Parenchym z.B. angelehnt an das Schema von Couinaud [8] in acht Versorgungsgebiete zu unterteilen. Ausgehend von dieser oder einer anderen Einteilung werden die Volumina für die potenzielle Organteilspende abgeschätzt. Je nach Bedarf des Empfängers werden für eine LDLT die linkslateralen Anteile der Leber (Segment II und III) entnommen, eine Hemihepatektomie rechts (Segmente V-VIII, s. Abb. 1) oder eine erweiterte Rechtsresektion (Segmente IV-VIII) durchgeführt. Neben dem Volumen dieser Leberanteile wird speziell bei Spenden für kleine Kinder die Form berücksichtigt.

Die Ergebnisse der Datenanalyse wurden mit dem Transplantationsteam diskutiert. Dabei gingen die dreidimensionale, interaktiv manipulierbare Visualisierung aller relevanten Strukturen der Leber und die abgeschätzten Resektatvolumina wesentlich in die Entscheidung für oder gegen einen potenziellen Spender in die Planung des Eingriffes ein.
Während der Operationen wurde die Anatomie der Gefäßsysteme dokumentiert und die resezierten Leberanteile gewogen. Diese Gewichte wurden mit den präoperativ berechneten Volumina verglichen, wobei eine Dichte von 1g/ml des Leberparenchyms angenommen wurde.

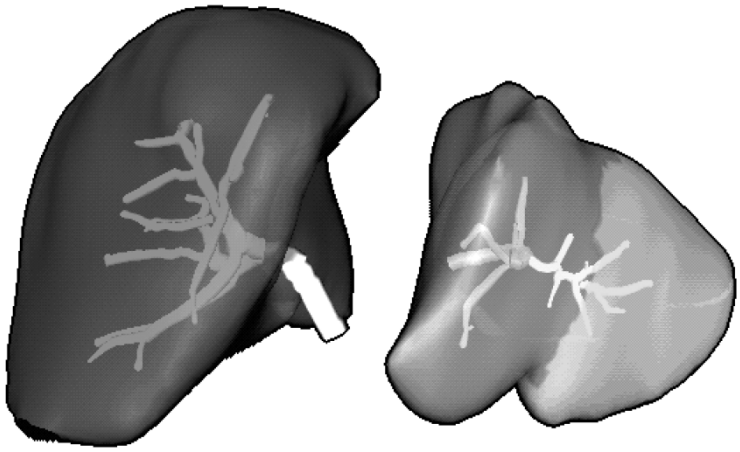

Abb.1: Mögliche Teilung einer Spenderleber für die Transplantation bei einem erwachsenen Empfänger. Die Leber ist entsprechend der Gefäßanatomie aufgeteilt (hellgrau: Segmente II und III, mittelgrau Segment IV, dunkelgrau: Segmente V-VIII)

3 Ergebnisse

Von den auf eine LDLT wartenden Patienten starben vor der Operation zwei, so dass sich die Zahl der potenziellen Spender auf 27 reduzierte. Acht Spender mussten abgelehnt werden, da sie zu geringe Volumina des Resektates bzw. der Restleber oder in einem Fall eine Gefäßvariation aufwiesen. Bei fünf Personen reichte z.B. das Volumen des verbleibenden Leberparenchyms nicht aus, da sie für einen jugendlichen oder erwachsenen Patienten spenden wollten und somit das zu spendende Resektat entsprechend groß hätte sein müssen.
Bei den durchgeführten 19 Transplantationen stimmte die intraoperativ gefundene Gefäßtopologie bis auf eine Ausnahme exakt mit dem präoperativen Befund überein. Bei einem Spender wurde eine akzessorische Lebervene gefunden, die knapp unterhalb der rechten Lebervene in die Vena cava inferior mündete und die nicht präoperativ segmentiert wurde.
Der Vergleich der präoperativen berechneten Volumina mit dem intraoperativen Gewicht der Leberresektate weist einen Korrelationskoeffizient von 0.97 bei einem Signifikanzniveau von $p < 0.001$ auf. Es traten jedoch absolute, systematische Abwei-

chungen auf, wie beispielsweise eine Überschätzung des Volumens von durchschnittlich 25% bei Hemihepatektomie rechts und Unterschätzung der linkslateralen Lebersegmentvolumina von 8%. Detailliert werden alle Studienergebnisse von Caldarone et al. [9] beschrieben.

4 Diskussion

Mit dem vorgestellten Untersuchungsprotokoll können auf Basis einer einzigen CT-Untersuchung und der anschließenden Analyse mit HepaVision fast alle relevanten Gefäß- und Volumeninformationen gewonnen werden. Die sonst übliche Angiographie zur Darstellung der hepatischen Gefäße mit ihren bekannten Risiken für den gesunden potenziellen Spender werden mit dieser nicht-invasiven Technik vermieden. Allein für die Darstellung der Gallengänge wird derzeit eine zusätzliche MRCP (Magnetresonanz-Cholangio-Pankreatikographie) angefertigt, für dessen Ersetzung innerhalb der CT-Untersuchung erste Versuche unternommen wurden.
Für die Abweichungen beim Vergleich der Volumina gibt es verschiedene Erklärungsansätze. Zum einen ist es kaum möglich, dass der Chirurg die vorher bestimmten Segmentgrenzen exakt einhält, zum anderen läuft bei der Entnahme des Leberresektates ein Teil des Blutes aus den Gefäßen ab, dessen Volumen präoperativ in der Abschätzung berücksichtigt wurde. Erste Studien an Schweinelebern zeigen, dass sich zwischen perfundiertem und nicht-perfundiertem Leberparenchym Abweichungen bis zu 35% ergeben können. Weitere Untersuchungen und eine größere Anzahl an Spenderevaluierungen sind Gegenstand derzeitiger Arbeiten.
Die bisherigen Ergebnisse haben gezeigt, dass sich mit der computergestützten Auswertung der Bilddaten mit HepaVision grundlegende Informationen für die präoperative Planung der LDLT gewinnen lassen, so dass dieses Verfahren mittlerweile bei allen Leberlebendspenden an der MHH eingesetzt wird.

5 Literatur

1. Raia S, Ney JR, Mies S et al.: Liver Transplantation from live donors, Lancet 2:497, 1989.
2. Transplant Patient Data Source, Richmond, VA. United Network for Organ Sharing, http://www.unos.org.
3. Eurotransplant: http://www.eurotransplant.nl
4. Trotter JF, Talamantes M, McClure M, et al. : Right hepatic Lobe Donation for Living Donor Liver Transplantation.: Impact on Donor Quality of Life, Liver Transpl. 7:6, 485-491, 2001.
5. UPMC Thomas E. Starzl Transplantation Institute, http://www.sti.upmc.edu/Liver.
6. Selle D, Peitgen HO: Analysis of the Morphology and Structure of Vessel System using Skeletonization, SPIE Medical Imaging: Physiology and Function from Multidimensional Images, Vol. 4321, S. 271-281, 2001.
7. Schenk A, Prause G, Peitgen HO: Efficient Semiautomatic Segmentation of 3D Objects in Medical Images, MICCAI'2000 Springer, S. 186-195, 2000.
8. Couinaud L.: Le Foie – Etudes anatomiques et chirurgicales, Paris, Masson, 1957.
9. Caldarone CC, Frericks BB, Stamm G, et al.: 3D CT Modelling of Hepatic Vessel Architecture and Volume Calculation in Living Related Liver Transplantation, (eingereicht für Radiology), 2002.

7.2 Formation of Venous Collaterals and Regeneration in the Donor Remnant Liver: Volumetric Analysis and Three-Dimensional Visualization.

Andrea Schenk, Milo Hindennach, Arnold Radtke, Massimo Malagó, Tobias Schroeder, and Heinz-Otto Peitgen

Presented at the Congress of the German Transplant Society 2008 and published in Transplant Proc 2009, 41(6), pp. 2515—2517.

Copyright 2008 Elsevier. Reprinted with permission.

Formation of Venous Collaterals and Regeneration in the Donor Remnant Liver: Volumetric Analysis and Three-Dimensional Visualization

A. Schenk, M. Hindennach, A. Radtke, M. Malagó, T. Schroeder, and H.-O. Peitgen

ABSTRACT

Purpose. We sought was to quantify and visualize the regeneration of the remnant liver after living donor liver transplantation using computed tomographic (CT) data.

Methods. For the evaluation of preoperative and follow-up data, we developed a software assistant that was able to compute the volume growth of the remnant liver and liver territories as well as visualize the individual growth of hepatic vessels over time. The software was applied to CT data of 20 donors who underwent right hepatectomy including the middle hepatic vein with at least 3 follow-up examinations in the first year after transplantation.

Results. After donation of a right lobe graft, the remnant liver regenerated by an average 77% of the original volume within the first 3 postoperative months and to 86% within the first year. The growth of the left lateral segments was increased compared with that of segment IV in all cases. The visualization showed the growth of the portal vein and the hepatic veins. With the simultaneous display of pre- and postoperative results, it was possible to detect the formation of collaterals between truncated segment IVb veins and the veins of segment IVa or of the left lateral lobe.

Conclusion. The software-assisted analysis of follow-up data yielded additional insight into territorial liver regeneration after living donor liver transplantation and allowed for reliable detection of relevant hepatic vein collaterals using CT data.

IN ADULT living donor liver transplantation (LDLT), the donor operation involves either a right or a left hepatectomy leaving the middle hepatic vein (MHV) in the donor or preserving it for the recipient. Ligated tributaries of the MHV can lead to territories with outflow obstruction bearing the risk of reduced or even insufficient liver function.[1–3] In the preoperative evaluation of donor livers, potentially congested territories are estimated based on computed tomography (CT) data or magnetic resonance imaging. The operative decision for MHV reconstruction depends on the remaining remnant volume, but there is no consensus about the optimal strategy and the lower limit. The purpose of our project was to better understand regeneration in partial livers with outflow obstructed territories. We developed specific software methods to investigate local volume growth and formation of collaterals.

PATIENTS AND METHODS

In our ongoing study, we applied software to the CT data of 20 donors with at least 3 follow-up examinations in the first year after LDLT. Preoperative imaging was performed according to the all-in-one multidetector CT protocol allowing for visualization of the hepatic artery, the portal and hepatic veins, and the bile ducts in 4 contrast phases.[1] Follow-up data were acquired on day 10 as well as at 3, 6, and 12 months after transplantation during the arterial, portal venous, and venous phases.

All pre- and postoperative data were analyzed with the software assistant MeVis LiverAnalyzer, which provided volume calculations of liver and local territories dependent on the supply of

From the Fraunhofer MEVIS (A.S., M.H., H.-O.P.), Institute for Medical Image Computing, Bremen; the Department of General, Visceral, and Transplantation Surgery (A.R., M.M.), University Hospital Essen; the Department of General and Abdominal Surgery (A.R.), Johannes Gutenberg University Hospital, Mainz, Germany; the Department of Surgery (M.M.), London, University College London, London, United Kingdom; and the Department of Diagnostic and Interventional Radiology and Neuroradiology (T.S.), University Hospital Essen, Essen, Germany.

Supported by a grant the German Research Foundation, KFO 177/1-2 and PE 199/14-2.

Address reprint requests to Andrea Schenk, Fraunhofer MEVIS, Institute for Medical Image Computing, Universitaetsallee 29, 28359 Bremen, Germany. E-mail: Andrea.Schenk@mevis.fraunhofer.de

© 2009 Published by Elsevier Inc.
360 Park Avenue South, New York, NY 10010-1710

0041-1345/09/$–see front matter
doi:10.1016/j.transproceed.2009.06.110

segmental portal veins or the drainage of MHV tributaries.[4,5] In the 3 dimensional reconstruction of the preoperative donor liver, the planned resection was performed virtually, and volumes of graft, of remnant, and of territories under the risk of venous congestion were computed subsequently.[6] Among the studied patient group, the MHV was given to the graft according to the typical operative technique leading in the remnant liver to potentially obstructed outflow zones.[7]

For comparison and detailed evaluation of preoperative and follow-up data, we developed a new software assistant that matched data analysis results at various times allowing computation of the territorial growth as well as visualization of the individual growth of the hepatic vascular systems over time. An important step was the registration of data at various times and phases. This step was a prerequisite for synchronous visualization of regenerating vascular branches and evaluation of dependent local territories. It also yielded insight into the shape deformation and rotation of the liver in the abdomen after resection (Fig 1).

RESULTS

After donation of a right lobe graft, the remnant liver regenerated within the first 3 postoperative months by an average of 77% and to 86% of the original volume within the first year. In all cases the growth of the left lateral segments increased compared to that of segment IV. The visualization showed portal vein and hepatic vein growth. With the simultaneous display of pre- and postoperative results, it was possible to detect the formation of collaterals and to identify new connections between truncated segment IVb veins and veins of segment IVa or of the left lateral lobe. Collaterals could not be detected in the first postoperative scan, but could be found in 12 (60%) donors with clearly visible CT images in the second and later scans.

DISCUSSION

The assignment of the MHV to the graft or to the remnant is a crucial decision in LDLT. It depends on anatomic and volumetric criteria as well as the metabolic demand of the recipient. It remains unclear whether existing or developing collaterals can substitute for the potential venous congestion of ligated MHV tributaries in the critical early postoperative phase.[8] A first visualization of intrahepatic collaterals between the MHV and the right hepatic vein (RHV) after LDLT was shown by Kaneko et al[9,10] using Doppler ultrasonography images and recently by Yan et al.[11] On computed tomography after LDLT, Hwang et al[12] observed early extensive hyperattenuation indicating interlobar arterial collaterals. Scatton et al[1] showed territories of venous congestion in segment IV of donor remnant livers with dissected MHV territories. These hypodense areas in computed tomography data at 10 days posttransplantation led the authors to state that the outflow obstruction was related

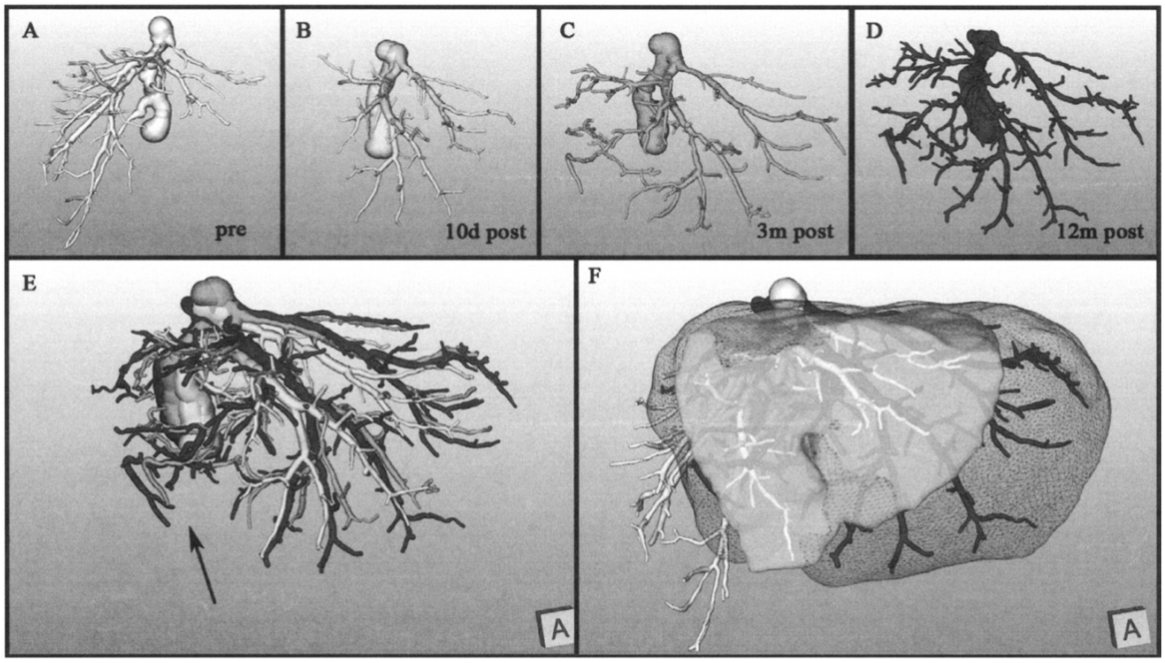

Fig 1. The registration of vascular structures from the different time points allows for additional evaluation of vascular substructures and dependent territories more precisely than with the images side by side (hepatic veins; **A–D**). In this donor, collaterals can be found in CT data 3 and 12 months after transplantation but not in the first postoperative scan (**B** and **E,** *arrow*). The shape deformation of the remnant can be compared for different time points more carefully when the rotation of the organ itself is removed (**F,** pre-OP remnant bright, 12 months post-OP dark).

to impaired functional recovery and volumetric regeneration.

In conclusion, the development of hepatic vein collaterals is an important factor for the regeneration and postoperative function of outflow-obstructed territories. Computer-assisted analysis of follow-up data provided a basis for quantitative analysis yielding additional insight into this process.

REFERENCES

1. Scatton O, Plasse M, Dondero F, et al: Impact of localized congestion related to venous deprivation after hepatectomy. Surgery 143:483, 2008

2. Kim DG, Moon IS, Kim SJ: Effect of middle hepatic vein reconstruction in living donor liver transplantation using right lobe. Transplant Proc 38:2099, 2006

3. Schroeder T, Radtke A, Kuehl H, et al: Evaluation of living liver donors with an all-inclusive 3D multi-detector row CT protocol. Radiology 238:900, 2006

4. Bourquain H, Schenk A, Link F, et al: HepaVision2: a software assistant for preoperative planning in living-related liver transplantation and oncologic liver surgery. In Lemke HU, Vannier MW, Inamura K, et al, eds. Computer Assisted Radiology and Surgery. Berlin: Springer; 2002. P 341

5. Selle D, Preim B, Schenk A, et al: Analysis of Vasculature for Liver Surgical Planning. IEEE Trans Med Imaging 21:1344, 2001

6. Radtke A, Nadalin S, Sotiropoulos GC, et al: Computer-assisted operative planning in adult living donor liver transplantation: a new way to resolve the dilemma of the middle hepatic vein. World J Surg 31:175, 2007

7. Malagó M, Molmenti EP, Paul A, et al: Hepatic venous outflow reconstruction in right live donor liver transplantation. Liver Transpl 11:364, 2005

8. Dirsch O, Madrahimov N, Chaudri N, et al: Recovery of liver perfusion after focal outflow obstruction and liver resection. Transplantation 85:748, 2008

9. Kaneko T, Kaneko K, Sugimoto H, et al: Intrahepatic anastomosis formation between the hepatic veins in the graft liver of the living related liver transplantation: observation by Doppler ultrasonography. Transplantation 70:982, 2000

10. Kaneko T, Sugimoto H, Hirota M, et al: Intrahepatic venous anastomosis formation of the right liver in living donor liver transplantation: Evaluations by Doppler ultrasonography and pulse-inversion ultrasonography with Levovist. Surgery 138:21, 2005

11. Yan L, Wu H, Chen Z, et al: Intrahepatic venous collaterals formation following outflow block in adult-to-adult living donor liver transplantation. J Surg Res 146:172, 2008

12. Hwang S, Lee SG, Lee YJ, et al: Postoperative changes in remnant medial segment parenchyma of living donor livers after procurement of left lateral segment graft. Hepatogastroenterology 53:773, 2006

7.3 Planning of Living Donor Liver Transplantations based on MRI and CT Data

Comparison of liver volume, portal and hepatic veins and their territories

Andrea Schenk, Milo Hindennach, Tobias Schroeder, Arnold Radtke, and Heinz-Otto Peitgen

Presented during a talk at the congress Computer Assisted Radiology and Surgery 2007 in Berlin and published in H. U. Lemke and M. W. Vannier, The International Journal of Computer Assisted Radiology and Surgery 2007, 2(S1), pp. 279-280.

Copyright 2007 Springer. Reprinted with permission.

Planning of living donor liver transplantations based on MRI and CT data: Comparison of liver volume, portal and hepatic veins and their territories

A. Schenk[a], M. Hindennach[a], T. Schroeder[b], A. Radtke[c], H.-O. Peitgen[a]

[a]*MeVis Research - Center for Medical Image Computing, Bremen*
[b]*Department of Diagnostic and Interventional Radiology and Neuroradiology, University Hospital of Essen*
[c]*Department of General, Visceral and Transplantation Surgery, University Hospital of Essen*

Abstract. Surgery planning of living donor liver transplantations is usually performed on the basis of preoperative CT imaging. To evaluate the performance of radiation-free MRI to serve as the sole imaging modality for donor evaluation and risk analysis of different resection strategies, we have analyzed CT and MRI data of potential donors. New methods for the analysis of MRI data have been developed and used for a first comparison of the liver volume, the portal and hepatic veins and the vascular territories with those extracted and computed from CT data of the same patient. The results of the first 13 pairs of datasets showed that the difference in liver volume is about 6%, the level of hierarchy for portal and hepatic veins extracted from MRI data is comparable to that from CT data while the differences between the territories are less than 1.5% of liver volume. Regarding the portal and hepatic vein, our study shows that the results of MRI are sufficient for the planning of living donor liver transplantations.

Keywords: Liver, Surgery, Planning, LDLT, Volume, Vessel, Segmentation

1. Introduction

In living donor liver transplantation (LDLT) the liver of a voluntary healthy donor is divided into the graft for the recipient and the remnant liver that remains in the donor. In contrast to the donation of the relatively independent left lateral lobe for a pediatric recipient, the adult living donor liver transplantation requires a subdivision of the right lobe near the middle hepatic vein (1;2). Due to the complex vascular liver anatomy and the restricted liver volume that has to be sufficient for both the healthy donor and the diseased recipient, a detailed evaluation of the donor and a dedicated image based planning is mandatory for this intervention.
Surgery planning for living donor liver transplantations is usually performed on the basis of preoperative CT imaging. For the evaluation of the healthy and mostly younger donor, it is worthwhile to accomplish the planning on basis of MRI data and thus to avoid the radiation dose. In an ongoing study, we evaluate the performance of MRI to serve as the sole imaging modality for LDLT planning and analyse CT and MRI data of potential donors of the right hemiliver. In this article, we present the methods developed and used for the analysis of MRI data and compare the liver volume, the portal and hepatic veins and vascular territories with those extracted and computed from CT data of the same patient.

2. Material and Methods

2.1 Preoperative Imaging

So far, twenty potential donors for LDLT underwent both CT and MR imaging. CT imaging was performed on a Sensation16 (Siemens, reconstruction increment 1 mm) and included simultaneous enhancement of hepatic vessels and bile ducts by injection

both of a biliary and conventional iodinated contrast agent (Biliscopin and Ultravist, Schering) as published by Schroeder et al. (3). MRI was performed on a 1.5 T scanner (Magnetom Avanto, Siemens), using an adapted Flash3D sequence (2mm slice thickness for venous phase and 1mm slice thickness with central field of view for biliary images) and involved administration of a liver specific contrast agent (Primovist, Schering).

2.2 Data Analysis

All MRI datasets were analyzed computer-assisted with an extended version of the MeVis Liver Analyzer (4;5). Liver extraction and segmentation of portal and hepatic veins was performed on the late phase of the enhanced Flash3D images where the liver appears bright with dark vascular structures (Fig. 1). The images were filtered using a statistical approach to eliminate the inhomogeneities that typically can be found in MR images (6;7).

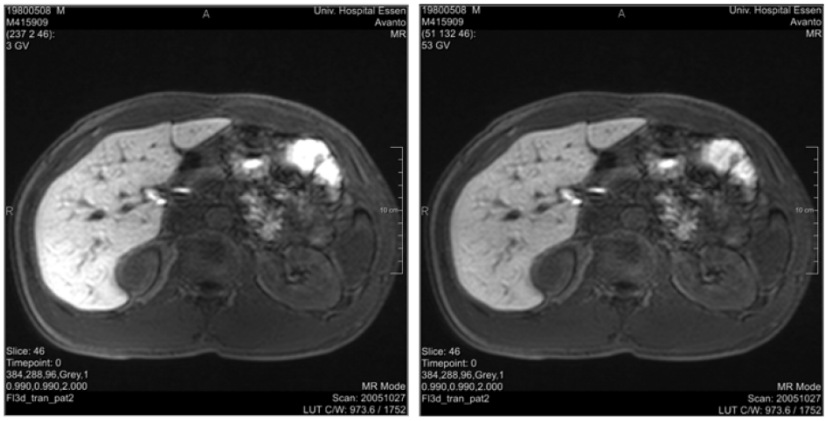

Fig. 1. Elimination of inhomogeneities in MR data: original slice (left) and resulting image after application of the correction filter.

After this preprocessing a semi-automatic segmentation approach based on three-dimensional region-growing and morphological operations was applied to extract the liver (8). Minor inaccuracies were corrected interactively with an intuitive tool for the modification of two-dimensional contours based on the live-wire approach (9).

Intrahepatic vascular structures were segmented also from the homogenised images of the late phase applying a region-growing method (10). Portal and hepatic veins were separated automatically and small vessels could be added interactively if necessary. Vascular trees were labelled according to Couinaud's scheme (11) for the portal vein, and the hepatic vascular system was subdivided into left, right, inferior veins and subtrees of the middle hepatic vein as it is advisable for a detailed LDLT planning.

Supplying and draining territories and their volumes were automatically computed on base of the liver mask and the labelled vascular systems utilizing a distance transformation.

The analysis of the CT data was performed according to our methods published by Bourquain et al. and Selle et al (4;10) and the results based on the two modalities were compared.

3. Results

So far, datasets from 13 donors have been analyzed and evaluated with our software. The liver volume ranged between 1366 ml and 2279 ml (mean 1724 ml) from CT and between 1309 ml and 2371 ml (mean 1749 ml) from MRI. The average difference was 98 ml or 5.6 % (of the liver volume from CT) with larger volumes from the MRI data in almost all cases.

Portal and hepatic veins from CT and MRI of the same patient showed similar vascular trees. Regarding a first visual comparison, the level of tree hierarchy is comparable with some minor branches missing in MRI (Fig. 2). A computer-assisted competitive evaluation of subtrees is under development. The mask for the portal vein extracted from MRI data, includes arterial and biliary structures due to the inverse contrast in the liver (enhanced liver parenchyma with hypodense vascular structures). Therefore the portal trunk appears broader as in CT but the topological information - important for the planning - is not influenced.

The territorial volumes for the portal vein showed a difference between MRI and CT of 1.1 % of CT liver volume on average with a standard deviation 0.3 %, and ranging between 0.6 and 1.7 %. Volume differences in the territories of the hepatic veins were 1.4 % (standard deviation 0.8 %), varying between 0.7 and 3.0 % (cf. Fig. 3).

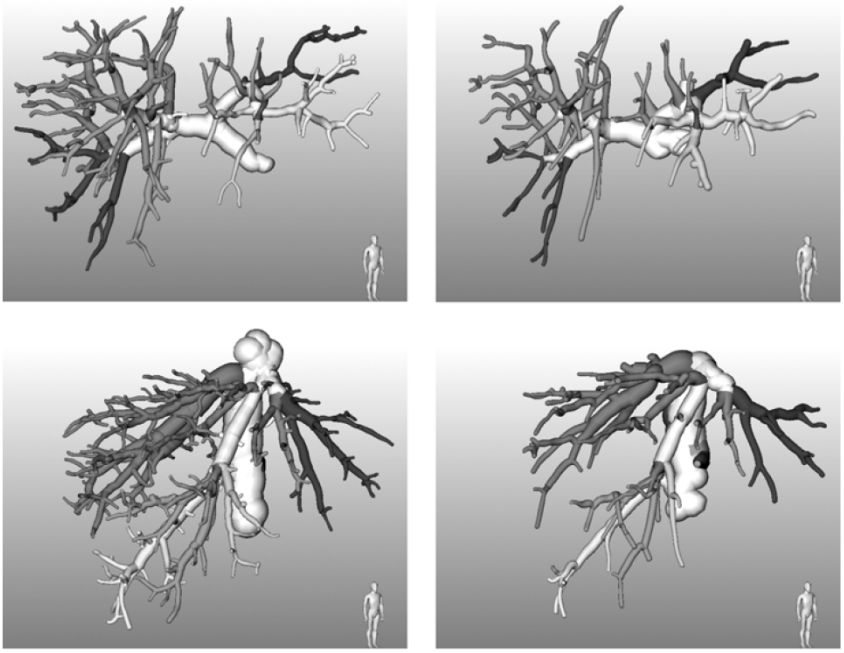

Fig. 2. Comparison of portal and hepatic veins from the same potential donor segmented in CT (left) and MRI (right) data.

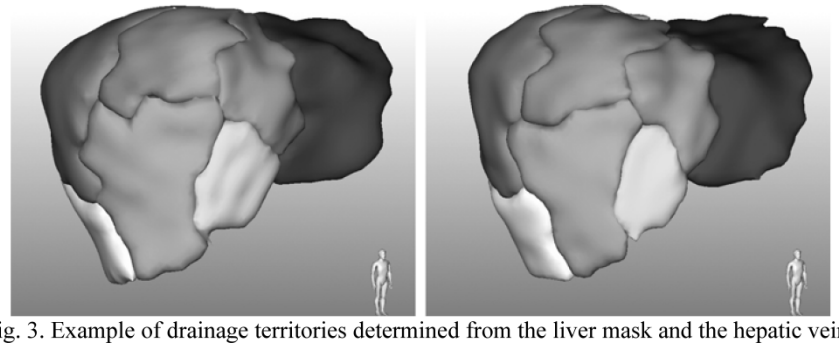

Fig. 3. Example of drainage territories determined from the liver mask and the hepatic veins of the same potential donor on basis of CT (left) and MRI data (right).

3. Conclusion

Regarding the portal and hepatic veins, the results of a MRI-based planning for LDLT is comparable to the results of CT. The liver volumes showed deviations in the range that has been published in the literature (12). The level of hierarchy for portal and hepatic veins extracted from MRI data is sufficient for the planning of LDLT. The differences of territorial volumes between MRI and CT are relatively small and the larger standard deviations for the hepatic veins originate from the small territories of the middle hepatic sub-veins.

In conclusion, the slice thickness which is larger in MRI than CT influences the territorial volume only to a limited extent and is of more importance for the smaller hepatic artery and bile ducts. The analysis and comparison of these structures in the context of LDLT planning is one of the next steps in the ongoing study. The project is supported by the German Research Foundation, grants Pe199/14 and KFO 117/1.

References

[1] Fan ST. Live donor liver transplantation in adults. Transplantation 2006; 82(6):723-732.
[2] Broelsch CE, Frilling A, Testa G, Malago M. Living donor liver transplantation in adults. Eur J Gastroenterol Hepatol 2003; 15(1):3-6.
[3] Schroeder T, Radtke A, Kuehl H, Debatin JF, Malago M, Ruehm SG. Evaluation of living liver donors with an all-inclusive 3D multi-detector row CT protocol. Radiology 2006; 238(3):900-910.
[4] Bourquain H, Schenk A, Link F, Preim B, Prause G, Peitgen HO. HepaVision2: A software assistant for preoperative planning in living-related liver transplantation and oncologic liver surgery. Computer Assisted Radiology and Surgery 2002;341-346.
[5] Schenk A, Bourquain H, Zidowitz S, Hindenach M, Konrad O, Peitgen HO. Software supported planning of liver interventions - Experience from more than 10 Years. LNI 2006; P-93 (1):529-535.
[6] Sied JG, Zijdenbos AP, Evans AC. A nonparametric method for automatic correction of intensity nonuniformity in MRI data. IEEE Transactions on Medical Imaging 1998; 17(1):87-97.
[7] Zidowitz S, Drexl H, Kröger T, Preusser T, Ritter F, Weihusen A, Peitgen H-O. Baysian Vessel Extraction for Planning of RF-Ablation. Bildverarbeitung für die Medizin 2007 (in press).
[8] Kuhnigk JM, Dicken V, Bornemann L, Bakai A, Wormanns D, Krass S et al. Morphological Segmentation and Partial Volume Analysis for Volumetry of Solid Pulmonary Lesions in Thoracic CT Scans. IEEE Trans Med Imaging 2006; 25(4):417-434.
[9] Schenk A, Prause G, Peitgen H-O. Efficient Semiautomatic Segmentation of 3D Objects in Medical Images. MICCAI - Medical Image Computing and Computer-Assisted Intervention 2000;186-195.
[10] Selle D, Preim B, Schenk A, Peitgen HO. Analysis of vasculature for liver surgical planning. IEEE Trans Med Imaging 2002; 21(11):1344-1357.
[11] Couinaud C. Le foie: etudes anatomiques et chirurgicales. Paris:Masson 1957;9-12.
[12] Schroeder T, Malago M, Debatin JF, Goyen M, Nadalin S, Ruehm SG. "All-in-one" imaging protocols for the evaluation of potential living liver donors: Comparison of magnetic resonance imaging and multidetector computed tomography. Liver Transplantation 2005; 11(7):776-787.

Appendix

Acknowledgements

"Finally, from so little sleeping and so much reading,
his brain dried up and he went completely out of his mind."
Miguel de Cervantes Saavedra, Don Quixote

First of all, I would like to thank my supervisor Prof. Dr. Heinz-Otto Peitgen, who gave me the opportunity to write this thesis at his research institute MeVis and without whose support, encouragement, and advice the presented work would not have been possible. He taucht me a special way of science and clinical understanding, and I am thankful to take part in this exciting journey of computer-assistance for liver surgery over the last fourteen years.

Secondly, my sincere gratitude goes to Prof. Dr. Bernhard Preim for his friendship, competence, outstanding effectiveness, and his creative and helpful advice. His open-mindedness and constructive comments supported me in many ways and helped me to complete this thesis.

I am also grateful to the people with whom I directly worked during the thesis. Particular thanks go to my mentor Dr. Guido Prause, who inspired me in the first years of my research on live wire, and supported me with knowledge and detailed answers to publication and funding issues during all the years. Many thanks go to my colleagues at Fraunhofer MEVIS and MeVis Medical Solutions for discussions, ideas, data analyses, proofreading, invisibly providing infrastructure for my thesis, and much more. In particular, I thank David Black, Dr. Holger Bourquain, Daniel Demedts, Christiane Engel, Dr. Christian Hansen, Milo Hindennach, Prof. Dr. Horst Hahn, André Homeyer, Michaela Jesse, Dr. Stefan Kraß, Dr. Darko Ojdanić, Prof. Dr. Tobias Preusser, Christian Rieder, Wolf Spindler, Dr. Christina Stöcker, Dr. Stefan Wirtz, Susanne Zentis, and Dr. Stephan Zidowitz.

Furthermore, I greatly acknowledge the cooperation with numerous clinical partners. My work has benefited enormously from the collaboration. In particular, I thank Prof Dr. Karl J. Oldhafer, Prof. Dr. Yasuhiro Fujimoto, Prof. Dr. Itaru Endo, PD Dr. Bernd B. Frericks, Prof. Dr. Uta Dahmen, Prof. Dr. Olaf Dirsch, Prof. Dr. Hauke Lang, and Prof. Dr. Christoph Wald.

Finally and most of all, I would like to express my love and gratitude to my family, to my parents, and especially to my husband York and my daughter Lea for putting up with me being absent so often, both mentally and physically, and supporting me in all the good and bad times.

Andrea Schenk

List of Own Publications

"If you always do what interests you, at least one person is pleased."
Katharine Hepburn

Journal Papers

Wang, Y., Zhang, Y., Peitgen, H.-O., Schenk, A., Yuan, L., Wei, G., and Sun, Y. (2012). Precise local resection for hepatocellular carcinoma based on tumor-surrounding vascular anatomy revealed by 3D analysis. Dig Surg, 29(2):99–106.

Homeyer, A., Schenk, A., Huang, H., Hahn, H., Dirsch, O., and Dahmen, U. (2011). A comparison of sampling strategies for histological image analysis. J Pathology Informatics, 2(2):11.

Radtke, A., Sgourakis, G., Sotiropoulos, G. C., Beckebaum, S., Molmenti, E. P., Saner, F. H., Schroeder, T., Nadalin, S., Schenk, A., Lang, H., Malagó, M., and Broelsch, C. E. (2010). Donor/recipient algorithm for management of the middle hepatic vein in right graft live donor liver transplantation. Am J Surg, 199(5):708–715.

Lehmann, K., Frericks, B., Holmer, C., Schenk, A., Weihusen, A., Knappe, V., Zurbuchen, U., Peitgen, H.-O., Buhr, H., and Ritz, J. (2011). In vivo validation of a therapy planning system for laser-induced thermotherapy (LITT) of liver malignancies. Int J Colorectal Disease, 26(6):799–808.

Schenk, A., Haemmerich, D., and Preusser, T. (2011). Planning of image-guided interventions in the liver. IEEE Pulse, 2:48–55.

Ivanovska, T., Schenk, A., Homeyer, A., Deng, M., Dahmen, U., Dirsch, O., Hahn, H., and Linsen, L. (2010). A fast and robust hepatocyte quantification algorithm including vein processing. BMC Bioinformatics, 11:124.

Kroeger, T., Paetz, T., Altrogge, I., Schenk, A., Lehmann, K. S., Frericks, B. B., Ritz, J.-P., Peitgen, H.-O., and Preusser, T. (2010a). Fast estimation of the vascular cooling in RFA based on numerical simulation. Open Biomed Eng J, 4:16–26.

Radtke, A., Sgourakis, G., Sotiropoulos, G. C., Beckebaum, S., Molmenti, E. P., Saner, F. H., Schroeder, T., Nadalin, S., Schenk, A., Lang, H., Malagó, M., and Broelsch, C. E. (2010). Donor/recipient algorithm for management of the middle hepatic vein in right graft live donor liver transplantation. Am J Surg, 199(5):708–715.

Hansen, C., Zidowitz, S., Hindennach, M., Schenk, A., Hahn, H., and Peitgen, H.-O. (2009). Interactive determination of robust safety margins for oncologic liver surgery. Int J Comput Assist Radiol Surg, 4(5):469–474.

Lehmann, K. S., Ritz, J. P., Valdeig, S., Knappe, V., Schenk, A., Weihusen, A., Rieder, C., Holmer, C., Zurbuchen, U., Hoffmann, P., Peitgen, H.-O., Buhr, H. J., and Frericks, B. B. (2009). Ex situ quantification of the cooling effect of liver vessels on radiofrequency ablation. Langenbecks Arch Surg, 394(3):475–481.

Radtke, A., Sgourakis, G., Sotiropoulos, G., Molmenti, E., Nadalin, S., Schroeder, T., Saner, F., Schenk, A., Cincinnati, V., Broelsch, C., Lang, H., and Malago, M. (2009). Vascular and biliary anatomy of the right hilar window: its impact on recipient morbidity and mortality for right graft live donor liver transplantation. World J Surg, 33(9):1941–1951.

Schenk, A., Hindennach, M., Radtke, A., Malagó, M., Schroeder, T., and Peitgen, H.-O. (2009). Formation of venous collaterals and regeneration in the donor remnant liver: volumetric analysis and three-dimensional visualization. Transplant Proc, 41(6):2515–2517.

Dahmen, U., Madrahimov, N., Madrahimova, F., Ji, Y., Schenk, A., and Dirsch, O. (2008). Small-for-size syndrome in the rat: does size or technique matter? J Surg Res, 149(1):15–26.

Dahmen, U., Radtke, A., Schröder, T., Chi, H., Madrahimov, N., Lu, M., Schenk, A., Peitgen, H.-O., and Dirsch, O. (2008b). Median liver lobe of woodchuck as a model to study hepatic outflow obstruction: a pilot study. Liver Int, 28(9):1236–1244.

Dirsch, O., Madrahimov, N., Chaudri, N., Deng, M., Madrahimova, F., Schenk, A., and Dahmen, U. (2008). Recovery of liver perfusion after focal outflow obstruction and liver resection. Transplantation, 85(5):748–756.

Frericks, B., Lehmann, K., Valdeig, S., Schenk, A., and Ritz, J.-P. (2008). Influence of intrahepatic vessels on volume and shape of percutaneous laser ablation zones: In-vivo evaluation in a porcine model. Invest Radiol, 43(4):211–218.

Ketelsen, D., Heuschmid, M., Schenk, A., Nadalin, S., and Horger, M. (2008). CT cholangiography–potential applications and image findings. Rofo, 180(12):1031–1034.

Lehmann, K. S., Ritz, J.-P., Valdeig, S., Schenk, A., Holmer, C., Peitgen, H.-O., Buhr, H.-J., and Frericks, B. B. (2008). Portal vein segmentation of a 3D-planning system for liver surgery–in vivo evaluation in a porcine model. Ann Surg Oncol, 15(7):1899–1907.

Radtke, A., Nadalin, S., Sgourakis, G., Sotiropoulos, G., Molmenti, E., Schroeder, T., Fouzas, I., Saner, F., Schenk, A., Malago, M., and Lang, H. (2008). Liver compliance: A previously unrecognized preoperative predictor of small-for-size syndrome in adult living donor liver transplantation. Transplant Proc, 40(9):3142–3146.

Radtke, A., Sgourakis, G., Sotiropoulos, G., Molmenti, E., Fouzas, I., Schroeder, T., Saner, F., Schenk, A., Beckebaum, S., Malago, M., and Lang, H. (2008). Anatomical classification of the peripheral right hepatic duct: early identification of a preventable source of morbidity and mortality in adult live donor liver transplantation. Transplant Proc, 40(9):3155–3157.

Radtke, A., Sgourakis, G., Sotiropoulos, G., Molmenti, E., Nadalin, S., Fouzas, I., Schroeder, T., Saner, F., Schenk, A., Cincinnati, V., Malago, M., and Lang, H. (2008). Intrahepatic biliary anatomy derived from right graft adult live donor liver transplantation. Transplant Proc, 40(9):3151–3154.

Radtke, A., Sgourakis, G., Sotiropoulos, G., Molmenti, E., Nadalin, S., Fouzas, I., Schroeder, T., Saner, F., Cicinnati, V., Schenk, A., Malago, M., and Lang, H. (2008). A new systematic classification of peripheral anatomy of the right hepatic duct: experience from adult live liver donor transplantation. Transplant Proc, 40(9):3158–3160.

Radtke, A., Sgourakis, G., Sotiropoulos, G., Molmenti, E., Nadalin, S., Fouzas, I., Schroeder, T., Saner, F., Schenk, A., Cicinnati, V., Malago, M., and Lang, H. (2008). Hepatic hilar and sectorial vascular and biliary anatomy in right graft adult live liver donor transplantation. Transplant Proc, 40(9):3147–3150.

Lang, H., Radtke, A., Hindennach, M., Schroeder, T., Bourquain, H., Schenk, A., Oldhafer, K. J., Prause, G., Peitgen, H.-O., and Broelsch, C. E. (2007). Virtual hepatic surgery - computer-assisted operation planning on the 3-dimensional reconstructed liver. Z Gastroenterol, 45(9):965–970.

Radtke, A., Sotiropoulos, G. C., Nadalin, S., Molmenti, E. P., Schroeder, T., Lang, H., Saner, F., Valentin-Gamazo, C., Frilling, A., Schenk, A., Broelsch, C. E., and Malagó, M. (2007). Preoperative volume prediction in adult living donor liver transplantation: how much can we rely on it? Am J Transplant, 7(3):672–679.

Frericks, B., Kirchhoff, T., Shin, H., Stamm, G., Merkesdal, S., Abe, T., Schenk, A., Peitgen, H., Klempnauer, J., Galanski, M., and Nashan, B. (2006). Preoperative volume calculation of the hepatic venous draining areas with multi-detector row CT in adult living donor liver transplantation: impact on surgical procedure. Eur Radiol, 16(12):2803–2810.

Radtke, A., Bockhorn, M., Schroeder, T., Lang, H., Paul, A., Nadalin, S., Saner, F., Schenk, A., Broelsch, C. E., and Malagó, M. (2006). Computer-assisted planning in living donor liver operation. Zentralbl Chir, 131(1):69–74.

Radtke, A., Sotiropoulos, G. C., Molmenti, E. P., Nadalinl, S., Schroeder, T., Schenk, A., Saner, F., Valentin-Gamazo, C., Dahmen, U., Spasov, L., Broelsch, C. E., and Malagò, M. (2006). The influence of accessory right inferior hepatic veins on the venous drainage in right graft living donor liver transplantation. Hepatogastroenterology, 53(70):479–483.

Radtke, A., Schroeder, T., Molmenti, E. P., Sotiropoulos, G. C., Nadalin, S., Schenk, A., Malamutmann, E., Saner, F., Valentin-Gamazo, C., Dahmen, U., Lang, H., Peitgen, H.-O., Broelsch, C. E., and Malagò, M. (2006). The "territorial belonging" of the middle hepatic vein: a troublesome dilemma in adult live donor liver transplantation–anatomical evidence based on virtual 3-dimensional-computed tomography-imaging reconstructions. Eur J Med Res, 11(2):66–72.

Radtke, A., Schroeder, T., Sotiropoulos, G. C., Molmenti, E., Schenk, A., Paul, A., Nadalin, S., Lang, H., Saner, F., Peitgen, H. O., Broelsch, C. E., and Malagò, M. (2005). Anatomical and physiological classification of hepatic vein dominance applied to liver transplantation. Eur J Med Res, 10(5):187–194.

Radtke, A., Schroeder, T., Sotiropoulos, G. C., Molmenti, E., Schenk, A., Paul, A., Nadalin, S., Lang, H., Saner, F., Peitgen, H. O., Broelsch, C. E., and Malagò, M. (2005). Anatomical and physiological classification of hepatic vein dominance applied to liver transplantation. Eur J Med Res, 10(5):187–194.

Frericks, B. B. J., Kiene, T., Stamm, G., Shin, H., and Galanski, M. (2004). CT-based liver volumetry in a porcine model: Impact on clinical volumetry prior to living donated liver transplantation. Rofo, 176(2):252–257.

Meier, S., Schenk, A., Mildenberger, P., Bourquain, H., Pitton, M., and Thelen, M. (2004). Evaluation of a new software tool for the automatic volume calculation of hepatic tumors. First results. Rofo, 176(2):234–238.

van Ooijen, P., Wolf, R., Schenk, A., Rouw, D., Slooff, M., Peitgen, H.-O., and Oudkerk, M. (2003). Recent developments in organ-selective reconstruction and analysis of multiphase liver CT. Imaging Decisions, 7(1):37–43.

Selle, D., Preim, B., Schenk, A., and Peitgen, H.-O. (2002). Analysis of vasculature for liver surgical planning. IEEE Trans Med Imaging, 21(11):1344–1357.

Selle, D., Spindler, W., Schenk, A., Preim, B., Boehm, D., Oldhafer, K., Galanski, M., Fasel, J., Klose, K., and Peitgen, H.-O. (2000). Computer-aided preoperative planning and risk analysis in liver surgery. Diagnostic Imaging Europe, 12:16–20.

Conference Proceedings

Demedts, D., Schenk, A., Hansen, C., and Peitgen, H.-O. (2010). Evaluation of resection proposals for liver surgery planning. In CURAC, pages 13–16.

Hansen, C., Lindow, B., Zidowitz, S., Schenk, A., and Peitgen, H.-O. (2010). Towards automatic generation of resection surfaces for liver surgery planning. In Computer Assisted Radiology and Surgery, volume 5, pages 119–120.

Hansen, C., Zidowitz, S., Schenk, A., Oldhafer, K., Lang, H., and Peitgen, H.-O. (2010). Risk maps for navigation in liver surgery. In SPIE Medical Imaging, volume 7625, pages 762528_1–8.

Zidowitz, S., Altrogge, I., Hansen, C., Hindennach, M., Kröger, T., Ojdanic, D., Rieder, C., Preusser, T., Schenk, A., Weihusen, A., Wirtz, S., Prause, G., and Peitgen, H.-O. (2010). Computer-assisted risk prevention in surgical and interventional treatment of liver tumor. In Zeitschrift für Biomedizinische Technik, volume 55, pages 74–77, BMT.

Zidowitz, S., Schenk, A., Hindennach, M., Hansen, C., Hahn, H., and Peitgen, H.-O. (2009). Reliability and robustness in image based surgical planning. In O, D., Schlegel, W., and Magjarevic, R., editors, World Congress on Medical Physics and Biomedical Engineering, volume 25 of IFMBE Proceedings, pages 1628–1631.

Hindennach, M. (2008). Automatische Segmentierung Intra- und Extrahepatischer Gefaesse mit Hilfe von Anatomischen Landmarken in CT-Daten. In CURAC, pages 189–192.

Ivanovska, T., Schenk, A., Dahmen, U., Hahn, H., and Linsen, L. (2008). Automatic hepatocyte quantification from histological images: Comparing presmoothing filters. In Botha, C. and Kindlmann, G., editors, Eurographics Workshop on Visual Computing for Biomedicine, pages 143–150.

Schenk, A., Weihusen, A., Rieder, C., Frericks, B., Valdeig, S., Lehmann, K., and Peitgen, H.-O. (2008a). Evaluation of radiofrequency ablation lesions: a new software tool for the quantification of heat sink effects. In Int J Comput Assist Radiol Surg, volume 3, pages S448–S449.

Schenk, A., Zidowitz, S., Bourquain, H., Hindennach, M., Hansen, C., Hahn, H., and Peitgen, H.-O. (2008b). Clinical relevance of model based computer-assisted diagnosis and therapy. In Giger, M. L. and Karssemeijer, N., editors, SPIE Medical Imaging, volume 6915, pages 691502_1–19.

Hindennach, M., Zidowitz, S., A.Schenk, H.Bourquain, and Peitgen, H.-O. (2007). Computer assistance for fast extraction and analysis of intrahepatic vasculature from contrast-enhanced CT-volume data for preoperative planning in liver surgery. In Int J Comput Assist Radiol Surg, volume 2, pages 451–452.

Metzen, J., Kroeger, T., Schenk, A., Zidowitz, S., Peitgen, H., and Jiang, X. (2007). Matching of tree structures for registration of medical images. volume 4538 of Lecture Notes Computer Science, pages 13–24.

Metzen, J., Kroeger, T., Schenk, A., Zidowitz, S., Jiang, X., and Peitgen, H.-O. (2007). Matching von baumstrukturen. In Horsch, A., Deserno, T., Handels, H., Meinzer, H.-P., and Tolxdorff, T., editors, Bildverarbeitung fuer die Medizin, pages 116–120.

Schenk, A., Hindennach, M., Schroeder, T., Radtke, A., and Peitgen, H.-O. (2007). Planning of living donor liver transplantations based on MRI and CT data: comparison of liver volume, portal and hepatic veins and their territories. In Lemke, H. and Vannier, M., editors, Int J Comput Assist Radiol Surg, volume 2, pages 279–280.

Weinhold, A., Wirtz, S., Schenk, A., Boehler, T., Jiang, X., Dahmen, U., Dirsch, O., and Peitgen, H.-O. (2007). Vollautomatische vorverarbeitung und rigide registrierung zur rekonstruktion von bildern histologischer stufenschnitte der rattenleber. In Bildverarbeitung fuer die Medizin, Bildverarbeitung für die Medizin, pages 419–423.

Hennemuth, A., Bourquain, H., Berghorn, W., Wetzel, I., Lang, M., Schenk, A., and Peitgen, H.-O. (2006). Web-based support of time-critical services for image-based intervention planning. In Hochberger, C. and Liskowsky, R., editors, Lecture Notes in Informatics, volume 93, pages 491–498.

Schenk, A., Bourqain, H., Zidowitz, S., Hindenach, M., Konrad, O., and Peitgen, H.-O. (2006). Software supported planning of liver interventions, experience of more than 10 years. In C, H., , and R, L., editors, Lecture Notes in Informatics, volume P-93, pages 529–535.

Zidowitz, S., Bourqain, H., Hennemuth, A., Schenk, A., Berghorn, W., and Peitgen, H.-O. (2005). SIMPL: Service center for medical image analysis, visualization, and therapy planning. In Kalender, W., Hahn, E., and Schulte, A., editors, Biomedizinische Technik, volume 50 (Suppl. 1), pages 151–152.

Littmann, A., Schenk, A., Preim, B., Lehmann, K., Ritz, J.-P., Germer, C.-T., Roggan, A., and Peitgen, H.-O. (2003a). Kombination von Bildanalyse und physikalischer Simultaion für die Planung von Behandlungen maligner Lebertumore

mittels laserinduzierter Thermotherapie. In Bildverarbeitung fuer die Medizin, pages 428–432.

Littmann, A., Schenk, A., Preim, B., Prause, G., Lehmann, K., Roggan, A., and Peitgen, H.-O. (2003b). Planning of anatomical resections and in-situ ablations in oncologic liver surgery. In Lemke, H. and et al., editors, Computer Assisted Radiology and Surgery, pages 684–689.

Preim, B., Hindennach, M., Spindler, W., Schenk, A., Littmann, A., and Peitgen, H.-O. (2003). Visualisierungs- und Interaktionstechniken für die Planung lokaler Therapien. In Simulation und Visualisierung, pages 237–248.

Schenk, A., Behrens, S., Meier, S., Mildenberger, P., and Peitgen, H.-O. (2003). Segmentierung von Hepatozellulären Karzinomen mit Fuzzy-Connectedness. In Wittenberg, T., editor, Bildverarbeitung fuer die Medizin, pages 408–412.

Scheuering, M., Schenk, A., Schneider, A., Preim, B., and Greiner, G. (2003). Intra-operative augmented reality for minimally invasive liver interventions. In SPIE Medical Imaging, volume 5029, pages 407–417.

Bourquain, H., Schenk, A., Link, F., Preim, B., Prause, G., and Peitgen, H.-O. (2002). HepaVision2: A software assistant for preoperative planning in living-related liver transplantation and oncologic liver surgery. In Lemke, H., Vannier, M., Inamura, K., Farman, A., Doi, K., and Reiber, J., editors, Computer Assisted Radiology and Surgery, pages 341–346.

Schenk, A., Bourqain, H., Frericks, B., Calderone, F., Galanski, M., and Peitgen, H.-O. (2002). Evaluierung von Gefaessanalyse und Volumetrie fuer die Planung von Leberlebendspenden. In Bildverarbeitung fuer die Medizin, pages 397–400.

Schenk, A., Prause, G., and Peitgen, H.-O. (2001). Local cost computation for efficient segmentation of 3D objects with live wire. In Sonka, M. and Hanson, M., editors, SPIE Medical Imaging, volume 4322, pages 1357–1364.

Schenk, A., Prause, G., and Peitgen, H.-O. (2001). Optimierte semi-automatische Segmentierung von 3D-Objekten mit Live Wire und Shape-Based Interpolation. In Handels, H. and et al., editors, Bildverarbeitung fuer die Medizin, pages 202–206.

Schenk, A., Prause, G., and Peitgen, H.-O. (2000). Efficient semiautomatic segmentation of 3D objects in medical images. In MICCAI, pages 186–195.

Schenk, A., Breitenborn, J., Selle, D., Schindewolf, T., Boehm, D., Spindler, W., Juergens, H., and Peitgen, H.-O. (1999). ILabMed-Workstation – Eine Entwick-

lungsumgebung für radiologische Anwendungen. Bildverarbeitung für die Medizin, pages 238–242.

Book Chapters

Lang, H. and Schenk, A. (2010). Planung von Leberresektionen, In Computerassistierte Chirurgie, pages 515–524. Elsevier.

Oldhafer, K., Hindennach, M., Ritter, F., Schenk, A., Bourquain, H., Preim, B., and Peitgen, H.-O. (2006). Computerunterstuetzung in der Operationsplanung, In Pichlmayrs Chirurgische Therapie, pages 369–390. Springer.

Bourquain, H., Schenk, A., and Peitgen, H.-O. (2003). Computer-assisted planning and decision-making in living-donor liver transplantation, In Living-donor liver transplantation – Surgical techniques and innovations, pages 23–28. Prous Science.

Peitgen, H.-O., Preim, B., Selle, D., Böhm, D., Schenk, A., and Spindler, W. (2000). Lanalisi del rischio nella chirurgia del fegato (Risk Analysis for Liver Surgery), In Matematica e Cultura, pages 331–340. Springer.

Schindewolf, T., Selle, D., Spindler, W., Schenk, A., Böhm, D., Preim, B., Oldhafer, K., Galanski, M., Klose, K., and Peitgen, H.-O. (1999). Virtuelle Operationsplanung in der Leberchirurgie, In Telemedizinführer Deutschland, pages 300–301. Minerva.

Supervised and Co-supervised Thesis

Demedts, D. (2010). Bewertung virtueller Resektionen fuer die Leberchirurgie. Master's thesis, University of Luebeck, Germany.

Ivanovska, T. (2009). Efficient Multichannel Image Partitioning: Theory and Application. PhD thesis, Jacobs University, Bremen, Germany.

Metzen, J. (2006). Matching von Baumstrukturen in der medizinischen Bildverarbeitung. Master's thesis, Westfaelische Wilhelms-Universitaet Muenster, Germany.

Weinhold, A. (2006). Vollautomatische Vorverarbeitung und rigide Registrierung zur Rekonstruktion von Bildern histologischer Stufenschnitte der Rattenleber. Master's thesis, Westfaelische Wilhelms-Universitaet Muenster, Germany.

Behrens, S. (2003). Segmentierung medizinischer Bilddaten mit Fuzzy-Connectedness. Master's thesis, University of Bremen, Germany.

Abbreviations

ALDLT	Adult Living Donor Liver Transplantation
BSA	Body Surface Area
BrdU	5-bromo-2-deoxyuridine
BZ	Border Zone
CT	Computed Tomography
ECR	Estimated Congestion Ratio
ERCP	Endoscopic Retrograde cholangiopancreatography
ESLV	Estimated Standard Liver Volume
Gd-EOB-DTPA	Gadolinium-Ethoxybenzyl-Diethylenetriamine Penta-Acetic Acid, Gadoxetic acid
GRWR	Graft-to-Recipient Weight Ratio
GT	Ground Truth
GUI	Graphical User Interface
HA	Hepatic Artery
HCC	Hepatocellular Carcinoma
HV	Hepatic Vein
HVT	Hepatic Vein Territories
IHV or Inf.V	Inferior Hepatic Vein
LDLT	Living Donor Liver Transplantation
LHV	Left Hepatic Vein
LWI	Live Wire and Interpolation

MHV	Middle Hepatic Vein
MR	Magnetic Resonance
MRI	Magnetic Resonance Imaging
MRCP	Magnetic Resonance Cholangiopancreatography
NZ	Normal Zone
OPS	Orthogonal Polarizations Spectroscopy
OZ	Obstructed Zone
PI	Proliferation Index
PV	Portal Vein
PVT	Portal Vein Territories
RFA	Radio-Frequency Ablation
RHV	Right Hepatic Vein
RMHV	Right Hepatic Vein in the Median Liver Lobe
SFSS	Small-For-Size Syndrom
LITT	Laser-Induced Thermotherapy
VC	Vena Cava

Bibliography

Aitsebaomo, J., Portbury, A. L., Schisler, J. C., and Patterson, C. (2008). Brothers and sisters: molecular insights into arterial-venous heterogeneity. *Circ Res*, 103(9):929–939.

Altendorf-Hofmann, A. and Scheele, J. (2003). A critical review of the major indicators of prognosis after resection of hepatic metastases from colorectal carcinoma. *Surg Oncol Clin N Am*, 12(1):165–192.

Altrogge, I., Büskens, C., Kröger, T., Peitgen, H.-O., Preusser, T., and Tiesler, H. (2012). Modeling, simulation and optimization of radio frequency ablation. *Constrained Optimization and Optimal Control for Partial Differential Equations*, 160(5):487–499.

Altrogge, I., Preusser, T., Kröger, T., Büskens, C., Pereira, P., Schmidt, D., and Peitgen, H.-O. (2007). Multi-scale optimization of the probe placement for radiofrequency ablation. *Academic Radiology*, 14(11):1310–1324.

Asakuma, M., Fujimoto, Y., Bourquain, H., Uryuhara, K., Hayashi, M., Tanigawa, N., Peitgen, H.-O., and Tanaka, K. (2007). Graft selection algorithm based on congestion volume for adult living donor liver transplantation. *Am J Transplant*, 7(7):1788–1796.

Asbach, P., Warmuth, C., Stemmer, A., Rief, M., Huppertz, A., Hamm, B., Taupitz, M., and Klessen, C. (2008). High spatial resolution T1-weighted MR imaging of liver and biliary tract during uptake phase of a hepatocyte-specific contrast medium. *Invest Radiol*, 43(11):809–815.

Bae, K. T., Giger, M. L., Chen, C. T., and Kahn, C. E. (1993). Automatic segmentation of liver structure in CT images. *Med Phys*, 20(1):71–78.

Barrett, W. A. and Mortensen, E. N. (1996). Fast, accurate and reproducible live-wire boundary extraction. In Höhne, K. H. and Kikinis, R., editors, *Visualization in Biomedical Computing*, volume 1131 of *Lecture Notes in Computer Science*, pages 183–192.

Barrett, W. A. and Mortensen, E. N. (1997). Interactive live-wire boundary extraction. *Medical Image Analysis*, 1(4):331–341.

Beck, A. and Aurich, V. (2007). Hepatux–a semiautomatic liver segmentation system. In *MICCAI 2007 Workshop: 3D Segmentation in the Clinic-A Grand Challenge*, pages 225–233.

Bois, D. D. and Bois, E. F. D. (1989). A formula to estimate the approximate surface area if height and weight be known. *Nutrition*, 5(5):303–311; discussion 312–313.

Borgefors, G. (1986). Distance transformations in digital images. *Computer Vision, Graphics, and Image Processing*, 34(3):344–371.

Bornik, A., Beichel, R., and Schmalstieg, D. (2006). Interactive editing of segmented volumetric datasets in a hybrid 2D/3D virtual environment. In *VRST*, pages 197–206.

Bourquain, H., Schenk, A., Link, F., Preim, B., Prause, G., and Peitgen, H.-O. (2002). HepaVision2: A software assistant for preoperative planning in living-related liver transplantation and oncologic liver surgery. In Lemke, H., Vannier, M., Inamura, K., Farman, A., Doi, K., and Reiber, J., editors, *Computer Assisted Radiology and Surgery*, pages 341–346.

Bourquain, H., Schenk, A., and Peitgen, H.-O. (2003). *Living-donor liver transplantation – Surgical techniques and innovations*, chapter Computer-assisted planning and decision-making in living-donor liver transplantation, pages 23–28. Prous Science.

Breitenstein, S., Apestegui, C., Petrowsky, H., and Clavien, P. A. (2009). State of the art in liver resection and living donor liver transplantation: a worldwide survey of 100 liver centers. *World J Surg*, 33(4):797–803.

Broelsch, C. E., Emond, J. C., Thistlethwaite, J. R., Whitington, P. F., Zucker, A. R., Baker, A. L., Aran, P. F., Rouch, D. A., and Lichtor, J. L. (1988). Liver transplantation, including the concept of reduced-size liver transplants in children. *Ann Surg*, 208(4):410–420.

Broelsch, C. E., Whitington, P. F., Emond, J. C., Heffron, T. G., Thistlethwaite, J. R., Stevens, L., Piper, J., Whitington, S. H., and Lichtor, J. L. (1991). Liver transplantation in children from living related donors. surgical techniques and results. *Ann Surg*, 214(4):428–437; discussion 437–439.

Calne, R. Y., Rolles, K., White, D. J., Thiru, S., Evans, D. B., McMaster, P., Dunn, D. C., Craddock, G. N., Henderson, R. G., Aziz, S., and Lewis, P. (1979). Cyclosporin a initially as the only immunosuppressant in 34 recipients of cadaveric organs: 32 kidneys, 2 pancreases, and 2 livers. *Lancet*, 2(8151):1033–1036.

Calne, R. Y., Williams, R., Lindop, M., Farman, J. V., Tolley, M. E., Rolles, K., MacDougall, B., Neuberger, J., Wyke, R. J., Raftery, A. T., Duffy, T. J., Wight, D. G., and White, D. J. (1981). Improved survival after orthotopic liver grafting. *Br Med J (Clin Res Ed)*, 283(6284):115–118.

Campadelli, P., Casiraghi, E., and Esposito, A. (2009). Liver segmentation from computed tomography scans: a survey and a new algorithm. *Artif Intell Med*, 45(2-3):185–196.

Caselles, V.; Kimmel, R. . S. G. (1997). Geodesic active contours. *International Journal of Computer Vision*, 22(1):61–79.

Castaing, D., Adam, R., and Azoulay, D. (2006). *Chirurgie du foie et de l'hypertension portale*. Masson.

Chan, S. C., Lo, C. M., Chok, K. S. H., Sharr, W. W., Cheung, T. T., Tsang, S. H. Y., Chan, A. C. Y., and Fan, S. T. (2011). Validation of graft and standard liver size predictions in right liver living donor liver transplantation. *Hepatol Int*, 5(4):913–917.

Chen, C. L., Chen, Y. S., Chiang, Y. C., Liu, P. P., Cheng, Y. F., Huang, T. L., Eng, H. L., Cheung, H. K., Jawan, B., and Lee, J. H. (1996). Initiation of living-related liver donor transplantation in Taiwan. *Transplant Proc*, 28(3):1704–1705.

Chen, C.-L., Fan, S.-T., Lee, S.-G., Makuuchi, M., and Tanaka, K. (2003). Living-donor liver transplantation: 12 years of experience in Asia. *Transplantation*, 75(3 Suppl):S6–11.

Cherkassky, B. V., Goldberg, A. V., and Radzik, T. (1994). Shortest paths algorithms: Theory and experimental evaluation. In *SODA*, pages 516–525.

Chi, Y., Cashman, P. M. M., Bello, F., and Kitney, R. I. (2007). A discussion on the evaluation of a new automatic liver volume segmentation method for specified CT image datasets. In T. Heimann, M. Styner, B. v. G., editor, *MICCAI 2007 Workshop: 3D Segmentation in the Clinic-A Grand Challenge*, pages 167–175.

Clark, H. P., Carson, W. F., Kavanagh, P. V., Ho, C. P. H., Shen, P., and Zagoria, R. J. (2005). Staging and current treatment of hepatocellular carcinoma. *Radiographics*, 25 Suppl 1:S3–23.

Clavien, P.-A. and Breitenstein, S. (2010). *Malignant Liver Tumors - Current and Emerging Therapies*. Wiley-Blackwell, 3rd edition.

Couinaud, C. (1957). *Le Foie – Études anatomiques et chirurgicales [The Liver: Anatomical and Surgical Studies]*. Masson.

Crossingham, J. L., Jenkinson, J., Woolridge, N., Gallinger, S., Tait, G. A., and Moulton, C.-A. E. (2009). Interpreting three-dimensional structures from two-dimensional images: a web-based interactive 3D teaching model of surgical liver anatomy. *HPB (Oxford)*, 11(6):523–528.

Dahmen, U., Madrahimov, N., Madrahimova, F., Ji, Y., Schenk, A., and Dirsch, O. (2008a). Small-for-size syndrome in the rat: does size or technique matter? *J Surg Res*, 149(1):15–26.

Dahmen, U., Radtke, A., Schröder, T., Chi, H., Madrahimov, N., Lu, M., Schenk, A., Peitgen, H.-O., and Dirsch, O. (2008b). Median liver lobe of woodchuck as a model to study hepatic outflow obstruction: a pilot study. *Liver Int*, 28(9):1236–1244.

Dawant, B. M., Li, R., Lennon, B., and Li, S. (2007). Semi-automatic segmentation of the liver and its evaluation on the MICCAI 2007 grand challenge data set. In *MICCAI 2007 Workshop: 3D Segmentation in the Clinic-A Grand Challenge*, pages 215–221.

de Hoop, B., Gietema, H., van Ginneken, B., Zanen, P., Groenewegen, G., and Prokop, M. (2009). A comparison of six software packages for evaluation of solid lung nodules using semi-automated volumetry: what is the minimum increase in size to detect growth in repeated CT examinations. *Eur Radiol*, 19(4):800–808.

DeLand, F. H. and North, W. A. (1968). Relationship between liver size and body size. *Radiology*, 91(6):1195–1198.

Demedts, D. (2010). Bewertung virtueller Resektionen fuer die Leberchirurgie. Master's thesis, University of Luebeck, Germany.

Demedts, D., Schenk, A., Hansen, C., and Peitgen, H.-O. (2010). Evaluation of resection proposals for liver surgery planning. In *CURAC*, pages 13–16.

Dijkstra, E. W. (1959). A note on two problems in connexion with graphs. *Numerische Mathematik*, 1:269–271.

Dirsch, O., Madrahimov, N., Chaudri, N., Deng, M., Madrahimova, F., Schenk, A., and Dahmen, U. (2008). Recovery of liver perfusion after focal outflow obstruction and liver resection. *Transplantation*, 85(5):748–756.

Eurotransplant (assessed in July 2012). http://www.eurotransplant.org.

Falcao, A. X., Jayaram, K., Udupa, J. K., and K., M. F. (1999). An ultra-fast user-steered image segmentation paradigm: Live-wire-on-the-fly. In M, K. and Hanson, editors, *SPIE Medical Imaging*, volume 3661, pages 184–191.

Falcao, A. X. and Udupa, J. K. (1997). Segmentation of 3D objects using live wire. In *SPIE Medical Imaging*, volume 3034, pages 228–235.

Falcao, A. X., Udupa, J. K., and Miyazawa, F. K. (2000). An ultra-fast user-steered image segementation paradigm: Live-wire-on-the-fly. *IEEE Trans Med Imaging*, 19(1):55–62.

Falcao, A. X., Udupa, J. K., Samarasekera, S., Sharma, S., and Hirsch, B. E. (1998). User-steered image segmentation paradigms: Live-wire and live-lane. *Graphical Models and Image Processing*, 60(4):223–260.

Fan, S., Lee, P., and Wei, W. (2011). *Living Donor Liver Transplantation*. World Scientific Publishing Company.

Fasel, J. H., Selle, D., Evertsz, C. J., Terrier, F., Peitgen, H.-O., and Gailloud, P. (1998). Segmental anatomy of the liver: poor correlation with CT. *Radiology*, 206(1):151–156.

Fasel, J. H. D., Majno, P. E., and Peitgen, H.-O. (2010). Liver segments: an anatomical rationale for explaining inconsistencies with Couinaud's eight-segment concept. *Surg Radiol Anat*, 32(8):761–765.

Forner, A., Llovet, J. M., and Bruix, J. (2012). Hepatocellular carcinoma. *Lancet*, 379(9822):1245–1255.

Frericks, B., Kirchhoff, T., Shin, H., Stamm, G., Merkesdal, S., Abe, T., Schenk, A., Peitgen, H., Klempnauer, J., Galanski, M., and Nashan, B. (2006). Preoperative volume calculation of the hepatic venous draining areas with multi-detector row CT in adult living donor liver transplantation: impact on surgical procedure. *Eur Radiol*, 16(12):2803–2810.

Frericks, B., Lehmann, K., Valdeig, S., Schenk, A., and Ritz, J.-P. (2008). Influence of intrahepatic vessels on volume and shape of percutaneous laser ablation zones: In-vivo evaluation in a porcine model. *Invest Radiol*, 43(4):211–218.

Frericks, B. B., Caldarone, F. C., Nashan, B., Savellano, D. H., Stamm, G., Kirchhoff, T. D., Shin, H.-O., Schenk, A., Selle, D., Spindler, W., Klempnauer, J., Peitgen, H.-O., and Galanski, M. (2004a). 3D CT modeling of hepatic vessel architecture and volume calculation in living donated liver transplantation. *Eur Radiol*, 14(2):326–333.

Frericks, B. B. J., Kiene, T., Stamm, G., Shin, H., and Galanski, M. (2004b). CT-based liver volumetry in a porcine model: Impact on clinical volumetry prior to living donated liver transplantation. *Rofo*, 176(2):252–257.

Fu-Gui, L., Lu-Nan, Y., Bo, L., Yong, Z., Tian-Fu, W., Ming-Qing, X., Wen-Tao, W., and Zhe-Yu, C. (2009). Estimation of standard liver volume in Chinese adult living donors. *Transplant Proc*, 41(10):4052–4056.

Gao, L., Heath, D. G., Kuszyk, B. S., and Fishman, E. K. (1996). Automatic liver segmentation technique for three-dimensional visualization of CT data. *Radiology*, 201(2):359–364.

Gurusamy, K., Aggarwal, R., Palanivelu, L., and Davidson, B. R. (2008). Systematic review of randomized controlled trials on the effectiveness of virtual reality training for laparoscopic surgery. *Br J Surg*, 95(9):1088–1097.

Haase, S., Süss, P., Schwientek, J., Teichert, K., and Preusser, T. (2012). Radiofrequency ablation planning: An application of semi-infinite modelling techniques. *European Journal of Operational Research*, 218(3):856–864.

Hahn, H. K., Preim, B., Selle, D., and Peitgen, H.-O. (2001). Visualization and interaction techniques for the exploration of vascular structures. In Ertl, T., Joy, K. I., and Varshney, A., editors, *IEEE Visualization*, pages 395–402.

Hansen, C., Lindow, B., Zidowitz, S., Schenk, A., and Peitgen, H.-O. (2010a). Towards automatic generation of resection surfaces for liver surgery planning. In *Computer Assisted Radiology and Surgery*, volume 5, pages 119–120.

Hansen, C., Zidowitz, S., Schenk, A., Oldhafer, K., Lang, H., and Peitgen, H.-O. (2010b). Risk maps for navigation in liver surgery. In *SPIE Medical Imaging*, volume 7625, pages 762528_1–8.

Harada, N., Shimada, M., Yoshizumi, T., Suehiro, T., Soejima, Y., and Maehara, Y. (2004). A simple and accurate formula to estimate left hepatic graft volume in living-donor adult liver transplantation. *Transplantation*, 77(10):1571–1575.

Hashikura, Y., Makuuchi, M., Kawasaki, S., Matsunami, H., Ikegami, T., Nakazawa, Y., Kiyosawa, K., and Ichida, T. (1994). Successful living-related partial liver transplantation to an adult patient. *Lancet*, 343(8907):1233–1234.

Healey, J. E. (1954). Clinical anatomic aspects of radical hepatic surgery. *J Int Coll Surg*, 22(5, Sect. 1):542–550.

Healey, J. E., Schroy, P. C., and Sorensen, R. J. (1953). The intrahepatic distribution of the hepatic artery in man. *J Int Coll Surg*, 20(2):133–148.

Heckel, F., Moltz, J.-H., Dicken, V., Geisler, B., Bauknecht, H.-C., Fabel, M., Meier, S., and Peitgen, H.-O. (2009). 3D contour based local manual correction of liver segmentations in CT scans. In *Int J Comput Assist Radiol Surg*, volume 4, pages 45–46.

Heimann, T., van Ginneken, B., Styner, M., Arzhaeva, Y., Aurich, V., Bauer, C., Beck, A., Becker, C., Beichel, R., Bekes, G., Bello, F., Binnig, G. K., Bischof, H.,

Bornik, A., Cashman, P., Chi, Y., Cordova, A., Dawant, B. M., Fidrich, M., Furst, J. D., Furukawa, D., Grenacher, L., Hornegger, J., Kainmüller, D., Kitney, R., Kobatake, H., Lamecker, H., Lange, T., Lee, J., Lennon, B., Li, R., Li, S., Meinzer, H.-P., Németh, G., Raicu, D. S., Rau, A.-M., van Rikxoort, E. M., Rousson, M., Ruskó, L., Saddi, K. A., Schmidt, G., Seghers, D., Shimizu, A., Slagmolen, P., Sorantin, E., Soza, G., Susomboon, R., Waite, J. M., Wimmer, A., and Wolf, I. (2009). Comparison and evaluation of methods for liver segmentation from CT datasets. *IEEE Trans Med Imaging*, 28(8):1251–1265.

Heinemann, A., Wischhusen, F., Püschel, K., and Rogiers, X. (1999). Standard liver volume in the Caucasian population. *Liver Transpl Surg*, 5(5):366–368.

Henderson, J. M., Heymsfield, S. B., Horowitz, J., and Kutner, M. H. (1981). Measurement of liver and spleen volume by computed tomography. Assessment of reproducibility and changes found following a selective distal splenorenal shunt. *Radiology*, 141(2):525–527.

Hennemuth, A., Bourquain, H., Berghorn, W., Wetzel, I., Lang, M., Schenk, A., and Peitgen, H.-O. (2006). Web-based support of time-critical services for image-based intervention planning. In Hochberger, C. and Liskowsky, R., editors, *Lecture Notes in Informatics*, volume 93, pages 491–498.

Herline, A. J., Herring, J. L., Stefansic, J. D., Chapman, W. C., Galloway, R. L., and Dawant, B. M. (1999). Surface registration for use in interactive image-guided liver surgery. In Taylor, C. J. and Colchester, A. C. F., editors, *MICCAI*, pages 892–899.

Herman, G. T., Zheng, J., and A., B. C. (1992). Shape-based interpolation. *IEEE Computer Graphics and Applications*, 12(3):69–79.

Hermoye, L., Laamari-Azjal, I., Cao, Z., Annet, L., Lerut, J., and Dawant, B. (2005). Liver segmentation in living liver transplant donors: comparison of semi-automatic and manual methods. *Radiology*, 234(1):171–178.

Heymsfield, S. B., Fulenwider, T., Nordlinger, B., Barlow, R., Sones, P., and Kutner, M. (1979). Accurate measurement of liver, kidney, and spleen volume and mass by computerized axial tomography. *Ann Intern Med*, 90(2):185–187.

Hindennach, M., Bourquain, H., Wald, C., Pomfret, E., Fujimoto, Y., Tanaka, K., and Peitgen, H.-O. (2006). Regionale Unterschiede der Drainage des rechten Leberlappens über inferiore rechte Lebervenen bei der Planung von Leberlebendspenden. In Saeger, H. D., Jauch, K. W., and Bauer, H., editors, *Chirurgisches Forum 2006*, volume 35, pages 329–330. Springer.

Hindennach, M., Zidowitz, S., A.Schenk, H.Bourquain, and Peitgen, H.-O. (2007). Computer assistance for fast extraction and analysis of intrahepatic vasculature from contrast-enhanced CT-volume data for preoperative planning in liver surgery. In *Int J Comput Assist Radiol Surg*, volume 2, pages 451–452.

Hjortsjo, C. H. (1951). The topography of the intrahepatic duct systems. *Acta Anat (Basel)*, 11(4):599–615.

Hoegemann, D., Stamm, G., Oldhafer, K. J., Selle, D., Schindewolf, T., and Galanski, M. (1999). Volumetric evaluation and 3-D visualization of the liver before living-related donation. In *Computer Assisted Radiology and Surgery*, pages 249–252.

Hoehne, K. H., Pflesser, B., Pommert, A., Priesmeyer, K., Riemer, M., Schiemann, T., Schubert, R., Tiede, U., Frederking, H., Gehrmann, S., Noster, S., and Schumacher., U. (2003). VOXEL-MAN 3D-Navigator: Inner organs. Springer Electronic Media.

Homeyer, A., Schenk, A., Huang, H., Hahn, H., Dirsch, O., and Dahmen, U. (2011). A comparison of sampling strategies for histological image analysis. *J Pathology Informatics*, 2(2):11.

Hu, H. H., Boernert, P., Hernando, D., Kellman, P., Ma, J., Reeder, S., and Sirlin, C. (2012). ISMRM workshop on fat-water separation: Insights, applications and progress in MRI. *Magn Reson Med*.

Hwang, S., Lee, S.-G., Lee, Y.-J., Sung, K.-B., Park, K.-M., Kim, K.-H., Ahn, C.-S., Moon, D.-B., Hwang, G.-S., Kim, K.-M., Ha, T.-Y., Kim, D.-S., Jung, J.-P., and Song, G.-W. (2006). Lessons learned from 1,000 living donor liver transplantations in a single center: how to make living donations safe. *Liver Transpl*, 12(6):920–927.

IHPBA (2000). The Brisbane 2000 terminology of liver anatomy and resections. *HPB*, 2:333–339.

Imamura, H., Makuuchi, M., Sakamoto, Y., Sugawara, Y., Sano, K., Nakayama, A., Kawasaki, S., and Takayama, T. (2000). Anatomical keys and pitfalls in living donor liver transplantation. *J Hepatobiliary Pancreat Surg*, 7(4):380–394.

Ivanovska, T. (2009). *Efficient Multichannel Image Partitioning: Theory and Application*. PhD thesis, Jacobs University, Bremen, Germany.

Ivanovska, T., Schenk, A., Dahmen, U., Hahn, H., and Linsen, L. (2008). Automatic hepatocyte quantification from histological images: Comparing pre-

smoothing filters. In Botha, C. and Kindlmann, G., editors, *Eurographics Workshop on Visual Computing for Biomedicine*, pages 143–150.

Ivanovska, T., Schenk, A., Homeyer, A., Deng, M., Dahmen, U., Dirsch, O., Hahn, H., and Linsen, L. (2010). A fast and robust hepatocyte quantification algorithm including vein processing. *BMC Bioinformatics*, 11:124.

Iwatsuki, S., Starzl, T. E., Todo, S., Gordon, R. D., Esquivel, C. O., Tzakis, A. G., Makowka, L., Marsh, J. W., Koneru, B., and Stieber, A. (1988). Experience in 1,000 liver transplants under cyclosporine-steroid therapy: a survival report. *Transplant Proc*, 20(1 Suppl 1):498–504.

Kainmueller, D., Lange, T., and Lamecker, H. (2007). Shape constrained automatic segmentation of the liver based on a heuristic intensity model. In *MICCAI 2007 Workshop: 3D Segmentation in the Clinic-A Grand Challenge*, pages 109–116.

Kamei, H., Fujimoto, Y., Nagai, S., Suda, R., Yamamoto, H., and Kiuchi, T. (2007). Impact of non-congestive graft size in living donor liver transplantation: new indicator for additional vein reconstruction in right liver graft. *Liver Transpl*, 13(9):1295–1301.

Kaneko, T., Kaneko, K., Sugimoto, H., Inoue, S., Hatsuno, T., Sawada, K., Ando, H., and Nakao, A. (2000). Intrahepatic anastomosis formation between the hepatic veins in the graft liver of the living related liver transplantation: observation by Doppler ultrasonography. *Transplantation*, 70(6):982–985.

Kaneko, T., Sugimoto, H., Hirota, M., Kure, S., Kiuchi, T., and Nakao, A. (2005). Intrahepatic venous anastomosis formation of the right liver in living donor liver transplantation: evaluations by Doppler ultrasonography and pulse-inversion ultrasonography with Levovist. *Surgery*, 138(1):21–27.

Kang, Y., Engelke, K., and Kalender, W. A. (2004). Interactive 3D editing tools for image segmentation. *Medical Image Analysis*, 8(1):35–46.

Kass, M., Witkin, A., and Terzopoulos, D. (1988). Snakes: active contour models. *Int J Comp Vision*, 1(4):321–331.

Ketelsen, D., Heuschmid, M., Schenk, A., Nadalin, S., and Horger, M. (2008). CT cholangiography–potential applications and image findings. *Rofo*, 180(12):1031–1034.

Kiuchi, T., Kasahara, M., Uryuhara, K., Inomata, Y., Uemoto, S., Asonuma, K., Egawa, H., Fujita, S., Hayashi, M., and Tanaka, K. (1999). Impact of graft size mismatching on graft prognosis in liver transplantation from living donors. *Transplantation*, 67(2):321–327.

Koc, Z., Oguzkurt, L., and Ulusan, S. (2007). Portal venous system aneurysms: imaging, clinical findings, and a possible new etiologic factor. *Am J Roentgenol*, 189(5):1023–1030.

Konrad-Verse, O., Preim, B., and Littmann, A. (2004). Virtual resection with a deformable cutting plane. In *Simulation und Visualisierung*, pages 203–214.

Koss, J. E., Newman, F. D., Johnson, T. K., and Kirch, D. L. (1999). Abdominal organ segmentation using texture transforms and a Hopfield neural network. *IEEE Trans Med Imaging*, 18(7):640–648.

Kroeger, T., Altrogge, I., Preusser, T., Pereira, P., Schmidt, D., Weihusen, A., and Peitgen, H.-O. (2006). Numerical simulation of radio frequency ablation with state dependent material parameters in three space dimensions. *Medical Image Computing and Computer Assisted Intervention*, 9(Pt 2):380–388.

Kroeger, T., Paetz, T., Altrogge, I., Schenk, A., Lehmann, K. S., Frericks, B. B., Ritz, J.-P., Peitgen, H.-O., and Preusser, T. (2010a). Fast estimation of the vascular cooling in RFA based on numerical simulation. *Open Biomed Eng J*, 4:16–26.

Kroeger, T., Pannier, S., Kaliske, M., Altrogge, I., Graf, W., and Preusser, T. (2010b). Optimal applicator placement in hepatic radiofrequency ablation on the basis of rare data. *Comput Methods Biomech Biomed Engin*, 13(3):431–440.

Lamecker, H., Lange, T., and Seebass, M. (2004). Segmentation of the liver using a 3D statistical shape model. Technical Report 04-09, ZIB, Berlin.

Lassen, B. (2009). Atlas-based liver segmentation of CT images. Master's thesis, University Bremen, Germany.

Lee, C.-C., Chung, P.-C., and Tsai, H.-M. (2003). Identifying multiple abdominal organs from CT image series using a multimodule contextual neural network and spatial fuzzy rules. *IEEE J ITBM*, 7(3):208–217.

Lee, J., Kim, N., Lee, H.and Seo, J. B. W. H. J. S. Y. M., and Shin, Y. G. (2007). Efficient liver segmentation exploiting level-set speed images with 2.5D shape propagation. In *MICCAI 2007 Workshop: 3D Segmentation in the Clinic-A Grand Challenge*, pages 189–196.

Lee, S. G., Lee, Y. J., Park, K. M., Kwon, T. W., Choi, K. M., Ha, H. S., Kim, K. M., Kim, S. C., Kim, I. K., Kim, S. K., Han, S. H., Koh, K. S., and Min, P. C. (1996). Living related donor liver transplantation: the Seoul experience. *Transplant Proc*, 28(4):2383–2384.

Lehmann, K., Drexl, J., Frericks, B., Bourquain, H., Schenk, A., Germer, C.-T., Peitgen, H.-O., and Buhr, H.-J. (2003). Fusionierung von 3D-Bildgebung der Leber mit einem Planungs-System für die in-situ-Ablation maligner Lebertumoren. In *CURAC, presented Nov. 2003*.

Lehmann, K., Frericks, B., Holmer, C., Schenk, A., Weihusen, A., Knappe, V., Zurbuchen, U., Peitgen, H.-O., Buhr, H., and Ritz, J. (2011). In vivo validation of a therapy planning system for laser-induced thermotherapy (LITT) of liver malignancies. *Int J Colorectal Disease*, 26(6):799–808.

Lehmann, K. S., Ritz, J. P., Valdeig, S., Knappe, V., Schenk, A., Weihusen, A., Rieder, C., Holmer, C., Zurbuchen, U., Hoffmann, P., Peitgen, H.-O., Buhr, H. J., and Frericks, B. B. (2009). Ex situ quantification of the cooling effect of liver vessels on radiofrequency ablation. *Langenbecks Arch Surg*, 394(3):475–481.

Lehmann, K. S., Ritz, J.-P., Valdeig, S., Schenk, A., Holmer, C., Peitgen, H.-O., Buhr, H.-J., and Frericks, B. B. (2008). Portal vein segmentation of a 3D-planning system for liver surgery–in vivo evaluation in a porcine model. *Ann Surg Oncol*, 15(7):1899–1907.

Leppek, R., Zahlten, C., Juergens, H., Evertsz, C., Peitgen, H.-O., and Klose, K. (1993). In situ visualization of portal vein branching. *Eur Radiol*, 19:96–100.

Littmann, A., Schenk, A., Preim, B., Lehmann, K., Ritz, J.-P., Germer, C.-T., Roggan, A., and Peitgen, H.-O. (2003a). Kombination von Bildanalyse und physikalischer Simultaion für die Planung von Behandlungen maligner Lebertumore mittels laserinduzierter Thermotherapie. In *Bildverarbeitung fuer die Medizin*, pages 428–432.

Littmann, A., Schenk, A., Preim, B., Prause, G., Lehmann, K., Roggan, A., and Peitgen, H.-O. (2003b). Planning of anatomical resections and in-situ ablations in oncologic liver surgery. In Lemke, H. and et al., editors, *Computer Assisted Radiology and Surgery*, pages 684–689.

Liu, F., Zhao, B., Kijewski, P. K., Wang, L., and Schwartz, L. H. (2005). Liver segmentation for CT images using GVF snake. *Med Phys*, 32(12):3699–3706.

Liu, J. and Udupa, J. K. (2009). Oriented active shape models. *IEEE Trans Med Imaging*, 28(4):571–584.

Lo, C.-M. (2003). Complications and long-term outcome of living liver donors: a survey of 1,508 cases in five Asian centers. *Transplantation*, 75(3 Suppl):S12–S15.

Lo, C. M., Fan, S. T., Liu, C. L., Chan, J. K., Lam, B. K., Lau, G. K., Wei, W. I., and Wong, J. (1999). Minimum graft size for successful living donor liver transplantation. *Transplantation*, 68(8):1112–1116.

Lohe, T. (2007). Hierarchical matching of anatomical trees for medical imaging applications. Master's thesis, Westfaelische Wilhelms-Universitaet Muenster, Germany.

Maema, A., Imamura, H., Takayama, T., Sano, K., Hui, A.-M., Sugawara, Y., and Makuuchi, M. (2002). Impaired volume regeneration of split livers with partial venous disruption: a latent problem in partial liver transplantation. *Transplantation*, 73(5):765–769.

Mall, F. P. (1906). A study of the structural unit of the liver. *Am J Anatomy*, 5(3):227–308.

Malladi, R. and Sethian, J. A. (1997). Level set methods for curvature flow, image enchancement, and shape recovery in medical images. In *Conf. on Visualization and Mathematics*, pages 329–345.

Mangold, S., Bretschneider, C., Fenchel, M., Seeger, A., Kramer, U., Klumpp, B., Nadalin, S., Königsrainer, A., Claussen, C. D., and Miller, S. (2012). MRI for evaluation of potential living liver donors: a new approach including contrast-enhanced magnetic resonance cholangiography. *Abdom Imaging*, 37(2):244–251.

MDS (2012). MeVis Distance Services, http://www.mevis.de/mms/Distant_Services.html.

Metzen, J. (2006). Matching von Baumstrukturen in der medizinischen Bildverarbeitung. Master's thesis, Westfaelische Wilhelms-Universitaet Muenster, Germany.

Metzen, J., Kroeger, T., Schenk, A., Zidowitz, S., Peitgen, H., and Jiang, X. (2009). Matching of anatomical tree structures for registration of medical images. *Image and Vision Computing*, 27(7):923–933.

MeVisLab (2012). The rapid prototyping platform MeVisLab, www.mevislab.de.

MICCAI (2007). Segmentation of the liver, http://www.sliver07.org/.

Moltz, J., Bornemann, L., Kuhnigk, J., Dicken, V., Peitgen, E., Meier, S., Bolte, H., Fabel, M., Bauknecht, H., Hittinger, M., Kiessling, A., Puesken, M., and Peitgen, H.-O. (2009). Advanced segmentation techniques for lung nodules, liver metastases, and enlarged lymph nodes in ct scans. *IEEE Journal of Selected Topics in Signal Processing*, 3(1):122–134.

Montagnat, J. and HerveDelingette (1997). Volumetric medical images segmentation using shape constrained deformable models. In Troccaz, J., Grimson, W. E. L., and Moesges, R., editors, *CVRMed*, volume 1205, pages 13–22.

Mori, K., Nagata, I., Yamagata, S., Sasaki, H., Nishizawa, F., Takada, Y., Moriyasu, F., Tanaka, K., Yamaoka, Y., and Kumada, K. (1992). The introduction of microvascular surgery to hepatic artery reconstruction in living-donor liver transplantation–its surgical advantages compared with conventional procedures. *Transplantation*, 54(2):263–268.

Mortensen, E. N. and Barrett, W. A. (1995). Intelligent scissor for image composition. In *Computer Graphics (SIGGRAPH '95)*, pages 191–198.

Mortensen, E. N., Morse, B., Barrett, W. A., and Udupa, J. K. (1992). Adaptive boundary detection using live-wire two-dimensional dynamic programming. In Werner, R., editor, *IEEE Computers in Cardiology*, pages 635–638. I.

Mosteller, R. D. (1987). Simplified calculation of body-surface area. *N Engl J Med*, 317(17):1098.

Mulier, S., Ni, Y., Jamart, J., Ruers, T., Marchal, G., and Michel, L. (2005). Local recurrence after hepatic radiofrequency coagulation: multivariate meta-analysis and review of contributing factors. *Ann Surg*, 242(2):158–171.

Netter, F. H. (2006). *Atlas of human anatomy*. Elsevier.

NewsletterTransplant (2010). *International Figures on Donation and Transplantation 2009*, volume 15. Council of Europe.

Nicolau, S., Soler, L., Mutter, D., and Marescaux, J. (2011). Augmented reality in laparoscopic surgical oncology. *Surg Oncol*, 20(3):189–201.

Nilsson, H., Blomqvist, L., Douglas, L., Nordell, A., and Jonas, E. (2010). Assessment of liver function in primary biliary cirrhosis using Gd-EOB-DTPA-enhanced liver MRI. *HPB (Oxford)*, 12(8):567–576.

Nilsson, H., Nordell, A., Vargas, R., Douglas, L., Jonas, E., and Blomqvist, L. (2009). Assessment of hepatic extraction fraction and input relative blood flow using dynamic hepatocyte-specific contrast-enhanced MRI. *J Magn Reson Imaging*, 29(6):1323–1331.

Olabarriaga, S. D. and Smeulders, A. W. M. (2001). Interaction in the segmentation of medical images: A survey. *Medical Image Analysis*, 5(2):127–142.

Oldhafer, K. J., Hoegemann, D., Stamm, G., Raab, R., Peitgen, H. O., and Galanski, M. (1999). 3-dimensional (3-d) visualization of the liver for planning extensive liver resections. *Chirurg*, 70(3):233–238.

Oliveira, D., Feitosa, R., and Correia, M. (2011). Segmentation of liver, its vessels and lesions from CT images for surgical planning. *BioMedical Engineering Online*, 10(1):30.

OPTN (assessed in July 2012). Organ procurement and transplantation network. http://optn.transplant.hrsa.gov/.

Osher, S. and Sethian, J. A. (1988). Fronts propagating with curvature-dependent speed: algorithms based on Hamilton-Jacobi formulations. *J. Comput. Phys.*, 79:12–49.

Ozawa, K., Uemoto, S., Tanaka, K., Kumada, K., Yamaoka, Y., Kobayashi, N., Inamoto, T., Shimahara, Y., Mori, K., and Honda, K. (1992). An appraisal of pediatric liver transplantation from living relatives. Initial clinical experiences in 20 pediatric liver transplantations from living relatives as donors. *Ann Surg*, 216(5):547–553.

Paetz, T., Kroeger, T., and Preusser, T. (2009). Simulation of radiofrequency ablation including water evaporation. *IFMBE Proceedings*, 25(4):1287–1290.

Pan, S. and Dawant, B. M. (2001). Automatic 3-D segmentation of the liver from abdominal CT images: A level-set approach. In Sonka, M. and Hanson, K. M., editors, *SPIE Medical Imaging*, volume 4322, pages 189–196.

Park, H.; Bland, P. H. . M. C. R. (2003). Construction of an abdominal probabilistic atlas and its application in segmentation. *IEEE TMI*, 22(4):483–492.

Peterhans, M. (2010). *Ultrasound-based non-invasive referencing of anatomical Structures for computer-assisted soft tissue surgery*. PhD thesis, Uninversity Bern, Switzerland.

Pichlmayr, R., Ringe, B., Gubernatis, G., Hauss, J., and Bunzendahl, H. (1988). Transplantation of a donor liver to 2 recipients (splitting transplantation)–a new method in the further development of segmental liver transplantation. *Langenbecks Arch Chir*, 373(2):127–130.

Platero, C., Poncela, J. M., González, P. M., Tobar, M. C., Sanguino, J., Asensio, G., and Santos, E. (2008). Liver segmentation for hepatic lesions detection and characterisation. In *ISBI*, pages 13–16.

Pohle, R. and Toennies, K. D. (2001). A new approach for model-based adaptive region growing in medical image analysis. In *CAIP*, pages 238–246.

Pomposelli, J. J., Tongyoo, A., Wald, C., and Pomfret, E. A. (2012). Variability of standard liver volume (SLV) estimation compared to software assisted total liver volume measurement. *Liver Transpl*, page Epub ahead of print.

Poovathumkadavil, A., Leung, K. F., Ghamdi, H. M. A., Othman, I. E. H., and Meshikhes, A.-W. (2010). Standard formula for liver volume in Middle Eastern Arabic adults. *Transplant Proc*, 42(9):3600–3605.

Preim, B., Hindennach, M., Spindler, W., Schenk, A., Littmann, A., and Peitgen, H.-O. (2003). Visualisierungs- und Interaktionstechniken für die Planung lokaler Therapien. In *Simulation und Visualisierung*, pages 237–248.

Preim, B., Spindler, W., Oldhafer, K. J., Galanski, M., and Peitgen, H.-O. (2001a). Visualization and analysis techniques for liver surgery planning. In Lemke, H. U., Vannier, M. W., Inamura, K., Farman, A. G., and Doi, K., editors, *Computer Assisted Radiology and Surgery*, volume 1230, pages 1251–1252.

Preim, B., Spindler, W., Oldhafer, K. J., and Peitgen, H.-O. (2001b). 3D-interaction techniques for planning of oncologic soft tissue operations. In *Graphics Interface*, pages 183–190.

Preim, B., Tietjen, C., Spindler, W., and Peitgen, H.-O. (2002). Integration of measurement tools in medical 3D visualizations. In *IEEE Visualization*, pages 21–28.

Preusser, T., Weihusen, A., and Peitgen, H.-O. (2005). On the modelling of perfusion in the simulation of RF-ablation. In Schulze, T., Horton, G., Preim, B., and Schlechtweg, S., editors, *Simulation and Visualization*, pages 259–269, Ghent. SCS-Verlag.

Radtke, A., Bockhorn, M., Schroeder, T., Lang, H., Paul, A., Nadalin, S., Saner, F., Schenk, A., Broelsch, C. E., and Malagó, M. (2006a). Computer-assisted planning in living donor liver operation. *Zentralbl Chir*, 131(1):69–74.

Radtke, A., Nadalin, S., Sotiropoulos, G. C., Molmenti, E. P., Schroeder, T., Valentin-Gamazo, C., Lang, H., Bockhorn, M., Peitgen, H.-O., Broelsch, C. E., and Malagó, M. (2007a). Computer-assisted operative planning in adult living donor liver transplantation: a new way to resolve the dilemma of the middle hepatic vein. *World J Surg*, 31(1):175–185.

Radtke, A., Schroeder, T., Molmenti, E. P., Sotiropoulos, G. C., Nadalin, S., Schenk, A., Malamutmann, E., Saner, F., Valentin-Gamazo, C., Dahmen, U.,

Lang, H., Peitgen, H.-O., Broelsch, C. E., and Malagò, M. (2006b). The "territorial belonging" of the middle hepatic vein: a troublesome dilemma in adult live donor liver transplantation–anatomical evidence based on virtual 3-dimensional-computed tomography-imaging reconstructions. *Eur J Med Res*, 11(2):66–72.

Radtke, A., Schroeder, T., Sotiropoulos, G. C., Molmenti, E., Schenk, A., Paul, A., Nadalin, S., Lang, H., Saner, F., Peitgen, H. O., Broelsch, C. E., and Malagò, M. (2005). Anatomical and physiological classification of hepatic vein dominance applied to liver transplantation. *Eur J Med Res*, 10(5):187–194.

Radtke, A., Sgourakis, G., Sotiropoulos, G., Molmenti, E., Nadalin, S., Fouzas, I., Schroeder, T., Saner, F., Schenk, A., Cicinnati, V., Malago, M., and Lang, H. (2008a). Hepatic hilar and sectorial vascular and biliary anatomy in right graft adult live liver donor transplantation. *Transplant Proc*, 40(9):3147–3150.

Radtke, A., Sgourakis, G., Sotiropoulos, G., Molmenti, E., Nadalin, S., Fouzas, I., Schroeder, T., Saner, F., Schenk, A., Cincinnati, V., Malago, M., and Lang, H. (2008b). Intrahepatic biliary anatomy derived from right graft adult live donor liver transplantation. *Transplant Proc*, 40(9):3151–3154.

Radtke, A., Sgourakis, G., Sotiropoulos, G., Molmenti, E., Nadalin, S., Schroeder, T., Saner, F., Schenk, A., Cincinnati, V., Broelsch, C., Lang, H., and Malago, M. (2009). Vascular and biliary anatomy of the right hilar window: its impact on recipient morbidity and mortality for right graft live donor liver transplantation. *World J Surg*, 33(9):1941–1951.

Radtke, A., Sgourakis, G., Sotiropoulos, G. C., Beckebaum, S., Molmenti, E. P., Saner, F. H., Schroeder, T., Nadalin, S., Schenk, A., Lang, H., Malagó, M., and Broelsch, C. E. (2010). Donor/recipient algorithm for management of the middle hepatic vein in right graft live donor liver transplantation. *Am J Surg*, 199(5):708–715.

Radtke, A., Sotiropoulos, G. C., Nadalin, S., Molmenti, E. P., Schroeder, T., Lang, H., Saner, F., Valentin-Gamazo, C., Frilling, A., Schenk, A., Broelsch, C. E., and Malagó, M. (2007b). Preoperative volume prediction in adult living donor liver transplantation: how much can we rely on it? *Am J Transplant*, 7(3):672–679.

Radtke, A., Sotiropoulos, G. C., Sgourakis, G., Molmenti, E. P., Schroeder, T., Saner, F. H., Beckebaum, S., Schenk, A., Lang, H., Broelsch, C. E., and Malagó, M. (2011). "Anatomical" versus "territorial" belonging of the middle hepatic vein: virtual imaging and clinical repercussions. *J Surg Res*, 166(1):146–155.

Raia, S., Nery, J. R., and Mies, S. (1989). Liver transplantation from live donors. *Lancet*, 2(8661):497.

Raya, S. P. and Udupa, J. K. (1990). Shape-based interpolation of multidimensional objects. *IEEE Trans Med Imaging*, 9(1):32–42.

Rempp, H., Boss, A., Helmberger, T., and Pereira, P. (2011). The current role of minimally invasive therapies in the management of liver tumors. *Abdom Imaging*, 36(6):635–647.

Rex, H. (1888). Beitraege zur Morphologie der Saeugerleber. *Morphologisches Jahrbuch 1888*, 14:517–616.

Rieder, C., Altrogge, I., Kroeger, T., Zidowitz, S., and Preusser, T. (2010). Interactive approximation of the ablation zone incorporating heatsink effects for radiofrequency ablation. *CURAC*, pages 9–12.

Rieder, C., Kroeger, T., Schumann, C., and Hahn, H. (2011). GPU-based real-time approximation of the ablation zone for radiofrequency ablation. *IEEE Transactions on Visualization and Computer Graphics*, 17(12):1812–1821.

Rieder, C., Wirtz, S., Zidowitz, S., Bruners, P., Isfort, P., Mahnken, A. H., Strehlow, J., and Peitgen, H.-O. (2012). Automatic alignment of pre- and post-interventional CT images for assessment of radiofrequency ablation therapy. In *SPIE Medical Imaging*, volume 8316, pages 83163E–1–83163E–8.

Roggan, A., Ritz, J. P., Knappe, V., Germer, C. T., Isbert, C., Schaedel, D., and Mueller, G. (2001). Radiation planning for thermal laser treatment. *Med Laser Appl*, 16:65–72.

Ruskó, L., Bekes, G., and Fidrich, M. (2009). Automatic segmentation of the liver from multi- and single-phase contrast-enhanced CT images. *Medical Image Analysis*, 13(6):871–882.

Ruskó, L., Bekes, G., Németh, G., and Fidrich, M. (2007). Fully automatic liver segmentation for contrast-enhanced CT images. In *MICCAI 2007 Workshop: 3D Segmentation in the Clinic-A Grand Challenge*, pages 143–150.

Salhab, M. and Canelo, R. (2011). An overview of evidence-based management of hepatocellular carcinoma: a meta-analysis. *J Cancer Res Ther*, 7(4):463–475.

Salvalaggio, P. R. O., Baker, T. B., Koffron, A. J., Fryer, J. P., Clark, L., Superina, R. A., Blei, A. T., Nemcek, A., and Abecassis, M. M. (2005). Liver graft volume estimation in 100 living donors: measure twice, cut once. *Transplantation*, 80(9):1181–1185.

Scatton, O., Belghiti, J., Dondero, F., Goere, D., Sommacale, D., Plasse, M., Sauvanet, A., Farges, O., Vilgrain, V., and Durand, F. (2004). Harvesting the mid-

dle hepatic vein with a right hepatectomy does not increase the risk for the donor. *Liver Transpl*, 10(1):71–76.

Schenk, A., Bourqain, H., Frericks, B., Calderone, F., Galanski, M., and Peitgen, H.-O. (2002). Evaluierung von Gefaessanalyse und Volumetrie fuer die Planung von Leberlebendspenden. In *Bildverarbeitung fuer die Medizin*, pages 397–400.

Schenk, A., Breitenborn, J., Selle, D., Schindewolf, T., Boehm, D., Spindler, W., Juergens, H., and Peitgen, H.-O. (1999). ILabMed-Workstation – Eine Entwicklungsumgebung für radiologische Anwendungen. Bildverarbeitung für die Medizin, pages 238–242.

Schenk, A., Haemmerich, D., and Preusser, T. (2011). Planning of image-guided interventions in the liver. *IEEE Pulse*, 2:48–55.

Schenk, A., Hindennach, M., Radtke, A., Malagó, M., Schroeder, T., and Peitgen, H.-O. (2009). Formation of venous collaterals and regeneration in the donor remnant liver: volumetric analysis and three-dimensional visualization. *Transplant Proc*, 41(6):2515–2517.

Schenk, A., Hindennach, M., Schroeder, T., Radtke, A., and Peitgen, H.-O. (2007). Planning of living donor liver transplantations based on MRI and CT data: comparison of liver volume, portal and hepatic veins and their territories. In Lemke, H. and Vannier, M., editors, *Int J Comput Assist Radiol Surg*, volume 2, pages 279–280.

Schenk, A., Miller, S., Nadalin, S., Schroeder, T., Radtke, A., and Peitgen, H.-O. (2010). Volumetry and 3D reconstruction for LDLT based on Gd-EOB-DTPA-enhanced MRI. *Liver Transpl*, 16(6):S107.

Schenk, A. and Peitgen, H.-O. (2012). Accurate liver segmentation with live wire and interpolation: Evaluation on 2000 computed tomographies.

Schenk, A., Prause, G., and Peitgen, H.-O. (2000). Efficient semiautomatic segmentation of 3D objects in medical images. In *MICCAI*, pages 186–195.

Schenk, A., Prause, G., and Peitgen, H.-O. (2001a). Local cost computation for efficient segmentation of 3D objects with live wire. In Sonka, M. and Hanson, M., editors, *SPIE Medical Imaging*, volume 4322, pages 1357–1364.

Schenk, A., Prause, G., and Peitgen, H.-O. (2001b). Optimierte semi-automatische Segmentierung von 3D-Objekten mit Live Wire und Shape-Based Interpolation. In Handels, H. and et al., editors, *Bildverarbeitung fuer die Medizin*, pages 202–206.

Schenk, A., Weihusen, A., Rieder, C., Frericks, B., Valdeig, S., Lehmann, K., and Peitgen, H.-O. (2008a). Evaluation of radiofrequency ablation lesions: a new software tool for the quantification of heat sink effects. In *Int J Comput Assist Radiol Surg*, volume 3, pages S448–S449.

Schenk, A., Zidowitz, S., Bourquain, H., Hindennach, M., Hansen, C., Hahn, H., and Peitgen, H.-O. (2008b). Clinical relevance of model based computer-assisted diagnosis and therapy. In Giger, M. L. and Karssemeijer, N., editors, *SPIE Medical Imaging*, volume 6915, pages 691502_1–19.

Scheuering, M. (2003). *Fusion of Medical Video Images and Tomographic Volumes*. PhD thesis, University Erlangen-Nuernberg, Germany.

Scheuering, M., Schenk, A., Schneider, A., Preim, B., and Greiner, G. (2003). Intra-operative augmented reality for minimally invasive liver interventions. In *SPIE Medical Imaging*, volume 5029, pages 407–417.

Schindewolf, T., Frese, U., and Meissner, J. (1999). Segmentierung und Volumetrie der Hirnventrikel mit MRT-Datensätzen. In *Bildverarbeitung fuer die Medizin*, pages 92–96.

Schindewolf, T. and Peitgen, H.-O. (2000). Interaktive Bildsegmentierung von CT- und MR-Daten auf Basis einer modifizierten hierarchischen Wasserscheiden-Transformation. In *Bildverarbeitung fuer die Medizin*, pages 96–100.

Schroeder, T., Radtke, A., Kuehl, H., Debatin, J. F., Malagó, M., and Ruehm, S. G. (2006). Evaluation of living liver donors with an all-inclusive 3D multi-detector row CT protocol. *Radiology*, 238(3):900–910.

Schumann, C., Rieder, C., Bieberstein, J., Weihusen, A., Zidowitz, S., Moltz, J. H., and Preusser, T. (2010). State of the art in computer-assisted planning, intervention, and assessment of liver-tumor ablation. *Crit Rev Biomed Eng*, 38(1):31–52.

Schwarz, T., Heimann, T., Tetzlaff, R., Rau, A., Wolf, I., and Meinzer, H. (2008). Interactive surface correction for 3D shape based segmentation. In *SPIE Medical Imaging*, volume 6914, page 691430.

Schwier, M., Moltz, J. H., and Peitgen, H.-O. (2011). Object-based analysis of CT images for automatic detection and segmentation of hypodense liver lesions. *Int J Comput Assist Radiol Surg*, 6(6):737–747.

Selle, D., Preim, B., Schenk, A., and Peitgen, H.-O. (2002). Analysis of vasculature for liver surgical planning. *IEEE Trans Med Imaging*, 21(11):1344–1357.

Selle, D., Spindler, W., Schenk, A., Preim, B., Böhm, D., Oldhafer, K., Galanski, M., Fasel, J., Klose, K., and Peitgen, H.-O. (2000). Computer-aided preoperative planning and risk analysis in liver surgery. *Diagnostic Imaging Europe*, 12:16–20.

Seo, K.-S. and Park, J.-A. (2005). Improved automatic liver segmentation of a contrast enhanced CT image. In *PCM (1)*, pages 899–909.

Shimada, H., Tanaka, K., Endou, I., and Ichikawa, Y. (2009). Treatment for colorectal liver metastases: a review. *Langenbecks Arch Surg*, 394(6):973–983.

Shimizu, A., Kawamura, T., and Kobatake, H. (2005). Proposal of computer-aided detection system for three dimensional CT images of liver cancer. In *Int J Comput Assist Radiol Surg*, volume 1281, pages 1157–1162.

Shimizu, A., Ohno, R., Ikegami, T., Kobatake, H., Nawano, S., and Smutek, D. (2006). Multi-organ segmentation in three dimensional abdominal CT images. In *Int J Comput Assist Radiol Surg*, volume 1, pages 76–78.

Shimizu, A., Ohno, R., Ikegami, T., Kobatake, H., Nawano, S., and Smutek, D. (2007). Segmentation of multiple organs in non-contrast 3D abdominal CT images. *Int J Comput Assist Radiol Surg*, 2:135–142.

Silva, S. S., Santos, B. S., Madeira, J., Silva, A., and Silva, A. (2010). A 3D tool for left ventricle segmentation editing. In *ICIAR*, pages 79–88.

Sirlin, C. B. and Reeder, S. B. (2010). Magnetic resonance imaging quantification of liver iron. *Magn Reson Imaging Clin N Am*, 18(3):359–381, ix.

Sled, J. G., Zijdenbos, A. P., and Evans, A. C. (1998). A nonparametric method for automatic correction of intensity nonuniformity in MRI data. *IEEE Trans Med Imaging*, 17(1):87–97.

Soler, L., Delingette, H., Malandain, G., Montagnat, J., Ayache, N., Koehl, C., Dourthe, O., Malassagne, B., Smith, M., Mutter, D., and Marescaux, J. (2001). Fully automatic anatomical, pathological, and functional segmentation from CT scans for hepatic surgery. *Computer Aided Surgery*, 6(3):131–142.

Stalling, D. and Hege, H.-C. (1996). Intelligent scissors for medical image segmentation. In *Digitale Bildverarbeitung für die Medizin*, pages 32–36.

Starzl, T. E. and Demetris, A. J. (1990). Liver transplantation: a 31-year perspective. Part I. *Curr Probl Surg*, 27(2):49–116.

Starzl, T. E., Groth, C. G., Brettschneider, L., Moon, J. B., Fulginiti, V. A., Cotton, E. K., and Porter, K. A. (1968a). Extended survival in 3 cases of orthotopic homotransplantation of the human liver. *Surgery*, 63(4):549–563.

Starzl, T. E., Groth, C. G., Brettschneider, L., Penn, I., Fulginiti, V. A., Moon, J. B., Blanchard, H., Martin, A. J., and Porter, K. A. (1968b). Orthotopic homotransplantation of the human liver. *Ann Surg*, 168(3):392–415.

Starzl, T. E., Marchioro, T. L., Vonkaulla, K. N., Hermann, G., Brittain, R. S., and Waddell, W. R. (1963). Homotransplantation of the liver in humans. *Surg Gynecol Obstet*, 117:659–676.

Strong, R. W., Lynch, S. V., Ong, T. H., Matsunami, H., Koido, Y., and Balderson, G. A. (1990). Successful liver transplantation from a living donor to her son. *N Engl J Med*, 322(21):1505–1507.

Tanaka, K. and Ogura, Y. (2004). "Small-for-size graft" and "small-for-size syndrome" in living donor liver transplantation. *Yonsei Med J*, 45(6):1089–1094.

Taner, C. B., Dayangac, M., Akin, B., Balci, D., Uraz, S., Duran, C., Killi, R., Ayanoglu, O., Yuzer, Y., and Tokat, Y. (2008). Donor safety and remnant liver volume in living donor liver transplantation. *Liver Transpl*, 14(8):1174–1179.

Tiesler, H. (2011). *Identification of Material Parameters from Temperature Measurements in Radio Frequency Ablation.* PhD thesis, University of Bremen, Germany.

Udupa, J. K., Samarasekera, S., and Barrett, W. A. (1992). Boundary detection via dynamic programming. In *Visualization in Biomedical Computing*, pages 33–39.

Urata, K., Kawasaki, S., Matsunami, H., Hashikura, Y., Ikegami, T., Ishizone, S., Momose, Y., Komiyama, A., and Makuuchi, M. (1995). Calculation of child and adult standard liver volume for liver transplantation. *Hepatology*, 21(5):1317–1321.

van Ginneken, B., Heimann, T., and Styner, M. (2007). 3D segmentation in the clinic: A grand challenge. In Heimann T, Styner M, v. G. B., editor, *MICCAI 2007 Workshop: 3D Segmentation in the Clinic - A Grand Challenge*, pages 7–15.

Vauthey, J.-N., Abdalla, E. K., Doherty, D. A., Gertsch, P., Fenstermacher, M. J., Loyer, E. M., Lerut, J., Materne, R., Wang, X., Encarnacion, A., Herron, D., Mathey, C., Ferrari, G., Charnsangavej, C., Do, K.-A., and Denys, A. (2002). Body surface area and body weight predict total liver volume in Western adults. *Liver Transpl*, 8(3):233–240.

Vetter, M., Hassenpflug, P., Wolf, I., Thorn, M., S., C. E. C., Grenacher, L., Richter, G. M., Lamadé, W., Buechler, M. W., and Meinzer, H.-P. (2002). Intraoperative Navigation in der Leberchirurgie mittels Navigationshilfen und Verformungsmodellierung. In Meiler, M., Saupe, D., Kruggel, F., Handels, H., and Lehmann, T. M., editors, *Bildverarbeitung fuer die Medizin*, volume 56, pages 73–76.

West, D. B. (1996). *Introduction to Graph Theory*. Prentice Hall, Upper Saddle River.

Wood, B. J., Kruecker, J., Abi-Jaoudeh, N., Locklin, J. K., Levy, E., Xu, S., Solbiati, L., Kapoor, A., Amalou, H., and Venkatesan, A. M. (2010). Navigation systems for ablation. *J Vasc Interv Radiol*, 21(8 Suppl):S257–S263.

Xu, C. and Prince, J. L. (1997). Gradient vector flow: a new external force for snakes. In *IEEE Proc. Conf. on Comp. Vis. Patt. Recog. (CVPR'97)*, pages 66–71.

Xu, C. and Prince, J. L. (1998). Snakes, shapes, and gradient vector flow. *IEEE Trans Med Imaging*, pages 359–369.

Yeung, C. K., Ho, J. K., Lau, W. Y., Liu, K., Cho, A., Buckley, T., Aun, C., and Li, A. K. (1994). Institution of a pediatric liver transplantation program with living-related orthotopic liver transplantation: initial experience in Hong Kong. *Transplant Proc*, 26(4):2215–2217.

Yoshizumi, T., Gondolesi, G. E., Bodian, C. A., Jeon, H., Schwartz, M. E., Fishbein, T. M., Miller, C. M., and Emre, S. (2003). A simple new formula to assess liver weight. *Transplant Proc*, 35(4):1415–1420.

Yoshizumi, T., Taketomi, A., Kayashima, H., Yonemura, Y., Harada, N., Ijichi, H., Soejima, Y., Nishizaki, T., and Maehara, Y. (2008). Estimation of standard liver volume for Japanese adults. *Transplant Proc*, 40(5):1456–1460.

Yuan, D., Lu, T., Wei, Y. G., Li, B., Yan, L. N., Zeng, Y., Wen, T. F., and Zhao, J. C. (2008). Estimation of standard liver volume for liver transplantation in the Chinese population. *Transplant Proc*, 40(10):3536–3540.

Zahlten, C., Jürgens, H., Evertsz, C. J., Leppek, R., Peitgen, H.-O., and Klose, K. J. (1995). Portal vein reconstruction based on topology. *Eur J Radiol*, 19(2):96–100.

Zappa, M., Dondero, F., Sibert, A., Vullierme, M.-P., Belghiti, J., and Vilgrain, V. (2009). Liver regeneration at day 7 after right hepatectomy: global and segmental volumetric analysis by using CT. *Radiology*, 252(2):426–432.

Zhou, X., Kitagawa, T., Hara, T., Fujita, H., Zhang, X., Yokoyama, R., Kondo, H., Kanematsu, M., and Hoshi, H. (2006). Constructing a probabilistic model for automated liver region segmentation using non-contrast X-ray torso CT images. *Med Image Comput Comput Assist Interv*, 9:856–863.